AN INVESTIGATION ON THE EFFECTS OF LIME AND/OR PHOSPHORUS FERTILIZER APPLICATIONS ON SOIL ORGANIC MATTER PRESERVATION

A thesis presented in partial fulfilment of the requirements for the degree of

Doctor of Philosophy

in

Soil Science

At Massey University, Manawatu
New Zealand

Yang Li

2021

MASSEY UNIVERSITY
TE KUNENGA KI PŪREHUROA
UNIVERSITY OF NEW ZEALAND

ABSTRACT

The poor understanding of the mechanisms through which soil organic matter (OM) is lost with ongoing land-use intensification hampers the development of food security and climate-smart agricultural management practices. The overall objective of this thesis was to investigate the effect of lime and/or phosphorus (P) amendment on OM preservation in a volcanic soil classified as an Andosol – the mineral soil group with the largest organic carbon (OC) content worldwide and characterised by its abundance in aluminium (Al)-OM complexes (e.g., Al^{3+}-OM and allophane-OM complexes). Special attention was paid to the response of OM stabilisation and mineralisation with depth to these amendments.

Firstly, we hypothesised that (i) lime and P application has an impact on OM stabilisation through different mechanisms, and (ii) their effect is synergic. To have a direct understanding of the effect of lime and/or P application on OM preservation in the Andosol under study, we conducted a batch of water extractions. We extracted the bulk soil and its heavy fraction (>1.6 g/cm^3, indicative of the presence of OM-mineral associations) with added lime and/or P to reveal the individual and combined influence of lime and P amendments on water-extractable OM (WEOM), which has been deemed to be an indicator of OM destabilisation. The results obtained from quantitative analyses of WEOM showed that adding lime and/or P significantly increased the WEOM, along with a decrease in its carbon (C)/nitrogen (N) ratio (C/N) and an increase in its aromaticity. The chemical composition of WEOM measured by pyrolysis-gas chromatography/mass spectrometry suggested that lime and P addition (at high application rate) caused an enrichment in WEOM in the poly- and monophenolic, and nitrogenised fraction, as well as in plant-

derived polysaccharides. If we consider the effect on the heavy fraction, the increase in WEOM was still consistent with that observed in the bulk soil when lime was applied, but the response to P addition alone was smaller. These findings indicate that lime and P amendment to soils rich in Al-OM complexes cause destabilisation of OM, but through different mechanisms. Phosphate was found to mainly impact Al^{3+}-OM complexes (partly present in the removed free particulate OM) by outcompeting organic ligands for Al^{3+}, whereas alkalisation was able to disrupt both the Al^{3+}-OM and allophane-OM complexes, and the stability of aggregates. These could be hastened by combined lime and P addition, as made evident by the larger impact of combined lime and P amendments than that of either P or lime addition alone (Chapter 3).

After confirming the occurrence of OM destabilisation in the Andosol upon lime and/or P application, we hypothesised that the response of OM preservation (OM stabilisation and mineralisation) to these amendments varies with soil depth. We conducted a 6-month incubation experiment to have an in-depth understanding of the influence of these amendments on OM preservation in soil at different depths. A topsoil (rich in Al^{3+}-OM complexes) and a subsoil (with a greater abundance of allophane) of an alu-andic Andosol was incubated with/without inorganic amendments (either lime, phosphate or lime+phosphate) in the presence or absence of an organic amendment (^{13}C- and ^{15}N-labelled barley, *Hordeum vulgare* L.). By conventional chemical analyses of the bulk soil, we showed an increase in WEOM in both topsoil and subsoil samples that received amendments, particularly of lime (with/without P). However, through a nano-scale secondary ion mass spectrometry analysis of OM-mineral associations in soil microaggregates, we noted that lime amendments decreased OM coverage (particularly

plant-derived OM) on the mineral surface in topsoil, but increased it in subsoil (with enhanced coverage of plant-derived OM). These suggested that at these two soil depths with different biogeochemistry, lime addition resulted in OM destabilisation through different mechanisms associated with (i) the displacement of OM from inorganic surfaces in microaggregates in the topsoil, and (ii) the release of OM previously protected within macroaggregates in the subsoil. The total cumulative carbon dioxide (CO_2) emissions and stable C isotopic signature ($\delta^{13}C$) of CO_2 showed that lime amendments caused an increase in OM decomposition in the subsoil from both inherited OM (priming) and OM newly formed from barley litter decomposition, but not in topsoil. The increase in OM mineralisation observed in the subsoil (a harsher environment for microbes, with limited bioavailable OM) is consistent with the fact that more favourable conditions were generated by the lime and P addition, which caused an increase in WEOM (Chapter 4).

To further understand the distinct responses in OM mineralisation with depth to lime and/or P amendments, we investigated soil bacterial and fungal community composition and their functional profile through high-throughput sequencing analysis. A shift in bacterial and fungal community composition and their functional composition was found in the limed topsoil but not in the limed subsoil. Through structural equation modelling analysis, it was found that in the topsoil, microbial properties, particularly the fungal community composition and functional profile, had a significant relationship with OM mineralisation (with a relatively greater positive or negative coefficient value than other factors). However, in the subsoil, OM mineralisation was only significantly correlated with labile OM in the subsoil. These findings suggested that in the Andosol, the key regulator controlling the response of OM mineralisation to lime and/or phosphate addition shifted with depth from

microbial composition and functionality to bioavailable C substrate (Chapter 5).

All the results obtained in this thesis contribute to providing a mechanistic understanding of the effect of lime and/or P amendments on OM stabilisation and mineralisation, and have implications for designing climate-smart agricultural management practices of soils with abundant Al-OM complexes.

ACKNOWLEDGMENTS

I am profoundly grateful to my main supervisor, Prof. Marta Camps-Arbestain for her constant supervision, constructive suggestion, never-ending encouragement offered throughout my PhD study. I would also like to sincerely thank my co-supervisors, Dr. Catherine P. Whitby and Dr. Tao Wang who are very generous with their time, patience, and knowledge.

My special thanks go to the China Scholarship Council for awarding me a Doctoral Scholarship, and to the Massey University Research Fund (RM18670) and the New Zealand Ministry for Primary Industries for funding the research.

I am also indebted to Dr. Manuel Suárez-Abelenda (Universidade de Santiago de Compostela), A/Prof. Carsten W. Mueller (University of Copenhagen), Dr. Carmen Hoeschen (Technische Universität München), Dr. Mike Bear (New Zealand Institute for Plant & Food Research Limited), Ms. Gertraut Harrington (Technische Universität München), Mr. Johann Lugmeier (Technische Universität München) and Prof. Fei Shen (Sichuan Agricultural University) for assistant with the pyrolysis-gas chromatography/mass spectrometry, nano-scale secondary ion mass spectrometry, and microbial community composition analyses, help in data analysis and interpretation, and revision of manuscript.

My sincere acknowledge is extended to Dr. Qinhua Shen, Mr. Ian Furkert, Dr. Roberto Calvelo-Pereira, Dr. Peter Bishop, Mr. Bob Toes, Mr. John Sykes, Prof. David Harding, Dr. Jim Chen etc. for the guidance they provided me with the laboratory work.

Big thanks to all my other colleagues: Akinson Tumbure, Nilusha Ubeynarayana, Idri Siregar, Chao Kong, Stanislav Aleksandrovich Garbuz, Hamed Khan, Khadija Malik, May Sasikunya, Nguyen Truong Thi, Themba Dumsane, Fredy Monserrate, and many others. They provide me a very enjoyable and relaxed atmosphere to study in.

Appreciations are also conveyed to all friends in New Zealand: Cyrus Liu, Mark An, Xining Wang, Danxia Shi, Wei Cheng, Clyde Brunton, Yan Xia, Wenliang Xu, Yuwen Qi, etc. who give me concern and help during my stay in New Zealand.

Last, but not the least, my immense gratitude is offered to my patents and my family members, back in China, for their unconditional love, patience, and support. My lovely husband, Jin Li, is always appreciated for his endless love, understanding, encouragement and commitments over these years.

PUBLICATIONS

Journal articles

1. Li, Yang, Tao Wang, Marta Camps-Arbestain, Manuel Suárez-Abelenda, & Catherine P. Whitby (2020). Lime and/or phosphate application affects the stability of soil organic carbon: Evidence from changes in quantity and chemistry of the soil water-extractable organic matter. *Environmental Science & Technology, 54*(21), 13908–13916.

2. Yang Li, Marta Camps-Arbestain, Catherine P. Whitby, Tao Wang, Carsten W. Mueller, Carmen Hoeschen, Mike H. Beare (2021). Functional complexity explains the depth-dependent response of organic matter to lime and phosphorus fertilizer application (*Accepted, Geoderma*)

3. Yang Li, Marta Camps-Arbestain, Tao Wang, Catherine P. Whitby (2021). The key regulator controlling the response of soil organic matter mineralisation to lime and/or phosphate addition shifts with depth from microorganisms to bioavailable substrate carbon (*Under revision, Science of the Total Environment*)

TABLE OF CONTENTS

LIST OF TABLE AND FIGURES

LIST OF ABBREVIATIONS

Al	aluminium
Al_o	acid oxalate-extractable aluminium
Al_p	sodium pyrophosphate-extractable aluminium
AP ^{13}C	isotope enrichment of ^{13}C (atom-%)
AP ^{15}N	isotope enrichment of ^{15}N (atom-%)
C	carbon
C-C/N	carbon: nitrogen ratio of cold water-extractable organic matter
CO_2	carbon dioxide
C_{OMi}	carbon mineralisation from inherited organic matter
C_p	sodium pyrophosphate-extractable carbon
C-SUVA	aromaticity of cold water-extractable organic matter measured with specific UV absorbance at 245nm
Ctr-	negative control
Ctr+	positive control
CWEC	cold water-extractable organic carbon
DOM	dissolved organic matter
Fe	iron
Feo	acid oxalate-extractable iron
Fe_p	sodium pyrophosphate-extractable iron
f_{lime}	fractional contribution of lime
f_{OMi}	fractional contribution of inherited organic matter
f_{OMn}	fractional contribution of organic matter newly formed from the barley litter
fPOM	free particulate organic matter
GFI	goodness-of-fit index

H-C/N	carbon: nitrogen ratio of hot water-extractable organic matter
H-SUVA	aromaticity of hot water-extractable organic matter measured with specific UV absorbance at 245nm
HWEC	hot water-extractable organic carbon
IRMS	isotope ratio mass spectrometer
L	lime amendment
L2	individual lime amendment at application rate: 2 g/kg
L4	individual lime amendment at application rate: 4 g/kg
L4P0.2	combined amendment of lime (at 4 g/kg) and phosphorus (at 0.2 g P/kg)
L4P0.4	combined amendment of lime (at 4 g/kg) and phosphorus (at 0.4 g P/kg)
L6	individual lime amendment at application rate: 6 g/kg
L8	individual lime amendment at application rate: 8 g/kg
L8P0.2	combined amendment of lime (at 8 g/kg) and phosphorus (at 0.2 g P/kg)
L8P0.4	combined amendment of lime (at 8 g/kg) and phosphorus (at 0.4 g P/kg)
LR	labelled residue
MAHs	monocyclic aromatic hydrocarbons
N	nitrogen
NanoSIMS	nano-scale secondary ion mass spectrometry
OC	organic carbon
OM	organic matter
OMi	inherited organic matter
OMn	organic matter newly formed from the barley litter
P	phosphorus
P0.1	individual phosphorus amendment at application rate: 0.1 g P/kg
P0.2	individual phosphorus amendment at application rate: 0.2 g P/kg
P0.3	individual phosphorus amendment at application rate: 0.3 g P/kg

P0.4	individual phosphorus amendment at application rate: 0.4 g P/kg
PAHs	polycyclic aromatic hydrocarbons
PC	principal component
P-C/N	carbon: nitrogen ratio of sodium pyrophosphate-extractable organic matter
PCA	principal component analysis
PCo	principal coordinate
PCoA	principal coordinate analysis
PL	combined phosphorus and lime
P-SUVA	aromaticity of sodium pyrophosphate-extractable organic matter measured with specific UV absorbance at 245nm
Py-GC/MS	pyrolysis-gas chromatography/mass spectrometry
RMSE	root mean square error
ROIs	regions of interest
SDGs	sustainable development goals
SEM	structural equation modelling
Si	silicon
Sio	acid oxalate-extractable silicon
SS	subsoil incubated without amendments
SS-L	subsoil incubated with lime
SS-LR	subsoil incubated with residue
SS-LR-L	subsoil incubated with residue and lime
SS-LR-P	subsoil incubated with residue and phosphorus
SS-LR-PL	subsoil incubated with residue and combined phosphorus and lime
SS-P	subsoil incubated with phosphorus
SS-PL	subsoil incubated with combined phosphorus and lime
SUVA	specific UV absorbance at 245nm

TC	total carbon
TN	total nitrogen
TQPA	total quantified peak area
TS	topsoil incubated without amendments
TS-L	topsoil incubated with lime
TS-LR	topsoil incubated with residue
TS-LR-L	topsoil incubated with residue and lime
TS-LR-P	topsoil incubated with residue and phosphorus
TS-LR-PL	topsoil incubated with residue and combined phosphorus and lime
TS-P	topsoil incubated with phosphorus
TS-PL	topsoil incubated with combined phosphorus and lime
UV_{254}	UV absorbance at 254 nm
WEOC	water-extractable organic carbon
WEOM	water-extractable organic matter
WEON	water-extractable organic nitrogen
$\delta^{13}C$	stable carbon isotopic signature (per mil, ‰)
$\delta^{15}N$	stable nitrogen isotopic signature (per mil, ‰)

CHAPTER 1

GENERAL INTRODUCTION

1.1 General background

In recent years, there has been an increasing interest in the study of soil organic matter (OM), given the important role it plays in climate change and food security (Rumpel et al., 2020). Soil OM constitutes the largest terrestrial carbon (C) pool, which contains more C than the world's vegetation and atmosphere combined (Eswaran et al., 1993; Flato et al., 2013). For this reason, even small changes in the balance between inputs and outputs in the soil C pool can significantly influence global C cycling, particularly the CO_2 concentration in the atmosphere. In addition, soil OM is a primary indicator of soil health (Bünemann et al., 2018), as it plays a fundamental role in (i) providing essential nutrients to plants and energy to the soil food web (Lal, 2004; Tiessen et al., 1994), (ii) the stability of physical structure (Carter, 2002; Lefèvre et al., 2017), and (iii) the immobilisation of contaminants (Lamichhane et al., 2016). Maintaining or increasing soil OM preservation has been promoted as a multiple-win strategy for climate change and adaptation and mitigation, and to achieve food security (Rumpel et al., 2020).

In the current model, soil OM represents a continuum of decomposing organic compounds, which decrease in size and become more oxidised and water-soluble as decomposition progresses (Kleber et al., 2015; Lehmann and Kleber, 2015). The resultant organic species can be stabilised and become protected against further decomposition through (i) physical occlusion within soil micro- and macro-aggregates, and (ii) chemical interaction with inorganic constituents to form OM-mineral/metal complexes (Kleber et al., 2015). The decomposition of OM releases CO_2 to the atmosphere, this being the largest single source of CO_2 from global terrestrial ecosystems (Metcalfe et al., 2011). It has been proposed that

OM decomposition is controlled by two steps: firstly, abiological processes that convert some non-bioavailable OM into a bioavailable OM source for microorganisms (termed the Regulatory Gate hypothesis); secondly, biological mineralisation, which is associated with microbial properties (e.g., abundance, diversity and metabolic functions) (Kemmitt et al., 2008). Both steps can be explained on the basis of the soil's functional complexity (Lehmann et al., 2020)

The growing demand for food is increasing the pressure on soil systems through worldwide land use intensification. Many agricultural land management practices are causing a depletion in OM, including liming and/or phosphorus (P) fertilising the soil rich in aluminium (Al)-OM complexes (e.g., Al^{3+}-OM and allophane-OM complexes) (Kov et al., 2018; Miyazawa et al., 2013; Schneider et al., 2010; Shen et al., 2018). Upon addition of these amendments, OM can become destabilised by causing previously protected OM to become displaced and/or released to the aqueous phase, resulting in an increase in dissolved OM (DOM). This DOM fraction is an extremely dynamic fraction that plays an important role in soil C turnover, as it has a very fast turnover (releasing CO_2 to the atmosphere) and it is also susceptible to leaching down to groundwater (Seifert et al., 2016; Wang et al., 2015). An increase in DOM could indicate the occurrence of OM destabilisation. Therefore, it is important to study the effect of lime and P amendments on the quantity and quality of DOM, particularly the combined effect of lime and P application, as studies on the latter are sorely missing.

The potential mechanisms by which additions of lime and phosphate to the soil impact OM stabilisation include (i) soil alkalisation through the destabilisation of inner-sphere surface bonding between reactive Al or iron (Fe) (hydr)oxides and organic ligands, and favouring

the formation of weaker outer-sphere bonding (Greiner et al., 2014; Kang et al., 2008; Kleber et al., 2015; Ramesh et al., 2019), and (ii) competition by OH^- and phosphate ions with organic ligands for reactive sites of (hydr)oxides and metal cations (Hiemstra et al., 2010; Kaiser and Zech, 1997; Spohn and Schleuss, 2019). In order to have an in-depth understanding of these processes, direct microscale evidence is needed.

There is also a need to understand the specific impact of lime and P amendments on soil OM mineralisation (Hutchinson et al., 2007). The response of OM mineralisation to lime and P amendments has been reported to be associated with the above-mentioned increase in bioavailable OM resulting from OM destabilisation, and also with a shift in microbial properties (e.g., bacteria/fungi ratio, C use efficiency, community composition of either bacteria or fungi) caused by these amendments (Silva-Sánchez et al., 2019; Spohn and Schleuss, 2019). The contributions of abiotic (e.g., bioavailable OM) and biotic (e.g., microorganisms) factors to the changes in OM mineralisation are influenced by the soil biogeochemistry, which is affected not only by the distinct pedogenesis of the different soil orders, but also by soil heterogeneity across the soil profile (Chen et al., 2016).

Within the soil profile, (i) organic C (OC) content decreases with depth, but the OC in subsoil horizons accounts for more than half of the total soil OC stocks (Rumpel and Kögel-Knabner, 2010; Tarnocai et al., 2009); (ii) the relative abundance of microbial-derived OM (with high molecular complexity) tends to increase with depth (Lehmann et al., 2020); (iii) the availability of surfaces of inorganic constituents able to react with ligands (and, in some instances, their content, as is the case of allophane in Andosols; Macíasa and Camps-Arbestain, 2020; Zieger et al., 2017) increases with depth; and (iv) microbial richness and diversity decrease with soil depth (Eilers et al., 2012; Upton et al., 2020). Therefore, the

impact of lime and P amendments on OM stabilisation and OM mineralisation is expected to differ within soil profile, but less attention has been paid to their potential distinct impact with soil depth (Rumpel and Kögel-Knabner, 2010; Tarnocai et al., 2009).

This study of the effect of lime and P amendments on soils with andic properties (classified as 'Andosols' by the World Reference Base Classification system, and as 'Allophanic soil' by the New Zealand classification system, Hewitt and Shepherd, 1997; WRB, 2015) is highly relevant, given that Andosols have high P retention and tend to be acidic. Therefore, their agricultural management generally includes lime and P application (Dahlgren et al., 2004; Hedley and Bolan, 2003). Andosols are the mineral soil group with the largest C content worldwide (McDaniel et al., 2012) and have been proposed as an archetype of the soils rich in Al-OM and/or Fe-OM complexes (Possinger et al., 2020), which could be influenced by the increased OH^- and phosphate ions (as mentioned previously). In New Zealand, the intensification of dairy pastures has led to a decline in the OC stocks in C-rich Allophanic soils, with a loss of -1.37 kg C/m^2 in the top 30 cm, and -0.7 kg C/m^2 at 30–60 cm, which is higher than that in other soil types studied (e.g., Recent, Brown, Pumice and Pallic soils) (Schipper et al., 2014). Various studies have reported that the C loss in Andosols could be associated with alkalisation of the soil and an increase in phosphate content (Kov et al., 2018; Shen et al., 2018).

However, the impact of lime and P application (and particularly their combined addition) on OM preservation in Andosols remains largely unclear. There is a lack of (i) direct evidence of their impact on DOM, (ii) understanding of their effect on OM-mineral associations at the micro-scale and on the functional complexity of soil OM, (iii)

knowledge of the response of soil bacterial and fungal properties and their role in OM mineralisation, and (iv) studies addressing their impact on the subsoil and the role of these abiotic and biotic factors as soil depth increases. This thesis aimed to fill these research gaps by testing four hypotheses as follows:

- Lime and P application influences the quality and quantity of the water-extractable OM (WEOM) through different mechanisms.
- The combined effect of P and lime addition on WEOM is stronger than that of either P or lime addition alone, as phosphate impairs the bonding between OM and Ca^{2+} added with lime.
- The effect of lime and/or P amendment on OM-mineral associations differs with depth, with distinct molecular complexity of OM and reactive surfaces within the soil profile.
- The response of OM mineralisation to lime and/or P amendment depends on soil depth, with a heterogeneity of bioavailable OM and microbial properties found throughout the soil profile.

1.2 Research objectives

The main objective of this thesis was to obtain an in-depth understanding of the effect of lime and/or P amendment on soil OM preservation in an Andosol, particularly regarding the response of OM stabilisation and mineralisation with depth.

Four sub-objectives are associated or derived from the main objective, including the following:

- To study the changes in WEOM in the bulk soil and its heavy fraction (>1.6 g/cm^3, indicative of the OM-mineral association) upon lime and/or P amendment, to understand how, by impacting DOM, lime and/or P addition impairs OM stabilisation.
- To investigate the amendment-driven changes in OM-mineral associations (at the nano-scale) in the topsoil and the subsoil, to understand how, by impacting the formation of OM-mineral association, lime and/or P addition impairs OM stabilisation within the soil profile.
- To characterise the amendment-driven shifts in microbial properties in the topsoil and the subsoil, to understand how, by impacting soil microorganisms, lime and/or P addition affects OM mineralisation within the soil profile.
- To estimate the correlations that bioavailable OM (which is associated with OM stabilisation and functional complexity) and microorganisms have with OM mineralisation in either the topsoil or subsoil, to reveal the key regulator(s) controlling the response of OM mineralisation to these amendments within the soil profile.

1.3 Thesis outline

This thesis comprises six chapters in total. Chapters 1 and 2 are the general introduction and literature review, respectively. Chapters 3 to 5 are research chapters, which have been accepted, submitted, or are to be submitted as journal articles. As these standalone chapters were written according to the requirements of different journals, the structure of each chapter may differ slightly, and overlap and repetition between some sections occurs.

Chapter 1 (this chapter) gives a general introduction to the entire thesis, including the background, research hypotheses and objectives, and outline of this dissertation.

Chapter 2 composes a review of (i) soil OM and its importance in climate change and food security; (ii) soil OC storage, which has high spatial and vertical heterogeneity; (iii) soil OM preservation, considering inherent "chemical recalcitrance", physical and chemical protection and microbial metabolism; (iv) the effect of land use management practices (e.g., lime and P amendments) on soil OM preservation, including the effects on C inputs, OM stabilisation and OM mineralisation; and (v) research gaps.

Chapter 3 covers changes in the quantity and quality of the WEOM in the Andosol under study and its heavy fraction (>1.6 g/cm^3, indicative of the OM-mineral association) with lime and/or P addition. The results show that phosphate and lime caused OM destabilisation through different mechanisms, and there was a synergetic effect of combined lime and P.

Chapter 4 presents the results of quantitative analyses of OM mineralisation and OM fractions in the bulk soil, and the nano-scale secondary ion mass spectrometry (NanoSIMS) analysis of OM-mineral associations in microaggregates in the topsoil and subsoil of the Andosol incubated with/without inorganic amendments (either lime, phosphate or lime+phosphate) in the presence or absence of an organic amendment (^{13}C- and ^{15}N-labelled barley, *Hordeum vulgare* L.) for 6 months. The results provide nano-scale evidence that adding lime inhibits the formation of OM-mineral associations in the topsoil but favours it in the subsoil, but the latter does not occur to the extent to mitigate positive priming of OM mineralisation at depth.

Chapter 5 reports the results of microbial community composition analyses and structural equation modelling (to explore the interplays between microorganisms and OM turnover) of the topsoil and subsoil samples incubated for 6 months, as described above. These results provide evidence of the different effects these amendments have on microbial properties as soil depth increases. Microbial properties showed a significant correlation with OM mineralisation in the topsoil, but not in the subsoil, which was dependent on labile OM.

Chapter 6 includes a general summary of the whole thesis, the importance of the findings for agricultural systems and recommendations for future research.

CHAPTER 2

LITERATURE REVIEW

2.1 An overview of soil organic matter (OM)

The traditional model for soil OM describes it as plant litter being decomposed into a variety of organic molecules that then recombine into "humic substances". This model is being questioned, as modern analytical techniques have not been able to identify "humic substances" (Lehmann and Kleber, 2015). A new model (the soil continuum model) suggests that soil OM is, in fact, a continuum of decomposing organic compounds derived from plant inputs (e.g., leaf litter, roots and root exudates) and soil organisms (e.g., the biomass and necromass of animals and microorganisms) (Cotrufo et al., 2015; Lefèvre et al., 2017) to smaller, more oxidised and water-soluble molecules (Lehmann and Kleber, 2015).

Soil OM has received growing interest in these past years, owing to its critical role in food security, climate change mitigation (through its influence on the carbon (C) cycling) and other ecosystem functions. Maintaining or increasing soil OM storage has been promoted as a way to contribute to the 17 Sustainable Development Goals (SDGs) of the 2030 Agenda for Sustainable Development. For instance, soil OM has the potential to (i) maintain or improve soil productivity (SDG 2 "Zero Hunger" and SDG 3 "Good Health and Well Being"), (ii) store and supply cleaner water (SDG 3 and SDG 6 "Clean Water and Sanitation"), (iii) maintain biodiversity (SDG 15 "Life on Land") and (iv) increase ecosystem resilience in a changing climate (SDG 13 "Climate Action") (Lefevre et al., 2017).

2.1.1 Soil OM: its important role in climate change

It is well established that changes in the atmospheric abundance of greenhouse gases, such

as carbon dioxide (CO_2), methane and nitrous oxide, have an influence on the energy balance of the Earth. Carbon dioxide is the most abundant C-based gas in the atmosphere. The atmospheric CO_2 concentration has fluctuated between 180 and 290 parts per million (ppm) over the last 2.1 million years prior to the Industrial Era (Hönisch et al., 2009). However, industrialisation has caused an increase in atmospheric CO_2 concentration, which has now reached a peak of ca. 417 ppm (as measured in May 2020 at Mauna Loa; NOAA, 2020) and is over 40% higher than pre-industrialisation levels. This increase is attributed not only to fossil fuel combustion and cement production, but also to land use change and management (which accounts for 25% of the anthropogenic atmospheric CO_2 emissions) (Hutchinson et al., 2007; Pachauri et al., 2014).

Soil OM constitutes the largest terrestrial C pool, storing an estimated 1,500–2,400 Pg C (1 Pg=10^{15} g). It contains more C than the world's vegetation (450–650 Pg C) and atmosphere (819–839 Pg C) combined (Figure 2.1) (Chen et al., 2014; Flato et al., 2013). Therefore, increasing soil OC stocks could be a feasible strategy for removing C (between 0.79 and 1.54 Pg C yr^{-1}) from the atmosphere, thus mitigating climate change (Fuss et al., 2018; Shukla et al., 2019). For this reason, soil OM preservation has gained increasing attention in these recent years (Amelung et al., 2020; Paustian et al., 2016; Rumpel et al., 2018).

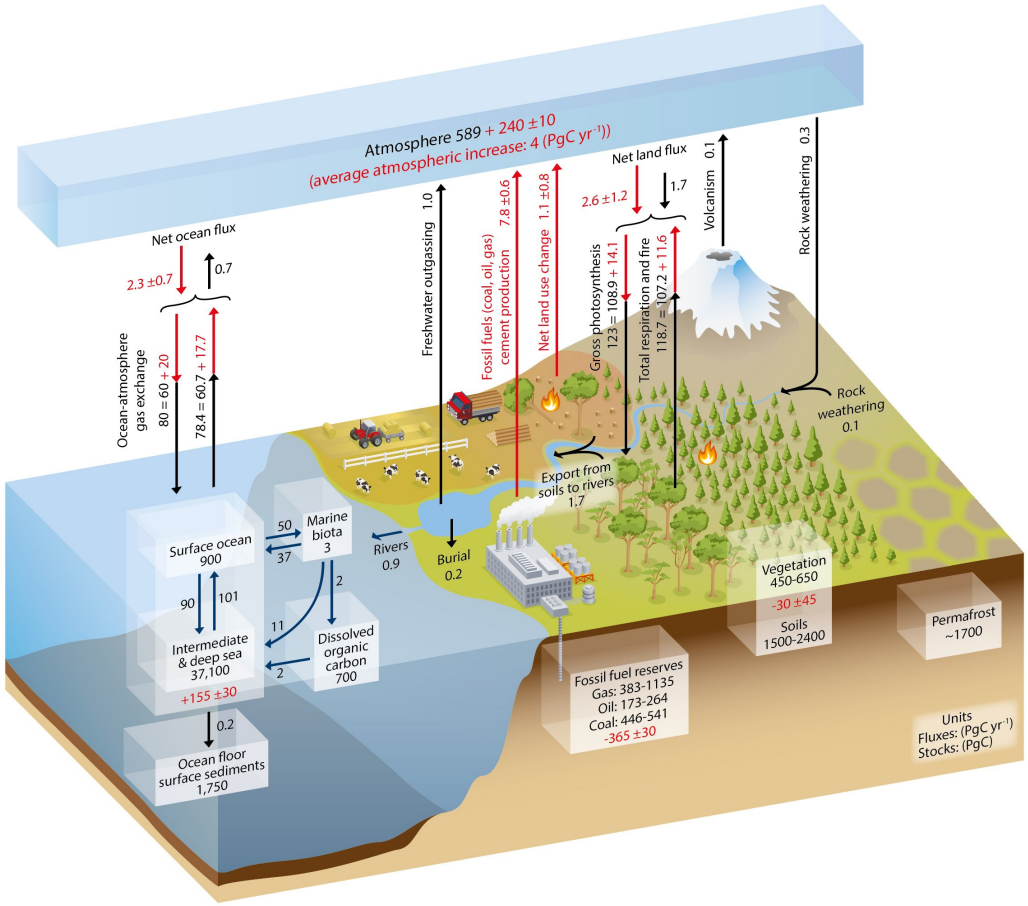

Figure 2.1 Simplified schematic of the global carbon (C) cycle. Source: IPCC AR5 report, Working Group 1, Chapter 6.

Three recent high-level initiatives focused on climate change have been created, including (i) the "4/1000 initiative" (launched at the 21st Conference of Parties of the United Nations Framework Convention on Climate Change under the framework of the Lima–Paris Action Plan in Paris in 2015), (ii) the Koronivia workshops on agriculture (initiated at the 23rd Conference of Parties in 2018), and (iii) RECSOIL, a program for the re-carbonisation of soils (launched by the Food and Agriculture Organisation of the United Nations in 2019). These initiatives consistently highlight that increasing soil OM sequestration can partly mitigate C emissions and improve the adaptation of soils (and agricultural systems) to

climate change. The latter is attributed to the improvement in soil quality (e.g., soil structure, as well as water and nutrient conditions) with increasing OM content (Lefèvre et al., 2017). These benefits are also crucial to sustaining agricultural productivity.

2.1.2 Soil OM: its important role in food security

The number of people suffering from hunger globally has kept increasing since 2014 and is expected to reach 840 million (or 9.8% of the world's population) by 2030. The number could be higher as a result of the COVID-19 pandemic. A recent preliminary assessment suggests that the pandemic may add 83–132 million people to the total number of undernourished people in the world in 2020 (FAO, 2020).

Soil OM preservation is a strategy to contribute towards food security. Soil OM is a primary indicator of soil health (Bünemann et al., 2018). As a source of nutrients for plant growth, soil OM generally contributes to the inherent fertility of soils (Lal, 2004; Tiessen et al., 1994). Soil OM promotes the aggregation and stability of the soil′s physical structure, which is important for root growth, soil aeration, retention of water and nutrients, and reducing soil erosion (Carter, 2002; Lefèvre et al., 2017). Soil OM also plays a pivotal role in immobilising contaminants (e.g., heavy metal and organic toxins) (Lamichhane et al., 2016). For instance, some heavy metals can be chemically adsorbed by OM (particularly by large molecular OM complexes) or physically occluded in soil aggregates favoured by the OM (Diagboya et al., 2015; Hou et al., 2020). The benefits provided by OM also favour soil biota growth (e.g., bacteria, fungi, protozoa, worms, other invertebrates and mammals) and thus improve soil biodiversity and function (Bardgett and Van Der Putten, 2014; Delgado-Baquerizo et al., 2020). Numerous studies have reported that an increase in soil

OM content causes (i) an increase in crop yields, especially where OM was originally low (Ghaley et al., 2018; Lal, 2004, 2020), and (ii) better resilience of agronomic systems (Chen et al., 2018). Therefore, maintenance of or even increases in soil OM content through the sustainable management of soils should contribute to food security.

2.2 Soil organic C (OC) storage

Soil OC storage is determined by the long-term difference between C inputs and outputs (Sollins et al., 1996). Across the globe, soil OC storage displays high spatial (shown in Figure 2.2) and vertical heterogeneity, which is controlled by variable environmental and or biogeochemical conditions (Batjes, 2016; Gomes et al., 2019; Weissert et al., 2016).

2.2.1 Spatial heterogeneity of soil OC

Soil OC accumulation differs between and within soil orders/groups, and this is associated with soil forming factors, including human activities (Kögel-Knabner and Amelung, 2021). Generally, high OC stocks are found in (i) soils in wetlands and peatlands, particularly located in permafrost and in the tropics, due to specific environmental conditions (either too cold and/or too wet) that impair biological activity and thus slow soil OM decomposition (Gougoulias et al., 2014; Köchy et al., 2015); and (ii) soils derived from specific parent materials, such as Andosols (most commonly formed from volcanic materials) and Vertisols (formed in confined areas where the formation of montmorillonite clay is favoured), mainly attributed to physicochemical protection and, in some instances, its burial in the subsoil when colluvial deposits are favoured (Kögel-Knabner and Amelung, 2021). As the mineral soil group with the greatest OC content worldwide, Andosols usually contain relatively up to 8–12% OC (McDaniel et al., 2012). They cover only ca. 0.8% of

the world's ice-free surface (McDaniel et al., 2012), but disproportionately sequester upwards of 1.8% of the total global soil C stocks to a depth of 1 m (Hillel and Rosenzweig, 2009; Matus et al., 2014; Takahashi and Dahlgren, 2016). Thus, they play an important role in contributing to soil C stocks (with ca. 19.07 kg OC/m^2 in the 1 m depth, shown in Table 2.1). Please note that the term 'Andosol' from the World Reference Base Classification system (WRB, 2015), will be used for this type of soil in this thesis, where possible. The other term used for the same soil in the literature are 'Allophanic soil' from the New Zealand classification system (Hewitt and Shepherd, 1997).

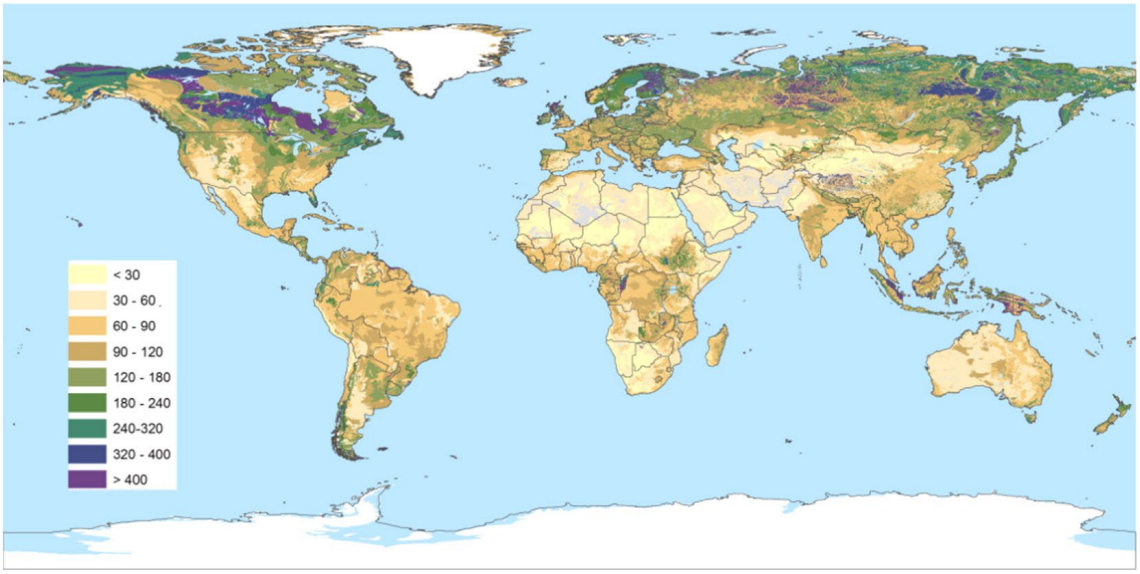

Figure 2.2 Map of soil organic carbon (OC) content to 1 m depth (Mg C/ha). From Batjes, 2016

Table 2.1 Area and organic carbon (OC) stocks of the world's soils and deep soil ^{14}C activity. Data from IUSS Working Group WRB (2015), Duarte-Guardia et al. (2019) and Mathieu et al., (2015).

Soil order	Land area M ha	OC stocks in 1 m depth kg 10^{12}	Mean OC stock kg OC/m^2 and 1 m	Deep soil $\delta^{14}C$ (‰)
Podzols	485	114.41	23.59	-1
Cambisols	1,500	346.36	23.09	-28
Andosols	**110**	**20.98**	**19.07**	**-539**
Cryosols	1,800	283.14	15.73	-
Phaeozems	190	24.13	12.7	-
Acrisols	1,000	115.8	11.58	-
Ferralsols	750	84.3	11.12	-190
Lixisols	435	37.32	8.58	-
Kastanozems	465	39.2	8.43	-
Chernozems	230	18.72	8.14	-281
Luvisols	550	42.52	7.73	-175
Vertisols	335	21.11	7.56	-330

2.2.2 Vertical heterogeneity of soil OC

Soil OC stocks decreases with depth, further contributing to distribution heterogeneity (Gomes et al., 2019; Marinho et al., 2017; Mora et al., 2014). Surface horizons always contain the highest amount of soil OM because it is the layer that receives the greatest C inputs (from roots and also from aboveground decomposing detritus). Many studies have focused on OM turnover at this horizon (Rumpel and Kögel-Knabner, 2010). Although subsoil horizons (below 30 cm) have lower OM content than surface horizons, they account for more than half of the total soil OC stocks (Rumpel and Kögel-Knabner, 2010; Tarnocai et al., 2009). In addition, subsoil OC shows a higher radiocarbon age (generally >1,000

years, particularly in Andosols, Table 2.1) compared with topsoil OC, which indicates that the subsoil has a large proportion of OC, with high stability and long residence time (Rumpel and Kögel-Knabner, 2010; Trumbore, 2009). For this reason, OM stored in the subsoil might play a more important role in soil OC sequestration than OM stored in the topsoil.

2.3 Soil OM preservation

Through soil OM preservation, C originally fixed from the atmosphere via plants, then modified *ex vivo* and/or biosynthesised *in vivo* by soil biota, is retained in long-lasting pools in the soil (Lefèvre et al., 2017, Liang et al., 2017). This is controlled by many factors, such as the inherent "chemical recalcitrance" of OM, chemical and physical interactions between OM and inorganic constituents, and the various types of microbial metabolism involved in OM turnover (Kleber et al., 2015; Liang et al., 2017; Plaza et al., 2013; Stockmann et al., 2013).

2.3.1 Selective preservation of recalcitrant OM compounds

Many traditional numerical C models have assumed that the stable soil OM is made of organic detritus that has some inherent "chemical recalcitrance", which is resistant to degradation (Lutzow et al., 2006). Historically, the litter decomposition rate has been considered to be negatively related to the C/nitrogen (N) ratio, lignin content and lignin/N ratio, and positively related to N concentration (Kleber, 2010). However, there is now robust evidence that, under suitable conditions, the microbial community has the ability to decompose persistent materials more quickly than originally expected, with the exception of carbonised C. The carbonised C is rich in condensed aromatic C and can persist longer

in the soil because it is not a preferred substrate for fulfilling microbial energy needs (Lehmann and Joseph, 2015; Lehmann and Kleber, 2015). This new view of soil OM dynamics argues that OM persists in soil, not because of the intrinsic properties of the OM itself, but as a result of physical, chemical and biological mechanisms (Dungait et al., 2012; Kleber, 2010; Schmidt et al., 2011).

2.3.2 Physical and chemical protection of OM

In the current model, soil OM represents a continuum of decomposing organic compounds from biopolymers to small organic molecules, which decrease in size and become more oxidised and water-soluble as decomposition progresses (Kleber et al., 2015; Lehmann and Kleber, 2015). The resultant organic species can be protected through physical and chemical protection (Kleber et al., 2015), as shown in Figure 2.3.

Physical protection refers to the occlusion of soil OM within soil micro- and macroaggregates. This process can make organic compounds inaccessible to decomposers and, in some instances, limit oxygen availability (Keiluweit et al., 2017). The accessibility of occluded organic compounds largely depends on the specific surface area and pore properties (size, shape and distribution) of the aggregates (Dungait et al., 2012; Pulleman and Marinissen, 2004).

Soil OM can be chemically protected by interacting with mineral surfaces and metal cations to form OM-mineral associations and OM-metal complexes, respectively. The types of interactions involved include ligand exchange and polyvalent cation bridges, as well as weak interactions (e.g., van der Waals type, electrostatic attraction) (Kaiser and Guggenberger, 2003). It has been proposed that these OM-mineral/metal interactions

follow a discrete zonal sequence, similar to a "membrane-like bilayer" structure (Kleber et al., 2015; Kleber et al., 2007), as shown in Figure 2.4. The strength and stability of the bonds between OM and inorganic constituents is thought to decrease with increasing distance from the mineral surface. In the inner zone (the contact zone, Layer ① in Figure 2.4), the formation of associations between OM (particularly microbial derived N-rich OM, Possinger et al., 2020; Kopittke et al., 2020) and (OM-free) mineral surfaces occurs via strong bonding (e.g., covalent bonding). In the outer layers (Layer ② in Figure 2.4), which are further away from the surface, the interaction shifts from covalent bonds to either van der Waals type bonds between organic ligands or electrostatic binding, as cations (e.g., Ca^{2+}, Mg^{2+}, Al^{3+} and Fe^{3+}) play the role of bridges between organic ligands (Kleber et al., 2007). Despite this "membrane-like bilayer" structure being widely accepted, more direct and nanoscale evidence is needed to further support it.

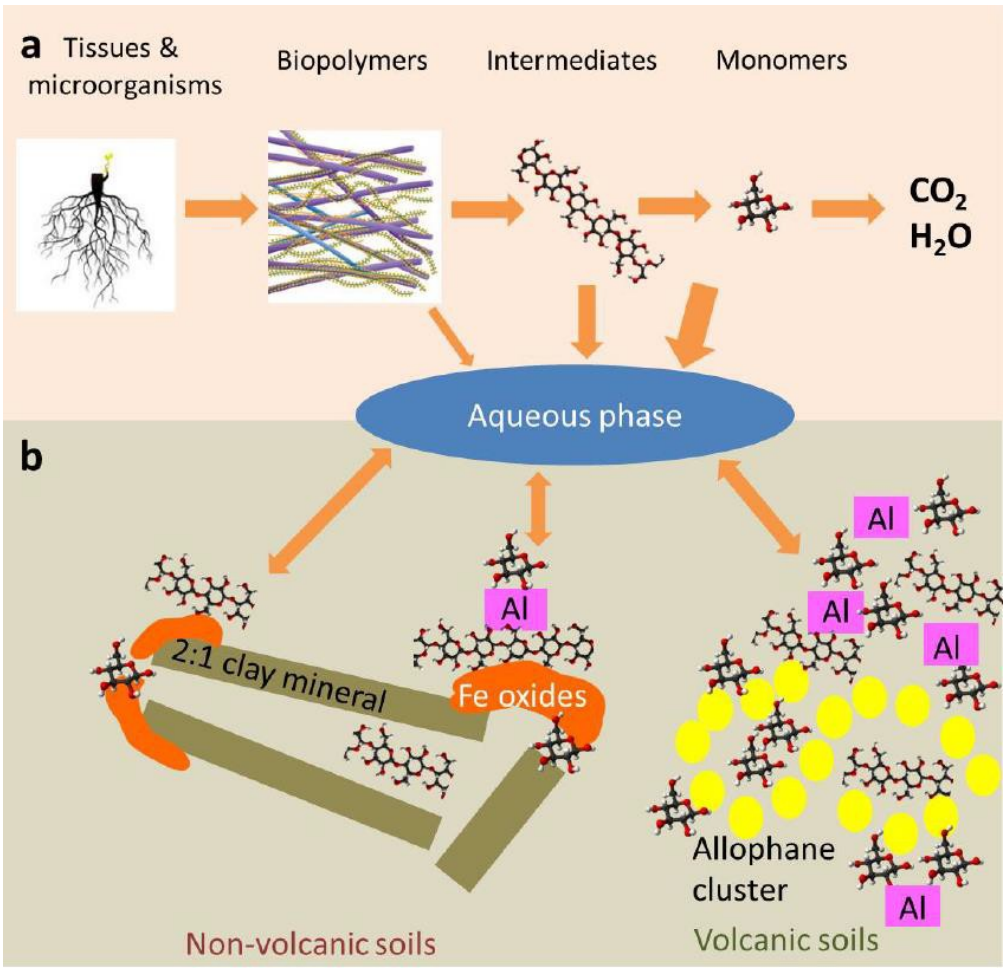

Figure 2.3 Schematic diagram of organo-mineral/metal association formation. (a) Soil continuum model view of the nature of soil organic matter. (b) Chemical and physical protection of organic ligands by a mineral or metal (e.g., aluminium, Al). These are more abundant in soils derived from volcanic materials (in the example, an Andosol, at right). Diagram courtesy of Marta Camps-Arbestain, modified from Kleber et al. (2015).

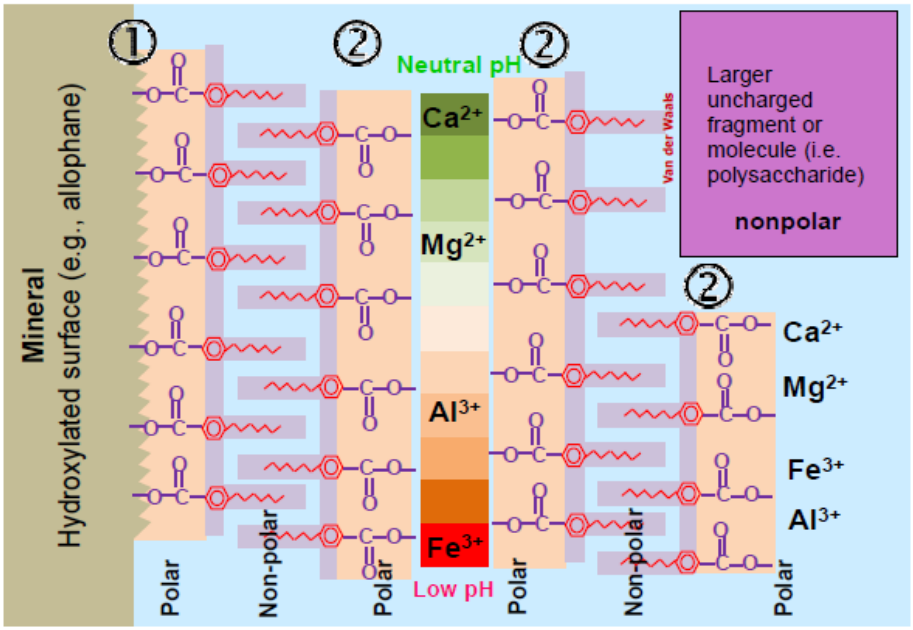

Figure 2.4 The "member-like bilayer model" of organo-mineral/metal interactions. Diagram courtesy of Marta Camps-Arbestain, adapted from Peter Buurman's course (original authorship is attributed to Markus Kleber).

2.3.3 Microbial metabolism

There is mounting evidence that soil microorganisms play an essential role in soil OM preservation, in which (i) microbial extracellular enzymes attack and break down plant litter (the dominant external C input) into smaller and more soluble plant-derived OM molecules (microbial catabolism, *ex vivo* modification); and (ii) microorganisms degrade plant-derived OM and form novel microbial-derived OM, by a cell uptake–biosynthesis–growth–death process (microbial anabolism, *in vivo* turnover) (Liang et al., 2017). During these processes, microorganisms contribute to the release of CO_2 to the atmosphere (through respiration), which is the largest single source of CO_2 from global terrestrial ecosystems (Metcalfe et al., 2011). In addition, the resultant smaller plant-derived or newly

formed microbe-derived OM molecules generally have higher potential to interact with inorganic constituents, which contributes to OM stabilisation (Kleber et al., 2015).

Organic matter preservation has been proposed to be associated with the (i) physical distance travelled by soil OC, (ii) richness and composition of microorganisms, and (iii) frequency and volume of C inputs (Sokol et al., 2018). This could also be understood on the basis of the functional complexity (e.g., molecular, spatial and temporal complexity) of OM, as recently proposed by Lehmann et al. (2020). In detail, (i) microbial-derived OM with higher complexity than plant-derived OM requires more metabolic investment, (ii) higher spatial heterogeneity of OM decreases the probability that microbes will come into contact with the organic substrates, and (iii) greater temporal complexity might weaken the ability of microorganisms to adapt to changes in their environment. As a result, the increase in functional complexity constrains OM decomposition by microorganisms (Lehmann et al., 2020).

2.4 Effect of land use management on soil OM preservation

The human population is predicted to reach 9.8 billion by the year 2050, requiring a projected increase in crop production by 2050 (increasing by 70% between 2005 and 2050) to ensure food security (ELD, 2015). The projected increase in food production is expected to be achieved by increased yields from existing agricultural land (via land-use intensification) rather than area expansion (Kopittke et al., 2019). However, current land use intensification is already unsustainable and degrading soils through several soil threats, including fertiliser over-application, acidification, salinisation, erosion, OM depletion and a decrease in biodiversity (Eze et al., 2018; Kopittke et al., 2019).

The change in the OC storage depends on an equilibrium level controlled by C inputs and outputs (these being influenced by OM stabilisation and mineralisation) and hence soil management practices. Cropping intensification has been found to reduce soil OC stocks by 30–60% (Kopittke et al., 2017). In New Zealand, the intensification of dairy pastures has led to a decline in the OC stocks of Allophanic soils by -1.37 kg OC/m^2 in the top 30 cm of the soil profile and by -0.7 kg OC/m^2 in soil at depth between 30–60 cm (Schipper et al., 2014).

2.4.1 Effect of land use management on C inputs

It is well known that agricultural amendments (e.g., lime, organic and inorganic fertiliser applications) increase crop and pasture yields, generally resulting in an increase in C inputs derived from plant tissues (e.g., shoots, reproductive organs and root biomass) and exudates. This benefits soil OM storage (Chen et al., 2018; Eze et al., 2018; Haynes and Naidu, 1998; Mathew et al., 2020). It is notable that only a very small proportion of C inputs become protected in the soil, this being dependent on the soil properties and environmental conditions (Stewart et al., 2007; Castellano et al., 2015).

2.4.2 Effect of land use management on OM stabilisation

Agricultural amendments can change the soil's physicochemical properties and inherited OM (and also a small proportion of the newly-formed OM) might become destabilised and thus be more vulnerable to (i) decomposition (causing a release of CO_2 to the atmosphere), and (ii) leaching to ground water, resulting in a rise in C outputs. This has been reported for soils that have been either limed or phosphorus (P)-fertilised (Kov et al., 2018; Miyazawa et al., 2013; Schneider et al., 2010; Shen et al., 2018).

Land use intensification can cause soil acidification through, for example, the addition of ammonium or urea fertilisers, or urea in urine patches (Hedley and Bolan, 2003). Acidification further enhances the risk of phytotoxic metal uptake by crops and an associated reduction in productivity (Zhao et al., 2015). It is thus important to apply lime to increase soil pH and offset soil acidification (Haynes, 1984).

It is notable that pH is deemed to be an important factor controlling the OM sequestration capacity of soil (Kleber et al., 2015). Low pH conditions generally favour the formation of strong inner-sphere surface complexes, whereas at neutral and alkaline pH, weaker outer-sphere complexation often dominates (Kleber et al., 2015). Moreover, when the pH increases, the competition between OH^- ions with organic ligands for active sites on the mineral surface and/or metal cations could be favoured. Thus organic ligands previously bound to the reactive surfaces can be displaced and released to the aqueous solution as dissolved organic matter (DOM), as shown in Figure 2.5 (Kleber et al., 2015; Newcomb et al., 2017; Ramesh et al., 2019). This DOM fraction is a more active OM pool and is particularly susceptible to microbial decomposition and percolation (Seifert et al., 2016; Wang et al., 2015). However, the flip side of the coin is that as soil becomes more acid, plant growth decreases; this has an impact on organic detritus returned to the soil.

Long-term land use intensification has often resulted in soils being overloaded with phosphate due to the increased use of P fertilisers. Numerous studies have demonstrated that phosphate can have a negative influence on soil OM stabilisation (Kleber et al., 2015; Luo et al., 2019; Spohn and Schleuss, 2019). Phosphate can become adsorbed on reactive Al and Fe sites through binding to Al-OH or Fe-OH sites or to metal cations through ligand exchange reactions at defective sites on the mineral surface (Harsh et al., 2002; Parfitt,

2009). The ligand exchange reactions responsible for phosphate adsorption also occur between phosphates and the reactive sites that are already associated with OM, resulting in disruption of these organo-metal/mineral complexes (Hiemstra et al., 2010; Kaiser and Zech, 1997). A study carried out by Camps-Arbestain et al. (2002) on Podzols proved that phosphate competed with organic ligands for Al, leading to an eventual disruption of OM-Al complexes. Addition of phosphate can also result in an increase in pH through the displacement of OH^- from reactive sites (Schneider et al., 2010), which further contributes to the destabilisation of OM.

The influence of liming and/or P addition on OM stabilisation is expected to be especially evident in Andosols, as (i) their management usually includes amendments of lime and P, as they have high P retention and are generally acidic (Dahlgren et al., 2004; Hedley and Bolan, 2003) and (ii) they have been proposed as an archetype of soils where reactive Al and Fe control soil OM persistence, which could be influenced by OH^- and phosphate (as mentioned above) (Possinger et al., 2020).

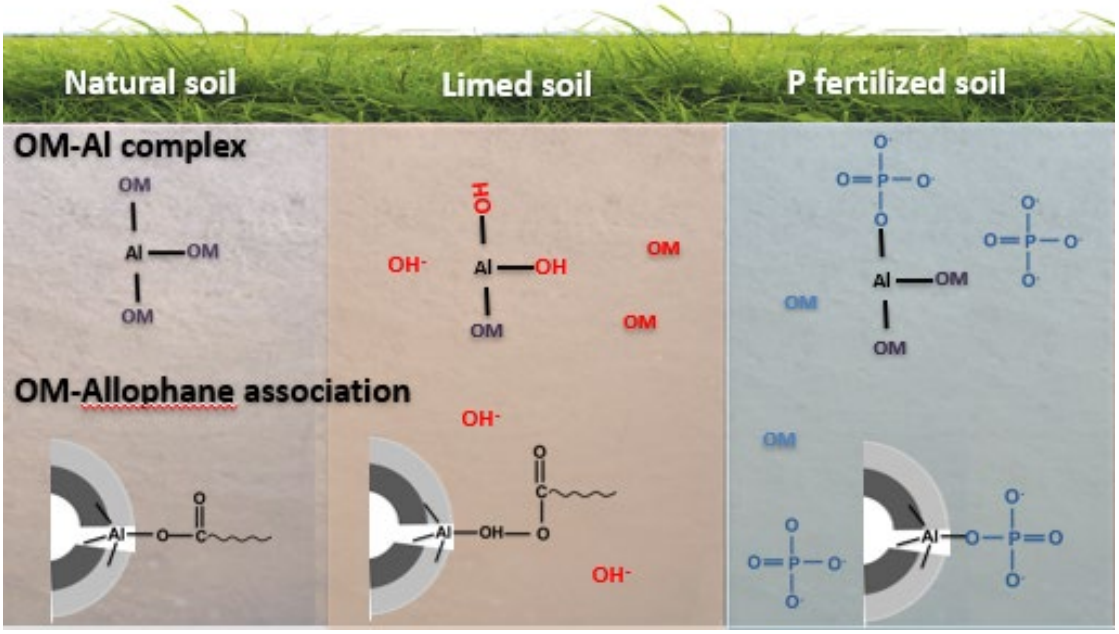

Figure 2.5 Schematic diagram of the influence of lime and phosphate on the interactions between organic matter (OM) and inorganic constituents. The increase in OH^- and phosphate loading caused by lime and phosphorus fertiliser application disrupts OM-Al complexes and OM-allophane associations, respectively. Red and blue indicate the OM being replaced by OH^- and phosphate, respectively.

2.4.3 Effect of land use management on OM mineralisation

The mineralisation of OM is basically controlled by two subsequent processes: (i) abiological processes through which non-bioavailable OM becomes bioavailable to microorganisms (termed the Regulatory Gate hypothesis) and (ii) the subsequent biological mineralisation of OM (Kemmitt et al., 2008). The response of soil OM mineralisation to soil amendments, used as part of land management, is thus related to the changes they drive in (i) the bioavailability of OM, which is associated with OM destabilisation and its functional complexity, and (ii) microbial properties, which are associated with its community composition and metabolic function (Malik et al., 2020; Razanamalala et al.,

2018; Schimel et al., 2007).

Many studies have reported that lime and P fertiliser applications impact the soil's bacterial and fungal composition and their metabolic functions (Camenzind et al., 2018; Cleveland et al., 2002; Fang et al., 2019). This might be attributed to (i) the impact these amendments have on soil alkalinity and available phosphate, respectively and (ii) the amendment-driven changes in OM fractions (not only in the quantity, but also in their functional complexity) through the impact on plant growth and OM stabilisation (Ma et al., 2018; Rousk et al., 2010; Zheng et al., 2019). An increase in soil pH resulting from lime application to acid soils causes an increase in the bacteria/fungi ratio, along with an increase in OM mineralisation (Silva-Sánchez et al., 2019). A significant correlation has also been found between changes in DOM (as covariance of soil alkalisation) and shifts in the bacterial and archaeal community composition (Zheng et al., 2019). The increase in phosphate in P-limited soil has been found to influence the microbial community composition, causing a drop in the abundance of some specific microbial groups i.e., those able to produce the exudates for mining P through mineralising OM (Fang et al., 2019; Zheng et al., 2015). The increase in DOM upon addition of P fertiliser causes an increase in OM mineralisation (Fisk et al., 2015; Spohn and Schleuss, 2019). The influence of amendment-driven abiotic and microbial changes in soil properties that influence OM mineralisation could differ within the profile, as a result of the differences in physicochemical and microbial properties as soil depth increases (Chen et al., 2016).

2.5 Conclusions and research gaps

To achieve climate- and food-smart agricultural management, it is necessary to have an in-depth understanding of the effects of lime and P application on soil OM preservation, particularly in the case of OM-rich Andosols. This literature review highlights that special attention should be paid to the current research gaps listed below:

- Despite the growing body of research on the influence of either lime or P application to soil, the combined effect of lime and P fertiliser applications on soil OM stabilisation remains unclear, with little direct evidence of how, by impacting DOM (quality and quantity), lime and/or P addition impairs the preservation of soil OM (e.g., particulate OM fraction and OM-mineral association).

- Although extensive research efforts have been made to investigate the effects of lime and P addition on the OM stabilisation in topsoil, less is known about the changes occurring in (i) OM-mineral associations at the micro-scale, and (ii) the functional complexity of soil OM, which are critical for understanding the mechanisms of OM preservation in soil.

- Compared with the effect of lime and/or P addition on the OM stabilisation in the soil (through physical and chemical protection), the effect on the interplay between soil microorganisms (bacteria and fungi) and OM turnover (i.e., how the changes in OM influence soil microorganisms and, in turn, how the shifts in microorganisms affect soil OM mineralisation) has received less attention.

- Compared with topsoil horizons, there is a shortage of research on the effect of lime

and/or P amendments on OM turnover in subsoil horizons. These have a distinct biogeochemistry, which may play an important role in OM preservation, as the subsoil contains a large proportion of OM with high stability and long residence time, and accounts for more than half of the total soil OC stocks.

CHAPTER 3

LIME AND/OR PHOSPHATE APPLICATION AFFECTS THE STABILITY OF SOIL ORGANIC CARBON: EVIDENCE FROM CHANGES IN QUANTITY AND CHEMISTRY OF THE SOIL WATER-EXTRACTABLE ORGANIC MATTER

Abstract

The mechanisms by which lime and/or phosphate addition impacts the preservation of soil organic matter (OM) are poorly understood. We explored the changes in quantity and chemistry of water-extractable organic matter (WEOM) in the bulk soil and its heavy density fraction (>1.6 g/cm^3) of an unmanaged C-rich volcanic soil caused by lime and/or phosphate application. The addition of lime or phosphate caused (i) a significant increase in the WEOM, along with a decrease in its C/N ratio and an increase in its aromaticity, and (ii) changes in the WEOM chemical composition, measured with pyrolysis-gas chromatography/mass spectrometry, this being most impacted by lime application. The combined effect of lime and phosphate addition on the quantity and chemistry of WEOM was larger than the effects of separate lime and phosphate additions. By comparing the response of the bulk soil and the heavy fraction, we infer that phosphate has a greater contribution to the destabilisation of vulnerable particulate OM, while lime causes a comparable disruption in both the particulate OM and the OM in heavy fraction. These findings provide a mechanistic insight into the decreased OM stability after liming and/or P fertilising Andosols. They have implications for the design of climate-smart management practices for these soils.

3.1 Introduction

Soil organic matter (OM) constitutes the largest terrestrial carbon (C) pool and contains more C than the world's vegetation and atmosphere combined (Chen et al., 2014; Flato et al., 2013). For this reason, even small changes in the balance between the input to and output from the soil organic C pool can significantly influence the global C cycling and, in particular, the carbon dioxide (CO_2) concentration in the atmosphere. Thereby, soil OM plays a fundamental role in climate change mitigation. If we are to limit global warming <2 °C compared with pre-industrial levels (Minasny et al., 2017), a better understanding of soil organic C turnover and the factors influencing it is needed.

Andosols play an important role in soil C sequestration as they are the mineral soils with the greatest C concentration worldwide – they cover only ca. 0.8% of the world's ice-free surface but store ca. 1.8% of total global soil C (Matus et al., 2014; McDaniel et al., 2012; Takahashi and Dahlgren, 2016; WRB, 2015). The abundance of short-range order constituents (allophane, imogolite and ferrihydrite) and/or OM-aluminium (Al) complexes in Andosols give these soils unique physicochemical properties, such as low bulk density, stable aggregation, and highly variable charge, which benefit the preservation of organic C in soil, but also cause a high phosphorus (P) retention (Dahlgren et al., 2004). Under humid temperate climate, most Andosols are acidic with conditions being aggravated by the addition of fertilisers (e.g., ammonium-nitrogen (N) forms) and/or under legume swards (Hedley and Bolan, 2003). Thus, management of these soils often includes the application of lime and P fertilisers to overcome the risk of Al toxicity to sensitive plant roots and P deficiency in crops.

Numerous studies have reported that increasing soil pH by the application of alkaline amendments (e.g., lime application) weakens the formation of stronger inner-sphere surface bonding between reactive Al/iron (Fe) (hydr)oxides and organic ligands, with weaker outer-sphere bonding becoming more prevalent (Das and Mahiuddin, 2007; Greiner et al., 2014; Kang et al., 2008; Kleber et al., 2015; Ramesh et al., 2019). The increase in phosphate concentration in soil solution resulting from the application of P fertilisers can also impair OM preservation (Luo et al., 2019), as phosphate competes with organic ligands for reactive sites of (hydr)oxides and metal cations more efficiently (Hiemstra et al., 2010; Kaiser and Zech, 1997; Spohn and Schleuss, 2019). Through the increases in the concentration of OH^- and/or phosphate, organic ligands previously bound to these reactive surfaces can be displaced and released to the aqueous solution, as dissolved organic matter (DOM). This DOM fraction plays an important role in soil C turnover, in particular by being susceptible to microbial decomposition and percolation (Seifert et al., 2016; Wang et al., 2015). Thereby the increases in DOM caused by specific management practices tend to indicate OM destabilisation (Chantigny, 2003; Kaiser and Guggenberger, 2000). Besides the increases in the concentration of DOM (Kaiser and Guggenberger, 2000; Curtin et al., 2016), lime or P application also changes the chemistry of the DOM. Namely, there is (i) an increase in hydrophilic DOM relative to hydrophobic DOM (Kaiser and Guggenberger, 2000); and (ii) an increase in C aromaticity (Curtin et al., 2016; Li et al., 2018; Scott and Rothstein, 2014). These findings have contributed to a more fundamental understanding of the loss of OM from soils, such that observed in Andosols under pasture in New Zealand over time (Schipper et al., 2007). Yet the combined effect of lime and P fertiliser applications on DOM and its composition still remains largely

unclear. Also, there is little direct evidence of how, by impacting DOM, lime and/or P additions impairs the preservation of soil OM. This knowledge is needed to get an in-depth understanding of the mechanisms that counteract soil OM preservation so that practical recommendations can be provided to farmers to ensure the preservation of organic C stocks in these organic C-rich soils.

In this study – using conventional wet chemical methods and pyrolysis-gas chromatography/mass spectrometry (Py-GC/MS) – we explored the changes in quantity and quality (chemical composition) of WEOM in a sil-andic Andosol (under unmanaged forest) from New Zealand upon the application of different rates of lime and/or P, assuming business-as-usual practices. The heavy fraction of the soil obtained after density fractionation was studied with the aim of obtaining a clearer understanding of the effects of these amendments on OM-mineral associations. We explored the hypotheses that (i) lime and P influence quality and quantity of the WEOM through different mechanisms; and that (ii) the combined effect of P and lime on WEOM is stronger than that of either P or lime addition alone.

3.2 Materials and methods

3.2.1 Soil sampling and characterisation

The top 15 cm of an Andosol under an unmanaged old pine (*Pinus radiata* L) forest stand located in Hawera, Taranaki, New Zealand (39°36'24"S 174°15'48"E) was used in this study. The soil was classified as Allophanic soil based on the New Zealand classification system and as a sil-andic Andosol based on the World Reference Base Classification system (Hewitt and Shepherd, 1997; WRB, 2015). Soil pH and the concentrations of Olsen

P, total C, total N and allophane were analysed (described in Supporting Information for Chapter 3, SI3) and shown in Table S3.1.

3.2.2 Soil density fractionation

The heavy fraction (>1.6 g/cm^3) of the soil was obtained by removing the floating free particulate organic matter (fPOM) fraction, following the methods described by Wagai et al. (2015), working with Andosols. In short, the 1.6 g/cm^3 sodium polytungstate solution was mixed with bulk soil, and the mixture shaken for 30 min. The floating material was collected after centrifugation and filtration. The procedure was repeated three times to maximise the removal of fPOM. Thereafter, both density fractions were separately washed by deionised water until the electrical conductivity was <50 µS/cm, then freeze dried and weighed. Total C and N contents in these fractions were measured (Table S3.2). The heavy fraction was used for further extractions.

3.2.3 Extractions

Batch extractions (5 g soil sample with 25 mL of extractant) were conducted (Figure S3.1) to study the individual and combined effects of lime and P application on WEOM of soils. There were 2 controls and 3 groups of treatments.

For the bulk soil, the first control involved extraction with 10 mM KCl (background electrolyte) as a negative control (Ctr-). The second control group was extracted with a solution containing 10 mM KCl and $CaCl_2$ (at concentrations ranging from 0.02 to 0.08 mol Ca^{2+}/kg). The concentrations used were equivalent to the Ca^{2+} concentrations in the $CaCO_3$ amendments (described below) in order to distinguish the effect of the alkalinity

added with $CaCO_3$ from that of Ca^{2+}. Soil extracted with 0.02 mol/kg $CaCl_2$ solution was chosen as the positive control (Ctr+), as there were no significant differences detected in water-extractable organic C (WEOC) at $CaCl_2$ concentrations ranging between 0.02 and 0.08 g/kg (Figure S3.2).

One group was amended with P alone. They were extracted with a solution containing 10 mM KCl and KH_2PO_4 (at concentrations of 0.1, 0.2, 0.3 and 0.4 g P/kg, simulating business-as-usual fertiliser practices (Dairy, 2012) and labelled as P0.1, P0.2, P0.3 and P0.4). The soil in the second treatment group was mixed with $CaCO_3$ at application rates of 2, 4, 6 and 8 g/kg (equivalent to 0.02, 0.04, 0.06, and 0.08 mol/kg, as well as 2.4, 4.8, 7.2 and 9.6 t/ha), and subsequently extracted with a 10 mM KCl solution, to model soil treated with lime alone (L2, L4, L6 and L8). Another group was mixed with $CaCO_3$ (at either moderate or large application rates, 4 or 8 g/kg), and subsequently extracted with a solution containing KCl and KH_2PO_4 (at either moderate or large application rates, 0.2 or 0.4 g P/kg), to model combined amendments of lime and P (L4P0.2, L4P0.4, L8P0.2 and L8P0.4). The heavy fraction was only extracted with moderate and large rates of lime (4 and 8 g/kg) and/or P (0.2 and 0.4 g P/kg), following the procedure described above. The extractions were performed on an end-over-end shaker for 24 hours at room temperature (Gu et al., 1994; Kaiser and Guggenberger, 2000). After extraction, the soil suspensions were centrifuged for 10 min at 8,000 g. The water-extractable fraction was collected after the supernatant was passed through a filter paper (Whatman No 42) (Jones and Willett, 2006).

3.2.4 Characterisation of the water-extractable fraction

The pH values of the extracts were measured. The WEOC and water-extractable nitrogen were determined using a Total Organic Carbon Analyser (TOC-LCSH, Shimadzu, Japan). The mineral nitrogen (NH_4^+ and NO_3^-) contents of the extracts were determined on a Technicon autoanalyser. The water-extractable organic N (WEON) was calculated by subtracting mineral N from water-extractable N. The UV absorbance at 254 nm (UV_{254}) of each extract was measured on a UV/Visible scanning spectrophotometer (Jenway 7315, UK) to estimate the content of conjugated unsaturated C (assumed to be mainly aromatic C) (Weishaar et al., 2003). The aromaticity of WEOM in the treated samples relative to that of the Ctr- was calculated as follows: Relative Aromaticity $\%=UV_{254(Amendment)}\times 100/UV_{254(Ctr-)}$. Specific UV absorbance at 254 nm (SUVA) was also calculated (Table S3.3) (Weishaar et al., 2003). The chemical composition of WEOM was characterised by Py-GC/MS. An aliquot of the freeze-dried extracts (1–2 mg) were pyrolysed using a Multi-Shot Pyrolyser (EGA/PY-3030D, Frontier Lab, Japan), connected to a GC/MS unit (GCMS QP2010 Ultra, Shimadzu, Japan). We used GCMS solution software (Shimadzu) for qualitative and semi-quantitative analyses, and the data were composed of the relative area of each pyrolysis product (% total quantified peak area, TQPA). More details are provided in the section S3.1.2 in SI3.

3.2.5 Data analysis

One-way ANOVA with a Tukey B test was used to evaluate the statistical difference ($P<0.05$) in means of different treatments by SPSS software (IBM SPSS Statistics Version 24). Principal component analysis (PCA) of pyrolysis products (either 76 compounds of

bulk soils or 119 compounds of heavy fraction samples) was performed by SPSS.

3.3 Results

3.3.1 Influence of individual amendments on the concentration of WEOM in bulk soil

The bulk soil that received lime addition had significantly greater WEOC ($P<0.05$) – ranging from 455.7 to 622.1 mg/kg – than the Ctr- (413.4 mg/kg) and Ctr+ (291.9 mg/kg) treatments (Figure 3.1a). Changes in WEOC were positively related to changes in soil pH ($r=0.98$, $P<0.01$) (Figure S3.3a). As lime application rates increased, there was an increase in the aromaticity of WEOM fraction as determined by the specific UV absorbance (Figures 3.2b and S3.4a), and this was later supported by the Py-GC/MS measurement (Figure S3.5), and a decrease in the C/N ratio (Figure 3.2c). Similar trends in the correlation between P addition and WEOC concentration ($r=0.96$, $P<0.01$) (Figures 3.1b and S3.3b), aromaticity, or C/N ratio of the WEOM were observed (Figure 3.2b-c).

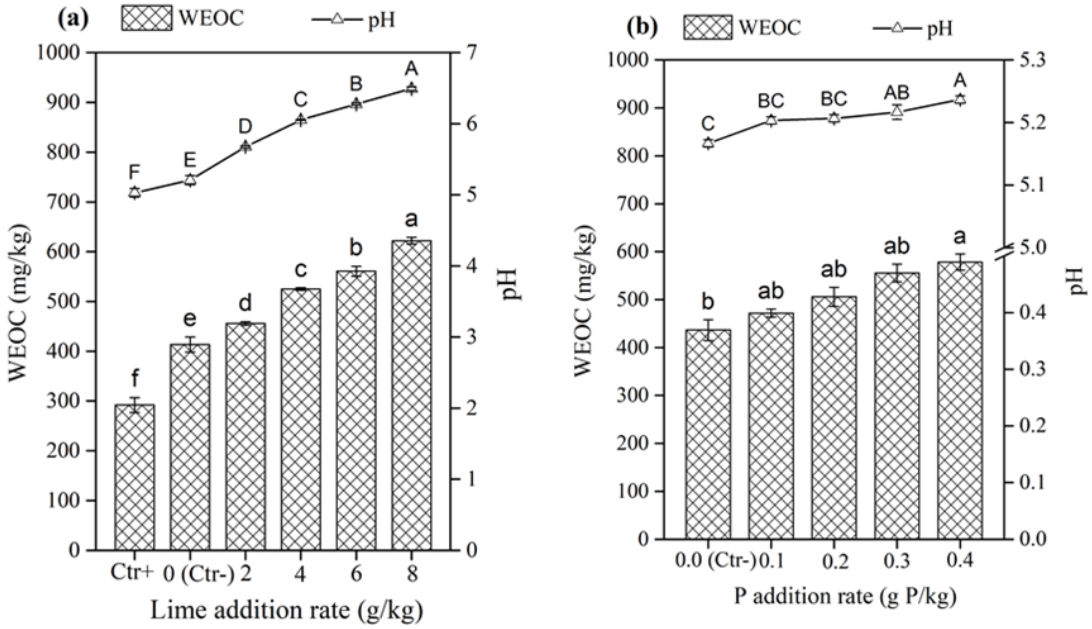

Figure 3.1 The water-extractable organic carbon (WEOC) concentration and pH of unamended (Ctr-) and amended bulk soils with (a) $CaCl_2$ (Ctr+) and lime additions, as well as (b) P additions. Graph bars and symbols marked with different letters on top represent statistically significant results (P<0.05) based on a one-way ANOVA followed by Tukey B test (n=3).

3.3.2 Influence of combined amendments on the concentration of WEOM in bulk soil

At a constant P addition rate, there was a significant increase (P<0.05) in WEOC at increasing rates of lime addition, e.g., P0.2 < L4P0.2 < L8P0.2; P0.4 < L4P0.4 < L8P0.4 (Figure 3.2a). Similar trends were also found with increasing rates of P addition at a constant lime application rate (following L4 < L4P0.2 < L4P0.4; L8 < L8P0.2 < L8P0.4). The aromaticity of the WEOM tended to increase with the combined amendments compared with the corresponding individual amendments (Figure 3.2b), while changes in the C/N ratio of WEOM were smaller (or non-existent) than those observed when amendments were applied separately (Figure 3.2c).

The effect of combined P and lime additions on WEOC concentration (increasing by 43.9–84.1% compared with Ctr-) was stronger than the sum of effects of the separate addition of P and lime (increasing by 39.0–75.5% compared to Ctr-). Likewise, the increase in aromaticity ranged between 112.1% and 134.4% with combined additions of P and lime, whereas the sum of effects of the separate addition of P and lime ranged between 61.4% and 119.5%.

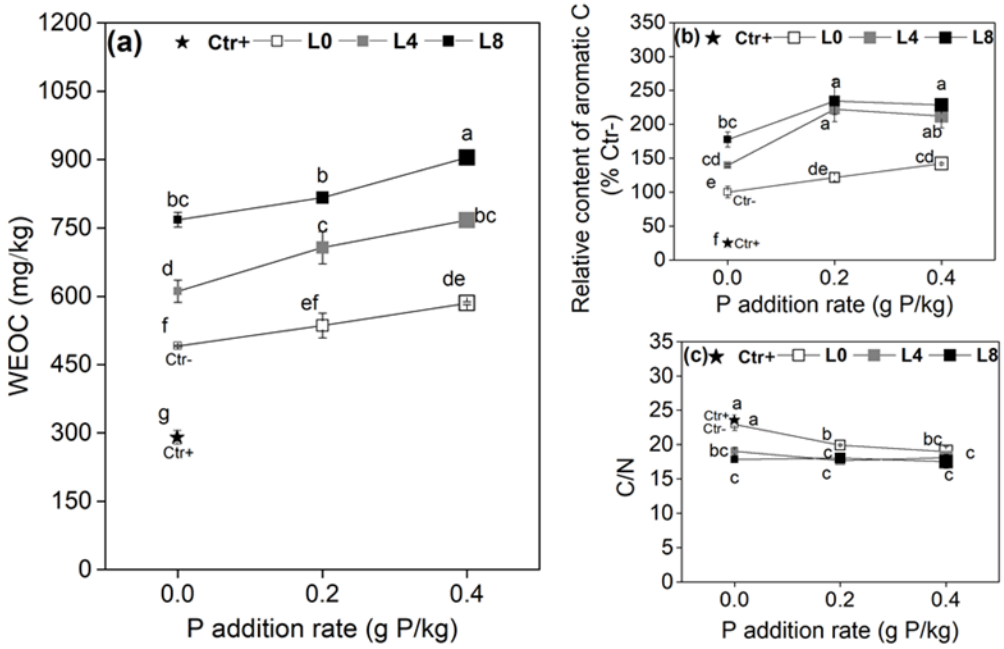

Figure 3.2 The (a) water-extractable organic carbon (WEOC) concentration, (b) relative content of aromatic carbon (C) and (c) C/nitrogen (N) ratio of water-extractable organic matter (WEOM) of controls and amended bulk soils with lime (at addition rates of 4 and 8 g/kg, L4 and L8) and/or P (at addition rates of 0.2 and 0.4 g P/kg). The negative control (Ctr-) was the unamended bulk soil, while the positive control was the amended bulk soil with $CaCl_2$ (Ctr+). Graph symbols marked with different letters represent statistically significant results (P<0.05) based on a one-way ANOVA followed by Tukey B test (n=3).

3.3.3 Influence of individual amendments on the concentration of WEOM in the heavy fraction

Increasing lime application rates up to 8 g/kg raised the pH of the heavy fraction from 5.1 to 6.3, and the WEOC concentration from 343.9 to 539.3 mg/kg (Figure 3.3a), along with an increase in aromaticity (2–2.6-fold increment) and a drop in the C/N ratio of the WEOM (decreasing from 19.9 to 16.8; Figure 3.4b-c). As with the bulk soil, the Ctr+ treatment had an opposite effect to that of lime at increasing Ca^{2+} concentration (e.g., decreased pH, WEOC, and aromaticity, and caused a slight increase in the C/N ratio). There was a strong positive linear correlation between WEOC and pH (r=0.98, P<0.01; Figure S3.3c). Individual P amendments did not significantly influence WEOC of the heavy fraction.

3.3.4 Influence of combined amendments on the concentration of WEOM in the heavy fraction

At a constant P addition rate, WEOC concentrations increased at increasing lime additions (P0.2 < L4P0.2 < L8P0.2; P0.4 < L4P0.4 < L8P0.4), while WEOC concentrations at increasing P additions were, in general, similar between treatments with a constant lime rate (Figure 3.4a). In contrast, for the aromaticity of WEOM, prominent positive effects of P were found by comparing the combined amendments with identical lime addition rates (L4 < L4P0.2 < L4P0.4; L8 < L8P0.2 < L8P0.4, Figure 3.4b). These positive effects were also found at increasing lime additions, except with L8P0.4, which was not significantly different from L4P0.4. Changes in the C/N ratio of WEOM in the heavy fraction were consistent with those observed in the bulk soil. A distinct decrease in the C/N ratio was only observed in the combined L4P0.2 and L8P0.2 treatments when compared with only P

addition (e.g., P0.2 > L4P0.2 ≈ L8P0.2, P0.4 ≈ L4P0.4 ≈ L8P0.4, Figure 3.4c).

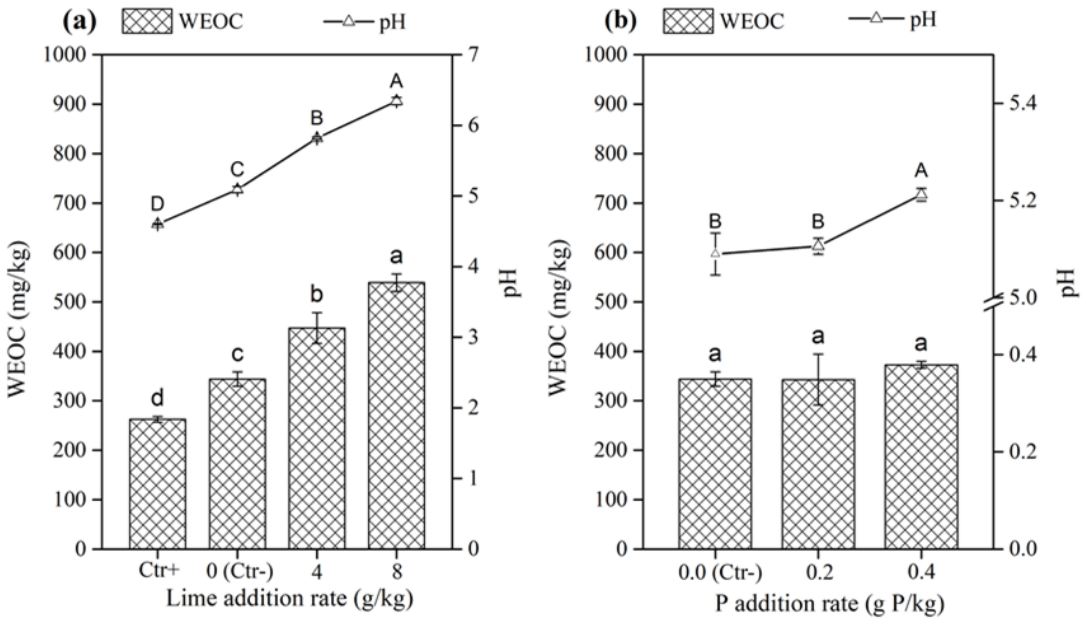

Figure 3.3 The water-extractable organic carbon (WEOC) concentration and pH of the unamended (Ctr-) and amended heavy fraction samples with (a) $CaCl_2$ (Ctr+) and lime additions, as well as (b) P additions. Graph bars and symbols marked with different letters on top represent statistically significant results (P<0.05) based on a one-way ANOVA followed by Tukey B test (n=3).

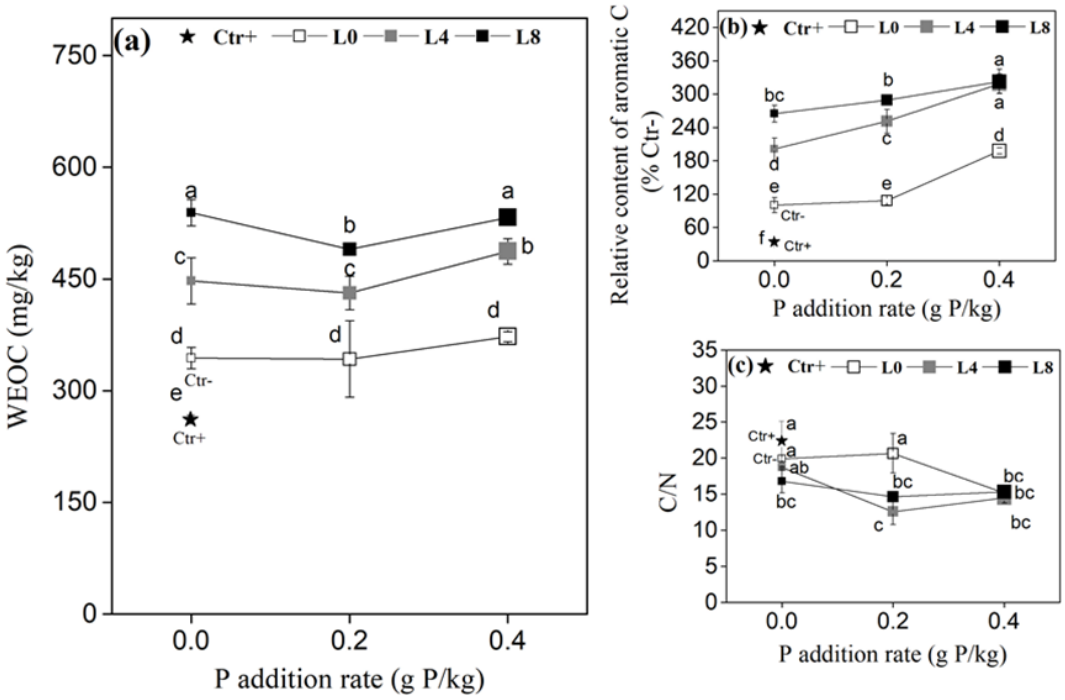

Figure 3.4 The (a) water-extractable organic carbon (WEOC) concentration, (b) relative content of aromatic carbon (C) and (c) C/nitrogen (N) ratio of water-extractable organic matter (WEOM) of controls and amended heavy fraction samples with lime (at addition rates of 4 and 8 g/kg, L4 and L8) and/or P (at addition rates of 0.2 and 0.4 g P/kg). The negative control (Ctr-) was the unamended heavy fraction, while the positive control was the amended heavy fraction with $CaCl_2$ (Ctr+). Graph symbols marked with different letters represent statistically significant results (P<0.05) based on a one-way ANOVA followed by Tukey B test (n=3).

3.3.5 Changes in WEOM chemical composition

For the Py-GC/MS analysis, a total of 129 pyrolysis products were identified (Table S3.4) and grouped as follows: polysaccharides, N-compounds, monocyclic aromatic hydrocarbons (MAHs), polycyclic aromatic hydrocarbons (PAHs), lignin, phenols, and aliphatic compounds including *n*-fatty acids, *n*-methylketones, *n*-alkanes and *n*-alkenes doublets and other aliphatics according to probable source or chemical structure (Buurman

et al., 2007; Suárez-Abelenda et al., 2014).

For the bulk soil comparison (Figure 3.5a), the Ctr- treatment was dominated by polysaccharides (91.8% TQPA), and to a lesser extent, MAHs (7.7% TQPA), and *n*-fatty acids (<1% TQPA). The Ctr+ treatment had a similar composition to the Ctr- treatment, but with no appreciable contribution of *n*-fatty acids. When the soil received either lime or combined lime and P addition(s), the chemical composition of the WEOM in the bulk soil underwent a drastic increase in MAHs and N-compounds and a decrease in relative proportions of polysaccharides. Changes in the composition of the grouped pyrolysis products caused by lime and/or P at different application rates followed the descending order: large lime amendments (L8, L8P0.2 and L8P0.4) > moderate lime amendments (L4, L4P0.2 and L4P0.4) > individual P amendments ≈ Ctr- and Ctr+ (Figures 3.5a, S3.6a and S3.7a).

For the heavy fraction comparison (Figure 3.5b), the Ctr- treatment had a similar composition to that of the bulk soil, but with a greater relative abundance of n-alkenes and *n*-fatty acids. Out of all treatments, the Ctr+ treatment had the greatest contribution of polysaccharides to TQPA (97.1%), and the smallest contribution of MAHs to TQPA (2.4%) and undetectable *n*-fatty acids. Moderate P application resulted in negligible molecular differences (i.e. P0.2 vs. Ctr-; Figure S3.7b) as opposed to large P application. Similar changes to those caused by large P application were also found after adding lime application. Namely, there was a relative increase in MAHs, N compounds, and the aliphatic fraction, including *n*-alkane and other aliphatic compounds (Figures 3.5b and S3.7b). The combined large P and/or large lime addition (L8P0.2, L8P0.4 and L4P0.4) to the heavy fraction caused the greatest differences in the relative composition of WEOM

pyrolysis products when compared with the corresponding Ctr- and Ctr+ treatments (Figure S3.7b). These changes were mainly related to the relative increase in aromatic compounds (including MAHs and PAHs), phenols, N compounds and aliphatic compounds (Figure 3.5b).

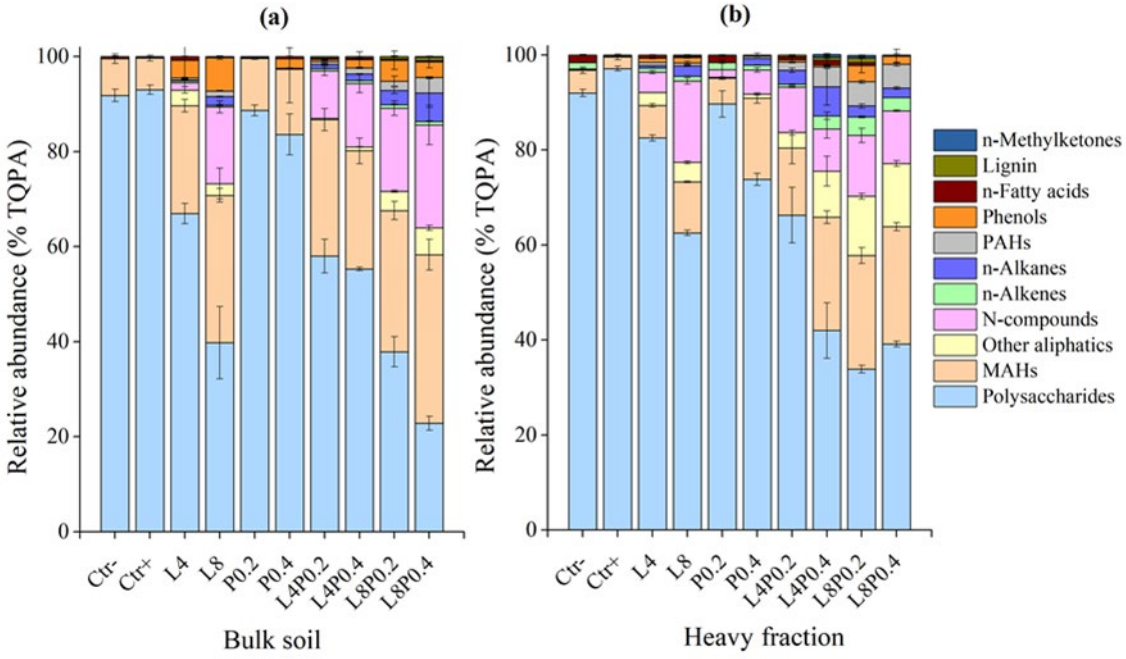

Figure 3.5 Average value of the relative abundances (% total quantified peak area, TQPA) of grouped pyrolysis products in (a) bulk soil and (b) heavy fraction samples, including controls and treatments with either individual lime (at addition rates of 4 and 8 g/kg, L4 and L8), individual P (at addition rates of 0.2 and 0.4 g P/kg, P0.2 and P0.4), or combined lime and P additions (L4P0.2, L4P0.4, L8P0.2 and L8P0.4). The negative control (Ctr-) was the unamended soil sample, while the positive control was the amended soil sample with $CaCl_2$ (Ctr+). Error bar indicates ± standard deviation (n=2).

3.3.6 Principal component analysis and cluster analysis

When PCA was applied to the bulk soil samples, the first four principal components accounted for 74.8% of total variation of WEOM composition data, with PC1 and PC2

accounting for 55.7% of it (Figure 3.6a). In the factor loadings of the first two components, a large group of compounds tended to plot on the high positive loading values (>0.5) of PC1 axis, which spread between both positive and negative loadings of PC2 axis. High positive values of PC1 were dominated by some plant-derived polysaccharides (specially levomannosan, Ps30 and (2H)-furan-2-one, Ps7, loadings >0.75), lignin moieties (mostly guaiacol, L1 and vinylphenol, L2), some phenols (e.g., Ph2, Ph7), N-containing compounds (mainly pyrroles, N2, N5–7), aromatics (e.g., M1–3, M8, PA11–12, PA2), and a large group of aliphatic compounds, i.e. all the quantified *n*-alkanes and n-alkenes (e.g., C13:1, C17:1) along with several other aliphatics (e.g., Al1, Al3, Al 10). Positive loadings of PC2 were dominated by some pyridines and pyrroles (e.g., N8, N1, N5), few cyclopentenones (e.g., Ps14, Ps22), 4H-pyran-4-one, 3-hydroxy-2-methyl (Ps26), MAHs and phenols, whereas several polysaccharides (e.g., Ps12–13, Ps8, Ps30), PAHs (e.g., PA3, PA8–9) and most n-alkanes were located at negative loadings of PC2. On high negative loadings of PC1, a group of unspecific polysaccharides, including several furaldehydes (e.g, Ps12, Ps18, Ps13) and acetic acid (Ps2) were found.

The PC1-PC2 scores of the bulk soil showed that the treatments without lime (Ctr+, Ctr-, P0.2 and P0.4) grouped together on negative PC1 and PC2 scores, whilst all samples treated with lime (including single-lime and lime/P-combined treatments) showed a gradient increasing from less negative to high positive PC1 scores as (i) lime application rates increased, and (ii) larger P contents were added along with lime (Figure 3.6b). Thus, the combination of the largest lime and P application rates accounted for the highest positive scores in PC1. The two-way cluster analysis (Figure S3.8) showed consistent trends with the PCA. There were two dominant groups: I (treatments with large lime application rate)

and II (the rest of bulk soil samples). Group II was further divided into two subgroups, II-1 (controls and treatments with individual P additions) and II-2 (treatments with moderate lime application rate).

When considering the heavy fraction, the first four principal components accounted for 68.2% of total variation of WEOM composition data, with PC1 and PC2 accounting for 31.7% and 18.0%, respectively (Figure 3.6c). The distribution plot is similar to that of the bulk soil analysis but with some remarkable differences. Negative PC1 loadings were dominated by the previously-mentioned undefined group of polysaccharides (e.g., Ps2 and Ps18) but also levomannosan (Ps30), 4-hydroxy-5,6-dihydro-2H-pyran-2-one (Ps20), and dianhydrorhamnose (Ps23), which were undetectable or negatively correlated with these in bulk soils. In addition, some aliphatics (e.g., C12:1 and C_{16} fatty acid, FA2) were located at lower negative PC1 loadings. Positive PC1 loadings included also several polysaccharides (mainly Ps7, Ps14, Ps22, Ps1), but with a less clear plant-polysaccharide signal. This sector of PC1 was also dominant in aliphatics (n-alkanes/n-alkenes and other aliphatics), lignin (L1–2), phenolic compounds (mostly Ph5–6 and Ph10–12, loadings >0.6), MAHs (mostly M2, M4 and M9, loadings >0.8), PAHs (mostly PA1–3, PA6–7 and PA12, loadings >0.8), and N-containing compounds (mostly N14 (3-hydroxypyridine), N11 (3-acetylpyrrole), N7, N2, and N9, loadings >0.6) including the plant marker indole (N16) (Nierop et al., 2005). On the PC2 axis, negative loadings were dominated by N-containing compounds (e.g., N9, N14; N16), phenols (e.g., Ph5–6, Ph11) and aromatics (e.g., PA5, PA11, M10), whilst positive PC2 was largely dominated by aliphatic compounds (including ketones, fatty acids, alkanes/alkenes and several other aliphatics).

For PC1 factor scores (Figure 3.6d), control treatments (Ctr+ and Ctr- of the heavy fraction and the Ctr- of the bulk soil) and samples that received small P application rates (P0.2) accounted for the most negative values (<-0.7), whilst large-P samples contained smaller negative scores (ca. -0.4). With lime addition, there was a similar gradient increasing from relatively higher to less negative PC1 scores (from -0.6 to -0.02) as rates of lime only addition increased. Treatments with combined high lime and/or high P addition (L4P0.4, L8P0.4 and L8P0.2) dominated the PC1 positive sector and accounted for the largest positive scores. These arrangements were further supported by cluster analysis (Figure S3.9), which showed that the combined treatments with large P and/or lime additions grouped together (I), whereas the rest of the samples (II) plotted separately and further divided into II-1 (P0.4, L4, L8 and L4P0.2) and II-2 (Ctr-, Ctr+, P0.2 and the Ctr- of the bulk soil in separated small branches).

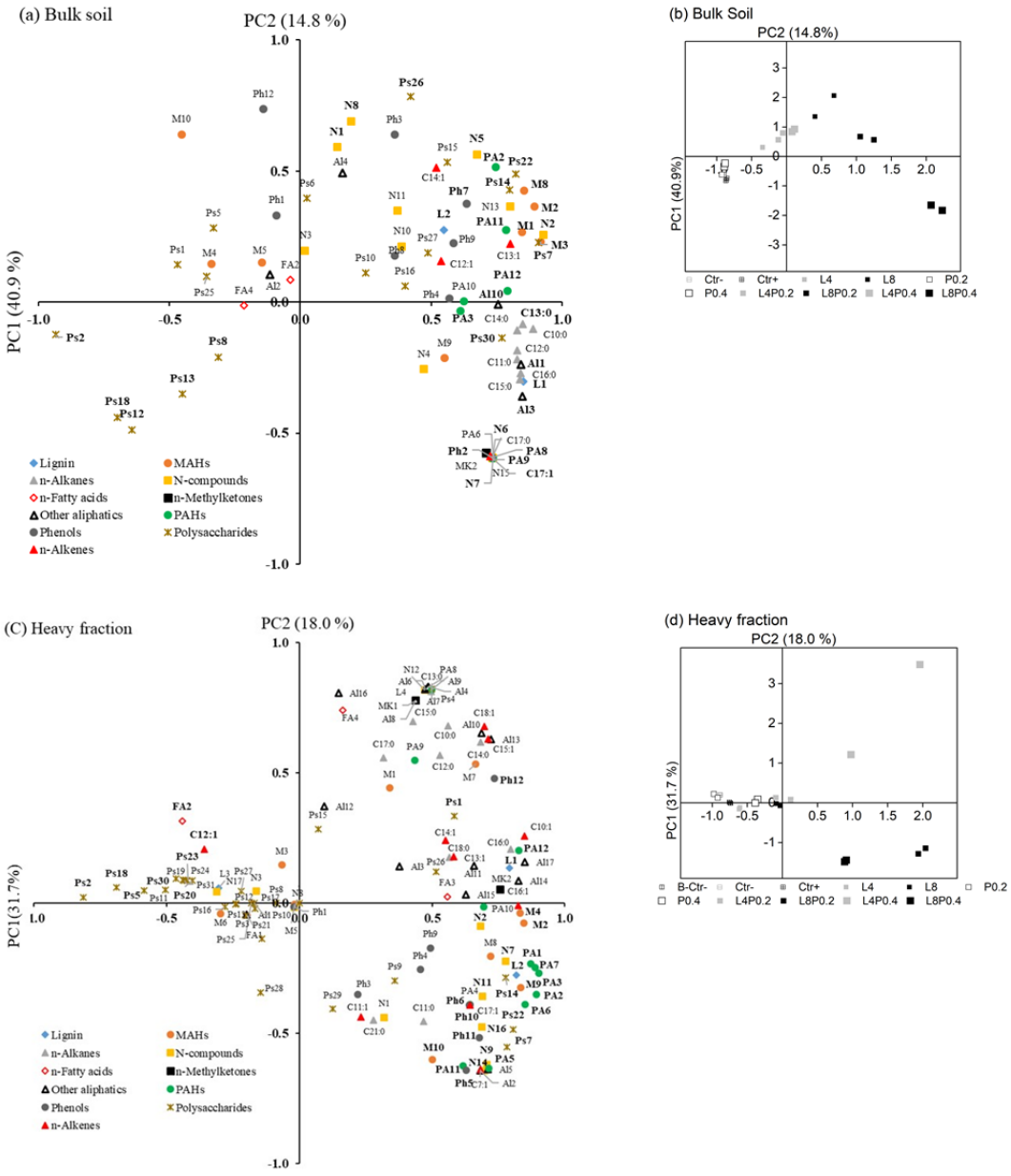

Figure 3.6 The (a) PC1-PC2 loadings of water-extractable organic matter (WEOM) pyrolysis products and (b) PC1-PC2 scores for the unamended (Ctr-) and amended bulk soils with either $CaCl_2$ (Ctr+), individual lime (at addition rates of 4 and 8 g/kg, L4 and L8), individual P (at addition rates of 0.2 and 0.4 g P/kg, P0.2 and P0.4), or combined lime and P additions (L4P0.2, L4P0.4, L8P0.2 and L8P0.4), as well as the (c) PC1-PC2 loadings of WEOM pyrolysis products and (d) PC1-PC2 scores for the unamended (Ctr-) and amended heavy fraction samples with these additions and the Ctr- of the bulk soil (B-Ctr-).

3.4 Discussion

3.4.1 Effects on the quantity of WEOM

This study was able to distinguish the effect of adding an alkaline Ca salt ($CaCO_3$) from that of a Ca-neutral salt ($CaCl_2$) on soil pH and the concentration of WEOC in a sil-andic Andosol. The decrease in WEOC observed upon the addition of Ca^{2+} as $CaCl_2$ was attributed to the drop in soil pH caused by this amendment. An increase in Ca^{2+} concentration in the soil solution may have caused a displacement of Al^{3+} from exchange sites, and this subsequently hydrolysed in solution and caused acidification (Ball et al., 1980; Kamprath and Adams, 2010). Acidification favours H-bonding between organic ligands, as well as inner-sphere complexes formation (Kleber et al., 2015), and thus decreases WEOC concentration. The opposite occurs with the addition of lime. The results thus show that the alkalinising effect of lime on OM solubilisation (in both the bulk and the heavy soil) was stronger than the flocculant effect of the Ca^{2+} present in lime.

The fact that P additions caused similar changes in WEOC concentration in the bulk soil to those that received lime was already observed by Miyazawa et al. (2013). The addition of phosphate displaced OH^- from soil inorganic constituents, as revealed by the increase in pH with increasing P concentrations, consistent with previous studies (Guan et al., 2006; Schneider et al., 2010). The smaller release of WEOC caused by P addition to the heavy fraction compared with that from the bulk soil could be related to the fact that P had a greater effect on OM-metal complexes, and these might have been partly removed by density fractionation. Yet despite the small impact on the amount of WEOC, phosphate had an influence on the chemistry of WEOC through the displacement of some weakly

bound N-rich compounds (as implied by the decrease in the C/N ratio) and aromatic compounds, particularly MAHs, as found in Py-GC/MS analysis at large application rate. These molecules have a low molecular mass and high solubility (Guggenberger and Zech, 1994; Scott and Rothstein, 2014).

The combined effect of lime and P amendments on WEOC of the bulk soil was greater than the sum of the individual effects of separate lime and P additions. A decrease in phosphate adsorption at increasing pH values (pH range: 5.2–6.5) would be expected as the positive charge of this variable-charge soil decreases and competition between OH^- and phosphate for reactive sites increases (Hiemstra et al., 2013; Lijklema, 1977; Rahnemaie et al., 2007). However, the rise in Ca^{2+} resulting from lime additions might have caused an increase in the competition between phosphate and OM for Ca^{2+} compared with the treatments with either lime or P only (Weng et al., 2011). This inhibits the formation of insoluble Ca-OM complexes (under neutral pH), particularly Ca-aromatic C complexes (Weng et al., 2005). There being few Ca-aromatic C complexes formed at small Ca^{2+} concentrations compared to large Ca^{2+} concentrations were supported by the significantly higher aromaticity of WEOM in the Ctr- treatment compared to the Ctr+ treatment with Ca^{2+} addition. Schneider et al. (2010) reported that, phosphate was able to compete for amorphous $Al(OH)_3$ reactive sites more efficiently than organic ligands at high dissolved organic C (DOC) loadings, whereas the aromatic moieties had higher affinity for these sites at lower DOC loadings. This could also explain the greater increase in aromaticity of WEOM caused by the combined lime and P additions.

3.4.2 Effects on the quality of WEOM.

The WEOM fraction of the untreated bulk sample (Ctr-) mainly consisted of carbohydrates (inferred from their pyrolysis products e.g., acetic acid, furaldehydes) and some MAHs, generally associated with soil OM degradation products (Buurman et al., 2007; Nierop et al., 2005). The removal of the fPOM fraction from the bulk soil resulted in a WEOM with a smaller relative contribution of MAHs and furaldehydes (Figure S3.9) and a greater relative contribution of (i) plant-derived polysaccharides, and (ii) hydrophobic straight chain n-alkenes (mostly derived from plant tissues, e.g., cutin and cutan in cuticle) and C_{16} fatty acids (possibly from pine needles waxes) compared with the bulk soil (Kov et al., 2018; Tegelaar et al., 1989). This suggests that some low-molecular weight compounds in bulk soil (either very soluble or weakly bound) that were dissolved/released into the sodium polytungstate solution were then removed along with the fPOM fraction by density fractionation step (Kleber et al., 2015; Kov et al., 201; Shen et al., 2018). The disruption caused by the removal of these forms could have favoured the release of some compounds of higher molecular weight (predominantly plant-derived material) that might have been weakly protected through occlusion in the heavy fraction (Buurman and Roscoe, 2011; Kleber et al., 2015; Shen et al., 2018).

Lime amendments, in addition to causing a larger concentration of WEOM than the Ctr treatments, had a more complex signature, especially in the case of the bulk soil. Soil alkalinisation caused an enrichment of WEOM in (i) the poly/mono-phenolic and nitrogenised fraction, and (ii) markers of plant polysaccharides, such as levomannosan and pyranones (Kov et al., 2018). The application of P did not result in changes in the WEOM chemical composition, except when applied at a large rate, especially in the heavy fraction

(Figures S3.7–S3.9), where there was a larger relative contribution of MAHs, benzofurans (Ps25) (rendering an accumulation of soil OM degradation products), non-specific N compounds (mostly pyrroles), and aliphatics (straight chain n-alkanes, <C17). These enhanced contributions could be associated with the weakening of bonds between Al/Fe (hydr)oxides and hydroxyl groups of polyphenols and aromatic hydrocarbons, and N functional group of microbial/fungal N-rich re-assimilation products, as the presence of OH^- or phosphate increases (Newcomb et al., 2017).

Compared with the individual lime or P addition, the combination of lime and P caused greater divergence in the soil OM signature with regard to the Ctr- treatment. The extent of divergence increased with increasing application rates of lime and phosphate. In the bulk soils, the greater influence caused by largest lime+P addition (L8P0.2 and L8P0.4) was evident by an enrichment in the lignin and plant-carbohydrate (cellulose marker) signatures, and that of aliphatic structures of plant and/or microbial origin (Jansen and Nierop, 2009), along with a further increment of N-compounds and aromatics. In the WEOM of the heavy fraction, the combined large P and/or large lime addition caused an increase in the signal of phenolic and N-compounds, as well as MAHs and PAHs (higher levels of recalcitrant aromatics), including hydroxylated structures (e.g., catechol, Ph12 an hydroxipyridine) and highly oxidised/reactive N form (acetylpyrrole). These treated heavy fraction samples were also enriched in derivatives of fresh litter, such as *p*-coumaryl acid of grasses, indole (plant marker) and, to a smaller extent, plant-carbohydrates (Sáiz-Jiménez and De Leeuw, 1986; Nierop et al., 2005). This indicates a synergistic effects of lime and P on the displacement of organic molecules with hydroxyl nature, N functional groups and high hydrophobicity from the solid phase to the aqueous solution (as explained above), along with disrupting

the stability of soil aggregates and releasing previously encapsulated fresh OM into solution when the largest amount of lime was applied (Ramesh et al., 2019).

3.5 Conclusions and implications

Our data corroborates and extends a recent finding that P and lime additions could increase soil respiration by increasing the organic C concentration in the soil solution (Spohn and Schleuss, 2019, Ahmad et al., 2020), likely resulting from (i) phosphate outcompeting OM for Al^{3+} in Al^{3+}-OM complexes, and (ii) alkalisation disrupting the OM association with both Al^{3+} and short-range order Al constituents. Given that both Al-OM complexes and/or short-range order Al constituents are abundant in Andosols worldwide, our data also provide mechanistic insight in the decreased soil OM stability after liming and P fertilising Andosols elsewhere, as observed in Spain, Japan, Chile, and New Zealand (Verde et al., 2010; Dumale et al., 2011; Undurraga et al., 2009; Kov et al., 2018; Shen et al., 2018). It is worth noting that both lime and P fertiliser addition will tend to favour plant growth, and thus increase the input of C to the soil. While this can cause a net increase in soil OM, our observations suggest that the formation of OM-mineral/metal complexes might be less favoured in the presence of these amendments and this can render an OM more vulnerable to environmental changes. More detailed lab/field studies with various factors (e.g., soil type and depth, vegetation, climate and time scale) are needed to further prove universality of these effects of lime and/or P on OM stability in soils with andic properties and factors controlling them.

Appendix I. Supporting Information for Chapter 3 (SI3)

S3.1 Supporting materials and methods

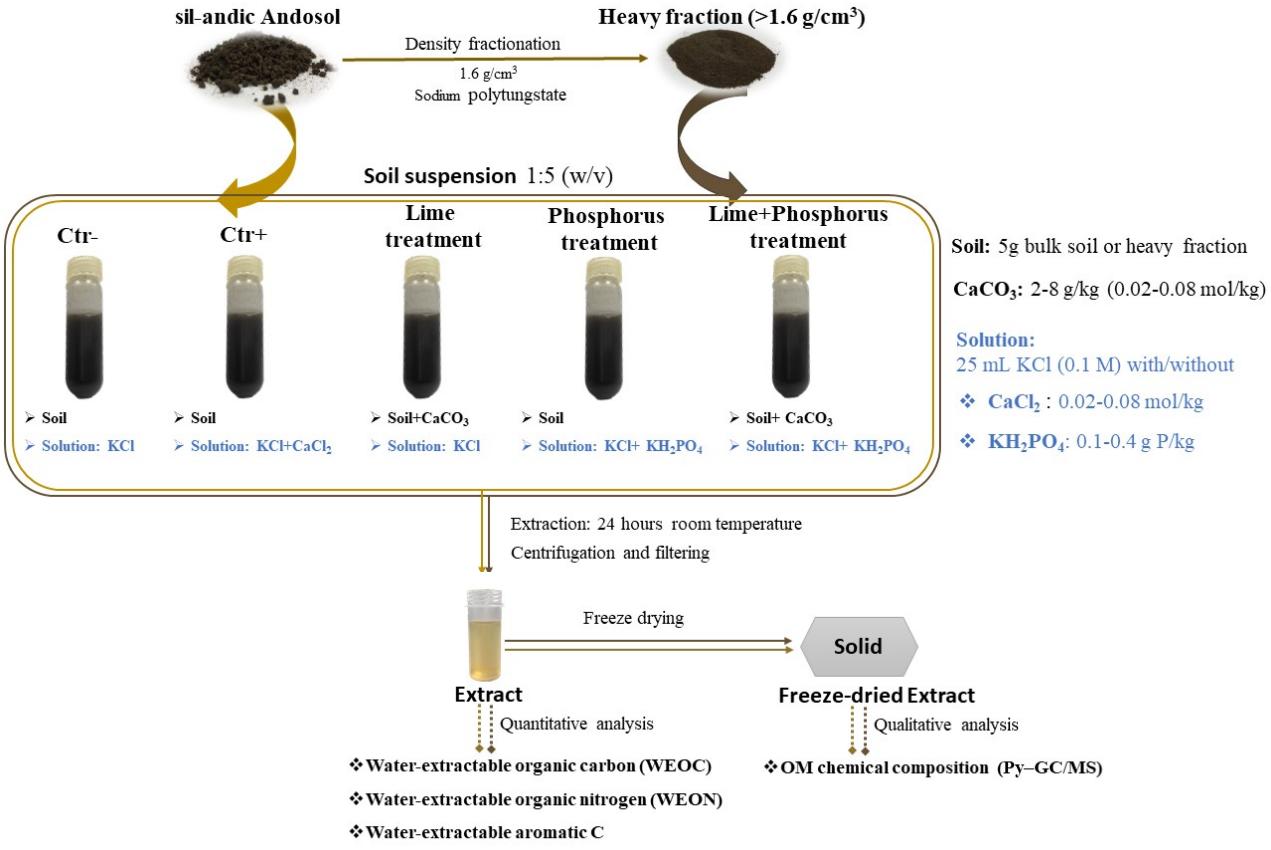

Figure S3.1 Schematic figure of the extraction procedure and quantitative and qualitative analyses of extracts.

S3.1.1 Characterisation of soil.

After removing identifiable plant residues and coarse material, and air drying, the bulk soil was sieved (<2 mm) and mixed further for homogenisation. Soil physicochemical characteristics (Table S3.1) were analysed as follows: (i) pH was measured (soil:water ratio=1:2.5) using a standard glass electrode; (ii) Olsen P was measured following the extraction method of Olsen et al. (1954) and analysis method of John (1970) and Murphy and Riley (1962); (iii) the total C and N contents were measured by using a vario MACRO cube CHNS elemental analyser (Elementar, Vario MACRO, Germany); and (iv) the Al_o, Fe_o and Si_o extracted by 0.1 M acid oxalate reagent (prepared by dissolving ammonium oxalate and oxalic acid, Blakemore, 1972), as well as the Al_p and Fe_p extracted with 0.1 M sodium pyrophosphate (Bascomb 1968), were measured by MP-AES (4200 MP-AES, Agilent Technologies, Singapore).

S3.1.2 Pyrolysis-gas chromatography/mass spectrometry (Py-GC/MS)

For GC/MS analysis, injection was carried out in a split mode (split ratio of 1:30). The pyrolysis products were separated using a stainless-steel capillary column [SH-Rxi-5 ms (Crossbond® 5% diphenyl/95% dimethyl polysiloxane): 30 m, 0.25 mm internal diameter, with a film thickness of 0.50 μm, Shimadzu]. High purity helium was used as the carrier gas (flow rate: 1 mL/min). The initial oven temperature was 40 °C, held for 12 s (same as the pyrolysis time) and then increased to 300 °C at a rate of 5 °C/min. The final column temperature was 300 °C and was held for 16 min. The temperature of the interface between GC and MS was 270 °C and that of the ion source was 230 °C. The ionisation energy was set as 70 eV, mass range *m/z* 45–650 and a cycle time 0.5 s (Shen et al. 2018). We used

GCMSsolution software (Shimadzu) for qualitative and semi-quantitative analysis. The peaks from the chromatograms were identified by "similarity search" function based on their distinctive mass spectra and compared with the NIST mass spec. library and published sources such as Buurman et al. (2007), Suárez-Abelenda et al. (2015), Shen et al. (2018), and Kov et al. (2018). The sum of the total quantified peak area (TQPA) of major fragment ion(s) (*m/z*) was set to 100% and the relative abundance of each pyrolysis product was then calculated. Peaks that contributed <0.1% of the TQPA were not considered in this study.

S3.1.3 Heatmap and cluster analysis

The heatmap and cluster analysis, revealing the pyrolysis products composition of WEOM, and the difference between controls and amendments, respectively, were performed using the "pheatmap" package in the R environment (R Version 3.2.5).

S3.2 Supporting results

The sil-andic Andosol had a high total C concentration of 93 g/kg, but a low pH (5.4) and Olsen P (7.5 mg/kg). Allophane content was 3.9% (Table S3.1). After the density fractionation through which the fPOM fraction was removed, the heavy fraction had a C and N concentration of 74 g/kg and 7 g/kg, respectively, which accounted for 69.3% total C and 75.2% total N in the bulk soil (Table S3.2). The C/N ratio of the heavy fraction was 10.7, which was lower than that of the bulk soil (11.6) and the fPOM fraction (13.2).

S3.2.1 General description of pyrolysis products

S3.2.1.1 Chemical composition of the WEOM from the bulk soil

The Ctr- had the greatest dominance of polysaccharides [mainly Ps2 (acetic acid), Ps12 (x-

furaldehyde) and Ps18 (2-furaldehyde, x-methyl-)] accounting for 91.8% TQPA, and to a lesser extent, MAHs (7.7% TQPA) [mainly M2 (toluene), and M3 (ethylbenzene)] and *n*-fatty acids (0.5%) [FA2 (C_{16} fatty acid iso)] (Figures 3.5a, S3.7a and S3.8). The Ctr+ treatment had a similar composition to the Ctr- treatment, but with no appreciable contributions of *n*-fatty acids (Figure S3.8). The chemical composition of the WEOM of the bulk soil evidenced a drastic increase of MAHs and/or N-compounds when the soil received either lime and/or P additions. Compared with the Ctr- treatment, lime and/or P amendments caused a relative increase in TQPA of MAHs, which ranged between 11.0% in P0.2 and 35.5% in L8P0.4 treatments, along with a notably increased M1(benzene), M2 and M3. Additionally, there was a relatively higher TQPA of N compounds, which were enriched in N2 (pyrrole), N5 (1H-pyrrole, 1-methyl) and N13 (benzonitrile, 2-methyl-) (Figures 3.5a and S3.8). This resulted in an intense decrease (from 91.8% to 22.8%) in relative proportions of polysaccharides in all treated soils, particularly when the soil received a high lime application rate (e.g., L8, L8P0.2, L8P0.4), ranging between 22.8% and 37.8%).

S3.2.1.2 Chemical composition of the WEOM from the heavy fraction

The Ctr- treatment contained a similar relative abundance of polysaccharides (91.4%) (Figure 3.5b) as that of the bulk soil. However, it had a different composition (Figure S3.9). The removal of fPOM resulted in (i) a relative increase of plant-derived polysaccharides, e.g., Ps30 (levomannosan), Ps20 (4-hydroxy-5, 6-dihydro-2H-pyran-2-one) and Ps23 (dianhydrorhamnose) (Nierop et al., 2005), and aliphatic compounds (*n*-alkenes and *n*-fatty acids); and (ii) a relative decline in MAHs (particularly M3). The Ctr+ had the greatest relative abundance of polysaccharides out of all treatments (97.1% TQPA) [mainly Ps2

and Ps11 (x-furaldehyde)], and the lowest relative contribution of MAHs (2.4% TQPA) (with less M2) and other groups with <0.3% TQPA.

The most striking changes in the composition of pyrolysis-product groups of the heavy fraction were caused by high P application, although low P application rates resulted in negligible molecular differences (i.e. P0.2 vs. Ctr- treatment; Figures S3.7b and S3.9). Namely, there was a relative increase in MAHs [e.g., M2 (toluene), M3,4 (ethylbenzenes) and M10 (benzene, 1,x,x-trimethyl-)], N compounds (e.g., N2, pyrrole) and in the aliphatic fraction including *n*-alkane (e.g., C10:0, C16:0 and C14:0) and other aliphatic compounds (mainly short/medium chain ones, <C17), along with a slightly larger contribution of PAHs [e.g., more PA10–11 (naphthalene, x-methyl-)] (Figures 3.5b and S3.9). Similar changes were also found after adding high lime application rates, with a relative increase in N compounds [e.g., more N2 (pyrrole) and N1 (pyridine)], MAHs [(e.g., M2–3, M8 (benzene, 1,x,x-trimethyl-)], aliphatics [e.g., C11:0, C16:0 and Al3] and phenols (with a small contribution).

The combined high P and/or high lime addition (L8P0.2, L8P0.4 and L4P0.4) to the heavy fraction caused the greatest differences in the relative composition of WEOM pyrolysis products when compared with the corresponding Ctr- and Ctr+ treatments. These changes were mainly related to the relative increase in (i) aromatic compounds, including MAHs and PAHs [e.g., greater contents of M4, M2, M8–10 (benzene, 1,x,x-trimethyl-), PA1 (indene), PA2–3 (1H-indene, X-methyl-), PA5 (naphthalene, 1,2-dihydro) and PA9–11 (naphthalenes, x-methyl-)], (ii) phenols [Ph3 and Ph5 (phenols, x-methyl-)], (iii) N compounds [e.g., greater N1–2, N7 (1H-pyrrole, 4-ethyl-) and N11 (3-acetylpyrrole)] and (iv) aliphatic compounds (mainly short or medium chain units) (Figures S3.7b and S3.9).

Also, a brief summary of the molecular characteristics of the 2% hydrofluoric acid-residue OM – carried out in a previous study of this same soil type (the Egmont soil) also under pine (Kov et al. 2018) – is provided. The OM is dominated by fresh organic (litter/root) inputs, as inferred by the cellulose markers and other plant-derived structural carbohydrates, aliphatic moieties from cutin/cutan and suberan-like signal from roots. The soil also contains (i) abundant degradation products of plant polysaccharides, (ii) largely oxidised lignin, and (iii) enriched on microbial-derived OM, as denoted by high contents of fungal/arthropods (chitin) and bacterial markers. This OM composition is consistent with that reported in other Py-GC/MS studies on the NaOH-extractable and 2% hydrofluoric acid-residue OM of soils with andic properties (Suárez-Abelenda et al., 2014; Buurman et al., 2007; Nierop et al., 2005; Wang et al 2016).

Table S3.1 Basic properties of the sil-andic Andosol

	pH (H_2O)	Olsen P mg/kg	C g/kg	N g/kg	C/N	Allophane %	$Al_o+{}^1/_2Fe_o$ g/kg	Al_p/Al_o
sil-andic Andosol	5.4	7.5	93	8	11.6	3.9	22.5	0.5

P (phosphorous), C (carbon), N (nitrogen), Al_o and Fe_o (acid oxalate-extractable aluminium and iron), as well as Al_p and C_p (sodium pyrophosphate-extractable aluminium and carbon).

Table S3.2 The carbon (C) and nitrogen (N) concentration and C/N ratio of free particulate organic matter (fPOM) and heavy fraction, the recovery of mass, C and N after fractionation and corresponding distribution of them in each fraction.

Fraction	Concentration in each fraction			Distribution in each fraction			Recovery		
	C g/kg	N g/kg	C/N	Mass %	C %	N %	Mass %	C %	N %
fPOM (<1.6 g/cm^3)	182	14	13.2	11.8	22.9	20.1	98.4	92.2	95.3
Heavy fraction (>1.6 g/cm^3)	74	7	10.7	86.6	69.3	75.2			

Table S3.3 The specific UV absorbance at 245nm (SUVA, mean±standard deviation) of water-extractable organic matter (WEOM) in bulk soils and heavy fraction samples, including negative control (Ctr-) without addition, positive control (Ctr+) with $CaCl_2$, and treatments with either individual lime (at addition rates of 4 and 8 g/kg, L4 and L8), individual P (at addition rates of 0.2 and 0.4 g P/kg, P0.2 and P0.4), or combined lime and P additions (L4P0.2, L4P0.4, L8P0.2 and L8P0.4).

Treatment	SUVA[1]	
	Bulk soil	Heavy fraction
Ctr+	1.91±0.24 e [2]	0.38±0.03 f
Ctr-	3.12±0.11 cd	0.84±0.11 e
L4	3.53±0.27 bc	1.30±0.08 cd
L8	4.22±0.15 a	1.42±0.10 cd
P0.2	3.34±0.06 c	0.96±0.12 e
P0.4	3.89±0.01 b	1.53±0.03 c
L4P0.2	4.44±0.64 a	4.15±0.15 b
L8P0.2	4.54±0.60 a	4.21±0.09 b
L4P0.4	4.19±0.13 ab	4.67±0.09 a
L8P0.4	4.34±0.18 ab	4.50±0.18 a

[1] SUVA (L/mg C/m)=UV absorbance at 245nm (UV_{254})/concentration of WEOC

[2] The values of the SUVA of WEOM in either bulk soils or heavy fraction samples with not shared letters are statistically different (P<0.05) based on a one-way ANOVA followed by Tukey B test (n=3).

Table S3.4 Pyrolysis products list, molecular mass (M^+), fragment ion used (*m/z*) and average retention time (RT).

Code	Group	M^+	*m/z*	RT	Compound
L1	Lignin	124	109+124	11.863	Guaiacol (Phenol, 2-methoxy-)
L2	Lignin	120	91+120	15.166	4-Vinylphenol (2-Methoxy-4-vinylphenol)
L3	Lignin	154	139+154	19.861	Syringol (phenol, 2,6-dimethoxy)
L4	Lignin	166	151+166	21.45	4-Acetylguaiacol
M1	MAHs	78	77+78	2.485	Benzene
M2	MAHs	92	91+92	3.769	Toluene
M3	MAHs	106	91+106	5.671	Ethylbenzene
M4	MAHs	106	91+106	5.82	Ethylbenzene
M5	MAHs	106	91+106	6.375	Benzene, 1,x-dimethyl-
M6	MAHs	104	78+104	6.387	Styrene
M7	MAHs	120	105+120	7.968	Benzene, 1,x,x-trimethyl-
M8	MAHs	120	105+120	8.225	Benzene, 1,x,x-trimethyl-
M9	MAHs	120	105+120	9.085	Benzene, 1,x,x-trimethyl-
M10	MAHs	120	105+120	9.868	Benzene, 1,x,x-trimethyl-
C10:0–21:0	n-Alkanes	-	57+71	-	C10:0-C21:0
C7:1–18:1	n-Alkenes	-	55+69	-	C7:1-C18:1
Al1-Al17	Others aliphatics	-	57+71	-	Branched alkanes
N1	N-compounds	79	55+69 52+79	3.491	Branched alkenes, Alkanols Pyridine
N2	N-compounds	67	67	3.65	Pyrrole
N3	N-compounds	59	59	4.396	Acetamide
N4	N-compounds	93	66+93	4.897	Pyridine, 2-methyl-
N5	N-compounds	81	80+81	5.365	1H-Pyrrole, 1-methyl
N6	N-compounds	81	80+81	5.565	1H-Pyrrole, 3-methyl
N7	N-compounds	95	80+95	7.56	1H-Pyrrole, 4-ethyl
N8	N-compounds	107	106+107	7.611	Pyridine, 2,4-dimethyl
N9	N-compounds	95	80+95	7.782	1H-Pyrrole, 2,4-dimethyl
N10	N-compounds	109	94+109	9.533	2-acetylpyrrole

N11	N-compounds	109	94+109	11.342	3-acetylpyrrole
N12	N-compounds	95	67+95	12.14	2-Hydroxypyridine (2(1H)-Pyridinone)
N13	N-compounds	117	116+117	12.945	Benzonitrile, 2-methyl-
N14	N-compounds	95	67+95	12.14	3-Hydroxypyridine (3(1H)-Pyridinone)
N15	N-compounds	117	116+117	13.24	Benzonitrile, 3-methyl
N16	N-compounds	117	90+117	16.803	Indole
N17	N-compounds	167	110+125	27.992	3-Acetamido-5-acetylfuran
FA1	n-Fatty acids	200	60+73	24.432	C12 Fatty acid
FA2	n-Fatty acids	256	60+73	32.323	C16 Fatty acid iso
FA3	n-Fatty acids	256	60+73	32.791	C16 Fatty acid anteiso
FA4	n-Fatty acids	284	60+74	39.442	C18 Fatty acid
MK1	n-Methylketones	226	58+59	20.239	C13-methylketone
MK2	n-Methylketones	282	58+59	31.567	C17-methylketone
PA1	PAHs	116	115+116	10.525	Indene
PA2	PAHs	130	115+130	13.563	1H-Indene, 2-methyl-
PA3	PAHs	130	115+130	13.745	1H-Indene, 3-methyl-
PA4	PAHs	130	129+130	14.406	Naphthalene, 1,x-dihydro-
PA5	PAHs	130	129+130	16.381	Naphthalene, 1,x-dihydro-
PA6	PAHs	130	129+130	16.485	Naphthalene, 1,x-dihydro-
PA7	PAHs	130	129+130	16.662	Naphthalene, 1,x-dihydro-
PA8	PAHs	128	128	16.838	Naphthalene
PA9	PAHs	142	141+142	17.623	Naphthalene, 1-methyl-
PA10	PAHs	142	141+142	18.066	Naphthalene, 2-methyl-
PA11	PAHs	142	141+142	19.704	Naphthalene, 3-methyl-
PA12	PAHs	156	141+156	20.949	Naphthalene, 1,7-dimethyl-
Ph1	Phenols	94	66+94	9.116	Phenol
Ph2	Phenols	108	107+108	9.821	Phenol, x-methyl
Ph3	Phenols	108	107+108	11.099	Phenol, x-methyl
Ph4	Phenols	108	107+108	11.713	Phenol, x-methyl
Ph5	Phenols	108	107+108	12.238	Phenol, x-methyl
Ph6	Phenols	122	107+122	12.434	Phenol, 1,x-dimethyl
Ph7	Phenols	122	107+122	12.511	Phenol, 1,x-dimethyl

Ph8	Phenols	122	107+122	13.449	Phenol, 1,x-dimethyl
Ph9	Phenols	122	107+122	14.438	Phenol, 3-ethyl
Ph10	Phenols	136	121+136	15.952	5-Ethyl, 2-methyl phenol
Ph11	Phenols	136	121+136	16.253	5-Ethyl, 3-methyl phenol
Ph12	Phenols	140	125+140	18.3	1,2-Benzenediol, 3-methoxy (3-methoxy catechol)
Ps1	Polysaccharides	82	53+82	2.061	Furan, 2-methyl-
Ps2	Polysaccharides	60	60	2.256	Acetic acid
Ps3	Polysaccharides	80	77+80	2.503	1,3-Cyclopentadiene, x-methyl
Ps4	Polysaccharides	82	53+82	2.653	Furan, 2-methyl-
Ps5	Polysaccharides	96	95+96	2.932	Furan, 2,5-dimethyl-
Ps6	Polysaccharides	96	95+96	3.043	Furan, 2,5-dimethyl-
Ps7	Polysaccharides	84	54+84	4.167	(2H)-Furan-2-one
Ps8	Polysaccharides	96	95+96	4.341	x-Furaldehyde
Ps9	Polysaccharides	96	95+96	4.725	x-Furaldehyde
Ps10	Polysaccharides	98	54+98	4.961	2,5 furandione
Ps11	Polysaccharides	96	95+96	5.121	x-Furaldehyde
Ps12	Polysaccharides	96	95+96	5.221	x-Furaldehyde
Ps13	Polysaccharides	96	95+96	5.23	x-Furaldehyde
Ps14	Polysaccharides	96	67+96	6.764	2-Cyclopenten-1-one, 2-methyl-
Ps15	Polysaccharides	110	109+110	7.002	2-Furaldehyde, x-methyl
Ps16	Polysaccharides	110	109+110	7.062	2-Furaldehyde, x-methyl
Ps17	Polysaccharides	98	55+98	7.338	2,3-Dihydro-5-methylfuran-2-one
Ps18	Polysaccharides	110	109+110	8.277	2-Furaldehyde, x-methyl-
Ps19	Polysaccharides	110	109+110	8.759	2-Furaldehyde, x-methyl
Ps20	Polysaccharides	114	114+58	9.261	4-Hydroxy-5,6-dihydro-2H-pyran-2-one
Ps21	Polysaccharides	112	55+112	10.252	3-Hydroxy-2-methyl-2-cyclopenten-1-one
Ps22	Polysaccharides	110	67+110	10.429	2,3-Dimethylcyclopent-2-en-1-one
Ps23	Polysaccharides	128	113+128	10.477	Dianhydrorhamnose
Ps24	Polysaccharides	128	57+128	11.767	2,5-Dimethyl-4-hydroxy-3(2H)-furanone
Ps25	Polysaccharides	132	131+132	12.437	Benzofuran, 2-methyl-
Ps26	Polysaccharides	126	71+126	12.646	4H-Pyran-4-one, 3-hydroxy-2-methyl
Ps27	Polysaccharides	130	69+100	14.511	1-Deoxy-2,4-methylene-3,5-anhydro-d-xylitol

Ps28	Polysaccharides	144	57+69	15.383	1,4:3,6-Dianhydro-.alpha.-d-glucopyranose
Ps29	Polysaccharides	-*	74+101	20.713	Arabinopyranose
Ps30	Polysaccharides	162	60+73	22.786	Levomannosan
Ps31	Polysaccharides	162	60+73	24.784	Levoglucosan

-* indicates unknown molecular mass.
MAHs: monocyclic aromatic hydrocarbons.
PAHs: polycyclic aromatic hydrocarbons.

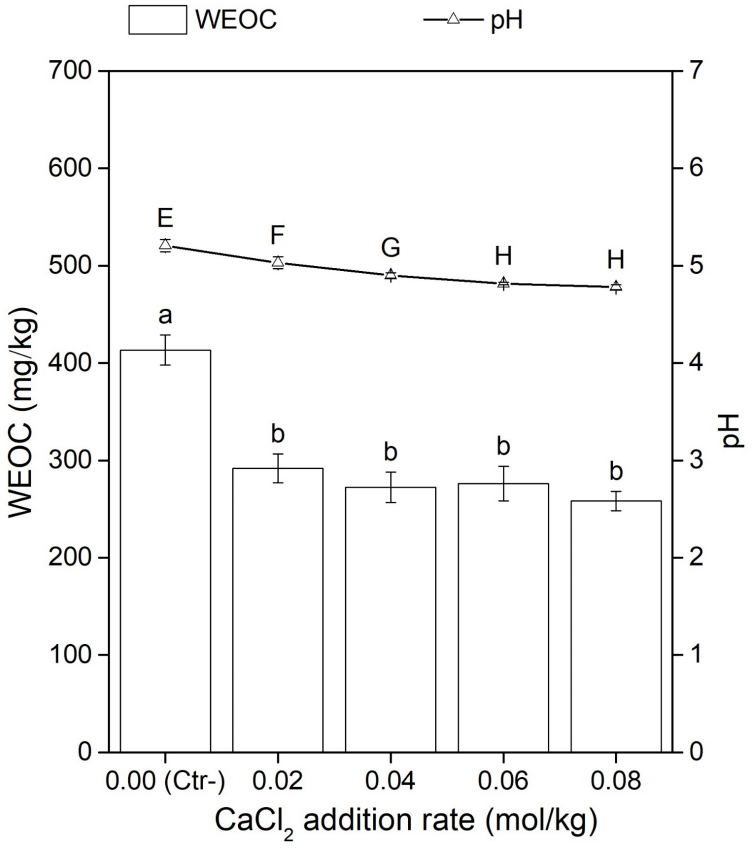

Figure S3.2 The water-extractable organic carbon (WEOC) concentration and pH of unamended (Ctr-) and amended bulk soils with $CaCl_2$ at different application rates. Graph bars and symbols marked with no shared letters on top represent statistically significant results (P<0.05) based on a one-way ANOVA followed by Tukey B test (n=3).

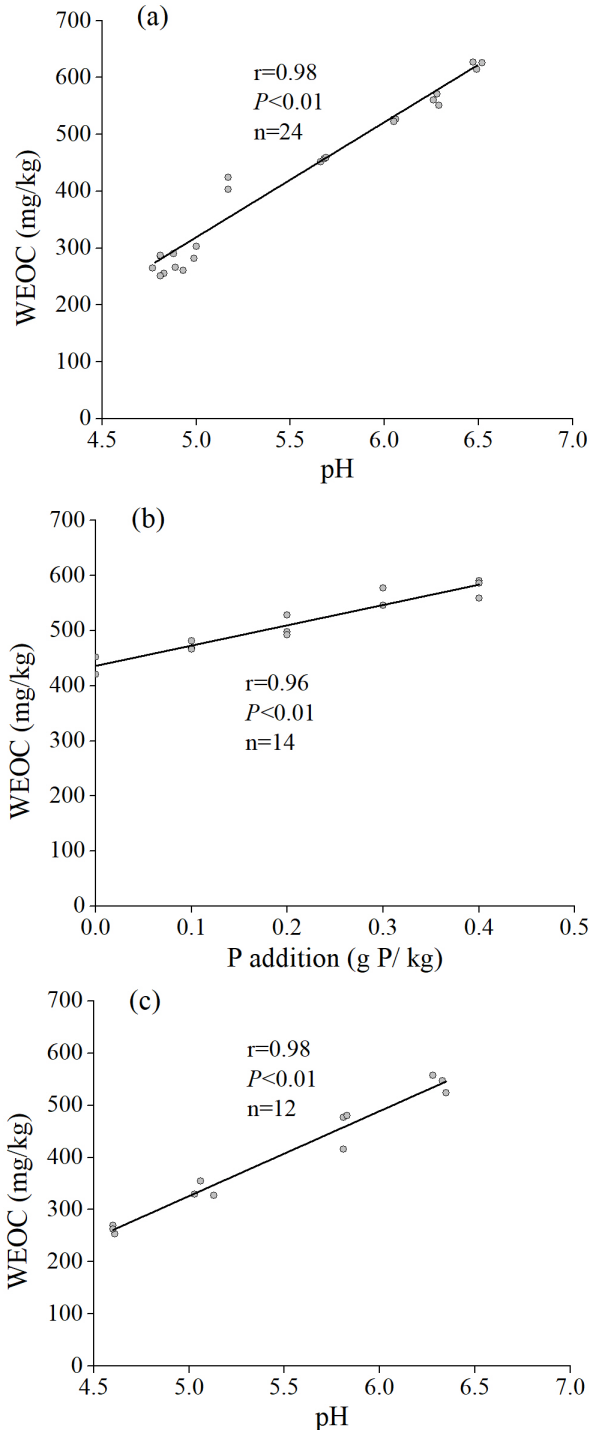

Figure S3.3 The correlation (Pearson's Correlation) between (a) pH and water-extractable organic carbon (WEOC) concertation of bulk soils, (b) P addition rate and WEOC concertation of bulk soils, as well as (c) pH and WEOC concertation of heavy fraction samples.

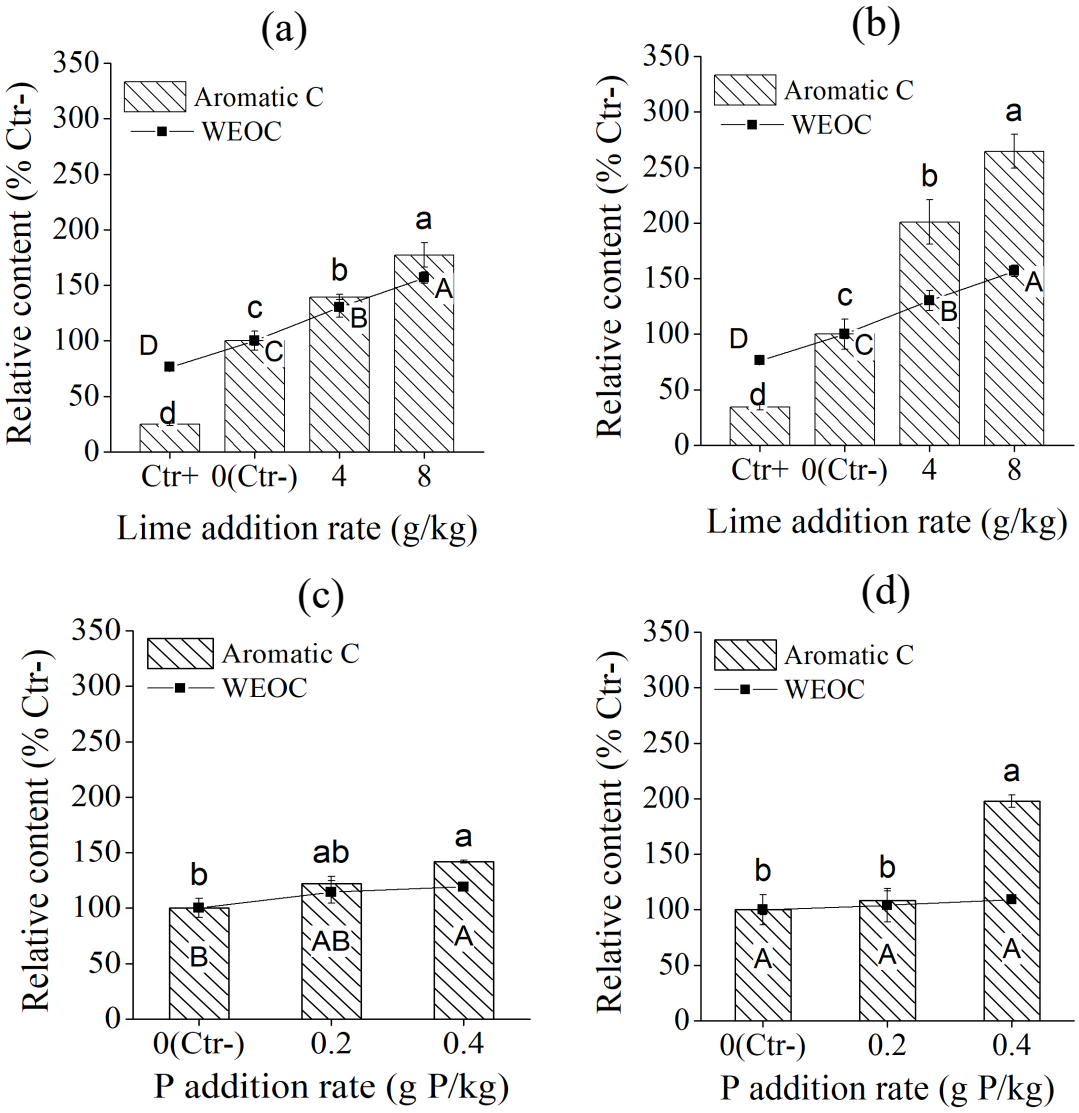

Figure S3.4 The relative content of aromatic carbon (C) and water-extractable organic carbon (WEOC) of the water-extractable organic matter (WEOM) in the (a and c) bulk soils as well as the (b and d) heavy fraction samples without (Ctr-)/with either $CaCl_2$ (Ctr+), lime or P additions. Graph bars and symbols marked with no shared letters represent statistically significant results (P<0.05) based on a one-way ANOVA followed by Tukey B test (n=3).

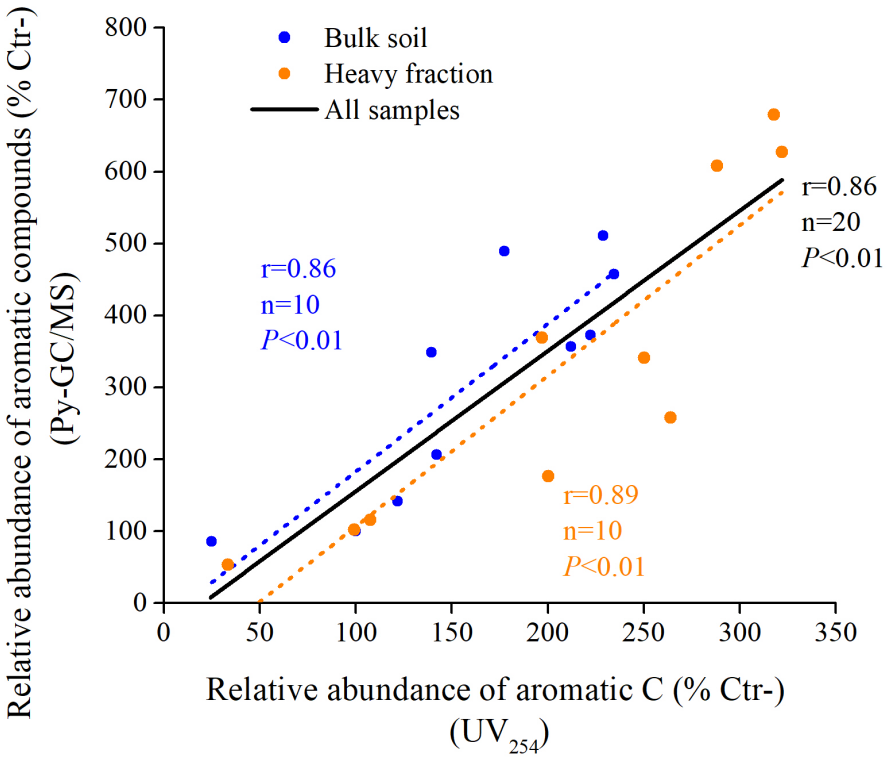

Figure S3.5 The correlation (Pearson's Correlation) between relative abundance of aromatic compounds analysed by pyrolysis-gas chromatography/mass spectrometry (Py-GC/MS) and relative abundance of aromatic carbon (C) measured by UV/Visible scanning spectrophotometer (UV absorbance at 245nm, UV_{254}).

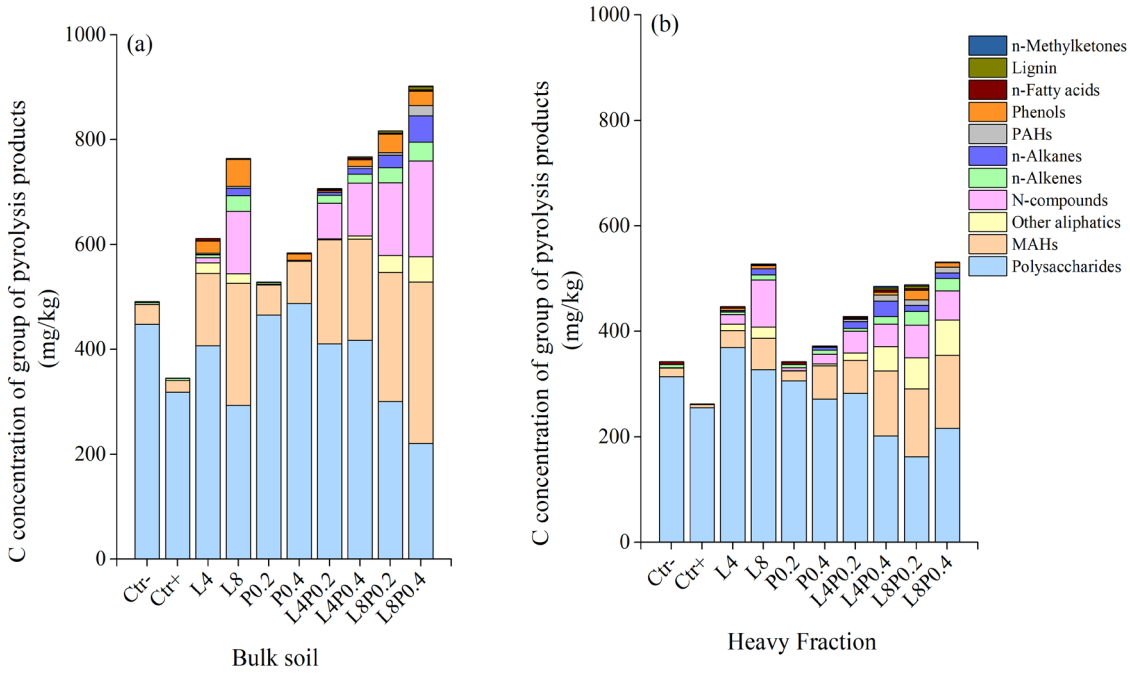

Figure S3.6 The estimated carbon (C) concentration of the 11 groups of pyrolysis products in the (a) bulk soils and (b) heavy fraction samples, including controls (Ctr- and Ctr+) and treatments with either individual lime (at addition rates of 4 and 8 g/kg, L4 and L8), individual P (at addition rates of 0.2 and 0.4 g P/kg, P0.2 and P0.4), or combined lime and P additions (L4P0.2, L4P0.4, L8P0.2 and L8P0.4). The C concentration of each group of pyrolysis products was calculated by multiplying the relative abundance of the group (% total quantified peak area, TQPA) by its water-extractable organic carbon (WEOC) concentration (mg/kg) to compare the chemical composition of water-extractable organic matter (WEOM) in a semi-quantitative manner.

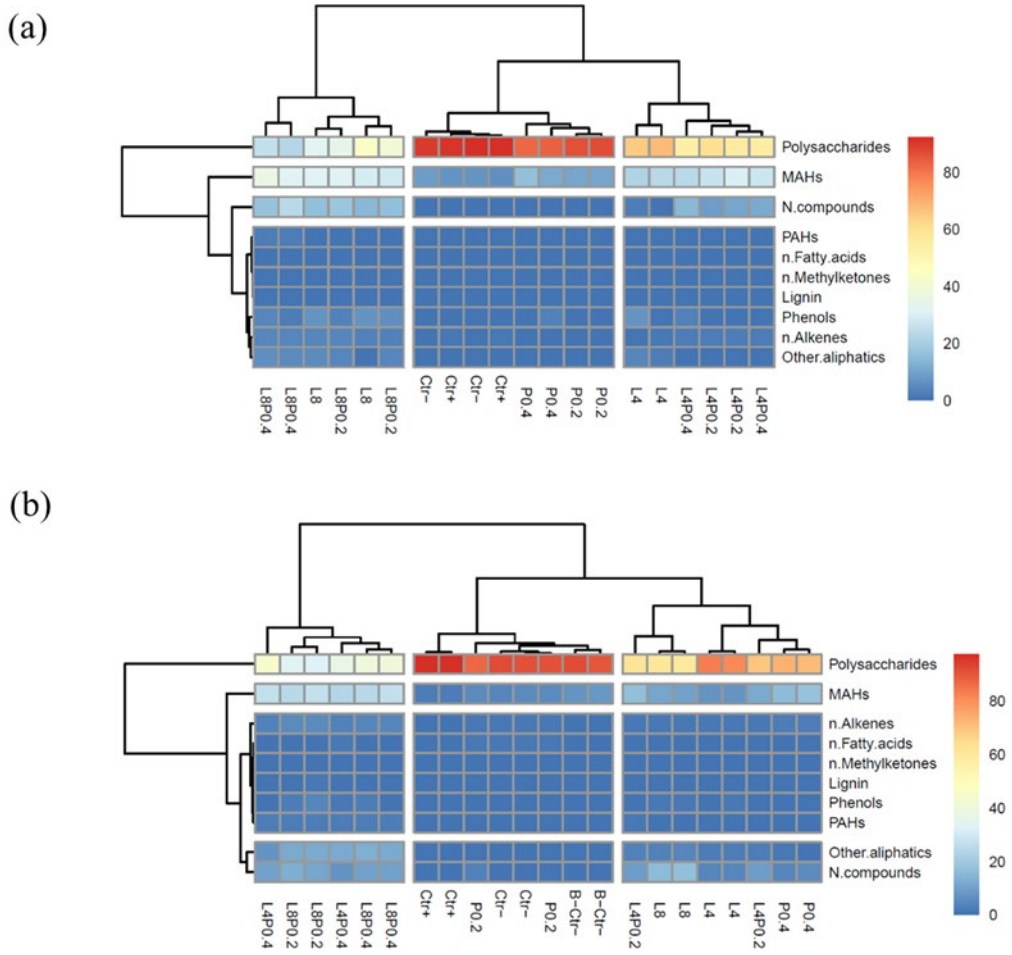

Figure S3.7 Heatmap displaying the two-way cluster analysis of grouped pyrolysis products in (a) the unamended (Ctr-) and amended bulk soils with either $CaCl_2$ (Ctr+), individual lime (at addition rates of 4 and 8 g/kg, L4 and L8), individual P (at addition rates of 0.2 and 0.4 g P/kg, P0.2 and P0.4), or combined lime and P additions (L4P0.2, L4P0.4, L8P0.2 and L8P0.4) at different application rates, as well as in (b) the unamended (Ctr-) and amended heavy fraction samples with these additions and the Ctr- of the bulk soil (B-Ctr-).

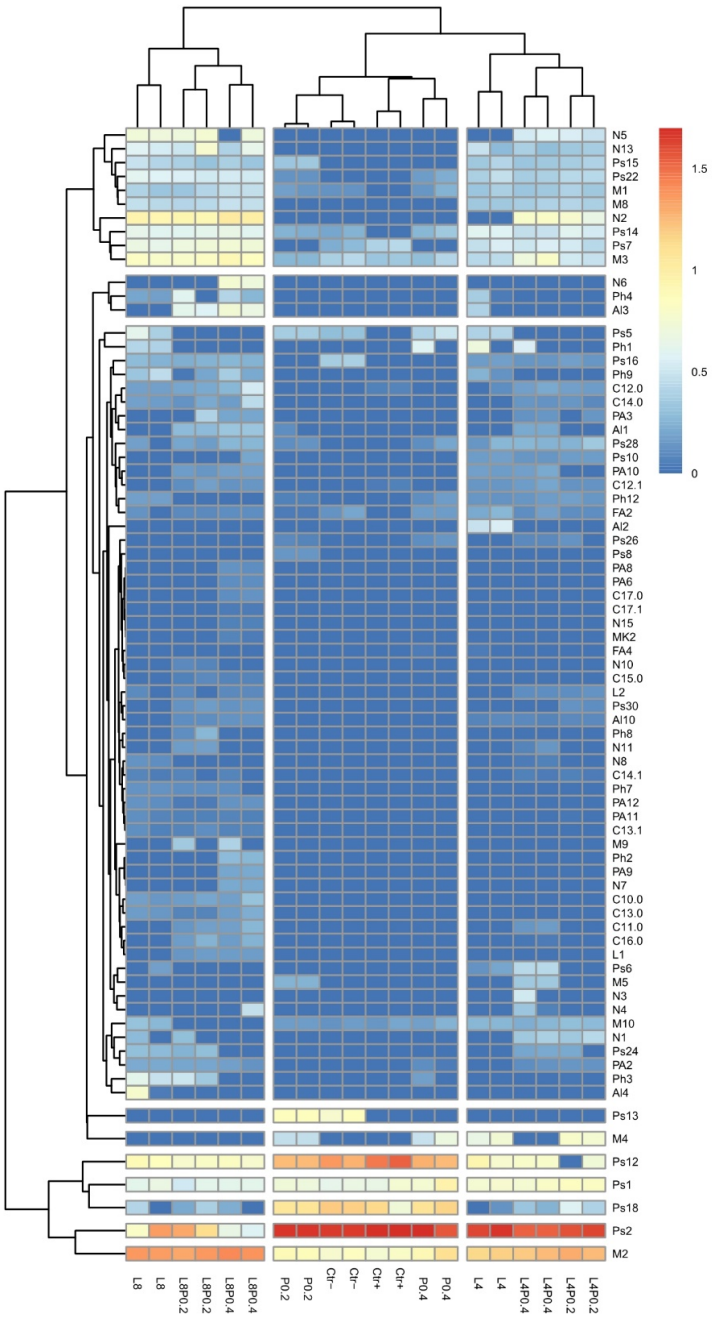

Figure S3.8 Heatmap displaying the two-way cluster analysis of pyrolysis products in the unamended (Ctr-) and amended bulk soils with either $CaCl_2$ (Ctr+), individual lime (at addition rates of 4 and 8 g/kg, L4 and L8), individual P (at addition rates of 0.2 and 0.4 g P/kg, P0.2 and P0.4), or combined lime and P additions (L4P0.2, L4P0.4, L8P0.2 and L8P0.4) at different application rates.

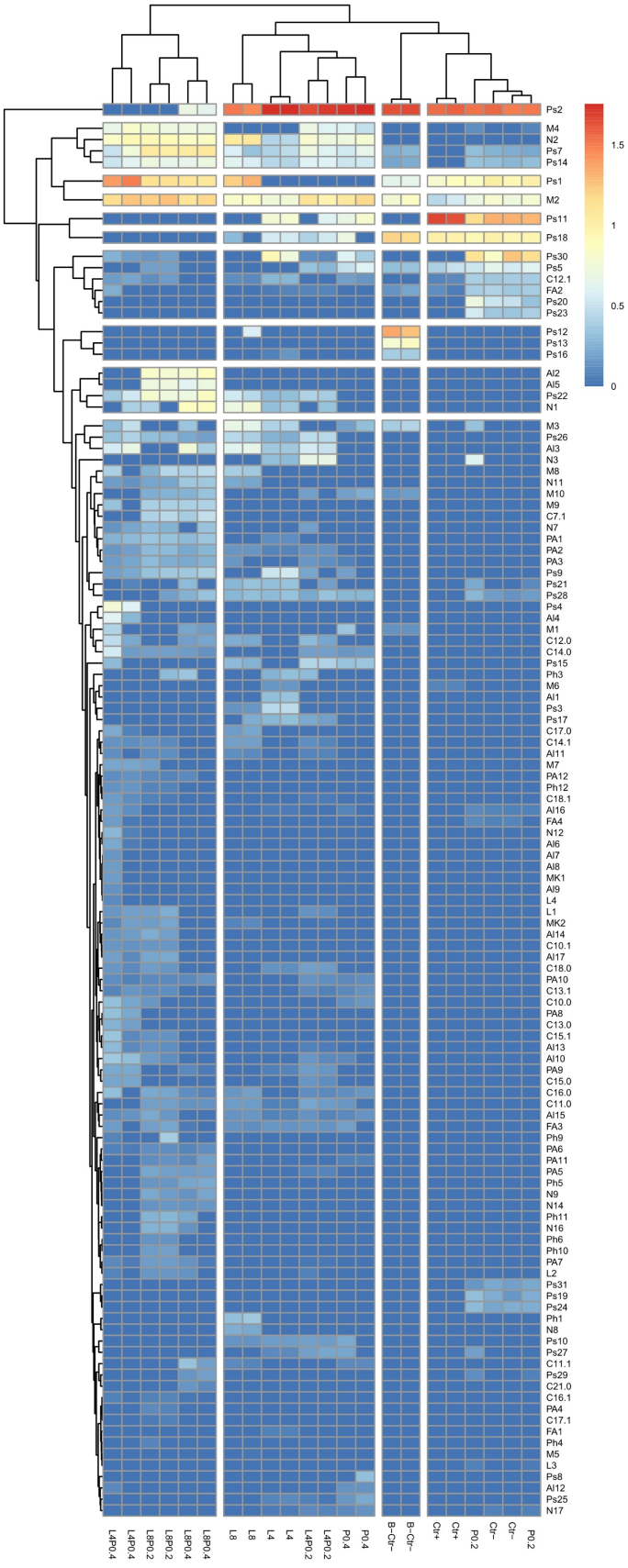
Ps2
M4
N2
Ps7
Ps14
Ps1
M2
Ps11
Ps18
Ps30
Ps5
C12.1
FA2
Ps20
Ps23
Ps12
Ps13
Ps16
AI2
AI5
Ps22
N1
M3
Ps26
AI3
N3
M8
N11
M10
M9
C7.1
N7
PA1
PA2
PA3
Ps9
Ps21
Ps28
Ps4
AI4
M1
C12.0
C14.0
Ps15
Ph3
M6
AI1
Ps3
Ps17
C17.0
C14.1
AI11
M7
PA12
Ph12
C18.1
AI16
FA4
N12
AI6
AI7
AI8
MK1
AI9
L4
L1
MK2
AI14
C10.1
AI17
C18.0
PA10
C13.1
C10.0
PA8
C13.0
C15.1
AI13
AI10
PA9
C15.0
C16.0
C11.0
AI15
FA3
Ph9
PA6
PA11
PA5
Ph5
N9
N14
Ph11
N16
Ph6
Ph10
PA7
L2
Ps31
Ps19
Ps24
Ph1
N8
Ps10
Ps27
C11.1
Ps29
C21.0
C16.1
PA4
C17.1
FA1
Ph4
M5
L3
Ps8
AI12
Ps25
N17
1.5
1
0.5
0
L4P0.4
L4P0.4
L8P0.2
L8P0.2
L8P0.4
L8P0.4
L8
L8
L4
L4
L4P0.2
L4P0.2
P0.4
P0.4
B−Ctr−
B−Ctr−
Ctr+
Ctr+
P0.2
Ctr−
Ctr−
P0.2

Figure S3.9 Heatmap displaying the two-way cluster analysis of pyrolysis products in unamended (Ctr-) and amended heavy fraction samples with either $CaCl_2$ (Ctr+), individual lime (at addition rates of 4 and 8 g/kg, L4 and L8), individual P (at addition rates of 0.2 and 0.4 g P/kg, P0.2 and P0.4), or combined lime and P additions (L4P0.2, L4P0.4, L8P0.2 and L8P0.4) at different application rates, as well as Ctr- of bulk soil (B-Ctr-).

CHAPTER 4

FUNCTIONAL COMPLEXITY EXPLAINS THE DEPTH-DEPENDENT RESPONSE OF ORGANIC MATTER TO LIME AND/OR PHOSPHORUS FERTILISER APPLICATION AT NANOMETRE-SCALE

Abstract

The development of effective strategies to maintain/increase soil carbon is hindered by the poor process-level understanding of the impact of management practices on carbon preservation at different soil depths. We have investigated the effect of the addition of plant litter, lime, and phosphorus fertilizer on organic matter (OM) turnover in a volcanic soil classified as Andosol – the mineral soil with the largest organic carbon content worldwide. By separately incubating the top- and sub-soil layers, we found that the inorganic amendments only impact the net CO_2 evolution from the subsoil. By combining nano-scale secondary ion mass spectrometry and isotope tracing, we show that lime addition favours the formation of OM-mineral associations in the subsoil but inhibits it in the topsoil. The increase in functional complexity with depth contributes to the depth-dependent response of soil OM to these amendments. Our study has major implications for designing climate-smart management practices.

4.1 Introduction

Soil organic matter (OM) makes up the largest reservoir of organic carbon (C) in terrestrial ecosystems (Flato et al., 2014; Lefèvre et al., 2017). Most soil OM forms through partial decomposition and transformation of plant residues by microorganisms – with this process generating the second largest terrestrial flux of carbon dioxide (CO_2) into the atmosphere (Bond-Lamberty and Thomson, 2010). In recent years, the potential of soils to sequester C has been recognized as a way to counterbalance the current increase in atmospheric CO_2 (Pachauri et al., 2014; Rumpel et al., 2020). Mounting evidence shows that OM preservation in soil is governed by interactions with minerals (either physically within aggregates or through chemical binding) rather than chemical recalcitrance against microbial decomposition (Dungait et al., 2012; von Lützow et al., 2008). In fact, the persistence of soil OM was recently proposed to be caused by functional complexity (e.g., molecular diversity, spatial heterogeneity, temporal variability in soil systems), with OM physical and chemical protection contributing to this complexity (Lehmann et al., 2008). The chemical association of OM with mineral surfaces and metal cations to form OM-mineral/metal complexes is considered one of the most important mechanisms for OM persistence in soil (Hemingway et al., 2019; Kleber et al., 2015; Kögel-Knabner et al., 2008). The strength and stability of the bonds between OM and minerals (inorganic constituents) decreases with increasing distance from the surfaces (Kleber et al., 2015; Kleber et al., 2007). Organo-mineral interactions are proposed to follow a discrete zonal sequence, forming a "membrane-like bilayer" consisting of an inner layer of species with charged functional groups that adsorb strongly due to electrostatic interactions and an outer layer of material held by weaker hydrophobic interactions (Kleber et al., 2007). These

interactions can also be viewed as an array of combinations of molecular diversity and spatial heterogeneity (Lehmann et al., 2008), and are regulated by many factors, such as soil properties, climatic conditions, and land use and management (Wiesmeier et al., 2019).

Soil management practices (e.g., fertilisation, liming and tillage) are known to affect organic C stocks in topsoils and subsoils (Smith et al., 2016; Wiesmeier et al., 2019). Phosphorus (P) fertiliser and lime are commonly added to soil to sustain soil fertility and offset soil acidity (Fornara et al., 2011; Haynes, 1984; Hedley and Bolan, 2003). In addition to their influence on (i) the OM input to soil by enhancing plant growth, and (ii) microbial decomposition of OM, P fertiliser and lime may also affect the mechanisms by which OM interacts with soil minerals. For instance, the alkalinisation of soil weakens the formation of inner-sphere bonding between reactive inorganic constituents (e.g., aluminium (Al)/iron (Fe) (hydr)oxides) and organic ligands, and favours the weaker outer-sphere bonding (Kleber et al., 2015). Phosphate ions added through the application of P fertilisers outcompete many organic ligands for reactive sites on soil inorganic constituents (Hiemstra et al., 2010; Kaiser and Zech, 1997; Spohn and Schleuss, 2019). These effects may vary with soil depth, given differences in molecular complexity of OM, soil pH, and reactive surfaces within the soil profile (Lehmann et al., 2008; Rumpel et al., 2015; Spielvogel et al., 2008). Yet less attention has been paid to the differential responses between soil horizons to these amendments.

In this study, a C-rich Andosol was chosen as a representative benchmark soil. Andosols are the mineral soils with the largest OM content worldwide (Eswaran et al., 1993), and have been deemed as an archetype of soils rich in OM associations with reactive Fe and Al (Possinger et al., 2020). Due to their high physical fertility, if managed properly, Andosols

can play an important role in agricultural production (Dahlgren et al., 2004). Their agricultural management includes amendments of lime and phosphorus, as these soils have low available P (due to high P retention) and an acid pH (Bolan and Hedley, 2003; Dahlgren et al., 2004). The two key chemical mechanisms through which OM is protected in Andosols are by the formation of OM-metal complexes (e.g., OM-Al^{3+} complexes, particularly abundant in alu-andic Andosol) and OM-mineral associations (e.g., OM-allophane association, particularly abundant in sil-andic Andosol) (Matus et al., 2014; Verde et al., 2010; Wagai et al., 2018). In the soil under study here, these two biogeochemical conditions can be observed within the profile, with OM-Al^{3+} complexes being dominant in the topsoil and allophane increasing in the subsoil. Studying these two biogeochemical systems within a single soil profile therefore provides a unique opportunity to disentangle how these two OM-protecting mechanisms are affected by P fertilisation and liming.

The aim of the study was to investigate how lime and P additions impact OM preservation in a topsoil (rich in OM-Al^{3+} complexes; pH 5.6) and a subsoil (with a greater abundance of allophane; pH 5.9) of an alu-andic Andosol, with a special attention to OM decomposition and OM surface coverage of soil particles in microaggregates upon addition of plant residue (simulating the incorporation of crop residues to soil). We incubated the topsoil and subsoil together with the different amendments (plant residue, lime, and phosphate fertiliser) for 6 months to investigate their effects on the fate of soil OM in the different soil horizons. The plant residue was ^{13}C- and ^{15}N-labelled barley litter, so that we could distinguish between C sequestered in inherited OM (OMi) and OM newly formed from the barley litter (OMn). We characterised the impact of the amendments on the fate

and distribution of soil OM using (i) conventional chemical analyses of the bulk soil, and (ii) nano-scale secondary ion mass spectrometry (NanoSIMS) analysis of soil microaggregates <30 μm in size. The major aim was to study how microscale heterogeneities in soil particle surface chemistry determines the OM coverage of soil microaggregates. The quantitative bulk and the microscale imaging approaches were combined to explore how (i) the changes at the microscopic scale could account for the changes in OM dynamics caused by the amendments, and (ii) the contrasting biogeochemistry and functional complexity of the two soil layers contributed to explain these changes.

4.2 Materials and methods

4.2.1 Soil and litter characterisation

The soil was sampled in February 2019 on the eastern flank of Mount Taranaki (New Zealand) at an elevation of 512 m (asl) (39°19'15.82"S; 174°11'18.05"E). Annual precipitation is ca. 2,022 mm and the mean annual temperature is ca. 8.6 °C at Stratford, Taranaki. Topsoil and subsoil samples were collected at 0–20 cm and 20–40 cm, respectively, under a C_3 native forest vegetation, which includes Kaikawaka (*Libocedrus bidwillii* Hook.f.) and Kohekohe (*Dysoxylum spectabile* (G.Forst.) Hook.f.) trees. After removing identifiable plant residues and other coarse material, soils were sieved (<4 mm) and stored for two weeks at ca. 4 °C prior to their use.

Soil characterisation was carried out as follows. Water holding capacity at -10 kPa was determined using a suction plate (Loveday, 1974). Soil pH was measured at a soil:solution ratio of 1:2.5 (in either deionised water or 1M KCl) using a standard glass electrode. Olsen

P was extracted following Olsen et al. (1954) and determined by the phosphomolybdate method of Murphy and Riley (1962). Total P was determined using a vanadomolydate method after Kjeldahl digestion (McKenzie and Wallace, 1954). Reactive Al, Fe and silicon (Si) in short-range constituents and/or OM-Al/Fe complexes (Al_o, Fe_o and Si_o, respectively) were extracted with 0.1 M acidic ammonium oxalate (pH=3) (Blakemore, 1972). The Al and Fe (mostly in OM-Al/Fe complexes) that could be removed by complexation with phosphate ions (Al_p and Fe_p) were quantified by extraction with 0.1 M sodium pyrophosphate (ca. pH=10) (Bascomb, 1968). The concentrations of Al, Fe and Si in all extractants were measured by microwave plasma atomic emission spectroscopy (4200 MP-AES, Agilent Technologies, Singapore). Allophane content was estimated following the method of Mizota and Van Reeuwijk (1989). Soil C and N contents were measured using an elemental analyser (Elementar, Vario MACRO, Germany). The sodium pyrophosphate-extractable C (C_p) content was determined using a Total Organic Carbon Analyser (TOC-LCSH, Shimadzu, Japan).

The ^{13}C- and ^{15}N-labelled barley residue (air dried, ground and sieved <2 mm) was provided by Plant & Food Research Limited (New Zealand). This isotope-labelled litter had a C content of 40.5% (d.w. basis), an N content of 0.6% (d.w. basis), and a C/N-ratio of 67.5. The ^{13}C and ^{15}N enrichment was 6.1 atom-% and 3.5 atom-%, respectively (section S4.1.1 in Supporting Information for Chapter 4, SI4). Isotope signatures were measured by a Carlo ErbaNA1500 elemental analyser connected to a Thermo Delta Plus Advantage isotope ratio mass spectrometer at Isotrace Research (Dunedin, New Zealand).

4.2.2 Soil incubation

Each soil sample (equivalent to 30 g oven-dried) was thoroughly mixed and incubated with (or without) inorganic amendments (either lime, phosphate or lime+phosphate) in the presence or absence of an organic amendment (^{13}C- and ^{15}N- labelled barley, *Hordeum vulgare* L.), as shown in Figure S4.1. The unamended topsoil and subsoil were considered the negative control (Ctr-). The topsoil and subsoil to which 3% (wt basis) ^{13}C- and ^{15}N-labelled barley residue (LR) was added were referred to as positive control (Ctr+). There were 3 treatments with inorganic amendments, including the addition of lime (3 mg $CaCO_3$/g, labelled as L), P (300 mg P/kg in the form of KH_2PO_4), and combined lime and P (labelled as PL) to either topsoil (TS-L, TS-P and TS-PL) or subsoil (SS-L, SS-P and SS-PL) without residue. The inorganic amendments were also added to the topsoil or subsoil that received labelled residue (LR-L, LR-P, and LR-PL). Given that lime (^{13}C enrichment=1.09 atom-%) also contributed to the isotopic signature, the topsoil and subsoil were incubated with unlabelled residue and lime additions (with or without P) only for partitioning of CO_2 sources, e.g., lime, OMi and OMn. After adjusting the soil moisture to 60% water holding capacity (Vogel et al., 2014), the soils were placed in a 50 mL plastic container and incubated in 0.5 L air-tight glass jars, under darkness at 20 °C for 6 months. There were three experimental replicates per treatment. The sealed jars were vented (for ca. 2 hours each time the NaOH solution was replaced) for air circulation and resealed thereafter. To keep the soil moisture constant, 5 mL 0.1% HNO_3 was added to the bottom of the jar to ensure a humid atmosphere and prevent from the CO_2 dissolved in water.

4.2.3 Soil CO_2 evolution measurement

During the incubation, emitted CO_2 was trapped by 0.25 M NaOH (20 mL) contained in a vial in the jar. The amount of trapped CO_2 was measured using an electrical conductivity meter (HI 8733, Hannah instrument, US) following a modified version of the protocol of Whitman et al. (2014). The NaOH solution was used instead of KOH here. There was a strong linear relationship between the injected CO_2 volume and electrical conductivity (EC) values of NaOH traps measured after 24-hour equilibrium. The CO_2 evolution measurements were taken at day 3, 7, 14, 21, 28, 35, 42, 49, 56 and 63, and thereafter every two weeks from day 64 to day 175.

The $\delta^{13}C$ of CO_2 from all the soils was measured using a Thermo Advantage Isotope Ratio Mass Spectrometer (IRMS) (Thermo, Bremen) following the method of Herath et al. (2015). The fractional contributions of OMi and OMn (f_{OMi} and f_{OMn}) to the total CO_2 evolution from unlimed soils that received residue either with or without P, as well as fractional contributions of OMi, OMn and lime (f_{OMi}, f_{OMn} and f_{lime}) to total CO_2 evolution from soils amended with both residue and lime additions were estimated. The equations used for the partitioning of CO_2 sources in the soils amended with different additions are provided in the section S4.1.2 in SI4.

The total priming effect of the residue amendment on OMi decomposition during the 6-month incubation was calculated based on the difference in cumulative C mineralisation from OMi (C_{OMi}) between the amended soil and the corresponding Ctr-:

$$Priming\ effect\ \% = \frac{C_{OMi(amended\ soil)} - C_{OMi(Ctr-)}}{C_{OMi(Ctr-)}} \times 100 \qquad \text{(eq. 4.1)}$$

4.2.4 Physicochemical characterisation of the incubated soils

At the end of the 6-month incubation, soil pH, and the contents of total C, total N, C_p, allophane and Al_o+½Fe_o were measured as described above. The water-extractable organic C (WEOC), was given by the sum of cold water-extractable organic C and hot water-extractable organic C. Samples of the incubated soils (equivalent to 3 g d.w.) were first extracted with 18 mL deionised water in a centrifuge tube at room temperature (ca. 20 °C) for 1 hour. After centrifugation, the supernatant was passed through a filter paper (Whatman No 42) and analysed. The soil residues in the tubes were resuspended with 18 mL deionised water before being placed in a water bath (80 °C) for a 16-hour hot water extraction. Thereafter, the hot water-extractable fraction was collected as described above (Curtin et al., 2015). The organic C content in cold water and hot water extracts determined using a Total Organic Carbon Analyser was only used for calculation of the total WEOC. Inorganic C in soil was determined by measuring CO_2 released after acid addition, following the method of Bundy and Bremner (1972) modified by Wang et al. (2014); CO_2 was measured by electrical conductivity analysis as described above (see section S4.1.3 in SI4).

4.2.5 Nano-scale secondary ion mass spectrometry analysis.

NanoSIMS (Cameca NanoSIMS 50l, France) was used to visualise and quantify the spatial distribution of OM (including OMi and OMn) on mineral surfaces in the free soil microaggregates. In addition to the unamended soils (Ctr-), which were chosen for the characterisation of the distribution of the OMi on the mineral surface, the soils that received ^{13}C- and ^{15}N-labelled residue incubated with (or without) inorganic amendment were studied to distinguish the OMn (enriched in ^{13}C and/or ^{15}N) from the OMi (with natural

isotopic signal) on the mineral surface. The soil microaggregates were prepared according to Kopittke et al. (2020) and Keiluweit et al. (2012) with some modifications. Specifically, the air-dried soil sample (20 mg) was dispersed in 10 mL of deionised water by gently shaking (1 min). The larger particles were allowed to settle (5 min), and 100 µL of the suspension containing the free stable microaggregates was placed on a GaAs wafer (7×7 mm) and dried overnight in a desiccator. After drying, microscopic images of the samples were taken by reflected-light microscope (Axio Imager Z2m, Zeiss, Germany) for documentation and later orientation on the sample.

The NanoSIMS analyses were performed at the Chair of Soil Science of the Technical University of Munich, Germany. To avoid charging during the measurements, the samples were coated with an Au/Pd layer (~30 nm). The Cs^+ primary ion probe was used with a primary ion impact energy of 16 keV. Prior to the measurement, contaminants and any additional Au/Pd coating layer were sputtered away by a high primary beam current (pre-sputtering). During the pre-sputtering, the reactive Cs^+ ions are implanted into the sample to enhance the secondary ion yields. The primary beam (~2 pA) focused at a lateral resolution of 100–200 nm was scanned over the sample, while $^{12}C_2^-$ ($^{12}C^{12}C^-$), $^{13}C^{12}C^-$, $^{12}C^{14}N^-$, $^{12}C^{15}N^-$, $^{16}O^-$ and $^{27}Al^{16}O^-$ secondary ions were detected using electron multipliers with an electronic dead time fixed at 44 ns. The instrument was tuned for high mass power resolution to accurately resolve any mass interferences (Nuñez et al., 2018). In addition to the Au/Pd layer, we compensated for the charging due to the non-conductive mineral particles by using the electron flood gun of the NanoSIMS instrument. All measurements were accomplished in imaging mode. The ion images were acquired using a dwell time of 1 ms/pixel, 40 planes, with 256×256 pixels for a 30×30 µm. For every sample, 5–9 spots

were analysed to obtain reliable data for the calculation of the fate of ^{13}C and ^{15}N.

NanoSIMS images were analysed using the OpenMIMS plugin (https://usermanual.wiki/Pdf/OpenMimsManual.682350371/view) within Fiji-ImageJ-win64 software (Schindelin et al., 2012). All images were corrected for electron multiplier dead time (44 ns), drift corrected and the planes accumulated. Regions of interest (ROIs) were selected using the threshold option of the ImageJ software with the Yen algorithm. The ROIs of the $^{12}C_2^-$ and $^{12}C^{14}N^-$ images were combined thereafter to obtain the ROIs for the OM distribution on mineral particles selected as ROIs on the basis of $^{16}O^-$ images. The OM coverage on the mineral surface was computed by dividing total area of OM coatings ($^{12}C_2^-$+$^{12}C^{14}N^-$) by total area of mineral particles ($^{16}O^-$). The entire ROIs for these images were further split into smaller ROIs through "split" option in the OpenMIMS plugin. All ROIs with an area greater than 5 pixels (ca. 0.6 µm) were used for $^{13}C^{12}C^-/^{12}C_2^-$, $^{12}C^{15}N^-/^{12}C^{14}N^-$, $^{12}C^{14}N^-/^{12}C_2^-$ and $^{12}C_2^-/^{27}Al^{16}O^-$ ratio calculations. These ratios were used to compute the $^{13}C/^{12}C$ and $^{15}N/^{14}N$ isotopic composition and represent N/C ratio (relative chemical composition) of OM patches, as well as indicate the relationship between Al and C, respectively. The isotope enrichment, expressed as AP ^{13}C and AP ^{15}N (atom-%), was calculated according to the $^{13}C^{12}C^-/^{12}C_2^-$ and $^{12}C^{15}N^-/^{12}C^{14}N^-$ ratio. It is noted that $^{13}C^{12}C^-/^{12}C_2^-$ ratio value is double compared to the $^{13}C^-/^{12}C^-$ (Nuñez et al., 2018). More details of these calculations are provided in the section S4.1.4 in SI4.

4.2.6 Statistical analysis

One-way ANOVA (analysis of variance) with a Tukey B test was used to analyse the statistical difference ($P<0.05$) in means of different treatments using the SPSS software (IBM

SPSS Statistics Version 24). Principal component analysis of $^{12}C_2^-$, $^{13}C^{12}C^-$, $^{12}C^{14}N^-$ and $^{12}C^{15}N^-$ secondary ions, the $^{13}C^{12}C^-/^{12}C_2^-$, $^{12}C^{15}N^-/^{12}C^{14}N^-$, $^{12}C^{14}N^-/^{12}C_2^-$, $^{12}C_2^-/^{27}Al^{16}O^-$, $^{13}C^{12}C^-/^{27}Al^{16}O^-$, $^{12}C^{14}N^-/^{27}Al^{16}O^-$ and $^{12}C^{15}N^-/^{27}Al^{16}O^-$ ratio and OM coverage obtained from the NanoSIMS analyses of topsoils and subsoils incubated with LR (Ctr+), LR-L and LR-PL, and the corresponding Ctr- (incubated without amendment) after 6 months, was performed by SPSS.

4.3 Results

4.3.1 Initial soil properties

The topsoil and subsoil of the Andosol had high total organic C content (95.07 and 67.87 g/kg, respectively), low pH (topsoil: pH_{H_2O}=5.58, pH_{KCl}=4.42; subsoil: pH_{H_2O}=5.90, pH_{KCl}=4.59) and low Olsen P (14.21 and 2.60 mg/kg in topsoil and subsoil, respectively) (Table S4.1). There were notable differences in the content of short-range order constituents (e.g., allophane) and Al^{3+} from OM-Al^{3+} complexes at these two depths. Compared with the topsoil, the subsoil had a significantly greater allophane content (ca. 2.50% in subsoil vs. 0.24% in topsoil), more reactive Al and Fe (as inferred by Al_o+½Fe_o, ca. 2.29% in subsoil vs. 0.91% in topsoil), and a lower proportion of OM-Al^{3+} complexes out of total reactive Al (as inferred from the ratio of Al_p/Al_o, ca. 0.71 in subsoil vs. 1.15 in topsoil) (Table S4.1).

4.3.2 Influence of amendments on soil pH, mineral composition and organic C

Lime application (with and without P), increased the soil pH (regardless of soil depth) and caused an increase in Al_o +$^1/_2Fe_o$ and allophane contents in the subsoil (Table S4.2).

Phosphate alone tended to increase soil pH but had negligible effects on Al_o+½Fe_o and allophane content at either depth. The inorganic amendments did not cause significant changes in the total C and C_p contents of either the topsoil or the subsoil, except for the subsoil incubated with plant residue, lime and P (Figure 4.1a). It should be noted that amendments of P alone always had smaller (negligible) effect on C content at the application rate studied, compared with lime amendment (as shown in Figure S4.2). Thus, P was only used in combination with lime in the studies discussed here. Soil WEOC tended to be more sensitive to the different amendments than the total C and C_p contents (Figure 4.1b). In the topsoil (with or without plant residue), the largest and significant (P<0.05) soil WEOC increase was observed when lime was applied in combination with P (TS-PL and TS-LR-PL, Figure 4.1b). In the subsoil, the additions of either plant residue and/or inorganic addition caused a significant increase in WEOC when compared with the corresponding negative (Ctr-, without any amendment) and positive (Ctr+, with only residue) control. The greatest increase was again observed with the combined amendment of lime and P (SS-PL and SS-LR-PL, Figure 4.1b).

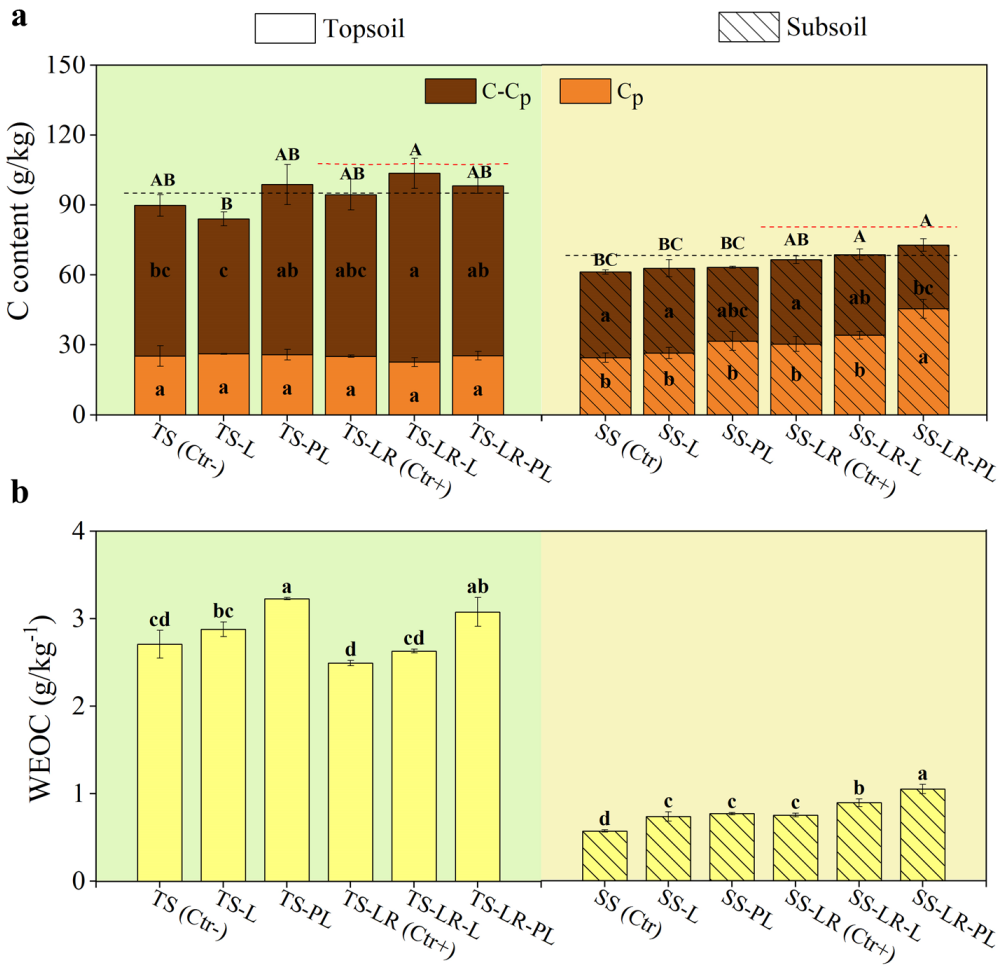

Figure 4.1 Influence of amendments on soil organic carbon (C) content. (a) Total C, $Na_4P_2O_7$-extractable C (C_p) and difference of total C and C_p ($C\text{-}C_p$), and (b) water-extractable organic C (WEOC) content of the topsoil and subsoil after 6 months of incubation with the lime (TS-L and SS-L), combined lime and P (TS-PL and SS-PL), combined residue and lime (TS-LR-L and SS-LR-L), and combined residue, lime and P (TS-LR-PL and SS-LR-PL). The negative control soil samples (TS and SS, Ctr-) were incubated without amendments, while the positive control samples (TS-LR and SS-LR, Ctr+) were treated with plant residue before incubation. The black and red dashed lines show the mean value of total C content of the Ctr- and Ctr+ prior to incubation, respectively. The letters above and in the bars indicate results that are statistically different ($P<0.05$) based on a one-way ANOVA followed by Tukey B test (n=3).

The changes in the CO_2 emission rates of the topsoil and subsoil in response to incubation with the organic residue and inorganic amendments are evident in the cumulative CO_2 emission profiles shown in Figure 4.2. The amount of CO_2 emitted was normalised to the bulk soil total C. Topsoil amended with the organic residue tended to generate similar CO_2 amounts, regardless of the addition of inorganic amendments. On the contrary, subsoil that received both organic residue and lime (SS-LR-L and SS-LR-PL) released more CO_2 than the corresponding Ctr+ (subsoil incubated with residue alone, SS-LR). Less CO_2 was emitted by soils treated only with inorganic amendments. It should be noted that amendments of phosphate alone (TS-P, SS-P, TS-LR-P and SS-LR-P) had little effect on CO_2 emission (as shown in S4.3 in SI4).

The different C sources contributing to the total CO_2 released by the top- and sub-soil samples over the 6-month incubation is shown in Figure 4.3. Adding plant residue caused a drop (significant at $P<0.05$ when comparing TS-PL with TS-LR-PL, Figure 4.3a) in total CO_2 evolution from OMi in topsoil (i.e., a negative priming effect on OMi decomposition, Figure 4.3b) and a rise (significant at $P<0.05$ when comparing SS-PL with SS-LR-PL, Figure 4.3a) in total CO_2 evolution from OMi in subsoil (i.e., a positive priming effect on OMi decomposition, Figure 4.3b). The direct contribution of C in lime to total CO_2 evolution was similar in all limed treatments (ca. 0.4 mg C/g soil from ca. 100% dissolution of $CaCO_3$, Table S4.3). Lime amendments also caused an increase in the decomposition of OM in some cases, particularly in SS-LR-PL.

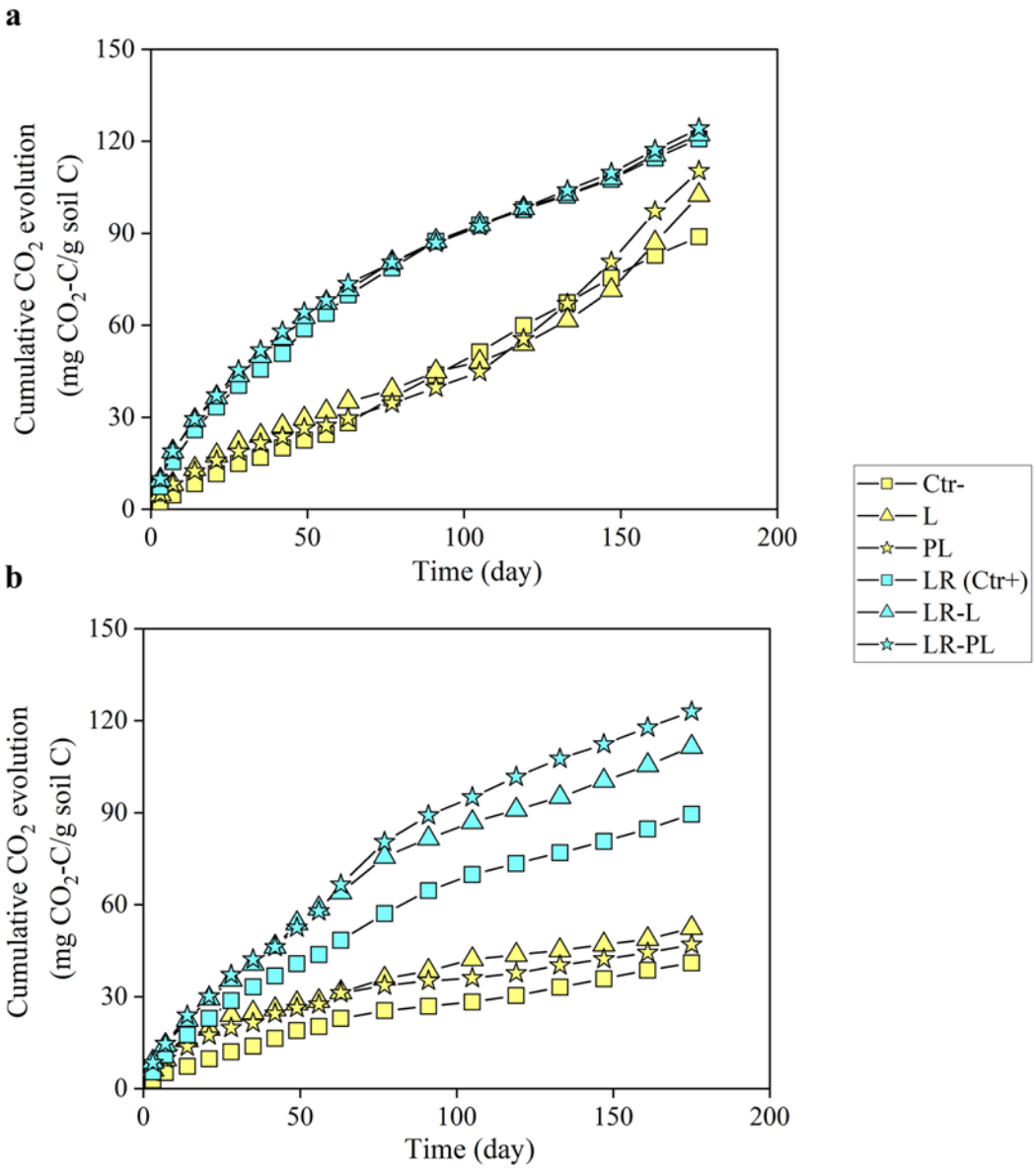

Figure 4.2 Influence of amendments on carbon dioxide (CO_2) evolution from soils during incubation period. Cumulative CO_2 evolved from (a) topsoil and (b) subsoil samples during 6 months of incubation with either lime (L), combined lime and P (PL), combined residue and lime (LR-L), or combined residue, lime and P (LR-PL). The negative control soil samples (Ctr-) were incubated without amendments, while the positive control samples were treated with plant residue (LR, Ctr+) before incubation.

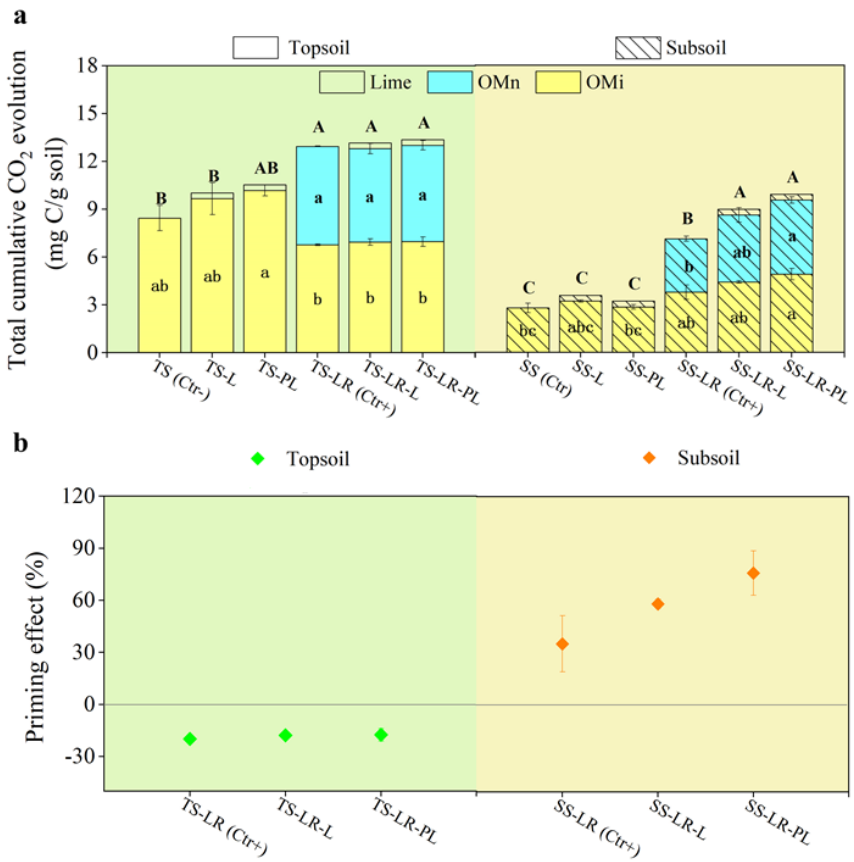

Figure 4.3 Influence of amendments on carbon dioxide (CO_2) released from different carbon (C) sources in soils. (a) Total amount of CO_2 evolved from the lime, organic matter newly formed from plant residue (OMn) and inherited organic matter (OMi) in topsoil and subsoil during 6 months of incubation with the lime (TS-L and SS-L), combined lime and P (TS-PL and SS-PL), combined residue and lime (TS-LR-L and SS-LR-L), and combined residue, lime and P (TS-LR-PL and SS-LR-PL). The negative control soil samples (TS and SS, Ctr-) were incubated without amendments, while the positive control samples (TS-LR and SS-LR, Ctr+) were treated with plant residue before incubation. The letters above and in the bars indicate results that are statistically different (P<0.05) based on a one-way ANOVA followed by Tukey B test (n=2) for the total cumulative CO_2 evolution (capital letters) and the total CO_2 from OMi (small letter) and from OMn (bold small letter). (b) The priming effect is expressed here as the percentage difference between the total amount of C mineralised from OMi in an organic amended soil compared to the corresponding (unamended) Ctr- for different amendments.

4.3.3 Organo-mineral associations at the microscale by NanoSIMS analysis

The soils chosen for this analysis were those that received ^{13}C- and ^{15}N-labelled barley residue and lime amendments (TS-LR-L, TS-LR-PL, SS-LR-L and SS-LR-PL), as well as both Ctr- (incubated without amendments, TS and SS) and Ctr+ (incubated with only labelled residue, TS-LR and SS-LR) controls. This is because the above-mentioned results indicated that P addition alone always had little effects on soil organic C dynamics, as shown in Figures S4.2–S4.4, probably due to the small P application rate used, as noted by Li et al. (2020). It should also be noted that treatment with lime alone and combined lime and P addition (TS-LR-L and TS-LR-PL, SS-L-LR-L and SS-LR-PL) had the same effect on the distribution of OM on mineral surfaces, and thus the results of the latter treatment (TS-LR-PL and SS-LR-PL) are shown only in the SI4 (Table S4.4 and Figures S4.5 and S4.7–S4.9).

In this Andosol, a high proportion (calculated to be 44.5%, Table S4.4) of the topsoil mineral particles were covered with OM (i.e., the coloured areas, Figure 4.4a). The OM coverage of mineral particles was three-times lower in the subsoil compared to the topsoil (Figure 4.4b, Table S4.4). The distribution of OM on the mineral surfaces was not homogeneous (Figure 4.4a, b). Some mineral particles had no detectable OM attached. Many OM patches were observed on the surfaces of inorganic constituents highly enriched with Al. This was inferred from the correlation between the $^{12}C_2^-$ and $^{12}C^{14}N^-$ signatures from the OM coatings and the $^{27}Al^{16}O^-$ signature from the inorganic constituents, as shown in Figure S4.6.

The $^{12}C^{14}N^-/^{12}C_2^-$ ratio of the OM patches was used to assess the N/C ratio of OM coating,

based on the work of Alleon et al. (2015) who reported that the $^{12}C^{14}N^{-}/^{12}C_2^{-}$ ratio of some organic compounds had direct relationship with their N/C ratio. The variability in the $^{12}C^{14}N^{-}/^{12}C_2^{-}$ ratio of OM coatings in the topsoil and subsoil is apparent in Figure 4.4c, d. Some OM patches showed a ratio >1 (yellow to orange to pink colours), which indicates OM rich in N (high N/C ratio). Other OM patches had a ratio <1 (blueish colours), indicative of N-poor OM (low N/C) (Schweizer et al., 2018). The topsoil showed a larger relative proportion of the OM coatings with low $^{12}C^{14}N^{-}/^{12}C_2^{-}$ ratio (as blue patches in Figure 4.4c), resulting in a lower mean $^{12}C^{14}N^{-}/^{12}C_2^{-}$ ratio of the OM coating (0.87, marked as a red line in the gradient colour bar). In comparison, the subsoil was dominated by OM coatings (as pink patches in Figure 4.4d) with high $^{12}C^{14}N^{-}/^{12}C_2^{-}$ ratio (mean=1.06, marked as a red line in the gradient colour bar).

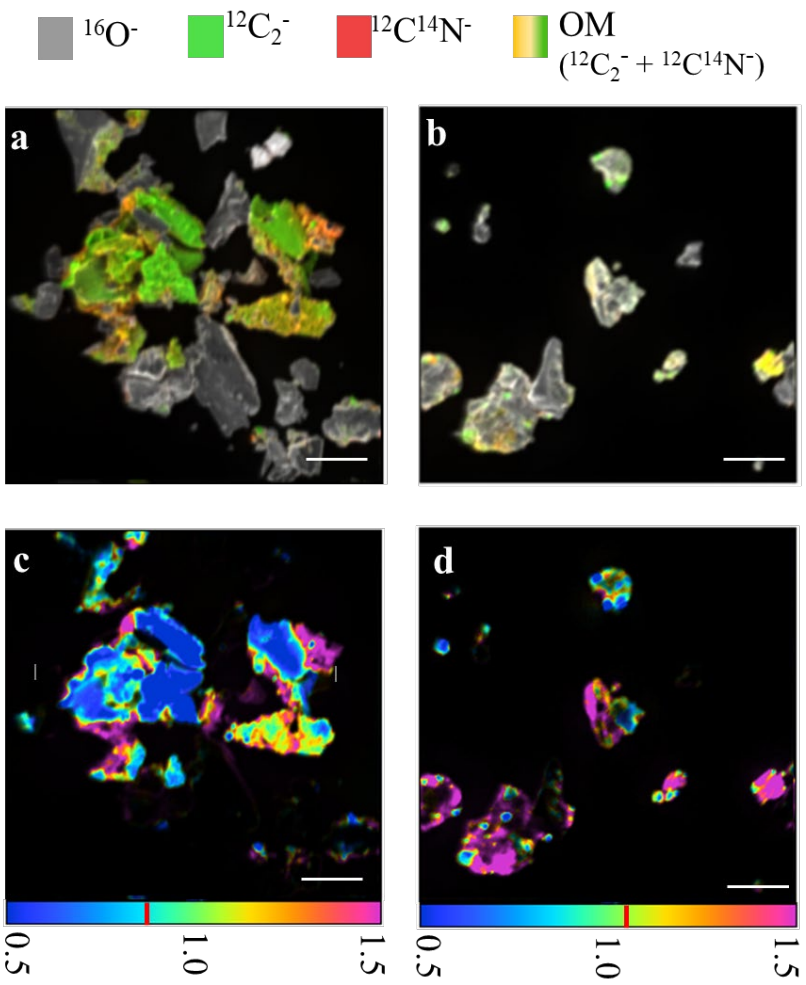

Figure 4.4 Difference between inherited organic matter (OMi) coatings on mineral surfaces in topsoil (left panels) and subsoil (right panels) incubated without amendments for 6 months (TS and SS, Ctr-). The upper images (a, b) are maps of the spatial distribution of ion species derived from organic and inorganic components. They show that a larger proportion of (a) topsoil particles are coated with organic matter (OM) compared to the (b) subsoil, and that there is a heterogeneous distribution of organic carbon ($^{12}C_2^-$), organic nitrogen ($^{12}C^{14}N^-$) and OM ($^{12}C_2^-$+$^{12}C^{14}N^-$) coatings on the mineral particles (identified by a $^{16}O^-$ signal). The lower images (c, d) are hue-saturation-intensity (HSI) maps of the ratio of $^{12}C^{14}N^-/^{12}C_2^-$ indicating the relative proportion of nitrogen in the OM coatings in (c) topsoil and (d) subsoil. The red marker in the gradient colour bar indicates the average ratio of $^{12}C^{14}N^-/^{12}C_2^-$. Scale bar is 5 µm.

The impact of the amendments of labelled plant residue and combined residue and lime on the chemical composition of the OM coatings on the soil particle surfaces is illustrated in Figure 4.5. The sole addition of labelled plant residue to topsoil and subsoil caused an increase in the OM coverage on the mineral surfaces, as quantified in Table S4.4. The largest increase in relative terms was in the subsoil (SS-LR), where the OM coverage increased by about 10%. This was also reflected in an increase in the total C content of the microaggregates in each soil depth measured by elemental analysis (Table S4.4). The OM coatings on the mineral surfaces showed a high spatial heterogeneity (Figure 4.5a, c). Some were enriched in ^{13}C and/or ^{15}N which led to higher $^{13}C^{12}C^{-}/^{12}C_2^{-}$ and/or $^{12}C^{15}N^{-}/^{12}C^{14}N^{-}$ isotopic ratios, shown as spots with brighter colour than OM patches with natural abundance in Figure 4.5e, g, i, and k. This suggested that OMn had formed, either directly through *ex vivo* microbial modification of plant residue (plant-derived OM), or by the *in vivo* OM turnover via microbial assimilation of plant-derived OM (microbial-derived OM) (Kopittke et al., 2020; Liang et al., 2017; Kopittke et al., 2018). These OMn patches had highly variable $^{13}C^{12}C^{-}/^{12}C_2^{-}$ (Figure 4.5e, g) and $^{12}C^{15}N^{-}/^{12}C^{14}N^{-}$ isotopic ratios (Figure 4.5i, k). Most OM patches comprising newly added OM were enriched in both ^{13}C and ^{15}N. Some OMn patches dominated by fresh OM had a high $^{13}C^{12}C^{-}/^{12}C_2^{-}$ ratio and a relatively low $^{12}C^{15}N^{-}/^{12}C^{14}N^{-}$ ratio (see arrows in Figure 4.5e, i), the latter being closer to its natural ^{15}N abundance. The relative magnitudes of the isotope ratios were reversed for other OMn which, instead, showed a relatively low (or undetectable) $^{13}C^{12}C^{-}/^{12}C_2^{-}$ ratio, like its natural ^{13}C abundance (see arrows in Figure 4.5g, k).

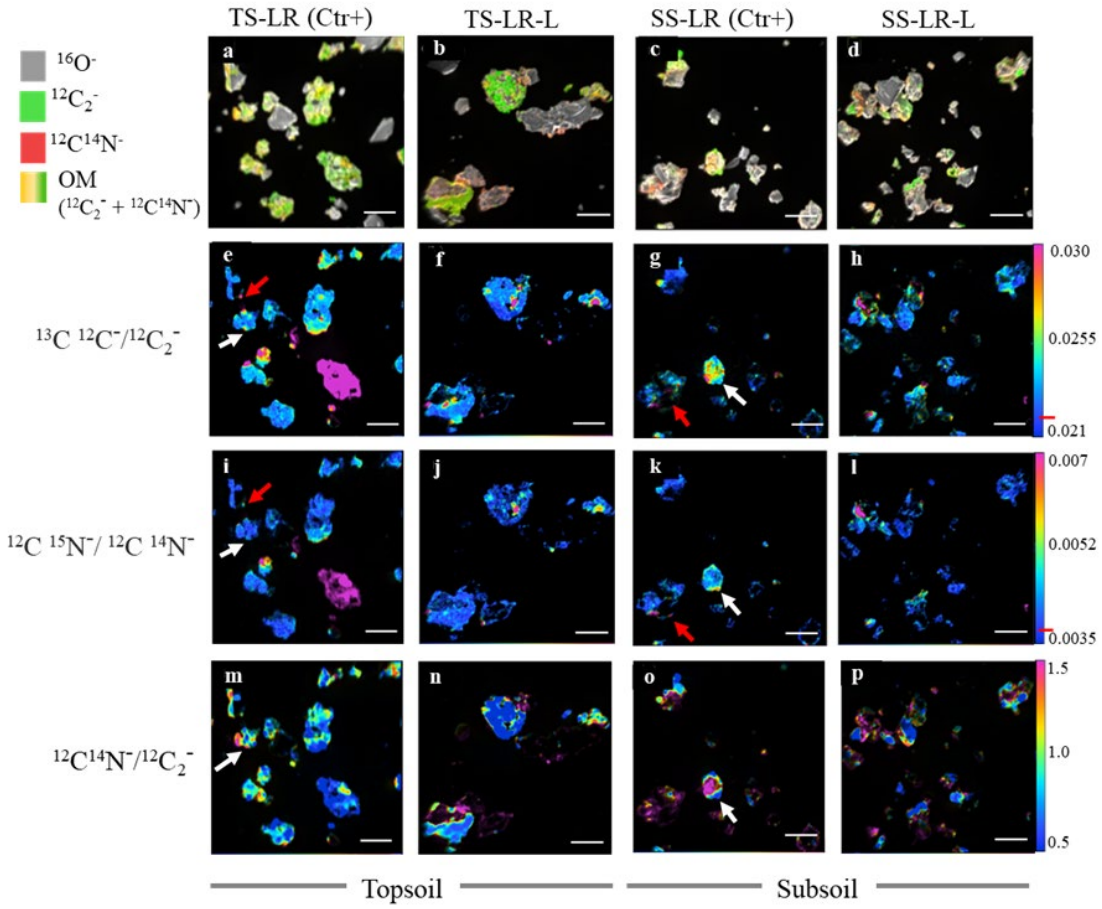

Figure 4.5 Influence of amendments on the organic matter (OM) coatings on mineral surfaces. The images show free stable microaggregates in topsoils (left panels) and subsoils (right panels) incubated for 6 months with either labelled plant residue (TS-LR and SS-LR, Ctr+) or plant residue and lime (TS-LR-L and SS-LR-L). (a-d) Overlay images showing the distribution of OM (indicated by the $^{12}C_2^-$, $^{12}C^{14}N^-$ signals) on the mineral particles (indicated by the $^{16}O^-$ signal). (e-h) Hue-saturation-intensity (HSI) maps of $^{12}C^{13}C^-/^{12}C_2^-$ ratios and (i-l) maps of $^{12}C^{15}N^-/^{12}C^{14}N^-$ ratios indicating the extent of enrichment of the OM coatings with components from the ^{13}C- and ^{15}N-labelled barley residue. The red markers in the gradient colour bars (h and l) indicate the average ratio of $^{12}C^{13}C^-/^{12}C_2^-$ (ca. 0.022) and $^{12}C^{15}N^-/^{12}C^{14}N^-$ (ca. 0.0039) in inherited OM (OMi), respectively. (m-p) HSI maps of $^{12}C^{14}N^-/^{12}C_2^-$ ratios indicating the relative proportion of nitrogen in the OM coatings.

To evaluate this in more detail, the isotope enrichment (AP ^{13}C and AP ^{15}N) was calculated from the relative abundance of the ^{13}C (^{15}N) isotopes to the ^{12}C (^{14}N) isotopes in the OM coatings identified in images of each soil sample. In the unamended topsoil and subsoil (TS and SS, Ctr-), the isotope enrichment of OMi ranged between 0.89 and 1.43 atom-% for AP ^{13}C. The mean value (1.08–1.09 atom-%, as indicated by a red dash line Figure 4.6a) was about the same as that in bulk soil (1.1 atom-% for ^{13}C enrichment) measured by IRMS. Similar observations were made for the ^{15}N enrichment (Figure S4.7b). The addition of labelled residue to the topsoil and the subsoil increased the heterogeneity in the OM. This was made evident by the wider ranges of AP ^{13}C in the amended topsoil (TS-LR: 0.99–8.92 atom-%, Figure 4.6a). In TS-LR, there were a few OMn patches having extremely high AP ^{13}C (and AP ^{15}N). These outliers in Figure 4.6a, could represent either unprocessed or poorly-processed plant residue. Adding labelled residue also affected the overall N/C ratio in the topsoil, as shown by the $^{12}C^{14}N^-/^{12}C_2^-$ ratio of OM coatings in Figure 4.6b. There was a decrease in the mean value of the ratio from 0.87 in the unamended topsoil (TS, Ctr-) to 0.76 in topsoil incubated with labelled plant residue (TS-LR, Ctr+). There were no appreciable changes in the overall N/C ratio in subsoil amended with labelled residue (SS-LR, Figure 4.6b).

Incubation with lime and barley litter caused opposite effects on the OM distribution on the mineral surface of the topsoil and subsoil. In the topsoil treatments, these amendments caused an apparent drop in the OM coverage as shown in Table S4.4. There was a rise in the mean $^{12}C^{14}N^-/^{12}C_2^-$ ratio (increasing from 0.76 in soil amended with only residue to 1.27 when amended with residue+lime, Figure 4.6b). In contrast, for the subsoil treatments, the lime amendments resulted in an apparent increase in OM coverage (Table S4.4), along

with a drop in the mean $^{12}C^{14}N^{-}/^{12}C_2^{-}$ ratio of the OM coatings (Figure 4.6b).

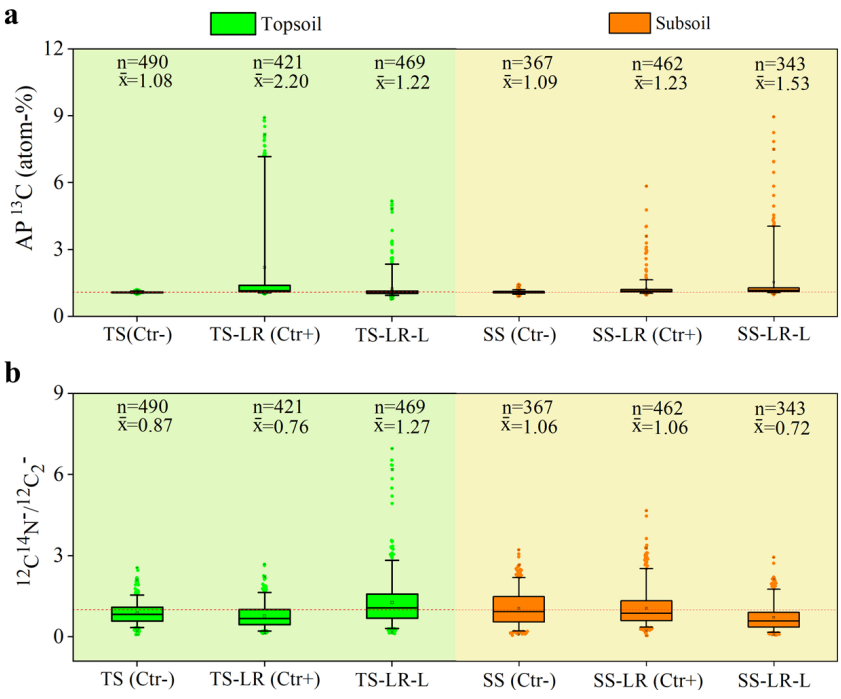

Figure 4.6 The influence of amendments on heterogeneity of organic matter (OM) coatings on mineral surfaces. Box plots of (a) isotope enrichment AP ^{13}C, and (b) $^{12}C^{14}N^{-}/^{12}C_2^{-}$ ratios of OM coatings on the mineral surfaces in the free stable microaggregates of the topsoil and subsoil after 6 months of incubation with either plant residue (TS-LR and SS-LR, Ctr+) or plant residue and lime (TS-LR-L and SS-LR-L). The negative control soil samples (TS and SS, Ctr-) were incubated without amendments. The boxes indicate the 25th to the 75th percentiles and the whiskers indicate the 10th and 90th percentiles. The line in each box indicates the median. The number of regions of interest (ROIs) analysed (n) and the mean values ($\bar{x}$) are indicated at the top of each panel. The mean AP ^{13}C of the unamended topsoil and subsoil (Ctr-), which represents the ^{13}C enrichment in inherited OM (OMi), are indicated by the red dotted lines, respectively in (a). The red dotted line in (b) indicates a $^{12}C^{14}N^{-}/^{12}C_2^{-}$ ratio of 1.

The decrease in surface coverage of OMn observed in the topsoil samples incubated with lime and barley litter (TS-LR-L, Figure 4.5e, i vs. f, j) led to a lower variability in the ^{13}C and ^{15}N enrichment of the OM coatings (Figures 6a and S4.7b, respectively). The lower

mean values of AP ^{13}C and AP ^{15}N were closer to the values in OMi (Ctr-) than the mean isotope enrichment values of the topsoil incubated with litter alone (TS-LR, Ctr+, Figures 4.6a and S4.7b). However, for subsoil samples, there was no apparent decrease in OM coatings on the mineral surfaces of limed samples (SS-LR-L, Figure 4.5g, k vs. h, l), and there was an increase in the number of ROIs with high AP ^{13}C and AP ^{15}N and in the mean value of these ratios (Figures 4.6a and S4.7b).

4.4 Discussion

Our data highlight the different responses of the top- and sub-soil layers to the addition of plant residue, lime, and P. Adding plant litter alone increased the amount of organic material associated with mineral particle surfaces in both soil layers. In the topsoil, the addition of plant residue caused negative priming of OMi, but this was not further affected by either lime, or lime and P addition, neither was the rate of CO_2 evolution, despite liming causing a decrease in the OM coverage of the topsoil mineral particles and an increase in WEOC. In contrast, the addition of the organic residue to the subsoil caused positive priming of OMi, which was enhanced by the addition of lime and P, and so was the release of WEOC and the rate of CO_2 evolution, although lime addition increased the OM coverage of the subsoil particles. Here we discuss how these different responses can be explained by considering the different biogeochemistry of the two horizons and the functional complexity framework proposed by Lehmann et al. (2020). Since the responses to adding lime, or lime and P were similar, here we focus on the effect of lime.

4.4.1 Differences in biogeochemistry between soil layers explain their distinct reactive Al

The difference in relative proportions of OM-Al^{3+} complexes and allophane in the two soil horizons is linked to their different acidity and organic ligand content. Greater acidity was observed in the topsoil than the subsoil. This is likely due to (i) the higher organic C content, and (ii) the smaller contribution of alkalinity from mineral weathering in the former (Panichini et al., 2017). The larger content of organic ligands able to compete with OH^- for reactive Al favours the formation of OM-Al^{3+} complexes over that of allophane in the topsoil. As the content of organic ligands and acidity decreases with depth, the formation of allophane is favoured in the subsoil. These findings are consistent with results reported elsewhere (Macíasa and Camps-Arbestain, 2020).

4.4.2 Differences in OMi availability between soil layers explain their contrasting priming response

Liming had an evident impact on soil organic C fractions. The increase in WEOC (the more active C fraction) after incubating the soil with lime was attributed to the enhanced competition between OH^- and organic ligands for reactive sites. This impairs the formation of OM-metal/mineral complexes, and disrupts soil aggregates and releases OM previously encapsulated in aggregates (Curtin et al., 2015; Kleber et al., 2015; Miyazawa et al., 2013). The latter might have a dominant contribution to the increase in WEOC in limed subsoil, given that there was no decrease in OM on their mineral surfaces (SS-LR-L, as found in NanoSIMS). The WEOC results also showed the only indication of an impact due to P addition alone. The addition of phosphate lead to the displacement of OM into the soil

solution as the phosphate anion competes with organic ligands for reactive sites (Spohn and Schleuss, 2019). The increase in WEOC was enhanced by combining P with lime. In some cases, the response was greater than that caused by lime alone, confirming that both species were displacing adsorbed organic ligands from the soil particle surfaces. This observation is consistent with our previous findings (Li et al., 2020).

The response of OM mineralisation to litter addition differed between soil horizons. In the topsoil, the additional CO_2 released was produced by mineralisation of the freshly added OM, which caused a negative priming effect (Figure 4.3b) through preferential substrate utilisation (i.e., OMn from additional plant litter) leading to pool substitution of OMi for OMn (Shahbaz et al., 2017). We hypothesise that the lower molecular diversity in the topsoil with higher abundance of closely related molecules, e.g., different forms of partly-degraded cellulose, as proposed by Lehmann et al (2020), compared with the subsoil, favours a more efficient soil biota (Table S4.5). Given that the favourable conditions are associated with an abundant OM substrate with a low molecular complexity in the residue-amended topsoil, the mineralisation of this highly bioavailable OM was thus independent from any additional labile OM caused by lime addition (Kemmitt et al., 2008).

In the subsoil, there was a larger fraction of organic ligands associated with inorganic constituents (as inferred from the hydrofluoric acid-extractable C content, which accounted for 50.2–61.8% of total C at depth between 20–40 cm, Table S4.6) and, thus, a smaller fraction of available OM. This results in a harsher environment for the microbes, which may have limited the capacity of the microbes to use OMi for growth. The addition of a new substrate with low-molecular complexity might have had contributed to generate an advantageous environment. This might have contributed to a shift in microbial composition

and functionality, which enhanced decomposition (Chapter 5); as a result, OMi decomposition increased (positive priming effect). This increase was accentuated along with an increase in decomposition of OMn, as more favourable conditions were generated by the lime and P addition, which caused the increase in WEOC.

4.4.3 Organo-mineral associations at the microscale

4.3.3.1 The distinct OM-mineral associations formed at the two soil layers supports the membrane-like bilayer model

The inorganic constituents of the Andosol under study provided a large reactive surface for adsorption of organic ligands as evident by the high OM coverage (up to ca. 45%), especially in the topsoil. Previous observations in the topsoil of other soil groups showed a 4% OM coverage on a Vertisol (typically dominated by smectite) and a 13–19% coverage on a lamellic Luvisol (dominated by illite and pedogenic iron oxides) (Kopittke et al., 2020; Vogel et al., 2014). Our results are consistent with the well-known role that reactive Al has in the formation of OM-mineral associations in Andosols (Inagaki et al., 2020). Crystalline minerals, as inferred by their smooth surfaces, tended to be devoid of OM coverage – compared to clusters of particles (see Figure 4.4) – as they have fewer defect sites that preferentially bind OM (Kleber et al., 2007; Vogel et al., 2014). The OM associated with surfaces rich in reactive Al species tended to have highly variable chemical composition, including N-poor OM (mainly plant-derived OM with low molecular complexity, particularly in topsoil) and N-rich OM (mainly microbial-derived OM with high molecular complexity, especially in subsoil) as inferred from the $^{12}C^{14}N^{-}/^{12}C_2^{-}$ ratio. In addition, these OM coatings showed an increase in spatial heterogeneity with depth.

For the soils incubated with ^{13}C- and ^{15}N-labelled barley residue, some new OM patches were identified on mineral surfaces of the topsoil and the subsoil. By comparing the coverage, spatial distribution and (relative) chemical composition of OM (including OMi and OMn) attached to mineral surfaces in the topsoil and the subsoil, we were able to infer that different mechanisms were operating in the formation of OM-mineral associations in these two soil horizons. This was supported by principal component analysis, as shown in Figure S4.8. In the topsoil, the highly variable forms of the OM coatings (see the wider range of AP ^{13}C signal on the topsoil incubated with plant residue compared to the range of the AP ^{13}C signal from the subsoil incubated with plant residue in Figure 4.6a, b) indicate the presence of non-selective bonding between OM and inorganic surfaces (Kleber et al., 2015; Mikutta and Kaiser, 2011; Spielvogel et al., 2008). More of the new OM patches in the topsoil coatings were N-poor (Figure 4.5e, i, m; and *cf* the $^{12}C^{14}N^-/^{12}C_2^-$ ratio of the OM coatings on the Ctr- and Ctr+ topsoil particles in Figure 4.6b). Some N-poor OMn might have been weakly associated with existing mineral-bound OM on the particles, and formed $OMn_{(N\text{-}poor)}$-OM-mineral associations, namely $OMn_{(N\text{-}poor)}$-$OM_{(N\text{-}rich)}$-mineral inferred by the OM patches (as indicated by white arrow, Figure 4.5e, i, m) that was solely enriched in ^{13}C, but had high $^{12}C^{14}N^-/^{12}C_2^-$ ratio >1. This co-location (indicative of the weaker outer layer of the "membrane-like bilayer", Kleber et al., 2007) could reduce the spatial complexity, resulting in decomposers being in close contact with new substrate. This also supports the occurrence of pool substitution of OMi for OMn in the topsoil that received residue.

In contrast, after having received the same amount and type of C inputs (^{13}C- and ^{15}N-labelled barley residue), the subsoil showed a preferential adsorption of OM with a high

N/C ratio on mineral surfaces (some of which could be allophane) (Rumpel et al., 2015; Spielvogel et al., 2008). This was evident by the high mean ratio of $^{12}C^{14}N^{-}/^{12}C_2^{-}$ of OMi coatings in the subsoil and negligible changes in the $^{12}C^{14}N^{-}/^{12}C_2^{-}$ ratio due to the addition of fresh OM in Figure 4.6b. This demonstrates that microbial-mediated processes producing microbial-derived OM (N-rich OM) play an important role in organic C preservation in the subsoil (Rumpel and Kögel-Knabner, 2010). In the subsoil, with a lower OM coverage and more available reactive sites than the topsoil, the preferential attachment of N-rich OM to the OM-free mineral particles by forming stronger OM $_{(N\text{-rich})}$-mineral associations (indicative of the inner layer of the "membrane-like bilayer", Kleber et al., 2007; Kopittke et al., 2020) was evident by the largest increase in OM coverage on the mineral surface caused by plant residue addition. This was also supported by the recent findings that OM-mineral interface showed ca. 88% enrichment of N at nanometre scale, as noted by Possinger et al. (2020).

4.3.3.2 Differences in the role of Ca^{2+} in the formation of OM-mineral associations between soil layers contribute to their distinct response to liming

In the topsoil, there was an obvious change in the relative chemical composition of the OM coatings (as inferred from the increase in the mean $^{12}C^{14}N^{-}/^{12}C_2^{-}$ ratio) remaining on the soil particle surfaces after lime addition (Figure 4.6b). This suggests that alkalinisation of the topsoil caused a preferential release of organic compounds with a low N/C ratio (e.g., N-poor plant-derived OM, with low molecular complexity) from the mineral surfaces. These N-poor organic compounds might be increasingly susceptible to destabilisation with the growing competition between organic ligands and OH^- (with or without PO_4^{3-}) for adsorption site as alkalinity increases (Kleber et al., 2015), which favours the hydroxylation

of reactive Al.

For the subsoil that received plant residue addition, the response to lime additions was opposite to that of topsoil, with an increase in total OM coverage (Table S4.4) and $^{12}C_2^-$ /$^{27}Al^{16}O^-$ (Figure S4.9). This indicates that, in the subsoil, these inorganic amendments favoured the formation of OM-mineral associations, e.g., OMn-mineral association. Changes in the chemical composition of the OM associated with minerals surfaces in the subsoil treatments were made evident by the wider ranges of the ^{13}C and ^{15}N enrichment. The drop in mean ratio of $^{12}C^{14}N^-/^{12}C_2^-$ upon the addition of lime suggested the increase in the proportion of N-poor OM coatings on the mineral surface in subsoil.

We hypothesise that Ca^{2+} in lime added to the soil might be retained at cation exchange sites (liming increases the cation exchange capacity of variable-charge soils) and provide new electrostatic binding sites for OM (mainly enriched in N-poor OM), forming ternary complexes (mineral-Ca-$OM_{(N\text{-}poor)}$) at the surface of inorganic constituents (Kleber et al., 2015; Kleber et al., 2007; Lützow et al., 2006; Weng et al., 2005). In the subsoil, this positive effect of Ca^{2+} on the formation of OM-mineral associations could overcome the negative effect that an increase in alkalinity has on the stability of these OM-mineral associations. In the surface horizon, the higher OM-saturation of reactive surfaces imply that the particle surfaces have fewer adsorption sites and higher negative electrostatic potentials. This might have attenuated the positive effect of Ca^{2+} on the formation of the OM-mineral association and favoured the de-stabilising effect of alkalisation on the weak $OM_{(N\text{-}poor)}$-OM-mineral and $OM_{(N\text{-}poor)}$-mineral associations (as inferred from the decrease in OM coverage with lime addition to the topsoil, Table S4.4) (Schneider et al., 2010). The different response of the two horizons suggests that the negative impact of liming on the

stability of OM-mineral associations might be more accentuated in an alu-andic Andosol, than in a sil-andic Andosol, given that alu-andic Andosols have a greater abundance of OM-Al^{3+} complexes and a larger OM content compared with sil-andic Andosols, where the greater alkalinity of sil-andic Andosols favours the formation of allophane instead (Matus et al., 2014; Verde et al., 2010; Wagai et al., 2018).

4.5 Conclusions and implications

In summary, this study provides evidence – obtained from bulk soil and micro-scale analyses – of existing differences in both OM decomposition and OM interactions with reactive surfaces, and in their response to amendments between the topsoil and the subsoil of an Andosol. These were associated with their distinct biogeochemistry and the increase in functional complexity of OM with depth. Our findings are in agreement with a conceptual model of the "membrane-like" bilayer (Kleber et al., 2015), with (i) the preferential adsorption of N-rich OM (over other organic compounds) to mineral surfaces in the inner layer; and (ii) the presence of non-selective bonding (e.g., hydrophobic interaction and electrostatic interaction with cations) between N-poor OM and inorganic surfaces, in the outer layer. Soil alkalinisation would preferentially disrupt the latter type of bonding, given its weaker nature. The findings also point to the essential role of OM bioavailability (as conditioned by molecular complexity and spatial heterogeneity) in the response of OM decomposition to litter, lime and P fertiliser addition, supporting the functional complexity framework proposed by Lehmann et al. (2020). Our study has major implications in the design of climate-smart management practices of acidic soils.

Appendix II. Supporting Information for Chapter 4 (SI4)

S4.1. Supporting materials and methods

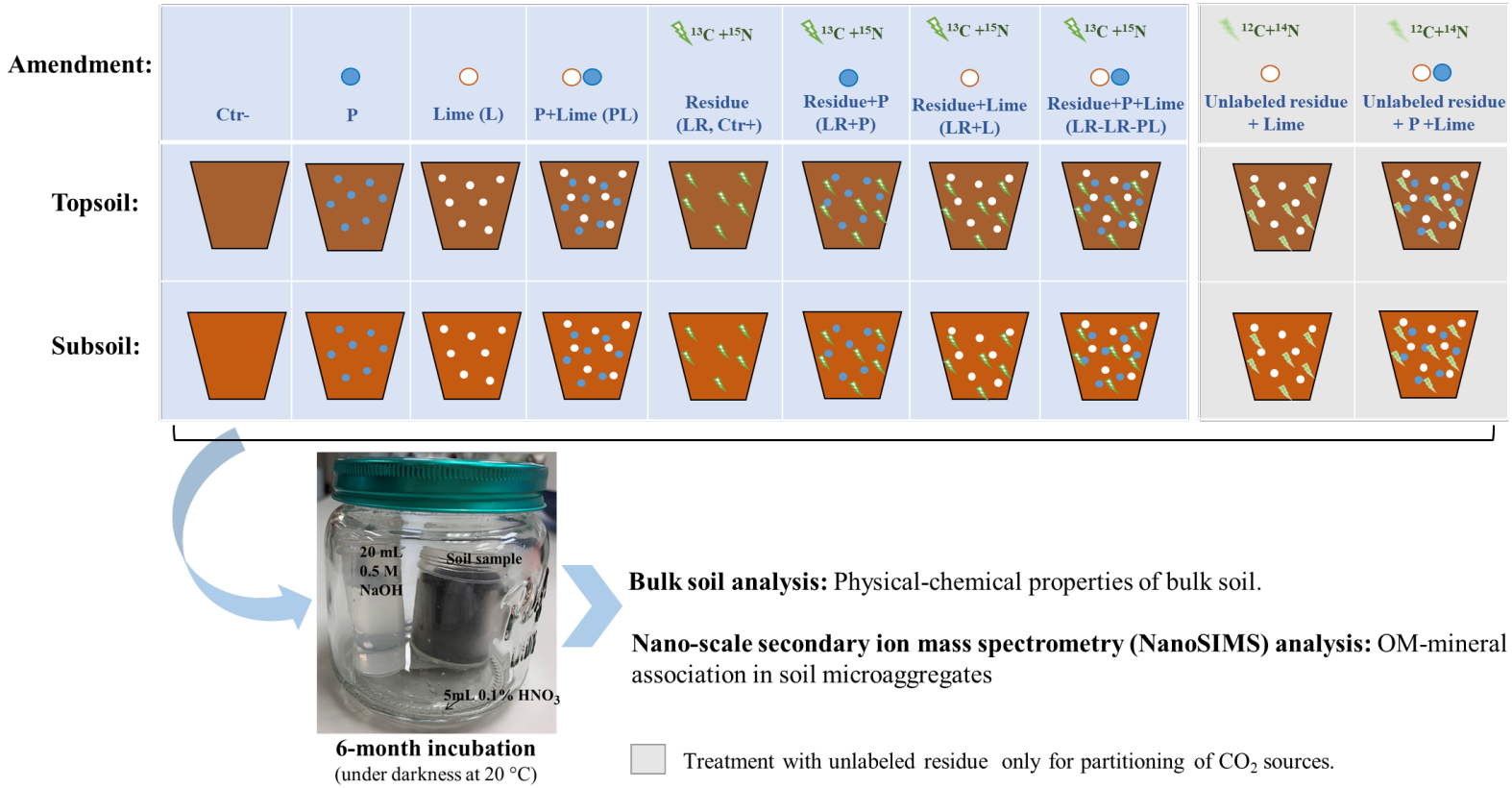

Figure S4.1 Schematic figure of the incubation experiment and analyses.

S4.1.1 Preparation of ^{13}C- and ^{15}N-labelled barley residue

A highly ^{13}C- and ^{15}N-labelled barley residue (^{13}C enrichment=12.1 atom-% and ^{15}N enrichment=7.9 atom-%) and an unlabelled barley residue (^{13}C enrichment=1.1 atom-% and ^{15}N enrichment=0.39 atom-%) were used in the study. To obtain labelled residue with a suitable ^{13}C and ^{15}N enrichment, we diluted highly labelled residue by mixing it with unlabelled barley residue at a mass ratio of 1:1. The diluted labelled barley prepared for the incubation had a ^{13}C enrichment of 6.1 atom-% and ^{15}N enrichment of 3.5 atom-%.

S4.1.2 Partitioning of CO_2 sources

All treatments amended with residue were grouped as (i) two-C source soils, including the topsoil and subsoil incubated with either labelled residue (TS-LR and SS-LR) or labelled residue+P (TS-LR-P and SS-LR-P), and (ii) three-C source soils, the topsoil and subsoil incubated with either labelled residue+lime (TS-LR-L and SS-LR-L) or labelled residue+combined P and lime (TS-LR-PL and SS-LR-PL).

For the two-C source soils, the fractional contributions of the inherited OM (f_{OMi}) and OM newly formed from the barley litter (f_{OMn}) to total CO_2 evolution were calculated according to a two-component isotopic mixing model (eqs. S4.1 and S4.2, as shown below) (Hall et al., 2017). The $\delta^{13}C_{(OMi)}$ and $\delta^{13}C_{(labelled\ residue)}$ are the measured ^{13}C isotopic signature (per mil, ‰) of the OMi (as inferred by the ratio of unamended topsoil and subsoil, TS and SS) and labelled residue (LR), respectively. $\delta^{13}CO_{2\ (total)}$ is the isotopic signature of the total CO_2 evolved from each soil sample.

$$1=f_{OMi}+f_{OMn} \quad \text{(eq. S4.1)}$$

$\delta^{13}CO_{2\,(total)} = f_{OMi} \times \delta^{13}C_{(OMi)} + f_{OMn} * \delta^{13}C_{(labelled\ residue)}$ (eq. S4.2)

For the three-C source soils, the fractional contributions of the OMn (f_{OMn}), OMi (f_{OMi}) and lime (f_{lime}) to total CO_2 evolution were calculated according to the eqs. S4.3–S4.5, as shown below. The $\delta^{13}C_{(soil+labelled\ residue+lime)}$ and $\delta^{13}C_{(soil+unlabelled\ residue+lime)}$ are the measured ^{13}C isotopic signature (per mil, ‰) of CO_2 from the soil that received labelled residue and lime amendments (TS-LR-L, TS-LR-PL, SS-LR-L and SS-LR-PL) and from corresponding soil that received unlabelled residue and lime amendments (TS-UR-L, TS-UR-PL, SS-UR-L and SS-UR-PL). The $\delta^{13}C_{(labelled\ residue)}$ and $\delta^{13}C_{(unlabelled\ residue)}$ are the measured ^{13}C isotopic signature (per mil, ‰) of the labelled residue and unlabelled residue. The $f_{residue}$ was calculated according to eq. S4.3. The $CO_{2\,(lime)}$ evolved from lime added, which was estimated based on the inorganic C present in lime, as the limed topsoils and subsoils had undetectable inorganic C at end of the 6-month incubation. The CO_2-C from the lime thus equalled to inorganic C of lime added. The $CO_{2\,(total)}$ refers to total CO_2 evolved from each treatment. The f_{lime} was calculated according to eq. S4.4. The fractional contribution of the OMi (f_{OMi}) was estimated according to eq. S4.5.

$$f_{OMn} = \frac{\delta^{13}C_{(soil+labelled\ residue+lime)} - \delta^{13}C_{(soil\ +unlabelled\ residue+lime)}}{\delta^{13}C_{(labelled\ residue)} - \delta^{13}C_{(unlabelled\ residue)}} \quad \text{(eq. S4.3)}$$

$$f_{lime} = \frac{CO_{2(lime)}}{CO_{2(total)}} \quad \text{(eq. S4.4)}$$

$1 = f_{OMi} + f_{OMn} + f_{lime}$ (eq. S4.5)

S4.1.3 Measurement of inorganic C

Briefly, 1 g air-dried sample was thoroughly wetted by deionised water (5 mL) in a 35-mL

polypropylene tube, which was placed with NaOH solution in a jar with an airtight lid. The 10 mL of 2 M HCl was injected to the soil slurry via the septum in the lid. The CO_2 trapped in the NaOH was measured using electrical conductivity meter after 5-day incubation at room temperature.

S4.1.4 Nano-scale secondary ion mass spectrometry (NanoSIMS) analysis

For each soil sample measured by NanoSIMS, the OM coverage on the mineral surface was calculated as the summed area of OM coatings ($^{12}C_2^-$+$^{12}C^{14}N^-$) divided by the summed area of the mineral surface ($^{16}O^-$), as eq. S4.6. The C_S and M_S denotes the area of OM coatings (μm^2) and mineral surface (μm^2) in each spot (with 256×256 pixels for a 30×30 μm) analysed, respectively. They were calculated by multiplying the specific number of pixels of the region of interest (ROI) with the size of each pixel (0.0138 μm^2). The *s* takes the values from 1 to *n* (number of analysed spots of every sample, ranging between 5 and 9).

$$OM\ coverage\ (\%) = \frac{\sum_{s=1}^{n} C_s}{\sum_{s=1}^{n} M_s} \times 100 \quad \text{(eq. S4.6)}$$

The AP ^{13}C and AP ^{15}N of the ROIs was computed according to corresponding $^{13}C^{12}C^-/^{12}C_2^-$ and $^{12}C^{15}N^-/^{12}C^{14}N^-$ ratio, as eqs. S4.7–S4.10.

$$R^{13}C/^{12}C = \frac{(^{13}C^{12}C^-/^{12}C_2^-)}{2} \quad \text{(eq. S4.7)}$$

$$R^{15}N/^{14}N = {}^{15}N^{12}C^-/^{14}N^{12}C^- \quad \text{(eq. S4.8)}$$

$$AP^{13}C\ (atom-\ \%) = \frac{^{13}C}{^{13}C+^{12}C} \times 100 = \frac{(R^{13}C/^{12}C)}{(R^{13}C/^{12}C)+1} \times 100 \quad \text{(eq. S4.9)}$$

$$\mathrm{AP}^{15}\mathrm{N}\ (atom-\ \%) = \frac{^{15}\mathrm{N}}{^{15}\mathrm{N}+^{14}\mathrm{N}} \times 100 = \frac{(\mathrm{R}^{15}\mathrm{N}/^{14}\mathrm{N})}{(\mathrm{R}^{15}\mathrm{N}/^{14}\mathrm{N})+1} \times 100 \qquad \text{(eq. S4.10)}$$

Table S4.1 Selected properties of the initial topsoil and subsoil of the Andosol.

	Topsoil (0–20 cm)	Subsoil (20–40 cm)
Moisture content (%)	46.30 ± 0.04	59.74 ± 1.24
Water holding capacity at -10 kPa (%)	74.29 ± 1.82	82.89 ± 7.42
pH (deionised water)	5.58 ± 0.01	5.90 ± 0.04
pH (KCl)	4.42 ± 0.01	4.59 ± 0.04
Total P (g/kg)	0.91 ± 0.03	0.73 ± 0.01
Olsen P (mg/kg)	14.21 ± 4.16	2.60 ± 0.06
Total C (g/kg)	95.07 ± 1.17	67.87 ± 0.13
Total N (g/kg)	7.51 ± 0.09	5.37 ± 0.01
C/N	12.66 ± 0.42	12.64 ± 0.48
^{13}C content (atom-%)	1.07	1.08
^{15}N content (atom-%)	0.39	0.39
Allophane (%)	0.24±0.05	2.50±0.13
Al_p (g/kg)	6.93±0.18	13.09±0.29
Al_p/Al_o	1.15±0.08	0.71±0.01
$(Al_p+Fe_p)/C_p$ atom ratio	0.16±0.02	0.26±0.02
$Al_o+½Fe_o$ (%)	0.91±0.07	2.29±0.08

P (phosphorous), C (carbon), N (nitrogen), Al_o and Fe_o (acid oxalate-extractable aluminium and iron), as well as, Al_p, Fe_p and C_p (sodium pyrophosphate-extractable Al, Fe and C).

Table S4.2 The pH and content of reactive aluminium and iron (Al_o +½Fe_o) and allophane of the topsoils and subsoils at the end of the 6-month incubation.

	Amendment*	pH (deionised water)	Al_o #+½Fe_o # (%)	Allophane (%)
Topsoil	Ctr-	5.04 ± 0.08 f	0.99 ± 0.03 c	0.28 ± 0.05 d
	L	5.56 ± 0.31 e	1.01 ± 0.03 c	0.26 ± 0.05 d
	P	5.12 ± 0.27 f	0.95 ± 0.05 c	0.23 ± 0.06 d
	PL	5.58 ± 0.05 e	0.94 ± 0.04 c	0.20 ± 0.05 d
	LR (Ctr+)	5.47 ± 0.23 e	0.84 ± 0.06 c	0.14 ± 0.05 d
	LR-L	6.35 ± 0.30 ab	1.01 ± 0.03 c	0.27 ± 0.01 d
	LR-P	5.98 ± 0.25 cd	1.04 ± 0.03 c	0.23 ± 0.03 d
	LR-PL	6.39 ± 0.05 ab	0.95 ± 0.03 c	0.22 ± 0.03 d
Subsoil	Ctr-	5.86 ± 0.07 E	2.13 ± 0.08 B	2.19 ± 0.02 C
	L	6.24 ± 0.03 BC	2.17 ± 0.07 AB	2.39 ± 0.02 C
	P	6.25 ± 0.03 BC	2.11 ± 0.04 B	2.19 ± 0.01 C
	PL	6.63 ± 0.22 A	2.17 ± 0.06 AB	2.38 ± 0.09 C
	LR (Ctr+)	5.95 ± 0.22 E	2.11 ± 0.06 B	2.20 ± 0.09 C
	LR-L	6.28 ± 0.20 BD	2.26 ± 0.02 AB	2.64 ± 0.05 AB
	LR-P	6.08 ± 0.20 D	2.29 ± 0.01 AB	2.42 ± 0.05 BC
	LR-PL	6.11 ± 0.05 D	2.35 ± 0.06 A	2.77 ± 0.07 A

Al_o and Fe_o: Acid oxalate-extractable aluminium (Al) and iron (Fe).

*Amendments include lime (L), P, combined lime and P (PL), combined residue and lime (LR-L), combined residue and P (LR-P), and combined residue, lime and P (LR-PL). The negative control soil samples (Ctr-) were incubated without amendments, while the positive control samples were treated with plant residue (LR, Ctr+) before incubation.

The values of either pH, Al_o +½Fe_o content or allophane content of either topsoils (with small letters) or subsoils (with capital letters) that do not share the same letter are significantly different (P<0.05) based on a one-way ANOVA followed by Tukey B test (n=3).

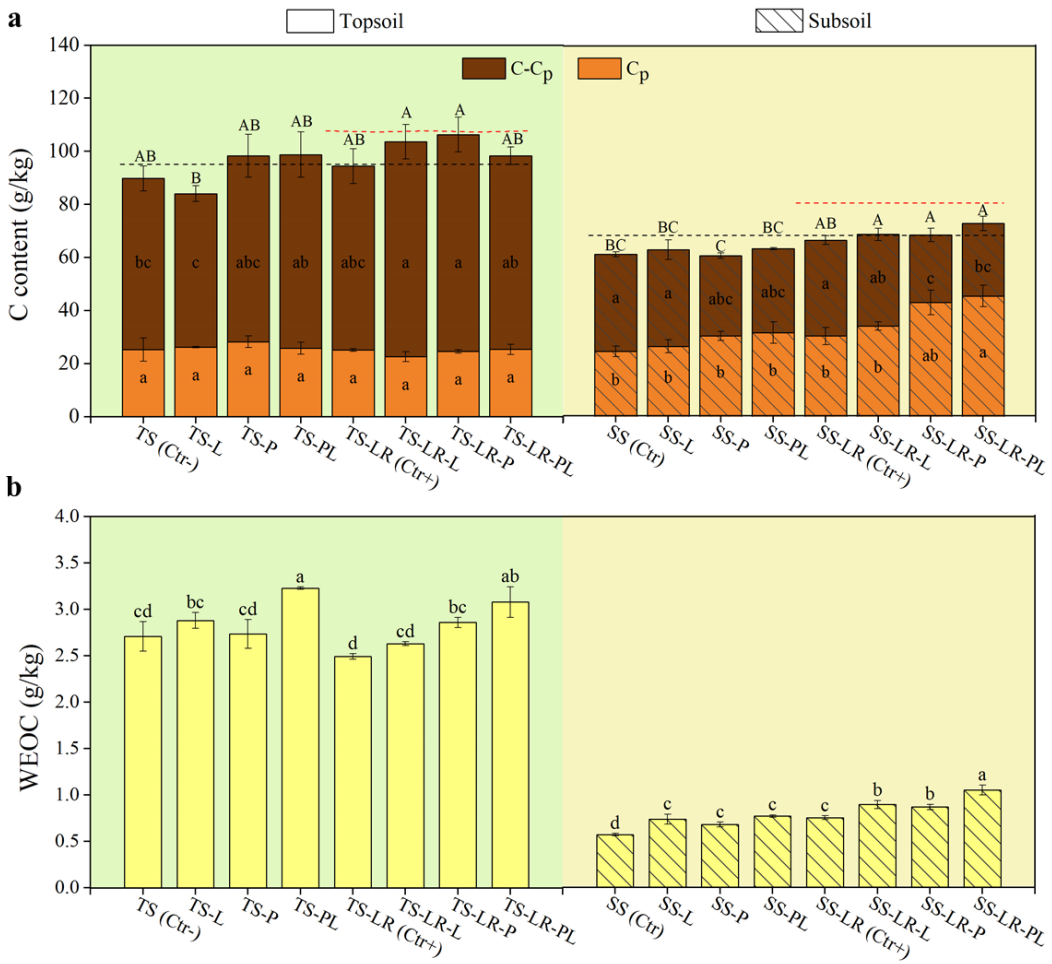

Figure S4.2 Influence of amendments on soil organic carbon (C) content. (a) Total C, $Na_4P_2O_7$-extractable C (C_p) and difference of total C and C_p (C-C_p), and (b) water-extractable organic C (WEOC) content of the topsoils and subsoils incubated with either lime (TS-L and SS-L), P (TS-P and SS-P), combined lime and P (TS-PL and SS-PL), combined residue and lime (TS-LR-L and SS-LR-L), combined residue and P (TS-LR-P and SS-LR-P), or combined residue, lime and P (TS-LR-PL and SS-LR-PL). The negative control soil samples (TS and SS, Ctr-) were incubated without amendments, while the positive control samples (TS-LR and SS-LR, Ctr+) were treated with plant residue before incubation. The black and red dashed lines show the mean value of total C content of the Ctr- and Ctr+ prior to incubation, respectively. The values of either total C (with capital letters), C_p (with small letter), C-C_p (with small letter), or WEOC (with smaller letter) in either topsoil samples or subsoil samples that do not share the same letter are statistically different (P<0.05) based on a one-way ANOVA followed by Tukey B test (n=3).

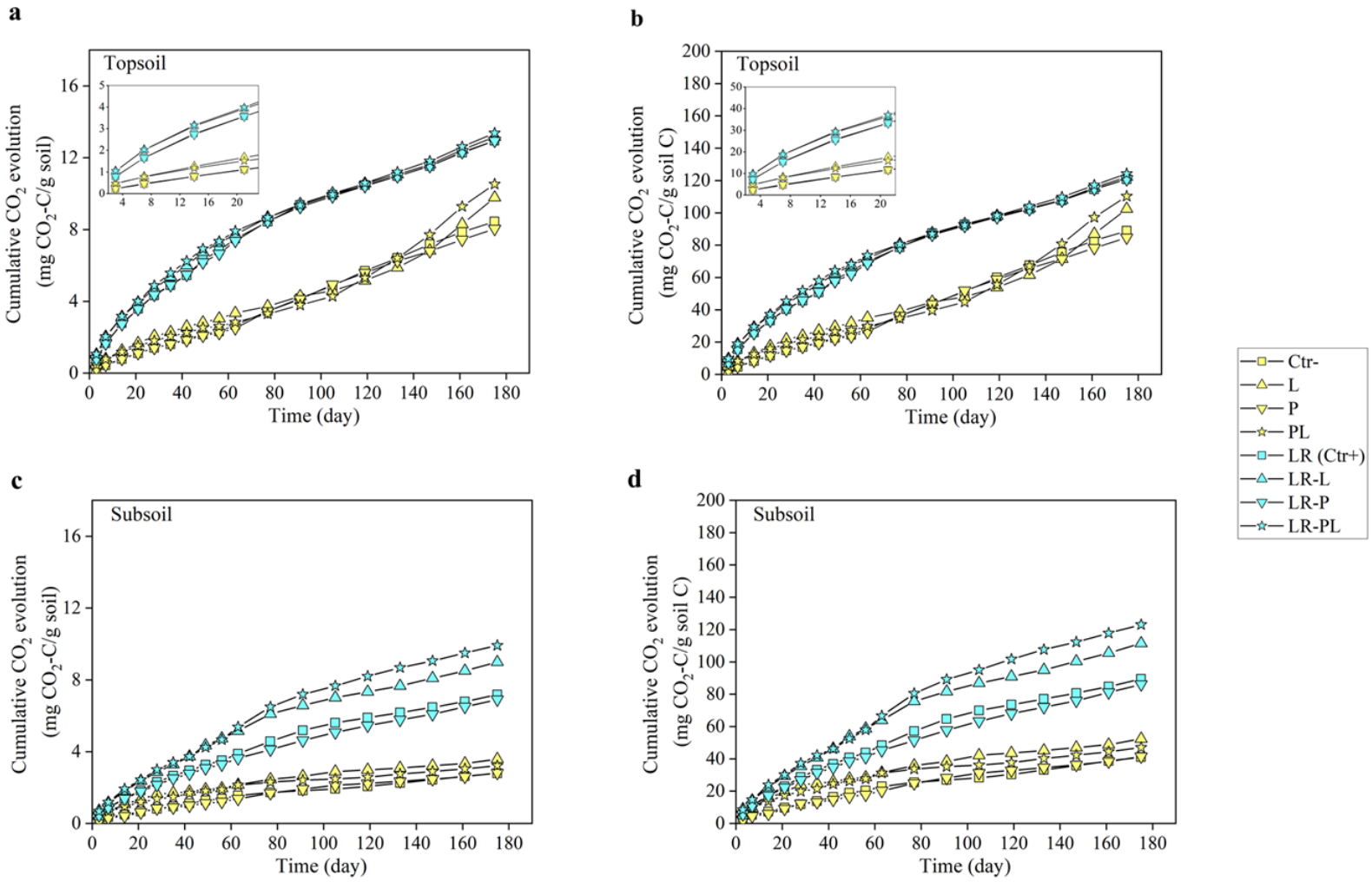
a
Topsoil
Cumulative CO_2 evolution (mg CO_2-C/g soil)
Time (day)
b
Topsoil
Cumulative CO_2 evolution (mg CO_2-C/g soil C)
Time (day)
c
Subsoil
Cumulative CO_2 evolution (mg CO_2-C/g soil)
Time (day)
d
Subsoil
Cumulative CO_2 evolution (mg CO_2-C/g soil C)
Time (day)
Ctr-
L
P
PL
LR (Ctr+)
LR-L
LR-P
LR-PL

Figure S4.3 Influence of amendments on carbon dioxide (CO_2) evolution from soils during incubation period. Cumulative CO_2 from (a and b) topsoils and (c and d) subsoils incubated without (Ctr-) /with either lime (L), P, combined lime and P (PL), residue (LR, Ctr+), combined residue and lime (LR-L), combined residue and P (LR-P), or combined residue, lime and P (LR-PL), during 6 months. The left panel shows the cumulative CO_2 evolution on basis of soil d.w., and the right panel shows the cumulative CO_2 evolution on the basis of the soil total carbon (C). Inset is a magnified view of cumulative CO_2 evolution from the topsoil during the first 21 days.

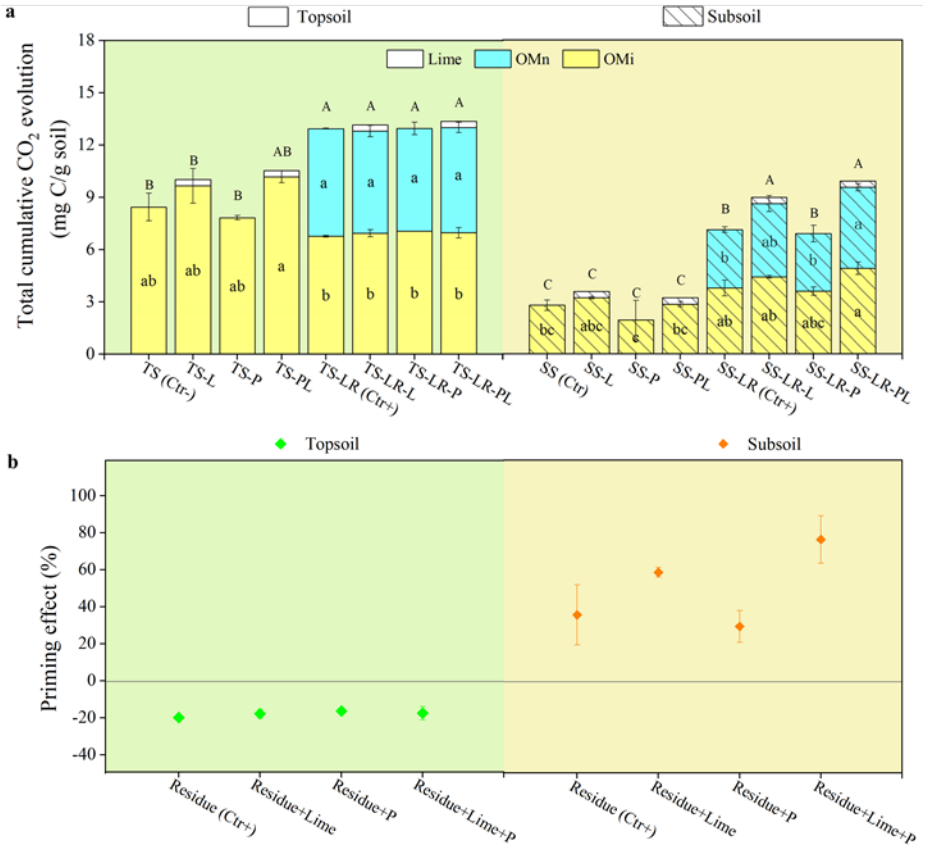

Figure S4.4 Influence of amendments on carbon dioxide (CO_2) released from different carbon (C) sources in soils. (a) Total amount of CO_2 evolved from the lime, organic matter newly formed from plant residue (OMn) and inherited organic matter (OMi) in topsoil and subsoil during 6 months of incubation with either lime (TS-L and SS-L), P, combined lime and P (TS-PL and SS-PL), combined residue and lime (TS-LR-L and SS-LR-L), combined residue and P (TS-LR-P and SS-LR-P) or combined residue, lime and P (TS-LR-PL and SS-LR-PL). The negative control soil samples (TS and SS, Ctr-) were incubated without amendments, while the positive control samples (TS-LR and SS-LR, Ctr+) were treated with plant residue before incubation. The letters above and in the bars indicate results that are statistically different (P<0.05) based on a one-way ANOVA followed by Tukey B test (n=2) for the total cumulative CO_2 evolution (capital letters) and the total CO_2 from OMi (small letter) and from OMn (small letter). (b) The priming effect is expressed here as the percentage difference between the total amount of C mineralised from OMi in a residue amended soil compared to the corresponding (unamended) Ctr- for different amendments.

Table S4.3 The proportion of total cumulative carbon dioxide (CO_2) evolution from inherited organic matter (OMi), organic matter newly formed from the barley litter (OMn), lime and total soil carbon (C) in either topsoils or subsoils after 6-month incubation. Data are presented as % C in each source and initial total C.

	Amendment*	Mineralisation of OMi (%)	Mineralisation of OMn (%)	C loss of lime (%)	C loss of initial total C (%)
Topsoil	Ctr-	8.88	\	\	8.88
	L	10.15	\	100	10.24
	P	8.23	\	\	8.23
	PL	10.69	\	100	11.03
	LR (Ctr+)	7.12	50.80	\	12.08
	LR-L	7.30	48.21	100	12.22
	LR-P	7.42	48.50	\	12.09
	LR-PL	7.32	49.76	100	12.42
Subsoil	Ctr-	4.11	\	\	4.11
	L	4.75	\	100	5.24
	P	2.86	\	\	2.86
	PL	4.20	\	100	4.69
	LR (Ctr+)	5.56	27.57	\	8.95
	LR-L	6.51	34.63	100	11.15
	LR-P	5.31	27.10	\	8.60
	LR-PL	7.24	38.23	100	12.30

*Amendments include sole lime (L), sole P (P), combined lime and P (PL), combined residue and lime (LR-L), combined residue and P (LR-P), and combined residue, lime and P (LR-PL). The negative control soil samples (Ctr-) were incubated without amendments, while the positive control samples were treated with plant residue (LR, Ctr+) before incubation.

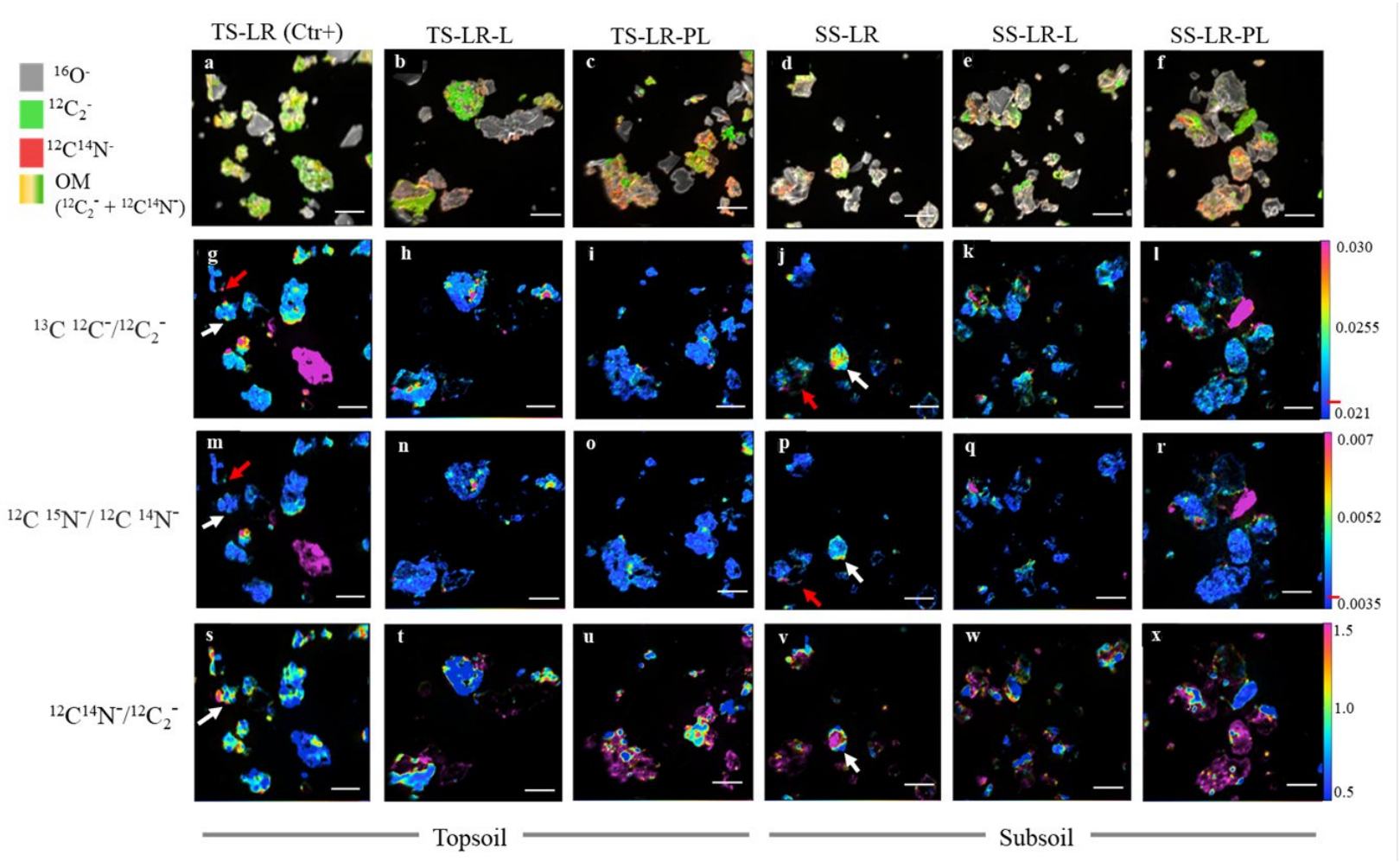

Figure S4.5 Influence of amendments on the organic matter (OM) coatings on mineral surfaces. The images show free stable microaggregates in topsoils (left panels) and subsoils (right panels) incubated for 6 months with either labelled plant residue (TS-LR and SS-LR, Ctr+), combined residue and lime (TS-LR-L and SS-LR-L), or combined residue, P and lime (TS-LR-PL and SS-LR-PL). (a-f) Overlay images showing the distribution of OM (indicated by the $^{12}C_2^-$, $^{12}C^{14}N^-$ signals) on the mineral

particles (indicated by the $^{16}O^-$ signal). (g-l) Hue-saturation-intensity (HSI) maps of $^{12}C^{13}C^-/^{12}C_2^-$ ratios and (m-r) maps of $^{12}C^{15}N^-/^{12}C^{14}N^-$ ratios indicating the extent of the enrichment of the OM coatings with components from the ^{13}C- and ^{15}N-labelled barley residue. The red markers in the gradient colour bars (l and r) indicate the average ratio of $^{12}C^{13}C^-/^{12}C_2^-$ (ca. 0.022) and $^{12}C^{15}N^-/^{12}C^{14}N^-$ (ca. 0.0039) in inherited OM (OMi), respectively. (s-x) HSI maps of $^{12}C^{14}N^-/^{12}C_2^-$ ratios indicating the relative proportion of N in the OM coatings.

Table S4.4 The summed areas of mineral and organic matter (OM) coating in spots measured by nano-scale secondary ion mass spectrometry analyses and computed coverage of OM on the mineral surface, as well as the carbon (C) content of the microaggregates measured by elemental analyser.

	Amendment*	Number of measurements	Total area of the mineral particles (μm^2)	Total area of OM (μm^2)	OM coverage %	C content %
Topsoil	Ctr-	9	2609.8	1162.0	44.5	18.8±0.7
	LR (Ctr+)	7	1699.5	830.3	48.9	21.9±1.0
	LR-L	6	1419.7	423.8	29.9	20.4±0.9
	LR-PL	6	1467.3	559.1	38.1	19.3±0.1
Subsoil	Ctr-	9	1984.1	262.4	13.2	12.8±0.1
	LR(Ctr+)	6	1240.5	287.0	23.1	15.0±0.5
	LR-L	7	1464.3	429.8	29.4	16.0±0.2
	LR-PL	6	1262.4	456.1	36.1	18.4±1.0

*Amendments include combined residue and lime (LR-L), as well as combined residue, lime and P (LR-PL). The negative control soil samples (Ctr-) were incubated without amendments, while the positive control samples were treated with plant residue (LR, Ctr+) before incubation.

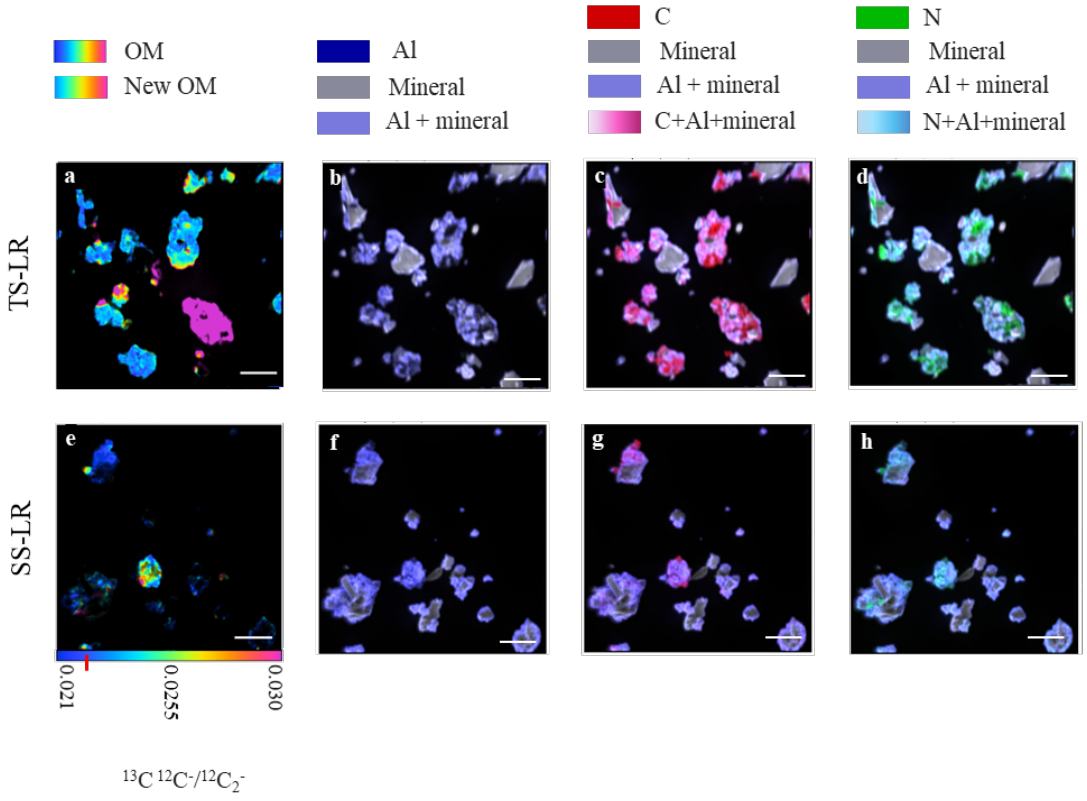

Figure S4.6 Relationship between organic matter (OM) coatings and aluminium (Al) signature from inorganic constituents. The images show free stable microaggregates in topsoil (upper panels) and subsoil (below panels) incubated for 6 months with labelled plant residue (TS-LR and SS-LR, Ctr+). (a and e) Hue-saturation-intensity (HSI) maps of $^{13}C^{12}C^{-}/^{12}C_2^{-}$ ratios showing the total OM and OM newly formed from residue added (OMn) coatings. Composite images showing the correlation between (b and f) Al and mineral; (c and g) Al, C and mineral; and (d and h) Al, N and mineral of TS-LR and SS-LR. The red line on the colour bar indicates the ratio of $^{13}C^{12}C^{-}/^{12}C_2^{-}$ at natural abundance (0.022). The scale bar is 5 µm.

.

Table S4.5 Total species of the fungi observed in topsoils and subsoils by the high throughput sequencing analyses.

	Amendment	Observed species
Topsoil	Ctr-	612 ± 129
	LR (Ctr+)	481 ± 39
	LR-L	582 ± 29
	LR- P	497 ± 8
	LR- PL	492 ± 11
Subsoil	Ctr-	304 ± 7
	LR (Ctr+)	314 ± 32
	LR-L	214 ± 35
	LR- P	203 ± 51
	LR- PL	289 ± 1

*Amendments include combined residue and lime (LR-L), combined residue and P (LR-P), as well as combined residue, lime and P (LR-PL). The negative control soil samples (Ctr-) were incubated without amendments, while the positive control samples were treated with plant residue (LR, Ctr+) before incubation.

Table S4.6 The content of hydrofluoric acid -extractable carbon (C) and its proportion out of total C at different soil depths.

Depth cm	g/kg soil	% C
10-15	28.3 ± 12.1	39.5 ± 4.4
20-25	28.3 ± 2.8	50.2 ± 2.4
35-40	33.9 ± 15.6	61.8 ± 1.54

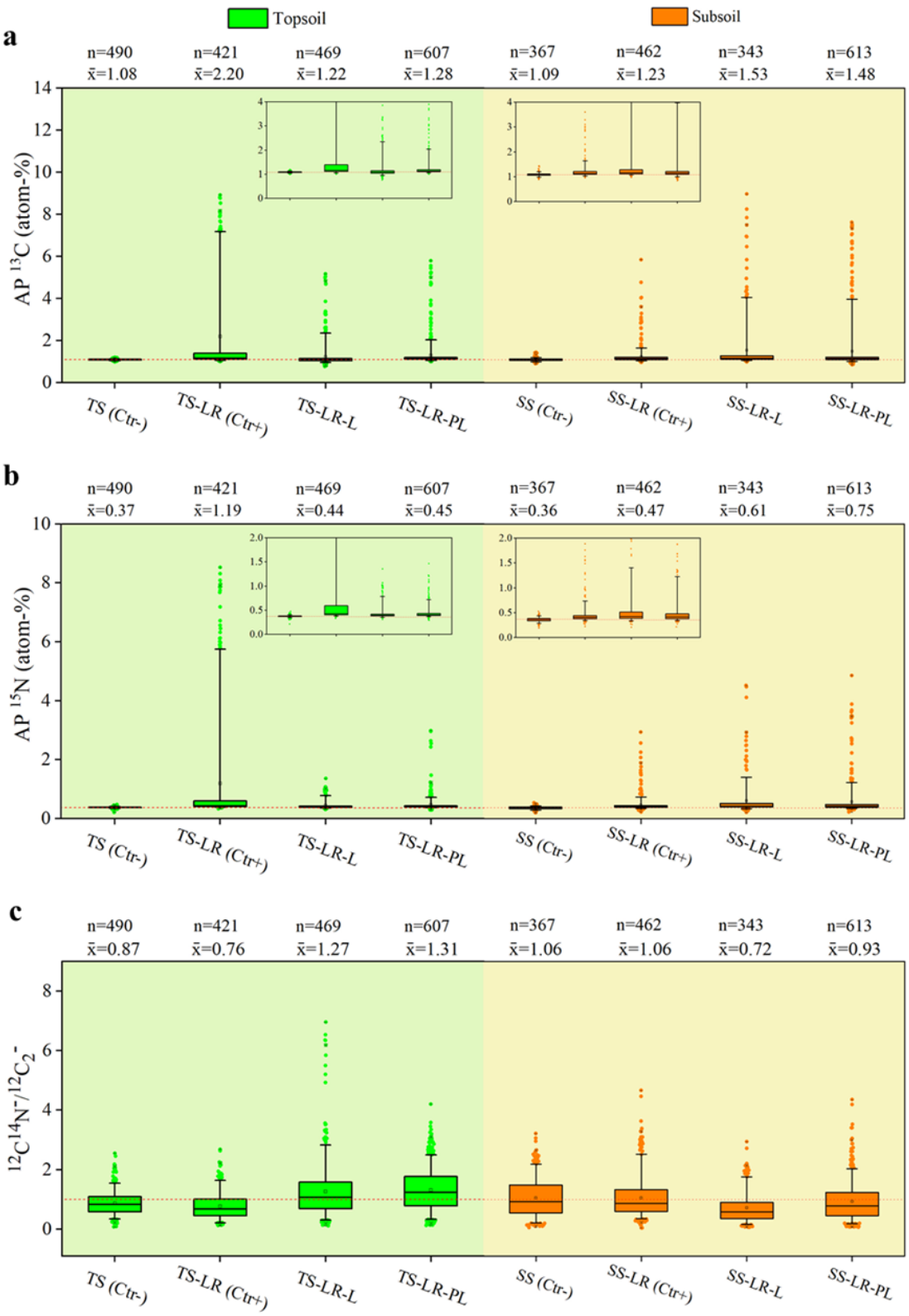
a
Topsoil
Subsoil
n=490 x̄=1.08
n=421 x̄=2.20
n=469 x̄=1.22
n=607 x̄=1.28
n=367 x̄=1.09
n=462 x̄=1.23
n=343 x̄=1.53
n=613 x̄=1.48
AP 13C (atom-%)
TS (Ctr-)
TS-LR (Ctr+)
TS-LR-L
TS-LR-PL
SS (Ctr-)
SS-LR (Ctr+)
SS-LR-L
SS-LR-PL
b
n=490 x̄=0.37
n=421 x̄=1.19
n=469 x̄=0.44
n=607 x̄=0.45
n=367 x̄=0.36
n=462 x̄=0.47
n=343 x̄=0.61
n=613 x̄=0.75
AP 15N (atom-%)
c
n=490 x̄=0.87
n=421 x̄=0.76
n=469 x̄=1.27
n=607 x̄=1.31
n=367 x̄=1.06
n=462 x̄=1.06
n=343 x̄=0.72
n=613 x̄=0.93
12C14N-/12C2-

Figure S4.7 Influence of amendments on heterogeneity of organic matter (OM) on mineral surfaces. Box plots of (a) the isotope enrichment AP ^{13}C, (b) the isotope enrichment AP ^{15}N and (c) the $^{12}C^{14}N^{-}/^{12}C_2^{-}$ ratios of OM coatings in the free stable microaggregates of the topsoils and subsoils incubated without (TS and SS, Ctr-)/with either plant residue (TS-LR and SS-LR, Ctr+), combined plant residue and lime (TS-LR-L and SS-LR-L) or combined plant residue, P and lime (TS-LR-PL and SS-LR-PL). The AP ^{13}C and AP ^{15}N value was calculated based on $^{13}C^{12}C^{-}/^{12}C_2^{-}$ and $^{12}C^{15}N^{-}/^{12}C^{14}N^{-}$ ratio. The boxes indicate the 25th to the 75th percentiles and the whiskers indicate the 10th and 90th percentiles. The line in each box indicates the median. The number of regions of interest (ROIs) analysed (n) and the mean values ($\bar{x}$) are indicated at the top of each panel. The mean AP ^{13}C and AP ^{15}N obtained from unamended topsoil and subsoil (Ctr-), which represent values of inherited OM (OMi) are indicated by red dash lines in (a) and (b), respectively. Inset is a magnified view of AP ^{13}C and AP ^{15}N ratios as the Y axis (atom-%) ranges between 0–4 for AP ^{13}C (a) and 0–2 for AP ^{15}N (b), respectively. The red dotted line in (c) indicates a $^{12}C^{14}N^{-}/^{12}C_2^{-}$ ratio of 1.

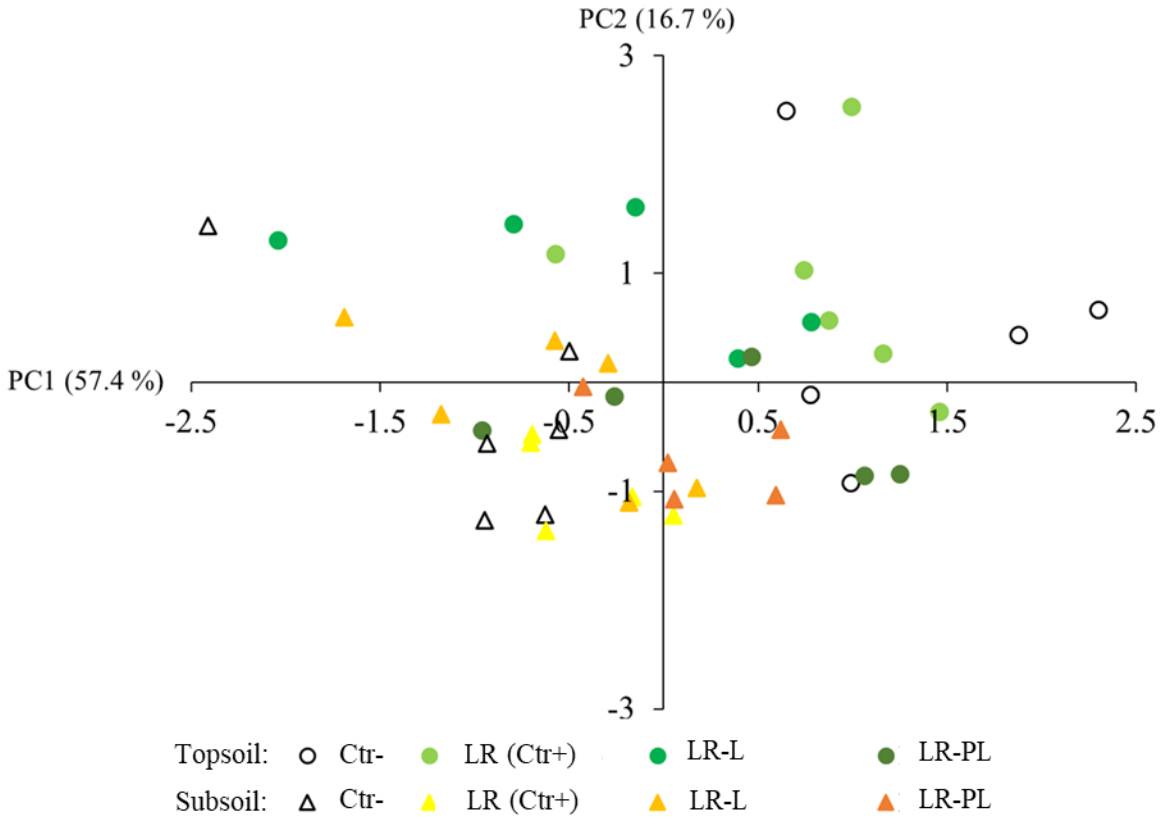

Figure S4.8 Principal component analysis of the properties of organic matter (OM) coatings on mineral surface in the free stable microaggregates from the topsoils and subsoils. The PC1-PC2 scores for topsoils and subsoils incubated without (Ctr-)/with either residue (LR, Ctr+), combined residue+lime (LR-L), or combined residue+lime+P (LR-PL) after 6 months, according to those results obtained from the nano-scale secondary ion mass spectrometry analysis, including $^{12}C_2^-$, $^{13}C^{12}C^-$, $^{12}C^{14}N^-$ and $^{12}C^{15}N^-$ secondary ions, the $^{13}C^{12}C^-/^{12}C_2^-$, $^{12}C^{15}N^-/^{12}C^{14}N^-$, $^{12}C^{14}N^-/^{12}C_2^-$, $^{12}C_2^-/^{27}Al^{16}O^-$, $^{13}C^{12}C^-/^{27}Al^{16}O^-$, $^{12}C^{14}N^-/^{27}Al^{16}O^-$ and $^{12}C^{15}N^-/^{27}Al^{16}O^-$ ratio and OM coverage.

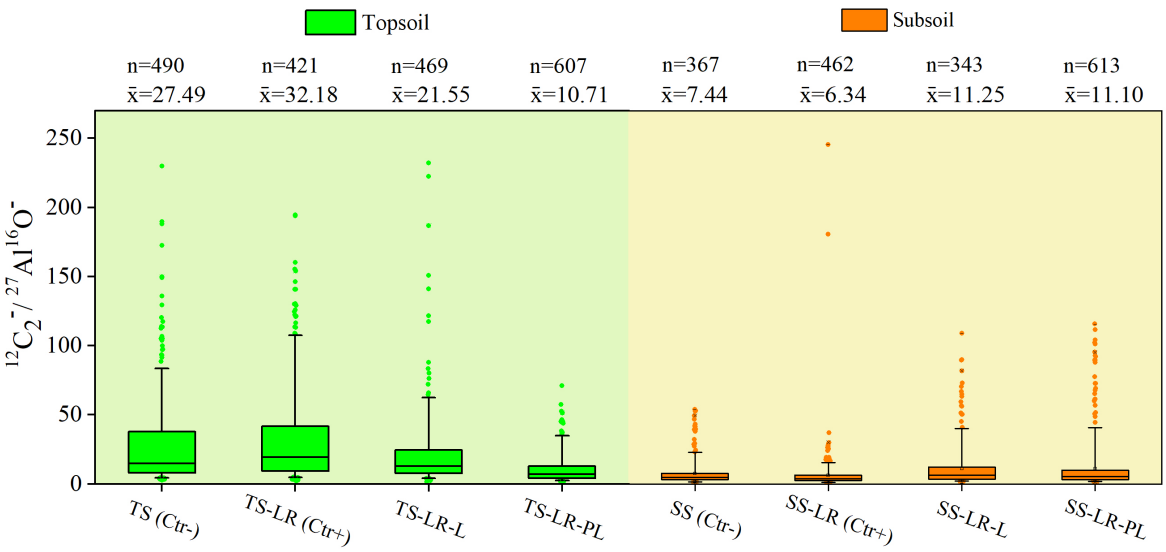

Figure S4.9 Influence of amendments on the organic matter (OM) coated with aluminium (Al) in the free stable microaggregates from the topsoils and subsoils. Box plot of the $^{12}C_2^-/^{27}Al^{16}O^-$ ratio of OM coatings on the mineral surfaces in the free stable microaggregates of the topsoil and subsoil after 6 months of incubation with either residue (LR, Ctr+), combined residue+lime (LR-L), or combined residue+lime+P (LR-PL). The negative control soil samples (TS and SS, Ctr-) were incubated without amendments. The boxes indicate the 25th to the 75th percentiles and the whiskers indicate the 10th and 90th percentiles. The line in each box indicates the median. The number of regions of interest (ROIs) across the OM coatings analysed (n) and the mean values ($\bar{x}$) are indicated at the top of the panel.

CHAPTER 5

THE KEY REGULATOR CONTROLLING THE RESPONSE OF SOIL ORGANIC MATTER MINERALISATION TO LIME AND/OR PHOSPHATE ADDITION SHIFTS WITH DEPTH FROM MICROORGANISMS TO BIOAVAILABLE SUBSTRATE CARBON

Abstract

To understand the dissimilar response of OM mineralisation with depth to lime and/or P addition, it is critical to know how microorganisms respond to the changes in soil properties caused by these amendments. Here we conducted a 6-month incubation of a topsoil and a subsoil of an Andosol with/without inorganic amendments (either lime, P or combined lime and P) in the presence or absence of plant residue. We looked at the changes in (i) microbial community composition, and (ii) abiotic factors (e.g., pH and labile OM), and investigated the influence of these changes in OM mineralisation. Under all conditions (included the unamended control), as soil depth increased, bacteria and fungi decreased in richness and diversity, and there was a decrease in the labile OM and nutrients. In the topsoil, lime amendment caused a shift in the microbial community composition and functional profile, but no effect was observed when P fertiliser was applied instead. Structural equation modelling suggested that, in the topsoil, OM mineralisation does not depend on the concentration of labile OM, but strongly relies on community composition (and specially on fungi) and functional profile. On the contrary, in the subsoil, the amendment-driven increase in labile OM showed significant correlation with the changes in OM mineralisation. These results indicated the fact that key regulator controlling the response of OM mineralisation to lime and/or P amendments shifts from microbial properties to bioavailability of OM source as soil depth increases.

.

5.1 Introduction

The need to produce enough food for a growing global population is expected to cause a 70–100% increase in crop production by 2050, which will foster land-use intensification worldwide (Foley et al., 2011; Tilman et al., 2011). Therefore, pressure on the environment will continue to rise (Godfray et al., 2010; Solaw, 2011) and we need a better understanding on how to achieve greater yields from a given land area (i.e., closing the yield gap) with minimal environmental impacts (i.e., by sustainably intensifying agriculture within planetary boundaries). For this, it is crucial to increase our knowledge of how different agricultural practices, such as the use of fertiliser and lime, influence soil functions and, more specifically, soil organic matter (OM) and soil life.

While the addition of conventional fertilisers and lime tends to increase soil OM because of the favoured crop growth compared with no amendments (Chen et al., 2018; Eze et al., 2018), ions such as phosphate from P fertilisers or OH^- generated upon lime application, causes destabilisation of OM, making it more vulnerable and, ultimately impacts soil microbial life (Kleber et al., 2015; Li et al., 2020; Ma et al., 2018; Spohn and Schleuss, 2019). As noted by our previous study (Chapter 3), increasing OH^- and/or phosphate ions in soil could disrupt the formation of OM-mineral/metal complexation and/or stability of aggregates through the increased competition between additional OH^- and phosphate ions and organic ligands for reactive sites, which causes some previously protected OM to become destabilised, thus being released to the aqueous phase and resulting in an increase in DOM. The fractions of DOM is generally deemed as labile OM fraction (bioavailable OM fraction), as it contains relatively low molecular weight OM and tends to be easily

decomposed and extremely high dynamic (Boddy et al., 2007). Changes in (i) bioavailability of OM source (as indispensable nutrients and energy source for microorganisms) and (ii) soil pH and phosphate, have each the potential to shift soil microbial community composition and functional profile, such as the bacteria/fungi ratio, K- vs. r- strategies, as well as C use efficiency (Fierer et al., 2007; Silva-Sánchez et al., 2019; Yang et al., 2019a; Zheng et al., 2019). The shifts, in turn, could affect the turnover of soil OM and the release of CO_2 to atmosphere, which is the largest single source of CO_2 from global terrestrial ecosystems (Metcalfe et al., 2011; Spohn and Schleuss, 2019).

Most of studies on the effects of soil amendments on the interplay between soil microorganisms (bacteria and fungi) and soil OM turnover have focused on the topsoil, despite the fact that (i) the subsoil contributes to more than half of the total soil C stocks, and (ii) its different biogeochemistry, e.g., mineral composition, microbial properties, quantity and functional complexity of OM (Rumpel et. al., 2015; Rumpel and Kögel-Kabner, 2010), will likely result in a different response from that of the topsoil. As noted by our previous findings (Chapter 4), when soil depth increased, lime and/or P addition caused a consistently increase in DOM, but contrasting effects on OM mineralisation, with negligible changes in the OM mineralisation of the topsoil, but an increase in that of the subsoil (Li et. al., 2020). Therefore, a better understanding of the amendment-driven influence on the relationships between microorganisms and OM through the soil profile is needed for a climate-smart land management practice.

In this study, we conducted a 6-month incubation of a topsoil and a subsoil of an Andosol with/without inorganic amendments (either lime, P or combined lime and P) in the presence or absence of plant residue (simulating the increase in C inputs resulting from the

incorporation of crop residues to soil). We used (i) high-throughput sequencing analysis to reveal the responses of the bacteria and fungi (e.g., community composition and functional profile) to these amendments as soil depth increases, and (ii) structural equation modelling to explore the correlations that the soil microbial properties and representative physicochemical properties have with OM mineralisation within the soil profile.

5.2. Materials and methods

5.2.1 Details of the soil and the plant residue used in the study

Topsoil (0–20 cm) and subsoil (20–40 cm) samples were taken in February 2019 at a site on the eastern flank of Mount Taranaki (New Zealand) with an elevation of 512 m (asl) (39°19'15.82"S; 174°11'18.05"E). Annual precipitation is ca. 2,022 mm and the mean annual temperature is ca. 8.6 °C. After removal of identifiable plant residues and other coarse material, the soil samples were sieved (<4 mm) and stored for two weeks at ca. 4 °C prior to their use. Topsoil and subsoil differed in pH (topsoil: pH_{KCl}=4.4; subsoil: pH_{KCl}=4.6), total C contents (TC: 95.1 g/kg in topsoil and 67.9 g/kg in subsoil), total N contents (TN: 0.8 g/kg in topsoil and 0.5 g/kg in subsoil), available P contents (Olsen P: 14.2 mg/kg in topsoil and 2.6 mg/kg in subsoil), and mineral composition (topsoil: allophane content=0.2%, Al_o+½Fe_o=0.9%, Al_p/Al_o ratio=1.2; subsoil: allophane content=2.5%, Al_o+½Fe_o=2.3%, Al_p/Al_o ratio=0.7, Table S5.1). Barley residue was air dried, ground and sieved <2 mm. It had an organic C content of 40.5% (d.w. basis), an N content of 0.6% (d.w. basis), and a C/N ratio of 67.5.

5.2.2 Incubation

Samples of topsoil and subsoil (equivalent to 30 g oven-dried) were each mixed thoroughly and incubated with the barley residue applied either (i) alone (3% wt basis; TS-LR and SS-LR), (ii) with lime (3 mg $CaCO_3$/g; TS-LR-L and SS-LR-L), (iii) with P (300 mg P/kg in the form of KH_2PO_4; TS-LR-P and SS-LR-P), or (iv) with both lime and P (TS-LR-PL and SS-LR-PL) (Figure S5.1). The topsoil and subsoil amended with only barley residue were referred to as controls (Ctr, TS-LR and SS-LR), whereas those incubated without amendments were considered as the negative controls (Ctr-, TS and SS). After adjusting the soil moisture at 60% water holding capacity (Vogel et al., 2014), the soils were placed in a 50-mL plastic container and incubated in 0.5-L air-tight glass jars, under darkness at 20 °C for 6 months, with three experimental replicates per treatment. To keep the soil moisture constant, 5 mL 0.1% HNO_3 was added to the bottom of the jar to ensure a humid atmosphere. At the end of the 6-month incubation, the soil samples were divided into two subsamples for (i) physicochemical properties analyses, including pH, TC (which was all organic C, even in lime-amended soils), cold and hot water-extractable C (CWEC and HWEC), sodium pyrophosphate-extractable C (C_p) and aromaticity (measure by the specific absorbance at UV 254, and labelled as SUVA) and/or C/N ratio of the OM (C/N), cold and hot water-extractable OM (C-SUVA, H-SUVA, C-C/N and H-C/N) and sodium pyrophosphate-extractable OM (P-SUVA and P-C/N) (more details provided in section S5.1 in Supporting Information for Chapter 5, SI5), and (ii) for microbiological analyses (as detailed below), respectively.

5.2.3 DNA extraction

Total genomic DNA samples were extracted using the OMEGA Soil DNA Kit (D5625-1) (Omega Bio-Tek, Norcross, GA, USA), following the manufacturer's instructions, and stored at -20 °C prior to further analysis. The quantity and quality of extracted DNAs were measured using a NanoDrop ND-1000 spectrophotometer (Thermo Fisher Scientific, Waltham, MA, USA) and agarose gel electrophoresis, respectively.

5.2.4 16S rRNA gene amplicon sequencing

PCR amplification of the bacterial 16S rRNA genes V3-V4 region was performed using the forward primer 338F (5'-ACTCCTACGGGAGGCAGCA-3') and the reverse primer 806R (5'-CGGACTACHVGGGTWTCTAAT-3'). Sample-specific 7-bp barcodes were incorporated into the primers for multiplex sequencing. The PCR components contained 5 μL of buffer (5×), 0.25 μL of Fast pfu DNA Polymerase (5U/μL), 2 μL (2.5 mM) of dNTPs, 1 μL (10 μM) of each Forward and Reverse primer, 1 μL of DNA Template, and 14.75 μL of ddH_2O. Thermal cycling consisted of initial denaturation at 98 °C for 5 min, followed by 25 cycles consisting of denaturation at 98 °C for 30 s, annealing at 53 °C for 30 s, and extension at 72 °C for 45 s, with a final extension of 5 min at 72 °C. PCR amplicons were purified with Vazyme VAHTSTM DNA Clean Beads (Vazyme, Nanjing, China) and quantified using the Quant-iT PicoGreen dsDNA Assay Kit (Invitrogen, Carlsbad, CA, USA). After the individual quantification step, amplicons were pooled in equal amounts, and pair-end 2×250 bp sequencing was performed using the Illumina MiSeq platform with MiSeq Reagent Kit v3 at Shanghai Personal Biotechnology Co., Ltd (Shanghai, China).

5.2.5 ITS amplicon sequencing

PCR amplification of the fungal ITS1 region was performed using the forward primer 1737F (5'-GGAAGTAAAAGTCGTAACAAGG-3') and the reverse primer 2043R (5'-GCTGCGTTCTTCATCGATGC-3'). Sample-specific 7-bp barcodes were incorporated into the primers for multiplex sequencing. The PCR components contained 5 μL of buffer (5×), 0.25 μL of Fast pfu DNA Polymerase (5U/μL), 2 μL (2.5 mM) of dNTPs, 1 μL (10 μM) of each Forward and Reverse primer, 1 μL of DNA Template, and 14.75 μL of ddH_2O. Thermal cycling consisted of initial denaturation at 98 °C for 5 min, followed by 28 cycles consisting of denaturation at 98 °C for 30 s, annealing at 55 °C for 30 s, and extension at 72 °C for 45 s, with a final extension of 5 min at 72 °C. PCR amplicons were purified with Vazyme VAHTSTM DNA Clean Beads (Vazyme, Nanjing, China) and quantified using the Quant-iT PicoGreen dsDNA Assay Kit (Invitrogen, Carlsbad, CA, USA). After the individual quantification step, amplicons were pooled in equal amounts, and pair-end 2×250 bp sequencing was performed using the Illumina MiSeq platform with MiSeq Reagent Kit v3 at Shanghai Personal Biotechnology Co., Ltd (Shanghai, China).

5.2.6 Sequence analysis

Microbiome bioinformatics were performed with QIIME2 2019.4 (Bolyen et al., 2019) with slight modification according to the official tutorials (https://docs.qiime2.org/2019.4/tutorials/). Briefly, raw sequence data were demultiplexed using the demux plugin following by primers cutting with cutadapt plugin (Martin, 2011). Sequences were then quality filtered, denoised, merged and chimera removed using the DADA2 plugin (Callahan et al., 2016). Non-singleton amplicon sequence variants (ASVs)

were aligned with mafft (Katoh et al., 2002), and then used to construct a phylogeny with fasttree2 (Price et al., 2010). A total of 2,010,929 valid sequences of bacteria (16S rRNA gene) and 1,630,610 valid sequences of fungi (ITS) were obtained across all soil samples studied. The sequences were classified into OTUs at the similarity level of 97%, including 2,523–4,516 bacterial OTUs, and to a lesser extent, 203–583 fungal OTUs (Table S5.2). Taxonomy was assigned to ASVs using the classify-sklearn naïve Bayes taxonomy classifier in feature-classifier plugin (Bokulich et al., 2018) against the SILVARelease 132 (bacteria)/UNITERelease 8.0 (fungi) Database (Koljalg et al., 2013).

5.2.7 Bioinformatics and statistical analysis

Sequence data analyses were mainly performed using QIIME2 and R packages (v3.2.0). ASV-level alpha diversity (α-diversity) indices, such as Chao1 richness estimator and Shannon diversity index were calculated using the ASV table in QIIME2. One-way ANOVA (analysis of variance) with a Tukey B test was used to analyse the statistical difference ($P<0.05$) in means of either Chao1 or Shannon index of bacteria and fungi in different treatments using the SPSS software (IBM SPSS Statistics Version 24). Beta diversity analysis was performed to investigate the structural variation of microbial communities (at OTU level) across all samples using Bray-Curtis metrics (Bray and Curtis, 1957) and visualised via principal coordinate analysis (PCoA) in R. Significant physicochemical variables ($P<0.05$) based on permutated data were selected and fitted onto the PCoA ordination space using the 'envfit' function in the 'vegan' R package, and significances of correlations were tested with 999 permutations. The functional composition of bacteria and fungi in topsoil and subsoil was based on the functional genes predicted by PICRUSt2 and MetaCyc metabolic pathway database. Differences in the

functional profile of either bacteria or fungi in soil treatments were studied using principal component analysis (PCA) conducted with SPSS. The Spearman's correlation analysis of richness, diversity and relative abundance of dominant phyla of bacteria and fungi, as well as selected soil physicochemical properties – including soil pH, TC and C/N ratio, as well as quantity and quality of cold and hot water- and sodium pyrophosphate-extractable OM fractions (CWEC, HWEC, C_p, C-SUVA, H-SUVA, P-SUVA, C-C/N, H-C/N and P-C/N) (Table S5.3) – was conducted with SPSS. The network of bacteria and fungi (top 200 OTUs) at these two depths was analysed with Cytoscape 3.2.1 (Shannon et al., 2003), which allowed to present the strong ($r>0.7$ or $r<-0.7$) correlations (via Spearman's rank correlation analysis) between either bacterial phyla or fungal phyla at each soil depth.

To reveal the importance of the soil physicochemical properties (mainly those associated with OM bioavailability) as well as the microbial (either bacterial or fungal) community composition and its functional composition on OM mineralisation (shown in Table S5.3, obtained based on our previous study, Chapter 4), structural equation modelling (SEM) was separately used for topsoil and subsoil treatments via the IBM SPSS-Amos 26.0. More details are provided in section S5.2.1 and Table S5.4 in SI5.

5.3 Results

Below, we focus on the treatments applied to the topsoil and the subsoil that received either residue alone (Ctr) or both residue and inorganic amendments (lime and/or P amendments) to reveal the influence of the lime and/or P addition on the microbial community composition and functional profile, and the interplays between microorganisms and OM turnover. Given that the shift in the microbial community composition and increase in OM

mineralisation with residue addition (indicating the increased C inputs) is well-known, the changes in microbial community composition and functional profile caused by residue amendment alone (observed by comparing with the topsoil and subsoil without any amendments, TS and SS, Ctr-) are detailed in the SI5 (as shown in Figures S5.2–S5.7, Tables S5.2–S5.3, and sections S5.2 and S5.3).

5.3.1 Effects on microbial α-diversity

Greater richness and diversity (as inferred from the larger values of Chao 1 and Shannon index, respectively) of both bacteria and fungi were always found in the topsoil treatments compared with the subsoil treatments, regardless of the amendment used (Figure 5.1). The inorganic amendments (either L, P or PL) only caused minor changes in richness and diversity of bacteria, regardless of the depth considered (Figure 5.1a). However, there was a distinct response of fungal richness and diversity to the amendments between the topsoil and the subsoil. The addition of lime to topsoil cased a significant increase in fungal richness, while the addition of lime or P alone to the subsoil significantly decreased fungal richness and diversity compared with the corresponding Ctr (SS-LR), as shown in Figure 5.1b.

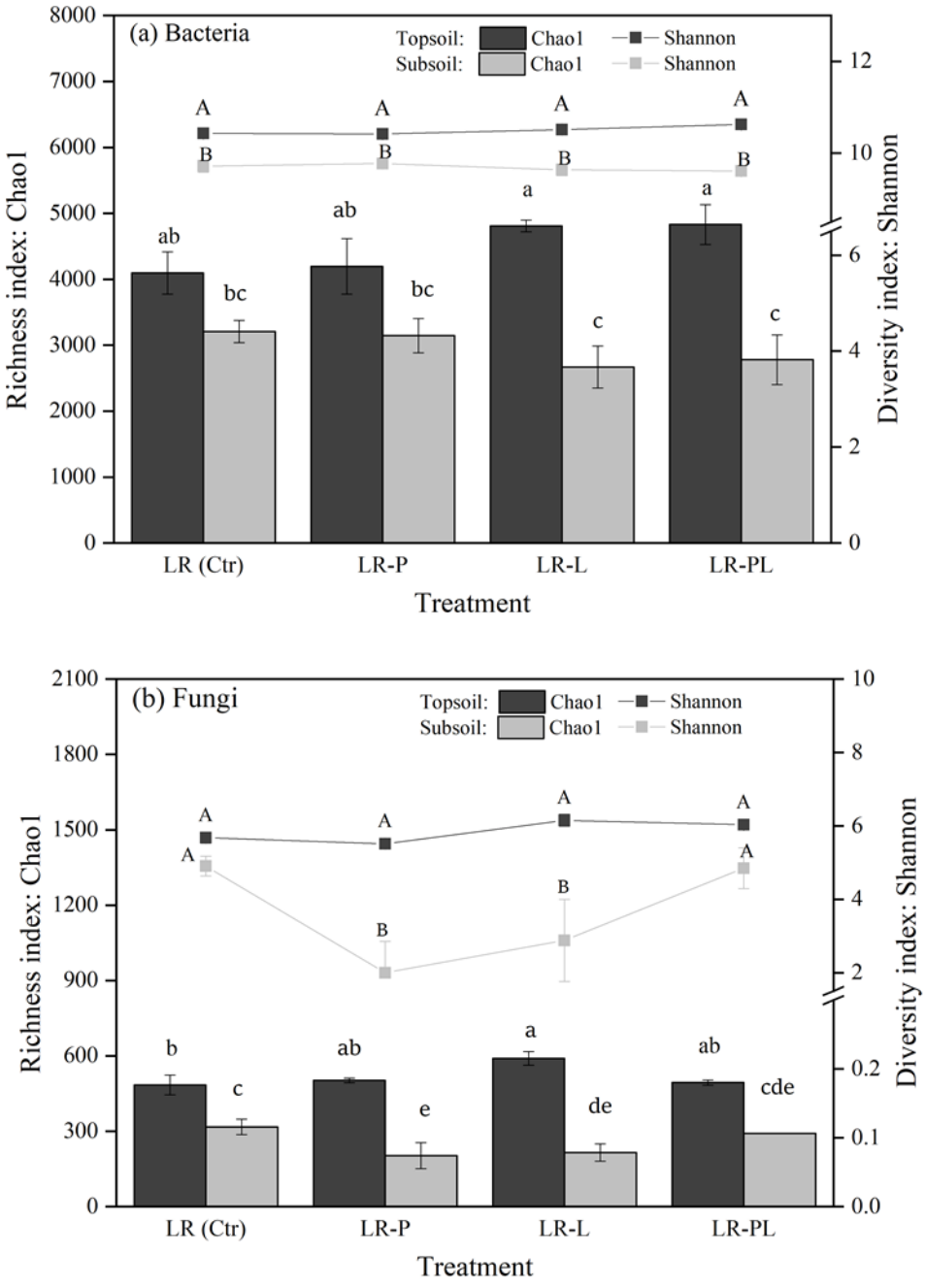

Figure 5.1 Richness (Chao1 index) and diversity (Shannon index) of the (a) bacteria and (b) fungi in the topsoil and subsoil that received either sole labelled residue (TS-LR and SS-LR, Ctr), residue+lime (TS-LR-L and SS-LR-L), residue+P (TS-LR-P and SS-LR-P) or residue+combined P and lime (TS-LR-PL and SS-LR-PL) at end of 6-month incubation.

5.3.2 Effects on microbial community composition at phylum level

There were 25–28 bacterial phyla identified across all treatments (Table S5.2). They were, in general, dominated by *Proteobacteria* (26.3–46.2%), *Acidobacteria* (17.1–23.8%), *Actinobacteria* (11.1–19.7%), *Chloroflexi* (5.1–19.8%) and, to a lesser extent, *Rokubacteria* (<6%), *Verrucomicrobia* (<4%), *Bacteroidetes* (<4%), *Planctomycetes* (<3%) and *Gemmatimonadetes* (< 2%) (Figure 5.2a). There were 5–9 fungal phyla identified, and *Ascomycota* (40.0–95.9%), *Basidiomycota* (1.4–41.4%) and *Mortierellomycota* (2.3–26.9%) were the dominant phyla in both topsoils and subsoils (Figure 5.2b).

There was an appreciable difference in the bacterial and fungal community composition at the phylum level with soil depth. Compared with the subsoil, the topsoil generally had greater abundance of *Proteobacteria*, *Actinobacteria* and *Bacteroidetes* of bacteria (Figure 5.2a), as well as *Basidiomycota* and *Mortierellomycota* of fungi (Figure 5.2b); but it also showed smaller proportions of *Chloroflexi* and *Rokubacteria* of bacteria (Figure 5.2a), as well as *Ascomycota* of fungi (Figure 5.2b). This was further supported by the cluster analysis based on the community composition of either bacteria or fungi, where the topsoil and subsoil treatments clustered separately, as two dominant branches (left panels, Figure 5.2).

In the topsoil, both bacterial and fungal composition (at phylum level) showed greater responses to lime additions (L and PL) than the sole addition of P (Figure 5.2). The lime (with/without P) addition structured (i) fungal phylum composition with a general increase in the relative abundance of the *Ascomycota* and *Mortierellomycota*, along with a drop in

the relative proportion of *Basidiomycota* (Figure 5.2b) and, to a lesser extent, (ii) bacterial phylum composition, in general, with a slight increase in relative abundance of *Chloroflexi* (Figure 5.2a). Based on the cluster analysis of either bacterial or fungal community composition at phylum level (Figure 5.2), all limed topsoil samples (TS-LR-L and TS-LR-PL) were grouped in a cluster; while Ctr (TS-LR) and P-amended topsoil (TS-LR-P) were grouped in another cluster.

In the subsoil, the inorganic amendments resulted in a different response between bacteria and fungi (Figure 5.2). The latter was more responsive, particularly to the P amendment alone, showing a greater relative abundance of the *Ascomycota*, and lower relative abundance of *Mortierellomycota* and *Basidiomycota* compared with Ctr (SS-LR). This was consistent with the cluster analysis, as subsoils that received individual P were in a separate subgroup, while the Ctr (SS-LR) and other treatments (SS-LR-L and SS-LR-PL) were grouped into another subgroup.

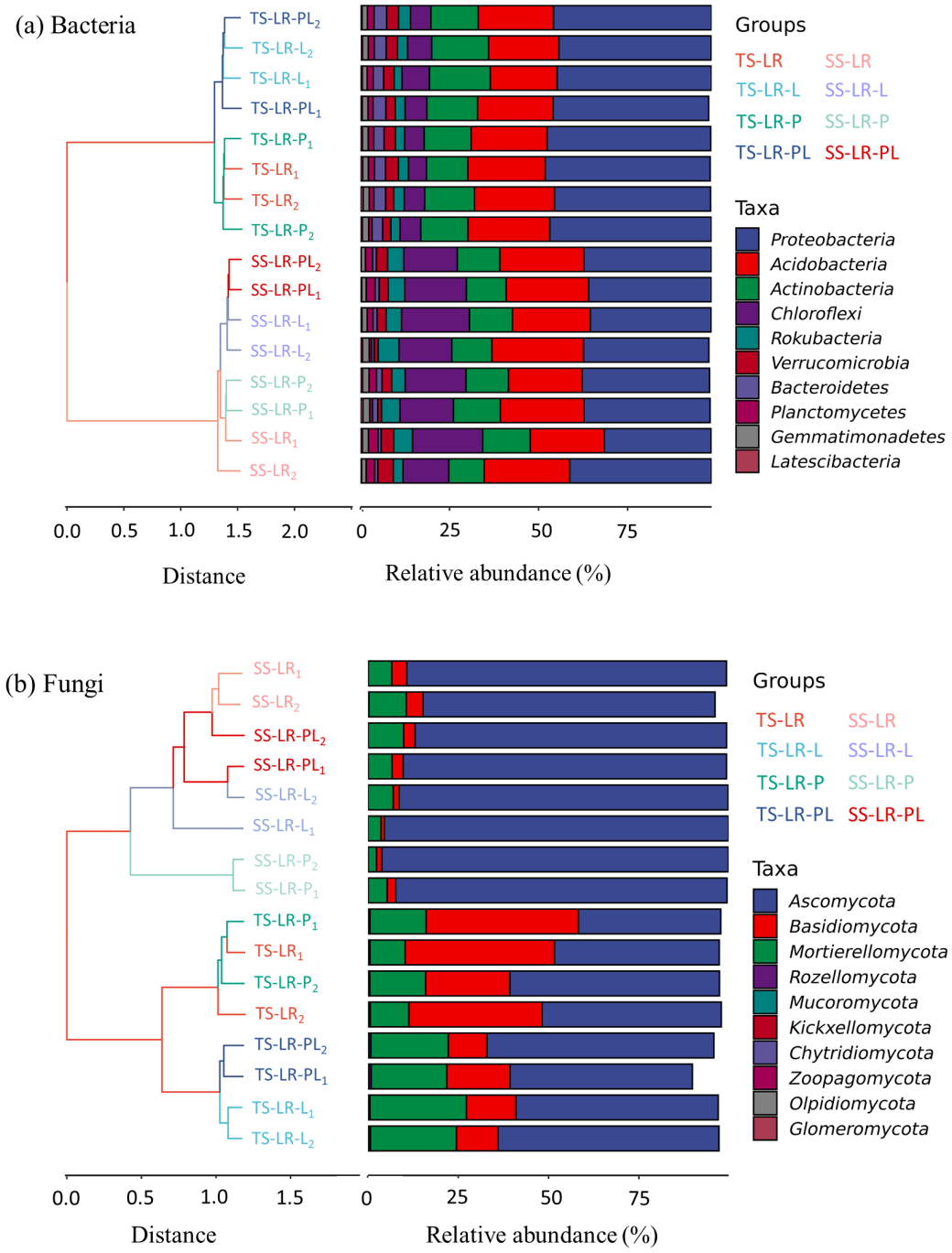

Figure 5.2 Relative abundance of the dominant phyla of (a) bacteria and (b) fungi in topsoil and subsoil that received either sole residue (TS-LR and SS-LR, Ctr), residue+lime (TS-LR-L and SS-LR-L), residue+P (TS-LR-P and SS-LR-P) or residue+combined P and lime (TS-LR-PL and SS-LR-PL) at end of 6-month incubation, with cluster analysis based on the similarity between the treatments (left panels).

5.3.3 Principal coordinate analysis of microbial community composition at OTU level

When considering the bacterial community composition at OTU level, the first two principal coordinates accounted for 69.3% of the total variation, with PCo1 and PCo2 accounting for 64.0% and 5.3%, respectively (Figure 5.3a). All topsoils were plotted on the negative sector of PCo1 and spread between negative (limed treatments, TS-LR-L and TS-LR-PL) and positive scores (TS-LR and TS-LR-P) of PCo2. All the subsoil samples were clustered on the positive axis of PCo1, with differences in PCo2 values between treatments being much less accentuated.

When considering the fungal community composition at OTU level, PCo1 and PCo2 accounted for 35.1% and 22.6% of the total variation, respectively (Figure 5.3b). Similar to the pattern of bacterial community composition, topsoils and subsoils were located on the negative and positive sides of PCo1 axis, respectively. On the PCo2 axis, the topsoils amended with P alone (TS-LR-P) and Ctr (TS-LR) were plotted together on the negative sector, while the topsoil treatments amended with lime (TS-LR-L and TS-LR-PL) plotted on the positive side. Subsoil Ctr (SS-LR) and treatments that were amended with lime (with/without P, SS-LR-L and SS-LR-PL) were generally allocated in the positive sector of the PCo2, while the P-amended subsoil (SS-LR-P) accounted for high negative value of PCo2.

These differences in bacterial and fungal community composition (at the OTU level) between the treatments were related to specific soil physicochemical properties such as soil OM and its fractions (quantity and quality) and/or soil pH (Figure 5.3). Differences in bacterial and fungal community composition at increasing soil depth were attributed to (i)

a decrease in content of TC and labile C (CWEC and HWEC), and aromaticity of labile OM (as inferred from C-SUVA and H-SUVA values), and (ii) an increase in the C/N ratio of OM and hot water-extractable OM (H-C/N). Changes in labile OM (e.g., CWEC, HWEC, C-SUVA, and H-SUVA), along with the enhanced alkalinity generated by lime addition, were particularly evident in the treatments of topsoil with lime addition (TS-LR-L and TS-LR-PL) and were paralleled by a distinct bacterial and fungal community composition. It was notable that P-amended subsoil had a different fungal community composition from other treatments of subsoil on the PCo2 axis, with a smaller contribution of the above-mentioned soil properties.

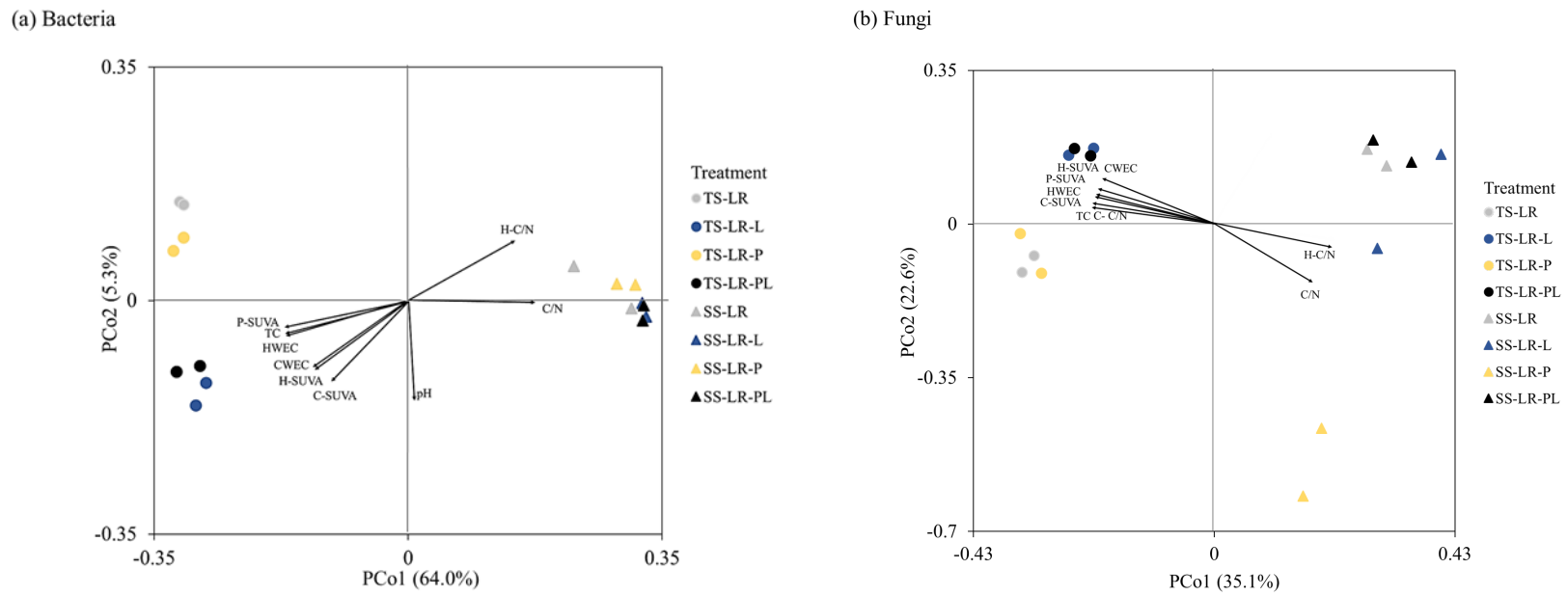

Figure 5.3 Principal coordinate analysis based on Bray-Curtis dissimilarity displaying samples and environmental vectors for the (a) bacterial and (b) fungal community composition (at OTU level) in topsoil and subsoil that received either sole residue (TS-LR and SS-LR, Ctr), residue+lime (TS-LR-L and SS-LR-L), residue+P (TS-LR-P and SS-LR-P) or residue+ P+lime (TS-LR-PL and SS-LR-PL) at the end of 6-month incubation. The selected environmental factors included pH, total carbon (TC), cold and hot water-extractable organic carbon (CWEC and HWEC), sodium pyrophosphate-extractable organic carbon (Cp), and chemistry of the organic matter (OM), namely, the ratio of carbon to nitrogen of soil (C/N) and its cold and hot water-extractable OM (C-C/N and H-C/N), and the aromaticity of cold and hot water- and sodium pyrophosphate-extractable OM (C-SUVA, H-SUVA and P-SUVA). These environmental factors had significant influence on bacterial and/or fungal community composition.

5.3.4 Principal component analysis of microbial functional composition

We ran PCA to reveal the response of functional profiles of either bacteria or fungi across all treatments that received residue (Figures 5.4 and S5.8). For the functional composition of bacteria, the first two principal components (PCs) accounted for 76.9% of the total variation, with PC1 and PC2 accounting for 57.0% and 19.9%, respectively (Figure 5.4a). The PC1-PC2 scores showed that (i) the driver of PC1 was soil depth, with topsoil samples and subsoil samples being located at positive and negative PC1 values, respectively; (ii) limed topsoil (TS-LR-L and TS-LR-PL) accounted for the lower positive or higher negative value of the PC2 axis compared with its corresponding Ctr (TS-LR), while there was no clear shift of the P-amended topsoil (TS-LR-P) from the Ctr (TS-LR); and (iii) despite the subsoil treatments spread between positive and negative sector of PC2, there was no clear difference in the distribution between them.

The factor loadings plot (Figure S5.8a) showed which bacterial metabolic functions were responsible for the arrangement of the soil samples in the scores plot (Figure 5.4a). A large group of functions, including generation of precursor of metabolites and energy, as well as degradation of organic compounds (aromatic compounds, carboxylates, secondary metabolites, fatty acids and lipids, Deg5, 8, 11 and 15, Figure S5.8a and Table S5.5), were found on positive loading of PC1, with either low positive or negative loadings of PC2. Thus, these functions had a relatively greater contribution to bacterial functional profile in the topsoil, particularly in the case of the limed topsoil, compared with that in the subsoil. Some functions pertaining to biosynthesis, degradation and metabolic clusters were located at negative PC1 and positive PC2 loadings.

For the functional composition of fungi, the PC1 and PC2 accounted for 53.5% and 25.1% of total variation, respectively (Figure 5.4b). The effects of depth and lime amendments (L and PL) were also evident in the fungal functional composition. The topsoil treatments were found on the positive PC1 score, and were located on both positive (limed treatments, TS-LR-L and TS-LR-PL) and negative sector (treatments without lime, TS-LR and TS-LR-P) of PC2, while subsoils generally clustered together on the negative sector of PC1.

In the factor loading (Figure S5.8b), almost all fungal functions studied plotted on the positive PC1 and PC2 loads, including biosynthesis processes (e.g., amino acids, carbohydrates, and fatty acids and lipids biosynthesis, Bio 2, 5 and 8, Table S5.5), the generation of precursor metabolites and the energy associated with 1,5-anhydrofructose degradation and fermentation (Gen1 and 4, Table S5.5). This suggests a greater fungal metabolic function in the topsoil treated with lime addition, compared with other treatments.

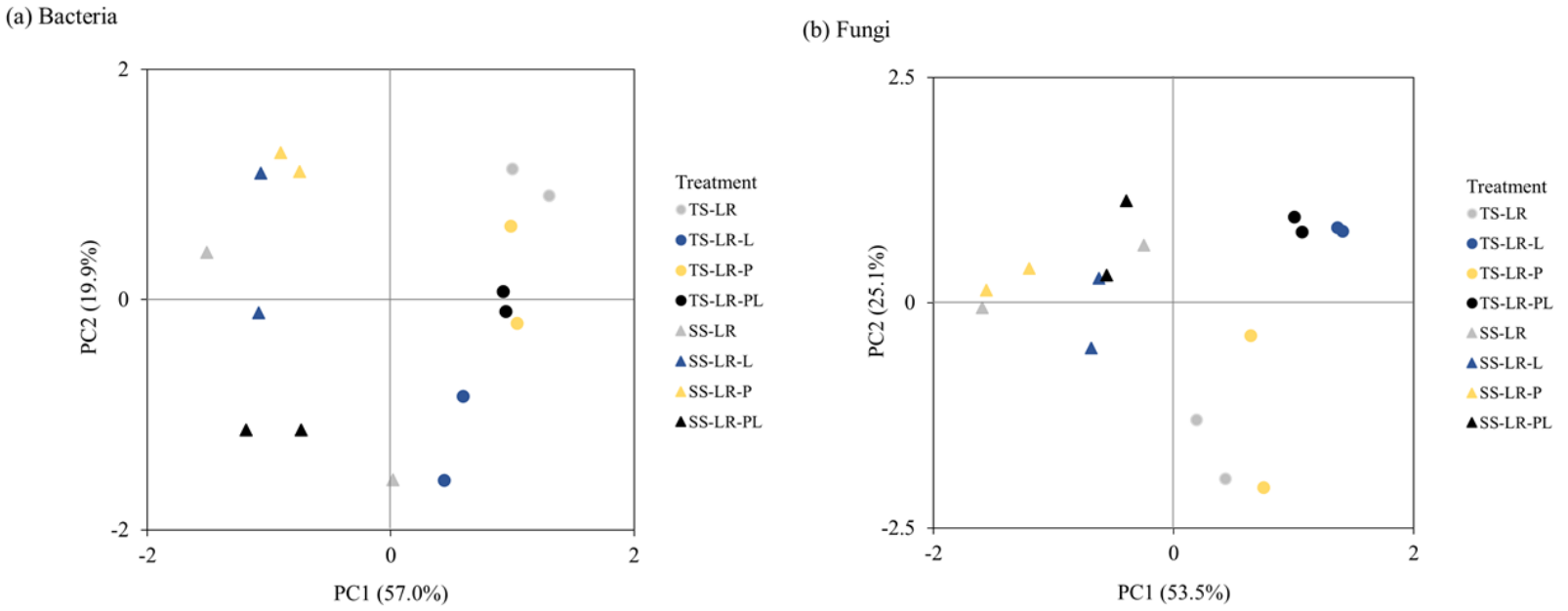

Figure 5.4 Principal component analysis of the functional composition of (a) bacteria and (b) fungi in topsoil and subsoil that received either residue (TS-LR and SS-LR, Ctr), residue+lime (TS-LR-L and SS-LR-L), residue+P (TS-LR-P and SS-LR-P) or residue+ P+lime (TS-LR-PL and SS-LR-PL) at the end of 6-month incubation. The microbial functional composition was predicted by PICRUSt2 and MetaCyc metabolic pathway database using the sequencing dataset.

5.3.5 Structural equation modelling of OM decomposition and its abiotic and biotic factors

The SEM applied to the topsoil treatments explained the 87% of total variance in the OM mineralisation at end of the 6-month incubation, which was significantly (directly) correlated with soil pH and the bacterial (community composition) and fungal (community composition and functional profile) properties considered (Figure 5.5a). Out of those drivers, fungal community composition and functional profile (as represented by the value of PC1 in the PCA analysis and accounted for 58% variance in composition of fungal dominant phyla and 72% variance in fungal functional composition, Table S5.4) played the most important role in OM decomposition, showing the relatively greater positive/negative coefficient value (being 1.85 between fungal composition and OM mineralisation, and -2.21 between fungal functional profile and OM mineralisation, $P<0.001$, Figure 5.5a). However, the driver of the labile OM was not evident in OM mineralisation ($P>0.05$). On the contrary, the SEM for the subsoils accounted for 98% of variance in the OM decomposition (Figure 5.5b), which was only significantly associated with labile OM (coefficient=0.72, $P<0.001$) out of the factors considered ($P>0.05$).

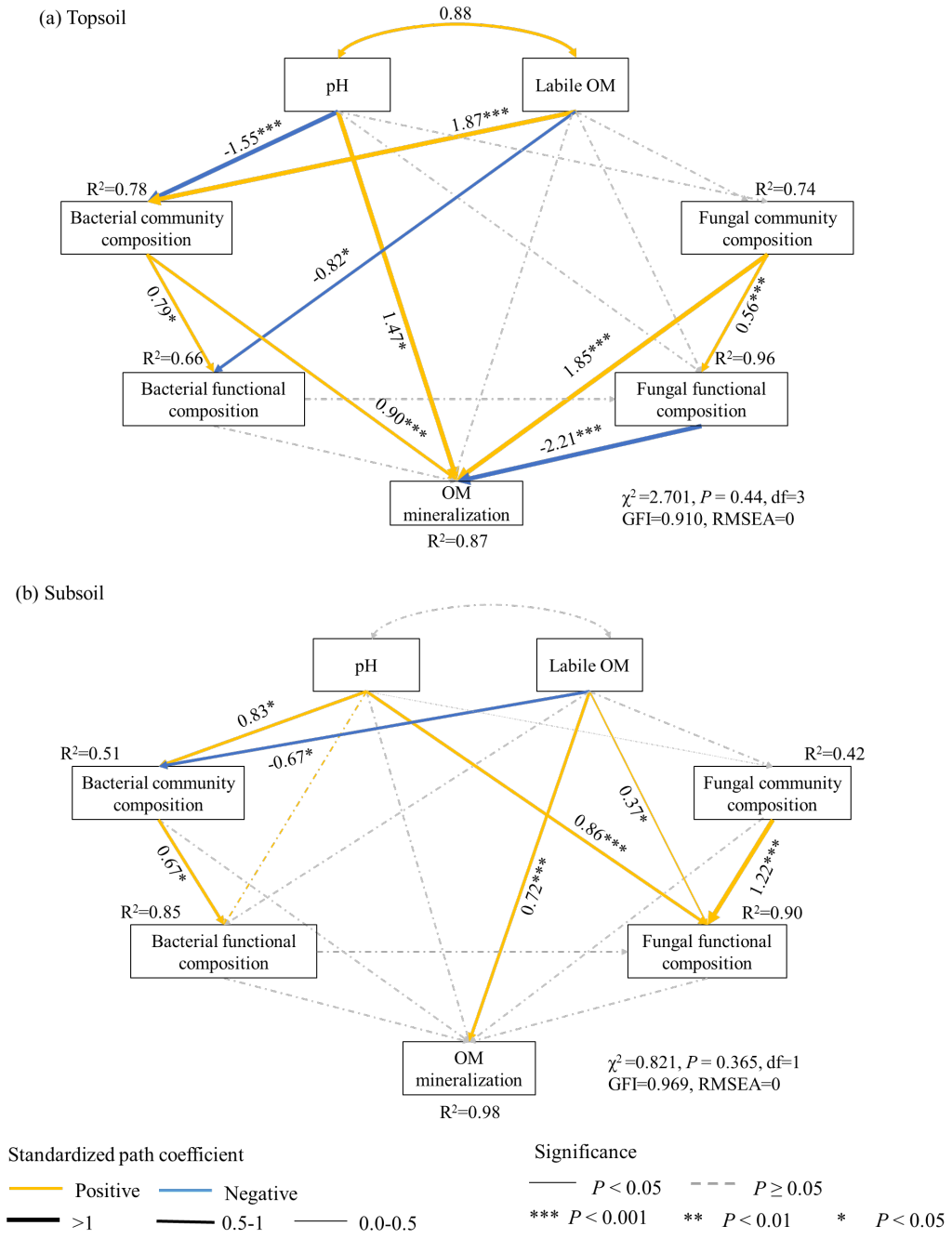

Figure 5.5 Structural equation model (SEM) analysis of the direct and indirect correlations between soil abiotic and biotic variables and OM mineralisation. Selected soil properties included pH, labile organic matter (OM) (indicated by the 1st component of the principal component analysis (PCA) of the carbon content and aromaticity of cold and hot water-extractable OM), bacterial and fungal composition (indicated by the 1st component of PCA of dominant phyla) and functional composition (indicated by the 1st component of PCA of

the functional composition), as well as OM mineralisation (i.e. accumulated carbon dioxide emission from OM) of all (a) topsoil and (b) subsoil treatments with plant residue at the end of the 6-month incubation. The solid and dash line represents the significant (P<0.05) and insignificant ($P \geqslant 0.05$) correlation, respectively, which is shown in yellow if positive or bule if negative. The path width is proportional to the strength of the correlations. Numbers adjacent to the path are standardised path coefficients with asterisks indicating their significance (* P<0.05, ** P<0.01, *** P<0.001). The proportion of variance explained (R^2) are shown alongside the box of the endogenous variables.

5.4 Discussion

5.4.1 Microbial community composition and functional profile differ with depth

The notable differences in microbial properties (e.g., richness, diversity and community composition) observed between the two soil layers of this alu-andic Andosol were attributed to their different environmental/biogeochemical conditions (Table S5.1), which have an impact on microbial life (Dixon and Tilston, 2010; Ramírez et al., 2020). Namely, as depth increased, there was a drop in total C and N (TC: from 95.1 g/kg to 67.9 g/kg; TN: from 7.5 g/kg to 5.4 g/kg), Olsen P (from 14.2 mg/kg to 2.6 mg/kg in original soils), and particularly labile OM fractions (e.g., CWEC: from 0.18 g/kg to 0.04 g/kg; HWEC: from 2.64 g/kg to 0.53 g/kg, shown in Tables S5.1 and S5.3). This contributed to the decrease in microbial richness and diversity with soil depth, along with the shift in the soil microbial community composition from fast-growing r-strategists (dominated by copiotrophs, e.g., *Proteobacteria*, *Actinobacteria*, *Bacteroidetes, Basidiomycota* and *Mortierellomycota*) (Cho et al., 2017; Xu et al., 2020; Yang et al., 2019b), to slow-growing K-strategists (dominated with oligotrophs, e.g., *Chloroflexi* and *Ascomycota*) (Lennon et al., 2012; Li et al., 2014; Su et al., 2020). While r-strategists are adapted to maximise their

intrinsic rate of growth when resources are abundant, K-strategists are able to compete and survive when resources are limited (Pianka, 1970). This was consistent with the results of network analyses of the topsoil and the subsoil under different treatments (Figure S5.9), which show that, compared with the topsoil, the subsoil had a more complex network of either bacteria or fungi (particularly fungi) that is dominated by more negative correlations, which indicates a stronger competitions between microorganisms for substrate (Wei et al., 2020).

The microbial (both bacterial and fungal) functional composition was highly depth-dependent, showing a decrease in bacterial degradation of organic compounds, and most of fungal metabolic functions as depth increased. These changes could be explained by (i) the decrease in amounts of the available nutrients and OM resources, as well as (ii) the drop in richness and diversity of bacteria and fungi resulting in a less capacity to degrade OM at depth (Figures 5.1 and S5.8, Cline and Zak, 2016; Zhonga et al., 2018).

5.4.2 The response of microorganisms to amendments differs with depth

When lime amendments were applied to the topsoil, there was an evident impact on both bacterial and fungal community composition and functional profile. This could be linked to the increase in the labile OM pool size (e.g., cold water-extractable OM, Haynes, 2005) and the changes in their chemistry (as inferred from the increased aromaticity of cold water-extractable OM, Figure 5.3) produced by the alkalisation caused by lime (as inferred with the positive correlation between pH and labile OM, Figure 5.5a). In the previous studies (Chapter 3 and Chapter 4), we proposed that the competition between organic ligands and newly generated OH^- by lime application for reactive sites disrupted OM-metal/mineral

complexes and/or aggregates, causing the release of previously-protected OM to the aqueous phase (Li et al., 2020). The lime amendments-driven shifts in microbial composition, particularly in the fungal community with (i) the increase in *Ascomycota* and *Mortierellomycota*, being attributed to increase in labile OM resulting from alkalisation; and (ii) the decreased *Basidiomycota*, likely due to the competition with favoured *Ascomycota*, were also noted by previous studies by Ye et al. (2020) and Liu et al. (2020). These changes in bacterial and fungal community composition further shaped functional profile, with an increase in OM degradation by bacteria, and in most fungal metabolic functions.

In the subsoil, the evident change was only found in the fungal community, with a distinct drop in richness and diversity resulting from the addition of either lime or P. This could be associated with the increase in alkalinity caused by these treatments (e.g., resulting from the addition of lime or through the displacement of OH^- from reactive sites by PO_4^{3-}, particularly at pH >6) (Li et al., 2020; Schneider et al., 2010), which might have decreased fungal diversity through the inhibition of some specific fungal groups, e.g., *Basidiomycota* and *Mortierellomycota* (Qiu et al., 2020; Ye et al., 2020). However, the latter (and *Ascomycota*) tended to be favoured with the increase in labile OM, and might have eclipsed the decrease in richness and diversity indexes and the shifts in composition (Liu et al., 2020). This could explain the negligible effects on fungal α-diversity found in subsoil treatments that received combined lime and P (SS-LR-PL) and the amended topsoils (TS-LR-L, TS-LR-P and TS-LR-PL), where there was a greater water-extractable OM concentration (e.g., CWEC and HWEC, Table S5.3) than in the subsoil treated with individual lime and P, despite the increase in alkalinity that also occurred in these systems.

However, P addition-driven changes had a negligible impact in functional profile of neither bacteria nor fungi. This might be due to microbial functional redundancy, which refers to the fact that the same functions are associated with many different microbial species, and thus the decrease in abundance of one or some species do not necessarily cause evident changes in the functional profile (Grządziel, 2017; Cline and Zak, 2016).

5.4.3 The links between abiotic/biotic drivers and OM mineralisation differ with depth

In the topsoil, the fungal properties (community composition of the dominant phyla and functional profile) were found to play a key role in mineralisation of OM (which had a predominance of plant-derived OM), as shown by the great abundance of fungi (richness index ranging between 453–602 in topsoil vs. 191–339 in subsoil, Figure 5.1b). This is consistent with previous findings that fungi are dominant decomposers of the high C/N plant-derived OM (Šnajdr et al., 2008; Zimmerman et al., 2011). However, there was a minor role of increased labile OM caused by the amendments in OM decomposition. This could be related to (i) the relatively large amounts of available OM already present in the topsoil, with relatively small increment of labile OM caused by amendments (e.g., CWEC increment <13%), and (ii) the fact that the labile OM molecular complexity, which was dominated by plant-derived OM, was barely changed with the amendments (Lehmann et al., 2020, Li et al., 2020). On the contrary, at depth, available resources (OM and nutrients) decreased, and an increase in labile OM (e.g., CWEC increment was up to 21%) had a key role in OM mineralisation, with the contribution of microbial community composition and functional profile being negligible. This was consistent with previous findings where the mineralisation of OM was found to be driven by the availability of C substrate, but was

independent of microbial properties (regulatory gate hypothesis, Kemmitt et al., 2008), as available OM sources for microorganisms are limited (Brookes et al., 2017; Chen et al., 2016; Xu et al., 2020).

5.5 Conclusions and implications

These results corroborate the distinct responses of OM mineralisation with depth to lime and/or P amendments, as reported in our previous study (Chapter 4). Regardless of soil depth, plant residue addition (simulating the incorporation of crop residues to soil) had the potential to (i) shift both bacterial and fungal community composition and functional profile, and (ii) increase OM mineralisation. In the topsoil, OM decomposition was mainly linked to the fungal community composition and functional profile. Although adding lime caused shifts in the fungal community composition and functional profile, these were not large enough to have an apparent influence in OM decomposition during the 6-month incubation. Shifts among the slow-growth fungal community and their contribution to OM decomposition might become more evident in longer-time incubations (Bastian et al., 2009; Nunan et al., 2020). In the subsoil, the different OM decomposition observed with the inorganic amendments (SS-LR-PL > SS-LR-L > SS-LR ≈ SS-LR-P) were dominantly attributed to the increase in labile OM caused by soil alkalinisation, which accentuated the increase in OM mineralisation caused by plant residue addition. Overall, our findings are valuable in advancing our understanding of the effects of lime and/or P on OM turnover within the soil profile and their implications in the design of climate-smart management practices for these soils.

Appendix III. Supporting Information for Chapter 5 (SI5)

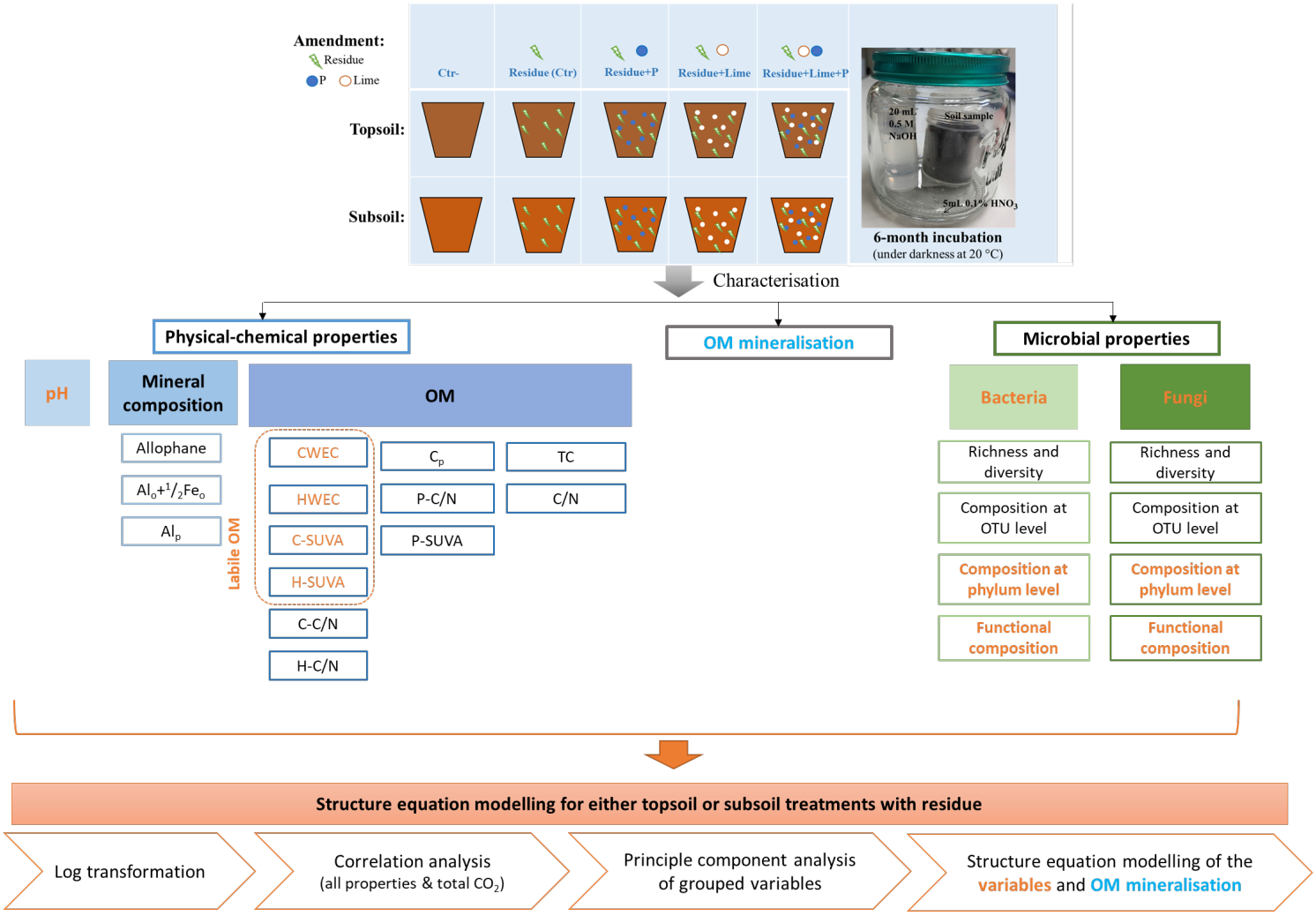

Figure S5.1 Schematic figure of the soil incubation, characterisation of the soil after incubation, and structure equation modelling process.

S5.1 Supporting materials and method

S5.1.1 Characterisation of the soil samples

Soil characterisation was carried out as follows. Water holding capacity at -10kPa was determined using a suction plate (Loveday, 1974). Soil pH was measured at a soil: solution ratio of 1:2.5 (in either deionised water or 1M KCl) using a standard glass electrode. Olsen phosphorus (P) was extracted following Olsen et al. (1954) and determined by the phosphomolybdate method of Murphy and Riley (1962). Total P was determined using a vanadomolydate method after Kjeldahl digestion (McKenzie and Wallace, 1954). The reactive aluminium (Al), iron (Fe) and silicon (Si) (in short-range constituents and/or organo-Al/Fe complexes) were extracted with 0.1 M acid ammonium oxalate (Al_o, Fe_o and Si_o) (Blakemore, 1972). The Al_p and Fe_p (mostly in organo-Al/Fe complexes) were extracted with 0.1 M sodium pyrophosphate (ca. pH=10) (Bascomb, 1968), despite relatively small amounts of Al and Fe from short-range order constituents are also able to be extracted by this reagent (Blakemore, 1972). The concentrations of Al, Fe and Si in all extracts were measured by MP-AES (4200 MP-AES, Agilent Technologies, Singapore). Allophane content was estimated following the method of the Mizota and Van Reeuwijk (1989). To investigate the OM associated with mineral, the bulk soil samples were treated with ca. 2% hydrofluoric acid to removing mineral fraction (Shen et al., 2018). Soil carbon (C) and nitrogen (N) contents were measured using an elemental analyser (Elementar, Vario MACRO, Germany). The sodium pyrophosphate-extractable C (C_p) content was determined using a Total Organic Carbon Analyser (TOC-LCSH, Shimadzu, Japan).

S5.1.2 Soil carbon dioxide (CO_2) evolution measurement

During the incubation, emitted CO_2 was trapped by 0.25 M NaOH (20 mL) and measured using an electrical conductivity (EC) meter (HI 8733, Hannah instrument, US) following a modified version of the protocol of Whitman et al. (2014). The NaOH solution was used instead of KOH herein. There was a strong linear relationship between the injected CO_2 volume and EC values of NaOH traps measured after 24-hour equilibrium. The CO_2 evolution measurements were taken at day 3, 7, 14, 21, 28, 35, 42, 49, 56 and 63, thereafter every two weeks from day 64 to day 175. The total cumulative CO_2 evolution was calculated as the sum of each measurement.

The organic matter (OM) mineralisation in limed soil was obtained by subtracting $CO_{2\ (lime)}$ released from lime added from the total cumulative CO_2 evolution. The $CO_{2\ (lime)}$ was estimated based on the inorganic C present in lime. The CO_2-C from the lime equalled to inorganic C of lime added, as the limed topsoils and subsoils had undetectable inorganic C at end of the 6-month incubation.

S5.1.3 Physicochemical characterisation of the incubated soils

At the end of the 6-month incubation, soil pH, and the contents of total C, total N and C_p were measured as described above. The fresh soil samples (equivalent to 3 g d.w.) were first extracted with 18 mL deionised water in a centrifuge tube at room temperature (ca. 20 °C) for 1 hour. After centrifugation, the supernatant was passed through a filter paper (Whatman No 42) and analysed. The soil residues in the tubes were resuspended with 18 mL deionised water before being placed in a water bath (80 °C) for a 16-hour hot water extraction. Thereafter, the hot water-extractable fraction was collected as described above

(Curtin et al., 2015). The organic C and total N contents in cold water, hot water and sodium pyrophosphate extracts were determined using a Total Organic Carbon Analyser. The mineral N (NH_4^+ and NO_3^-) contents of the extracts (with cold and hot water and sodium pyrophosphate, as mentioned above) were determined on a Technicon autoanalyser. The organic N of each extract was obtained by subtracting mineral N from corresponding extractable total N and used for their C/N ratio (C-C/N, H-C/N and P-C/N, respectively) calculation. The UV absorbance at 254 nm (UV_{254}) of each extract was measured on a UV/Visible scanning spectrophotometer (Jenway 7315, UK) to estimate the content of conjugated unsaturated C (assumed to be mainly aromatic C). Specific UV absorbance at 254 nm (SUVA) of cold and hot water (C-SUVA and H-SUVA) and sodium pyrophosphate (P-SUVA) extracts was calculated as eq. S5.1.

$$\text{SUVA (L/mg C/m)} = UV_{254}/\text{concentration of WEOC} \quad \text{(eq. S5.1)}$$

S5.1.4 Structural equation modelling (SEM) analysis

Before preforming SEM, all data of the variables were subjected to a log transformation according to an eq. Y=lg(Y+1). Thereafter, variables that had significant relationship with OM mineralisation (based on the Spearman's correlation analysis, $P<0.05$) were chosen for the SEM to simplify the model. We ran the principal components analysis (PCA) using (i) CWEC, HWEC, C-SUVA and H-SUVA (Tables S5.3), (ii) dominant phyla community composition of either bacteria or fungi, and (iii) metabolic functions of either bacteria or fungi, separately. The first principal component (PC1) of these analyses (which explained >48% of the variance, as shown in Table S5.4) was then represented as labile OM, bacterial and fungal composition, and metabolic functions, respectively, into the

subsequent SEM (Figure S5.1). The SEM analyses were performed using the IBM SPSS-Amos 26.0. First, we considered the hypothetical model with all possible pathways using the least squares generalised least squares and then sequentially eliminated nonsignificant pathways until we obtained the final models with a nonsignificant Chi-squared test (P>0.05), high $\chi 2$ goodness-of-fit index (GFI>0.85), low root mean square error of approximation (RSME<0.08).

S5.2 Supporting results

S5.2.1 Effects of residue on soil microbial community composition and functional profile

The Figure S5.3 showed that the treatments of topsoil amended with residue showed evident changes in the relative abundance of the dominant phyla, namely the increase in relative abundance of *Proteobacteria* (from 37.4% in Ctr- to 45.1%), *Acidobacteria* (from 17.1% in Ctr- to 22.0%), *Rokubacteria* (from 2.1% in Ctr- to 2.9%) and *Bacteroidetes* (from 2.3% in Ctr- to 3.2%), and a decrease in relative abundance of *Actinobacteria* (from 19.7% in Ctr- to 12.8%), *Chloroflexi* (from 11.3% in Ctr- to 5.4%) and *Gemmatimonadetes* (from 2.6% in Ctr- to 1.6%). The addition of residue alone to subsoil caused consistent effects to those observed in the topsoil on *Proteobacteria* (increasing from 26.6% in Ctr- to 34.9%), *Chloroflexi* (decreasing from 20.6% in Ctr- to 16.3%) and *Gemmatimonadetes* (decreasing from 2.4% in Ctr- to 1.5%). For the fungal composition at phylum level, an apparent increase in relative abundance of the *Basidiomycota* and drop in relative abundance of *Mortierellomycota* was found in topsoil amended with residue (TS-LR) compared with the corresponding Ctr- (TS), whereas at depth the opposed pattern was

observed. The residue amendment also influenced bacterial and fungal community composition at OTU level, as shown in Figure S5.4.

We ran PCA to reveal the response of functional profiles of either bacteria or fungi across all treatments (Figure S5.5). For the functional composition of bacteria, the first two principal components (PCs) accounted for 82.4% of the total variation, with PC1 and PC2 accounting for 64.4% and 18.0%, respectively (Figure S5.5a). The PC1-PC2 scores showed that unamended topsoil and subsoil were located at negative PC1 axis, accounting for a lower negative value of the PC1 axis compared with corresponding residue-amended topsoils and subsoils. For the functional composition of fungi, the PC1 and PC2 accounted for 50.1% and 23.2% of total variation, respectively (Figure S5.5b). The effect of residue amendment was also evident on the fungal functional composition. The unamended topsoil and subsoil accounted for a higher positive value of the PC1 axis compared with corresponding residue-amended topsoils and subsoils.

S5.2.2 The relationship between alpha-diversity and dominant phyla of bacteria and fungi and abiotic factors

The Figure S5.6 showed the results of Spearman's correlation analysis, as follows: (i) the Chao1 and the Shannon indices of bacteria and fungi were generally positively associated with total C and some more active organic C fractions (e.g., CWEC, HWEC) and aromaticity of C fractions (e.g., C-SUVA, H-SUVA, P-SUVA), but was negatively correlated with the content of C_p, and C/N ratio of OM and its fractions (e.g., C/N, C-C/N, H-C/N, P-C/N); (ii) consistent correlations were also found between the *Proteobacteria*, *Actinobacteria* and *Bacteroidetes* of bacteria, *Basidiomycota* and *Mortierellomycota* of

fungi, and these properties of soil C; (iii) on the contrary, the *Acidobacteria*, *Chloroflexi*, *Rokubacteria* and *Ascomycota* were negatively related with the C amount and extractable aromatic compounds, but positively correlated with the Cp and C/N ratio; (iv) generally, the C/N ratio had a significant influence on the dominant fungal community composition, but not on the dominant bacterial community composition; and (v) the selected microbial properties had a weak correlation with soil pH.

S5.3 Supporting discussion

S5.3.1 Response of the bacteria and fungi to the residue added

As expected, the presence of the additional mineralisable OM (with low complexity) and energy resulting from the residue added, influenced bacterial and fungal community composition (at both phylum and OTU level) in both topsoil and subsoil (Hale et al., 2019; Xu et al., 2015), with the consistent increase in the relative abundance of the copiotrophic *Proteobacteria* (Su et al., 2020; Whitman et al., 2016); and (ii) the drop in the relative proportion on of *Chloroflexi* and *Gemmatimonadetes* (consistent with their oligotrophic traits; Bernard et al., 2007; Xu et al., 2020). The response of *Basidiomycota* and *Mortierellomycota* to the residue amendments showed the depth-dependence with the varying abiotic conditions with depth (Yang et al., 2019b).

The changes in bacterial and fungal community composition could mediate the corresponding functional composition. There was an evident shift in bacterial functional profile with a stimulation of degradation/utilisation/assimilation, namely the degradation of carbohydrate (Deg 7), carboxylate (Deg 8), and secondary metabolic (Deg 15), found in both topsoil and subsoil when residue was applied. The functional profile of fungi in the

residue-amended topsoils and subsoils studied tended to be reduced (Figure S5.7), likely attributing to the competing bacteria (Silva-Sánchez et al., 2019), which might dominate the metabolic processes in both topsoil and subsoil.

Table S5.1 Selected properties of the original topsoil and subsoil of this Andosol studied.

	Topsoil (0–20 cm)	Subsoil (20–40 cm)
Moisture content (%)	46.30 ± 0.04	59.74 ± 1.24
Water holding capacity at -10 kPa (%)	74.29 ± 1.82	82.89 ± 7.42
pH (deionised water)	5.58 ± 0.01	5.90 ± 0.04
pH (KCl)	4.42 ± 0.01	4.59 ± 0.04
Total P (g/kg)	0.91 ± 0.03	0.73 ± 0.01
Olsen P (mg/kg)	14.21 ± 4.16	2.60 ± 0.06
Total C (g/kg)	95.07 ± 1.17	67.87 ± 0.13
Total N (g/kg)	7.51 ± 0.09	5.37 ± 0.01
C/N	12.66 ± 0.42	12.64 ± 0.48
Allophane (%)	0.24±0.05	2.50±0.13
Al_p (g/kg)	6.93±0.18	13.09±0.29
Al_p/Al_o	1.15±0.08	0.71±0.01
$(Al_p+Fe_p)/C_p$ atom ratio	0.16±0.02	0.26±0.02
$Al_o+½Fe_o$ (%)	0.91±0.07	2.29±0.08

P (phosphorous), C (carbon), N (nitrogen), Al_o and Fe_o (acid oxalate-extractable aluminium and iron), as well as Al_p, Fe_p and C_p (sodium pyrophosphate-extractable aluminium, iron and carbon).

Table S5.2 Number of the sequence, OTU and the group at different level of bacteria and fungi in topsoil and subsoil without (TS and SS, Ctr-)/with either residue (TS-LR and SS-LR, Ctr), residue+lime (TS-LR-L and SS-LR-L), residue+P (TS-LR-P and SS-LR-P) or residue+lime+P (TS-LR-PL and SS-LR-PL) at end of 6-month incubation.

	Sample	Sequence	OTU	Phylum	Class	Order	Family	Genus
Bacteria	TS (Ctr-)	101,676	3,976	25	55	112	139	170
	TS-LR (Ctr)	95,087	3,880	27	60	115	155	195
	TS-LR-L	108,465	4,480	26	62	119	161	211
	TS-LR-P	95,887	3,953	26	60	116	156	188
	TS-LR-LP	108,820	4,516	28	65	125	169	236
	SS (Ctr-)	96,812	3,052	27	62	99	128	152
	SS-LR (Ctr)	101,695	3,003	27	61	101	125	161
	SS-LR-L	97,258	2,523	27	59	98	129	169
	SS-LR-P	98,079	2,955	25	63	110	140	178
	SS-LR-LP	98,542	2,609	27	55	100	122	163
Fungi	TS (Ctr-)	83,605	522	9	22	44	61	89
	TS-LR (Ctr)	78,710	483	8	18	42	68	101
	TS-LR-L	83,220	583	8	19	43	71	110
	TS-LR-P	80,626	496	7	17	43	67	100
	TS-LR-LP	81,147	493	8	18	45	71	102
	SS (Ctr-)	97,112	305	6	13	27	40	59
	SS-LR (Ctr)	86,389	314	6	13	28	49	82
	SS-LR-L	76,414	216	4	10	23	44	67
	SS-LR-P	59,653	203	5	10	22	38	56
	SS-LR-LP	85,466	289	5	12	26	52	81

Table S5.3 Selected physicochemical properties and organic matter (OM) mineralisation (total cumulative carbon dioxide evolution from OM) of topsoil and subsoil without (TS and SS, Ctr-)/with either residue (TS-LR and SS-LR, Ctr), residue+lime (TS-LR-L and SS-LR-L), residue+P (TS-LR-P and SS-LR-P) or residue+lime+P (TS-LR-PL and SS-LR-PL) at end of 6-month incubation.

Sample	pH	TC g/kg	CWEC (mg/kg)	HWEC (mg/kg)	Cp (g/kg)	C/N	C-C/N	H-C/N	P-C/N	C-SUVA	H-SUVA	P-SUVA	OM mineralisation (mg C/g)
TS	5.05	85.8	0.18	2.64	22.26	14.23	21.23	9.38	14.06	2.72	2.25	7.77	9.00
TS-LR	5.48	92.8	0.14	2.36	25.07	14.73	25.45	10.79	14.13	3.24	2.16	7.23	12.94
TS-LR-L	6.33	103.4	0.16	2.47	21.53	14.98	25.15	10.37	14.85	3.58	2.34	7.59	13.16
TS-LR-P	6.01	105.2	0.13	2.75	24.72	14.98	26.66	11.52	14.84	3.16	2.32	7.19	12.95
TS-LR-PL	6.38	98.8	0.16	3.05	24.55	14.77	26.43	10.86	15.69	3.61	2.42	7.34	13.37
SS	5.87	60.7	0.04	0.53	24.53	14.31	17.47	10.46	16.64	1.64	1.42	5.31	2.79
SS-LR	5.95	65.6	0.08	0.66	29.72	15.53	24.83	13.09	17.90	1.84	1.68	4.76	7.13
SS-LR-L	6.26	70.2	0.10	0.76	33.16	15.76	16.25	12.89	18.04	2.50	2.00	4.49	8.99
SS-LR-P	6.08	70.8	0.09	0.78	40.87	16.46	21.23	13.54	21.26	2.41	1.79	3.48	6.90
SS-LR-PL	6.11	68.3	0.10	0.97	46.19	16.07	17.55	13.82	26.09	2.66	2.01	3.31	9.92

Total carbon, cold and hot water- and sodium pyrophosphate-extractable organic carbon was labelled as TC, CWEC, HWEC and Cp, respectively.

Ratio of carbon/nitrogen of soil, as well as the cold and hot water- and sodium pyrophosphate-extractable OM was labelled as C/N, C-C/N, H-C/N and P-C/N, respectively.

Aromaticity (indicated by specific UV absorbance at 254 nm, SUVA) of the cold and hot water- and sodium pyrophosphate-extractable OM was labelled as C-SUVA, H-SUVA and P-SUVA, respectively.

Table S5.4 Results of principal component analysis (PCA) of the abiotic and biotic properties in topsoils and subsoils amended with residue.

Factors	1st principal component (PC1) (%)	
	Topsoil	Subsoil
Labile OM	57.8	75.1
Bacterial composition	49.3	57.4
Fungal composition	57.5	67.2
Bacterial functional composition	48.5	61.0
Fungal functional composition	72.1	73.8

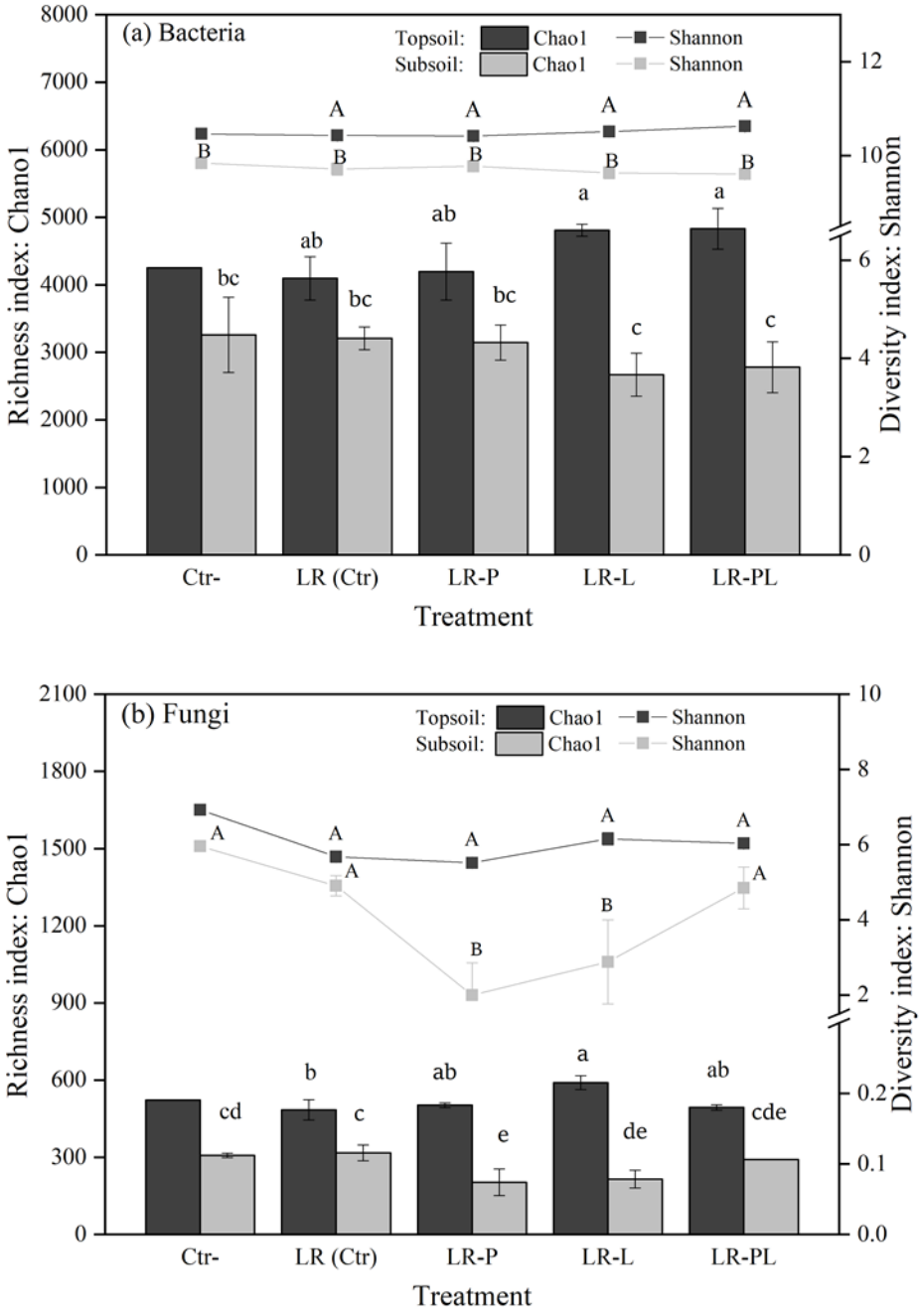

Figure S5.2 Richness (Chao1 index) and diversity (Shannon index) of the (a) bacteria and (b) fungi in the topsoil (TS) and subsoil (SS) incubated without (Ctr-)/with amendments: residue (LR, Ctr), residue+lime (LR-L), residue+P (LR-P) and residue+lime+P (LR-PL).

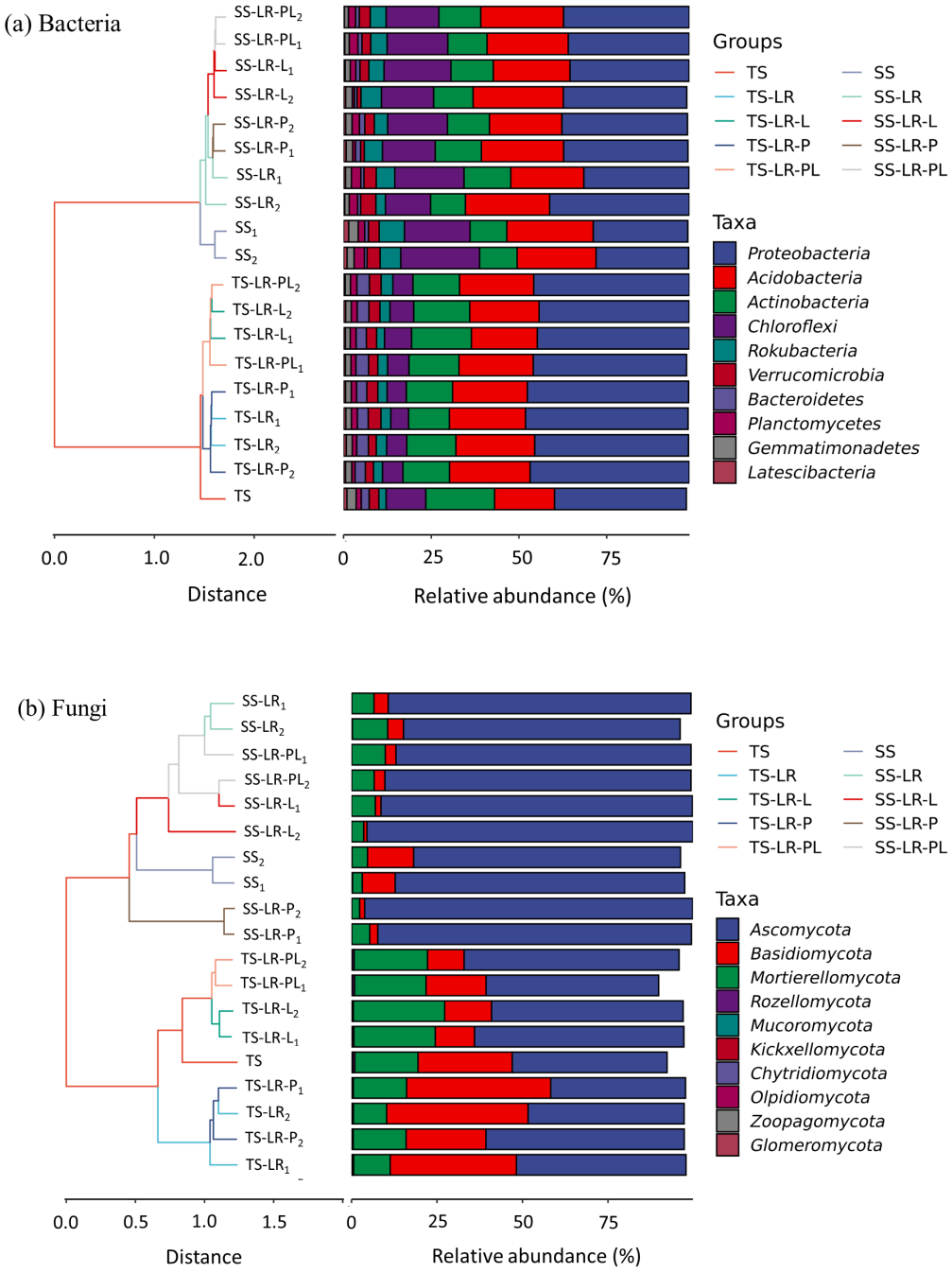

Figure S5.3 Relative abundance of the dominant phyla of (a) bacteria and (b) fungi in topsoil and subsoil incubated without (TS and SS, Ctr-)/with either residue (TS-LR and SS-LR, Ctr), residue+lime (TS-LR-L and SS-LR-L), residue+P (TS-LR-P and SS-LR-P) or residue+lime+P (TS-LR-PL and SS-LR-PL), with cluster analysis based on based on the similarity between the treatments (left panels).

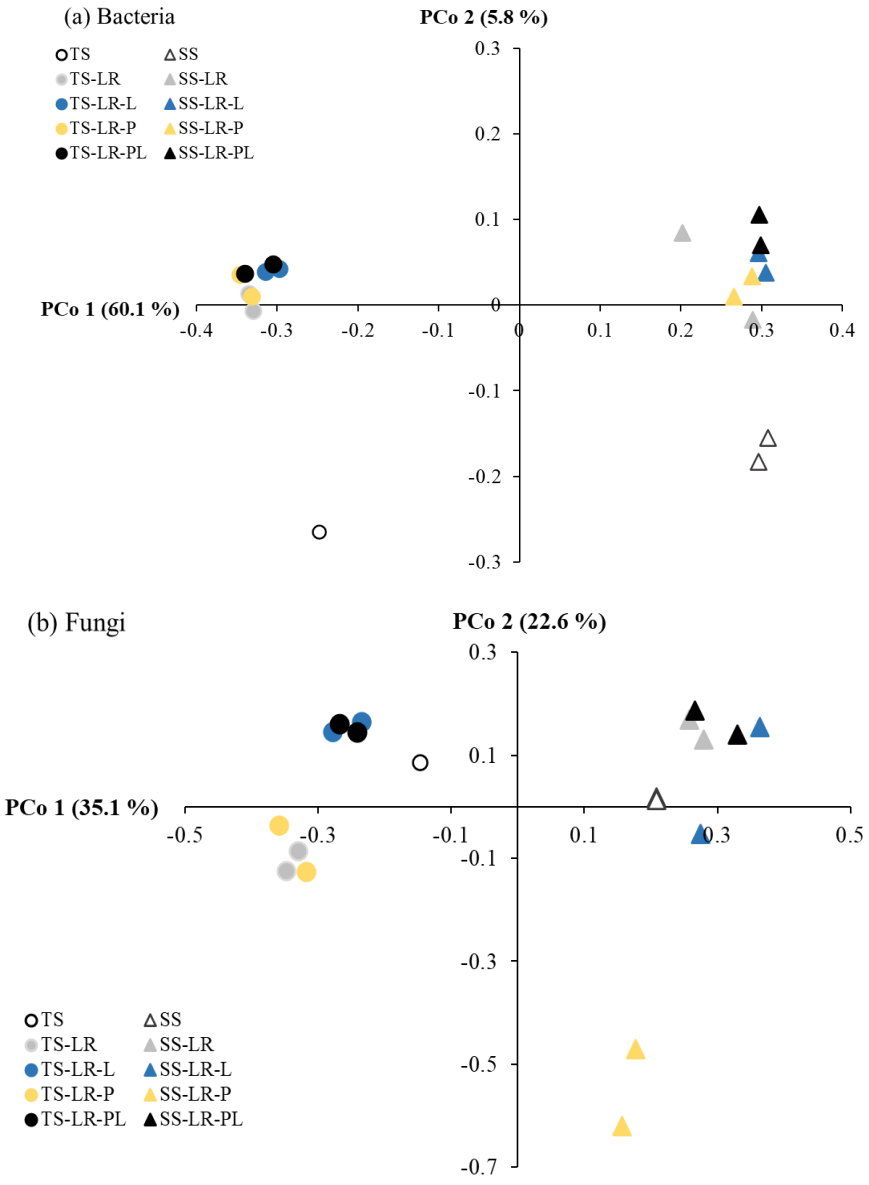

Figure S5.4 Principal coordinate analysis of the (a) bacterial and (b) fungal community composition (at OTU level) in treatments of topsoil and subsoil without (TS and SS, Ctr-) /with either residue (TS-LR and SS-LR, Ctr), residue+lime (TS-LR-L and SS-LR-L), residue+P (TS-LR-P and SS-LR-P) or residue+combined P and lime (TS-LR-PL and SS-LR-PL) at end of 6-month incubation.

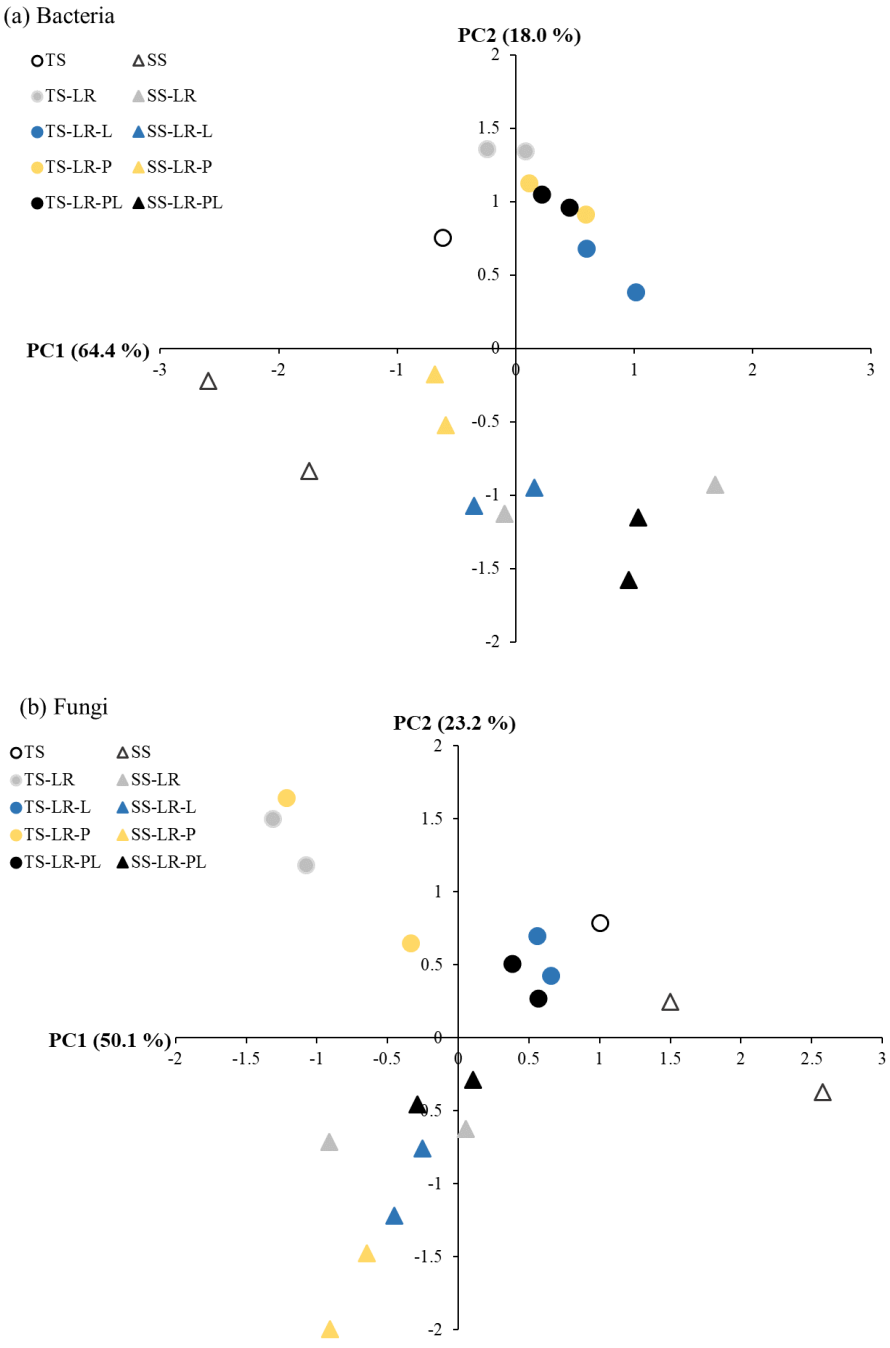

Figure S5.5 Principal compound analysis of the functional composition of (a) bacteria and (b) fungi in the treatments of topsoil and subsoil without (TS and SS, Ctr-)/with either residue (TS-LR and SS-LR, Ctr), residue+lime (TS-LR-L and SS-LR-L), residue+P (TS-LR-P and SS-LR-P) or residue+combined P and lime (TS-LR-PL and SS-LR-PL) at end of 6-month incubation. The microbial functional composition was predicted by PICRUSt2 and MetaCyc metabolic pathway database using the sequencing dataset.

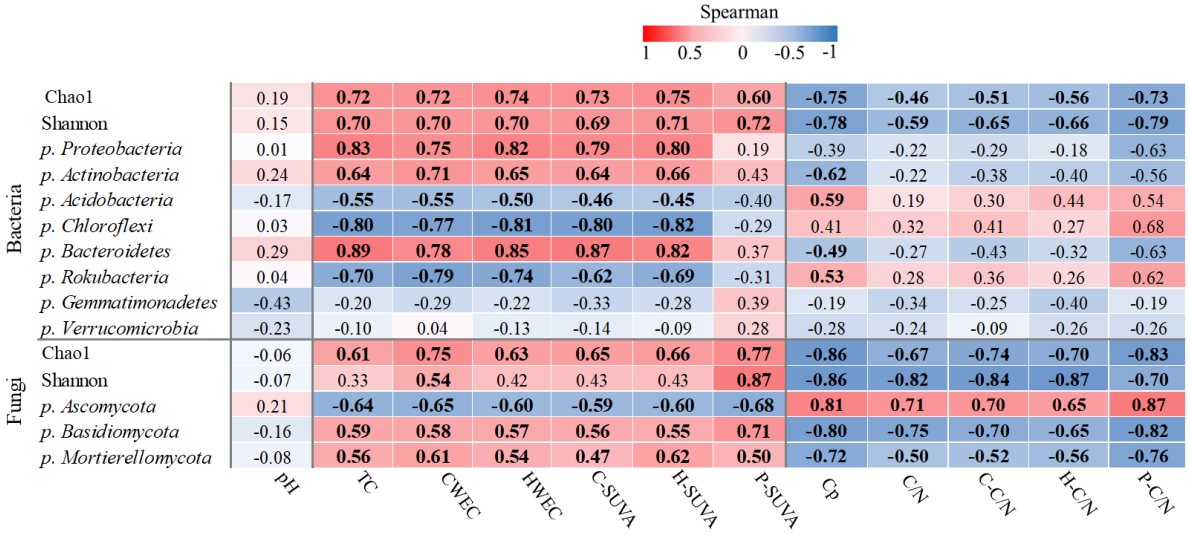

Figure S5.6 Spearman's correlations between richness (Chao1) and diversity (Shannon) index, and relative abundance of dominant phyla of bacteria and fungi, as well as selected soil physicochemical properties. The soil properties included pH, quantity of the total carbon (TC), cold and hot water-extractable organic carbon (CWEC and HWEC), and sodium pyrophosphate-extractable organic carbon (Cp), as well as chemistry of the organic matter (OM), namely, ratios of carbon to nitrogen of soil (C/N) and its cold and hot water- and sodium pyrophosphate-extractable OM (C-C/N, H-C/N and P-C/N), as well as the aromaticity of cold and hot water- and sodium pyrophosphate-extractable OM (C-SUVA, H-SUVA and P-SUVA). The bold numbers represent that the correlations are significant at $P<0.05$.

Table S5.5 List of the metabolic pathways of bacteria and fungi (based on the functional genes predicted by PICRUSt2 and MetaCyc metabolic pathway database) determined in topsoils and subsoils.

Code	Group	Pathway
Bio1	Biosynthesis	Amine and Polyamine Biosynthesis
Bio2	Biosynthesis	Amino Acid Biosynthesis
Bio3	Biosynthesis	Aminoacyl-tRNA Charging
Bio4	Biosynthesis	Aromatic Compound Biosynthesis
Bio5	Biosynthesis	Carbohydrate Biosynthesis
Bio6	Biosynthesis	Cell Structure Biosynthesis
Bio7	Biosynthesis	Cofactor, Prosthetic Group, Electron Carrier, and Vitamin Biosynthesis
Bio8	Biosynthesis	Fatty Acid and Lipid Biosynthesis
Bio9	Biosynthesis	Metabolic Regulator Biosynthesis
Bio10	Biosynthesis	Nucleoside and Nucleotide Biosynthesis
Bio11	Biosynthesis	Other Biosynthesis
Bio12	Biosynthesis	Secondary Metabolite Biosynthesis
Deg1	Degradation/Utilisation/Assimilation	Alcohol Degradation
Deg2	Degradation/Utilisation/Assimilation	Aldehyde Degradation
Deg3	Degradation/Utilisation/Assimilation	Amine and Polyamine Degradation
Deg4	Degradation/Utilisation/Assimilation	Amino Acid Degradation
Deg5	Degradation/Utilisation/Assimilation	Aromatic Compound Degradation
Deg6	Degradation/Utilisation/Assimilation	C1 Compound Utilisation and Assimilation
Deg7	Degradation/Utilisation/Assimilation	Carbohydrate Degradation
Deg8	Degradation/Utilisation/Assimilation	Carboxylate Degradation
Deg9	Degradation/Utilisation/Assimilation	Chlorinated Compound Degradation
Deg10	Degradation/Utilisation/Assimilation	Degradation/Utilisation/Assimilation - Other
Deg11	Degradation/Utilisation/Assimilation	Fatty Acid and Lipid Degradation
Deg12	Degradation/Utilisation/Assimilation	Inorganic Nutrient Metabolism
Deg13	Degradation/Utilisation/Assimilation	Nucleoside and Nucleotide Degradation
Deg14	Degradation/Utilisation/Assimilation	Polymeric Compound Degradation

Deg15	Degradation/Utilisation/Assimilation	Secondary Metabolite Degradation
Det1	Detoxification	Antibiotic Resistance
Det2	Detoxification	Methanol Oxidation to Carbon Dioxide
Gene1	Generation of Precursor Metabolite and Energy	1,5-anhydrofructose Degradation
Gene2	Generation of Precursor Metabolite and Energy	Electron Transfer
Gene3	Generation of Precursor Metabolite and Energy	Ethylmalonyl-CoA Pathway
Gene4	Generation of Precursor Metabolite and Energy	Fermentation
Gene5	Generation of Precursor Metabolite and Energy	formaldehyde oxidation I
Gene6	Generation of Precursor Metabolite and Energy	Glycolysis
Gene7	Generation of Precursor Metabolite and Energy	Glyoxylate Cycle
Gene8	Generation of Precursor Metabolite and Energy	Isopropanol Biosynthesis
Gene9	Generation of Precursor Metabolite and Energy	Methyl Ketone Biosynthesis
Gene10	Generation of Precursor Metabolite and Energy	Methylaspartate Cycle
Gene11	Generation of Precursor Metabolite and Energy	Pentose Phosphate Pathways
Gene12	Generation of Precursor Metabolite and Energy	Photosynthesis
Gene13	Generation of Precursor Metabolite and Energy	Respiration
Gene14	Generation of Precursor Metabolite and Energy	Superpathway of Glycolysis and Entner-Doudoroff
Gene15	Generation of Precursor Metabolite and Energy	Superpathway of Glycolysis, Pyruvate Dehydrogenase, TCA, and Glyoxylate Bypass
Gene16	Generation of Precursor Metabolite and Energy	TCA Cycle
Gly1	Glycan Pathways	Glycan Biosynthesis
Gly2	Glycan Pathways	Glycan Degradation
Mac1	Macromolecule Modification	Nucleic Acid Processing
Met1	Metabolic Clusters	L-glutamate and L-glutamine Biosynthesis
Met2	Metabolic Clusters	O-antigen Building Blocks Biosynthesis (E. coli)
Met3	Metabolic Clusters	Phospholipases
Met4	Metabolic Clusters	Pyrimidine Deoxyribonucleotide Phosphorylation
Met5	Metabolic Clusters	Pyrimidine Deoxyribonucleotides Biosynthesis from CTP
Met6	Metabolic Clusters	Pyrimidine Deoxyribonucleotides de novo Biosynthesis I
Met7	Metabolic Clusters	Pyrimidine Deoxyribonucleotides de novo Biosynthesis III
Met8	Metabolic Clusters	Pyrimidine Deoxyribonucleotides de novo Biosynthesis IV
Met9	Metabolic Clusters	Superpathway of L-aspartate and L-asparagine Biosynthesis

Met10	Metabolic Clusters	tRNA Charging

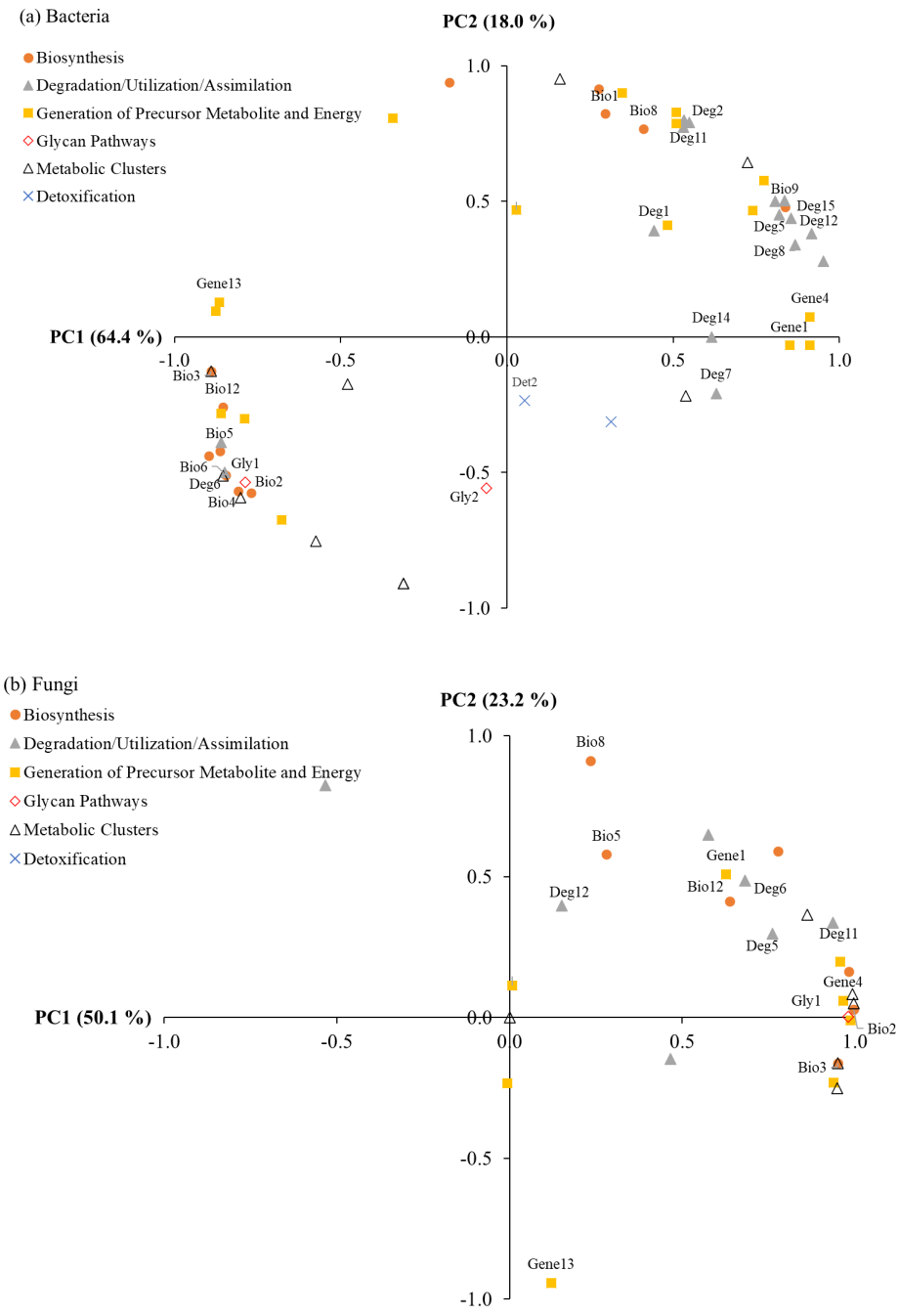

Figure S5.7 The PC1-PC2 loadings of (a) bacterial and (b) fungal functional composition (based on the functional genes predicted by PICRUSt2 and MetaCyc metabolic pathway database) in topsoils and subsoils incubated without (TS and SS, Ctr-)/with either residue (TS-LR and SS-LR, Ctr), residue+lime (TS-LR-L and SS-LR-L), residue+P (TS-LR-P and SS-LR-P) or residue+combined P and lime (TS-LR-PL and SS-LR-PL).

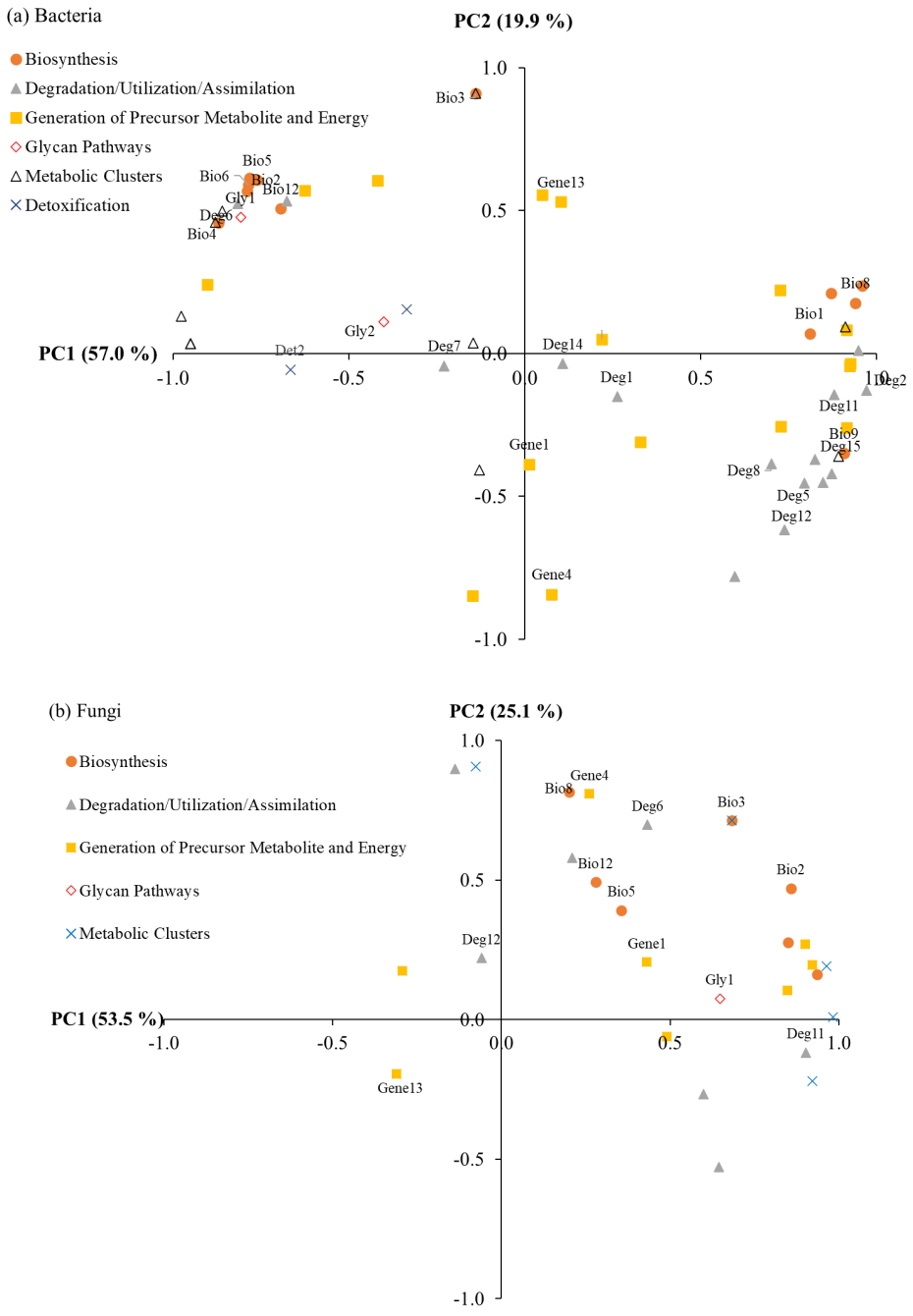

Figure S5.8 The PC1-PC2 loadings of (a) bacterial and (b) fungal functional composition (based on the functional genes predicted by PICRUSt2 and MetaCyc metabolic pathway database) in topsoils and subsoils incubated with either residue (TS-LR and SS-LR, Ctr), residue+lime (TS-LR-L and SS-LR-L), residue+P (TS-LR-P and SS-LR-P) or residue+combined P and lime (TS-LR-PL and SS-LR-PL).

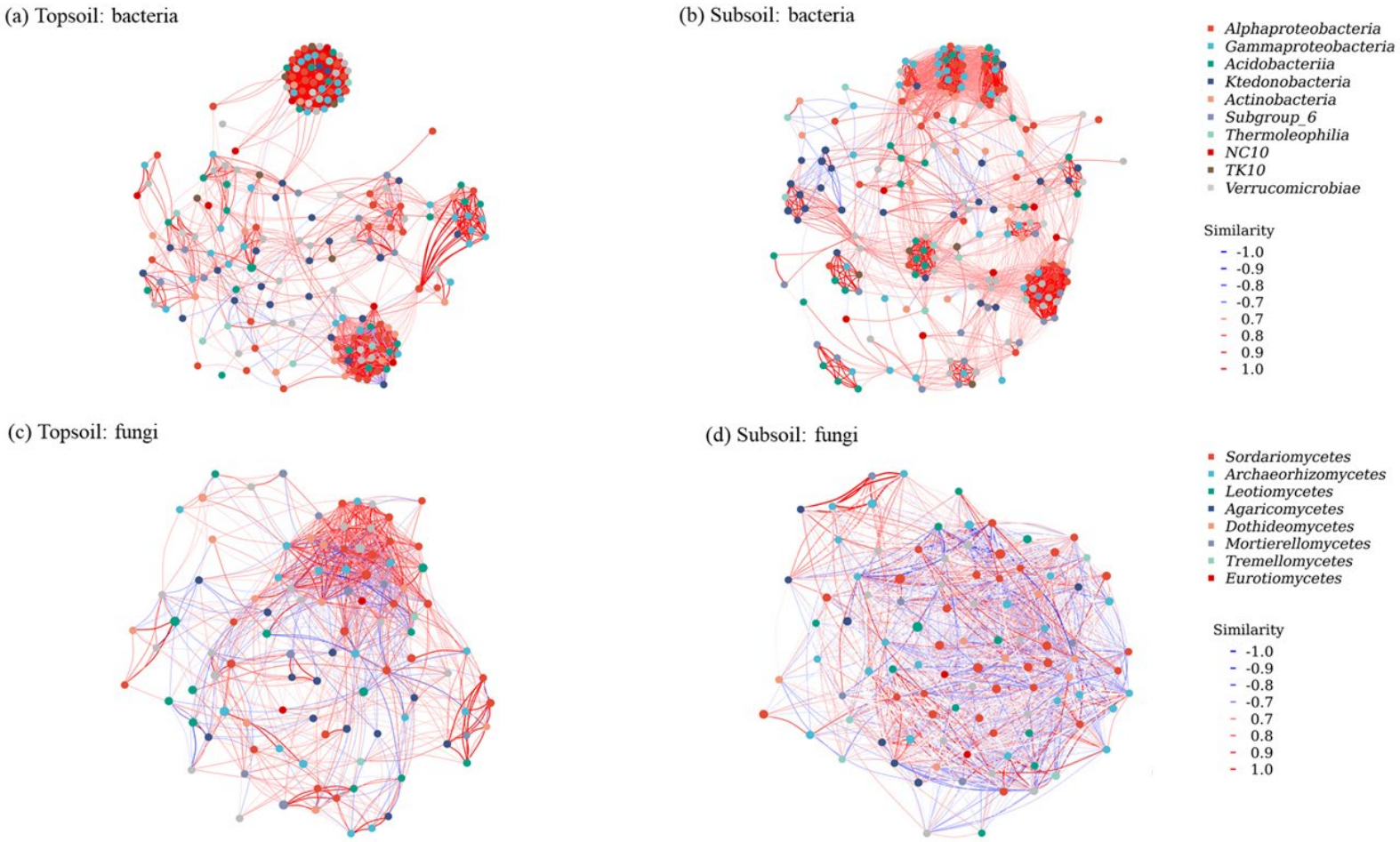

Figure S5.9 Network analysis showing (a and b) bacterial and (c and d) fungal classes co-occurrence in (a, c) topsoils and (b, d) subsoils studied. Top 200 OTUs of bacteria and 100 OTUs of fungi of each depth were selected for each network. Reddish lines represent significantly strong positive linear relationships ($r>0.7$); blueish lines represent strong negative relationships ($r<-0.7$).

CHAPTER 6

OVERALL SUMMARY AND RECOMMENDATIONS FOR FUTURE RESEARCH

6.1 Overall summary

Increasing soil organic matter (OM) storage has been promoted by scientists and policy makers as a prospective way to achieve climate change mitigation and food security. Given that land use intensification often entails a decrease in soil OM, it is essential to understand the effect of agricultural management practices on soil OM preservation, particularly in soils (e.g., Andosols) that play an important role in agricultural production and face a high risk of carbon (C) loss. Management practices such as liming and P fertilisation have the potential to negatively impact the preservation of OM in these soils. This thesis has investigated the effect of lime and/or P amendments on OM preservation in an Andosol used as a benchmark. Special attention has been paid to the different responses of OM stabilisation and mineralisation with depth to these amendments. The findings from this study contribute to providing a mechanistic understanding of how lime and/or phosphorus (P) amendment impairs soil OM preservation, and have implications for the design of climate-smart agricultural management practices.

6.1.1 Lime and/or P amendments impact soil OM stabilisation through different mechanisms

The addition of lime and/or phosphate to the soil caused a significant increase in the water-extractable OM (WEOM), along with a shift in the composition of organic compounds (e.g., the poly- and mono-phenolic and nitrogenised fractions), particularly when lime and P were applied in combination. The fact that, upon P-only addition, the changes in WEOM were larger in the bulk soil than in the heavy fractions points towards the evident impact of the phosphate ligand on vulnerable particulate OM (which contains some Al^{3+}-OM

complexes). The influence of lime applications on WEOM was observed in both the particulate and the heavy fractions, indicating that OM destabilisation was caused by the displacement and/or release of OM associated with inorganic constituents (Al^{3+} and allophane) and/or OM previously encapsulated in aggregates. There was a synergetic effect of lime and P on OM destabilisation (Chapter 3). These findings confirmed the hypotheses that (i) lime and P application to soil influences the OM stabilisation through different mechanisms, and (ii) the combined effect of P and lime addition on OM stabilisation is stronger than that of either P or lime addition alone.

6.1.2 Effects of lime amendments on OM preservation vary with soil depth

In the topsoil (rich in OM-Al^{3+} complexes) of the alu-andic Andosol, an increase in WEOM was, as expected, found in bulk soil that incubated with lime amendments for 6 months (Chapter 4), which was consistent with the previous extraction experiment (chapter 3). The nano-scale secondary ion mass spectrometry analyses of microaggregates showed that the topsoil had high OM coverage (with higher enrichment in N-poor OM) on the mineral surfaces with lower spatial complexity, mainly through non-selective adsorption (e.g., $OMn_{(N\text{-poor})}$-$OM_{(N\text{-rich})}$-mineral association). The N-poor OM was preferentially desorbed as soil pH increased with liming, consistent with the increase in WEOM found in bulk soil. These indicate that in the topsoil, lime addition destabilised soil OM, attributed to the disruption of OM (particularly N-poor OM)-mineral association in microaggregates (Chapter 4 and Figure 6.1). Despite liming increased OM availability, the changes in OM mineralisation were negligible after the short-term incubation. This was supported by the fact that the OM mineralisation process in topsoil showed a significant correlation with microbial properties, particularly fungal community composition and functional profile,

but not with OM availability (Chapter 5 and Figure 6.1).

In the subsoil (with a greater abundance of allophane) of the Andosol under study, the liming-driven increase in WEOM was also found in bulk soil, indicating the occurrence of the OM destabilisation in the limed subsoil. However, the microaggregates measured by NanoSIMS analysis showed a relatively lower OM coverage (more scattered) of the mineral surfaces (including allophane), with a greater contribution of $OM_{(N\text{-}rich)}$-mineral associations via preferential adsorption, reflecting a higher molecular and spatial complexity, compared with those found in topsoil. This was less disrupted by alkalisation, which might have favoured the formation of mineral-Ca-$OM_{(N\text{-}poor)}$ associations upon liming. Thus, the OM destabilisation (indicated by the increase in WEOM in bulk soil) found in the limed subsoil is probably the result of a disruption in the stability of the macroaggregates (Chapter 4 and Figure 6.1). This further increased OM mineralisation in the subsoil, as OM mineralisation was rate-limited by available OM (Chapter 5 and Figure 6.1).

These results confirmed the hypothesis that the amendment-driven changes in OM preservation (OM stabilisation and mineralisation) differ between the two soil layers studied, characterised by having a distinct biogeochemistry. The findings also supported the (i) conceptual model of the "membrane-like" bilayer, with strong inner-sphere bonding between N-rich OM (over other organic compounds) and mineral surfaces, and weaker outer-sphere bonding between N-poor OM and inorganic surfaces, as proposed by Kleber et al. (2015); (ii) the framework of functional complexity that controls the OM persistence, proposed by Lehmann et al. (2020); and (iii) the hypothesis of regulatory gate that soil OM mineralization is not regulated by the soil microbial properties, but mainly depends on the

bioavailability of OM, while the soil microorganisms are not able to access OM (Brookes et al., 2017).

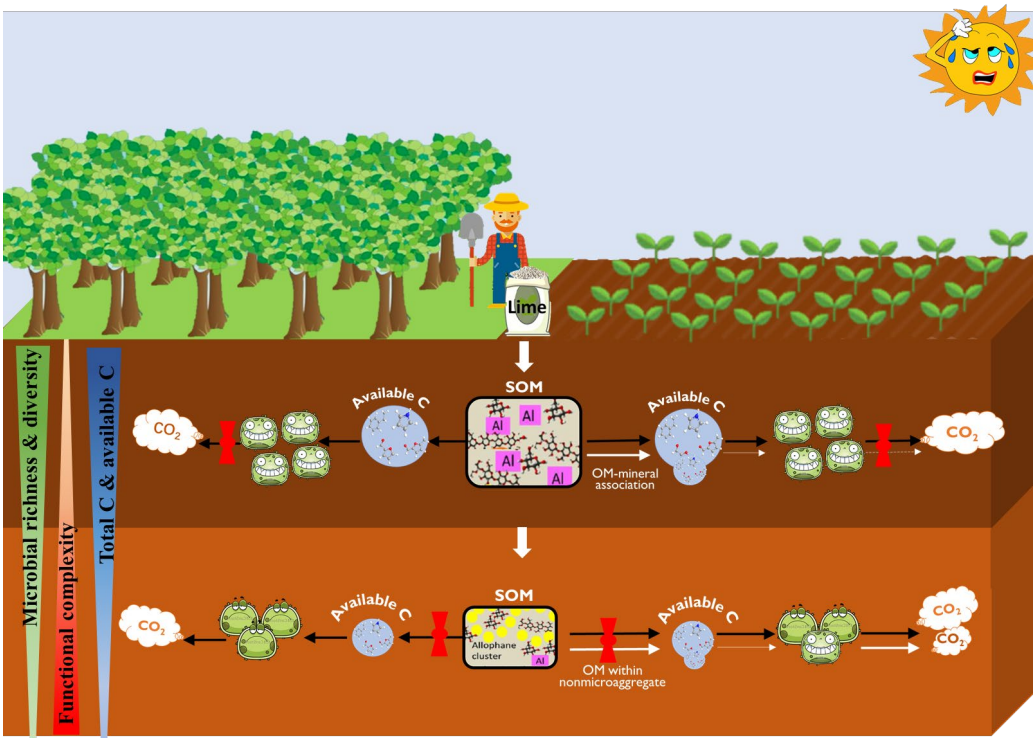

Figure 6.1 Conceptual illustration demonstrating the overall effects of liming on soil OM preservation within soil profile.

6.1.3 Highlights of this thesis

- An increase in phosphate ions in the Andosol caused by a high rate of P fertilisation produced OM destabilisation through phosphate displacing OM in Al^{3+}-OM complexes (Chapter 3).
- Soil alkalisation through liming resulted in the destabilisation of OM by disrupting both Al^{3+}-OM and allophane-OM associations, and also destabilising aggregates (Chapter 3).

- The effect of lime and P amendment on OM destabilisation was synergistic (Chapter 3).
- In the topsoil (with a larger ratio of Al in Al^{3+}-OM complexes to inorganic constituents than in the subsoil), lime-driven destabilisation of OM was associated with a decrease in OM (particularly plant-derived OM) surface coverage of inorganic constituents (Chapter 4).
- In the subsoil (with a greater abundance of allophane than in the topsoil), lime-driven destabilisation of OM was mainly attributed to the disruption of macroaggregates, as OM surface coverage of inorganic constituents in the microaggregates increased (Chapter 4).
- In the topsoil, which is rich in bioavailable OM, the negligible effect of lime and/or P amendments on OM mineralisation was mainly associated with the magnitude of the shifts in fungal community composition and functional profile (Chapter 5).
- In the subsoil, with limited bioavailable OM, liming accelerated OM mineralisation through an increase in labile OM (Chapter 5).

6.2 Importance of these findings for agricultural systems

In New Zealand, Andosols cover 5% of the country's land area and contribute to over 7% of total soil C stock. However, the studies showed that the OM is lost in New Zealand Andosols with ongoing land-use intensification. A field study done in New Zealand by Schipper et al. (2014) showed that the grazing practice of these soils has caused considerable OC losses throughout whole soil profiles (to a depth of 0.9 m) over the last four decades. Shen et al. (2018) studied the effects of land use on the OC content of New Zealand

soils and found a lower OC content in soils under cropping, compared with other land use studied (ungrazed grass and permanently grazed pasture), particularly in the case of the Andosols. It was notable that in Andosols, cropping decreased most soil C fractions (e.g., OC mainly associated with either Al^{3+} or mineral) and total C, with the increase in soil Olsen P and pH (Shen et al., 2018). The latter was due to the fact that the agricultural management of Andosols always involve application of lime and phosphorus, as these soils always have low available P (due to high P retention) and an acid pH under humid temperate climate (Bolan and Hedley, 2003; Dahlgren et al., 2004). Our study provides direct evidence and mechanistic understanding of lime and/or P amendment causing OM destabilisation, and of the liming negatively impacting OM preservation (by OM-allophane/Al^{3+} complexes) within the soil profile.

As a strategy to build the climate-smart practice of these soils where the OM is protected by reactive Al (Al^{3+} and allophane), it may be possible to use the swards adapted acidic condition so that lime use is minimised, but biomass production is maintained. Alternatively, the conversion of the pasture to cropping with the use of acidophilic plants, may achieve the same goal. This strategy could effectively reduce the risk of C loss in these soils.

6.3 Recommendations for future work

The study conducted in this thesis investigated the effect of lime and/or P amendments on OM stabilisation and mineralisation in a C-rich Andosol by considering the role of physical and chemical protection in OM stabilisation, and the role of OM bioavailability and microbial community composition in OM mineralisation. There are research areas on the

effect of lime and/or P applications on soil OM turnover that still require a better understanding, and thus future work could consider the following topics:

- The role of microorganisms in soil OM stabilisation

In addition to physical and chemical protection of soil OM, over recent years, mounting evidence has shown that the metabolism of soil microorganisms (particularly *in vivo* turnover) plays an essential role in soil OM stabilisation (Liang et al., 2017; Wang et al., 2021). Liang et al. (2019) reported that the role of microorganisms could be influenced by land use changes, as made evident by the distinct contributions of microbial necromass to total OC in topsoil of temperate agricultural soils (55.6%), grassland soils (61.8%) and temperate forest soils (30%). Ni et al. (2021) proposed that fertilisation increased the microbial residue content in soil. Thus, in future studies, it would be important to investigate the response of microbial-derived OM (microbial biomass and residue) at different soil depth to lime and/or P amendments.

- The role of different aggregates in soil OM stabilisation

In the subsoil that received lime, the increase in WEOM was assumed to be associated with disruption of the macroaggregates, as there was an increase in OM coverage on the mineral surface in microaggregates. To support this assumption, more studies on the response of OM protected within macroaggregates to liming with depth are needed. In future studies, it would be useful to consider changes in the representative OM fractions (e.g., free particulate OM, intra-aggregate particulate OM, silt+clay-associated OM) obtained by combined density and particle size fractionation (Herath et al., 2013).

- The role of enzyme activity in soil OM mineralisation

In the present study, we only considered the role of labile OM and microbial community composition in soil OM mineralisation. It is notable that the soil enzymes secreted or released by microorganisms, roots and soil fauna play a critical role in OM decomposition, in which enzymatic depolymerisation and oxidation jointly modify insoluble and/or macromolecular OM to a smaller size and to more oxidised and water-soluble OM. Some recent studies reported that, compared with microbial abundance and diversity, enzyme activity had a more important role in controlling OM mineralisation (Tan et al., 2021; Xu et al., 2020). We thus advise investigating the response of soil enzyme activity to lime and/or P amendments, and the relationship between enzyme activity and OM mineralisation.

- The addition of other inputs to soil and their impact on soil OM preservation

Abrupt changes in pH (along with changes in ionic strength) generated in urine patches could be another factor contributing to the destabilisation of OM preserved in soils. In future studies, an experiment on the soil with or without urine deposition (this causing soil alkalisation and an increase in ionic strength) is needed so that the contribution of urine to OM destabilisation is evaluated.

- A large-scale evidence with meta-analysis

In future studies, it will be important to carry out a meta-analysis of the effect of lime and/or P amendments on soil OM, considering factors such as soil type and depth, vegetation, climate and time scale. This could help to prove the universality of the effect

of lime and/or P on OM preservation in acid soils.

REFERENCES

Alleon, J., Bernard, S., Remusat, L, & Robert, R. (2015). Estimation of nitrogen-to-carbon ratios of organics and carbon materials at the submicrometer scale. *Carbon, 84*, 290–298.

Amelung, W., Bossio, D., de Vries, W., Kögel-Knabner, I., Lehmann, J., Amundson, R., . . . Leifeld, J. (2020). Towards a global-scale soil climate mitigation strategy. *Nature Communications, 11*(1), 1–10.

Ahmad, W.; Dijkstra, F.; Dalal, R.; & Singh, B. (2019). Plant roots are more important than temperature in modulating carbon release in a limed acidic soil. *European Journal of Soil Science*, 1−13

Ball, J. W., Nordstrom, D. K., & Jenne, E. A. (1980). Additional and revised thermochemical data for WATEQ-2 computerized model for trace and major element speciation and mineral equilibria of natural waters. *US Geological Survey, Water Resources Investigations, Washington*.

Bardgett, R. D., & Van Der Putten, W. H. (2014). Belowground biodiversity and ecosystem functioning. *Nature, 515*(7528), 505–511.

Bascomb, C. L. (1968). Distribution of pyrophosphate ‐ extractable iron and organic carbon in soils of various groups. *Journal of Soil Science*, 19(2), 251–268.

Bastian, F., Bouziri, L., Nicolardot, B., & Ranjard, L. (2009). Impact of wheat straw decomposition on successional patterns of soil microbial community structure. *Soil Biology & Biochemistry, 41*(2), 262–275.

Batjes, N. H. (2016). Harmonized soil property values for broad-scale modelling (WISE30sec) with estimates of global soil carbon stocks. *Geoderma, 269*, 61–68.

Bernard, L., Mougel, C., Maron, P. A., Nowak, V., Lévêque, J., Henault, C., . . . & Balesdent, J. (2007). Dynamics and identification of soil microbial populations actively assimilating carbon from ^{13}C-labelled wheat residue as estimated by DNA- and RNA-SIP techniques. *Environmental Microbiology*, *9*(3), 752–764.

Blakemore, L. (1972). Methods for chemical analysis of soils. *New Zealand Soil Bureau Scientific Report, 10*, A11. 11-A11. 17.

Boddy, E., Hill, P. W., Farrar, J., & Jones, D. L. (2007). Fast turnover of low molecular weight components of the dissolved organic carbon pool of temperate grassland field soils. *Soil Biology and Biochemistry, 39*(4), 827–835.

Bokulich, N. A., Kaehler, B. D., Rideout, J. R., Dillon, M., Bolyen, E., Knight, R., . . . & Caporaso, J. G. (2018). Optimizing taxonomic classification of marker-gene

amplicon sequences with QIIME 2's q2-feature-classifier plugin. *Microbiome, 6*(1), 1–17.

Bolan, N. S., & Hedley, M. J. (2003). Role of carbon, nitrogen, and sulfur cycles in soil acidification. *Handbook of soil acidity*, 29–56.

Bolyen, E., Rideout, J. R., Dillon, M. R., Bokulich, N. A., Abnet, C. C., Al-Ghalith, G. A., Alexander, H., Alm, E. J., Arumugam, M., and Asnicar, F. (2019). Reproducible, interactive, scalable and extensible microbiome data science using QIIME 2. *Nature biotechnology* **37**, 852–857.

Bond-Lamberty, B., & Thomson, A. (2010). A global database of soil respiration data. *Biogeosciences, 7*(6), 1915–1926.

Bray, J. R., & Curtis, J. T. (1957). An ordination of the upland forest communities of southern Wisconsin. *Ecological Monographs*, 27(4), 325–349.

Brookes, P. C., Chen, Y., Chen, L., Qiu, G., Luo, Y., & Xu, J. (2017). Is the rate of mineralization of soil organic carbon under microbiological control? *Soil Biology and Biochemistry, 112*, 127–139.

Bundy, L., & Bremner, J. (1972). A simple titrimetric method for determination of inorganic carbon in soils 1. *Soil Science Society of America Journal, 36*(2), 273–275.

Bünemann, E. K., Bongiorno, G., Bai, Z., Creamer, R. E., De Deyn, G., De Goede, R., . . . Mäder, P. (2018). Soil quality–A critical review. *Soil Biology and Biochemistry, 120*, 105–125.

Buurman, P., Peterse, F., & Almendros Martin, G. (2007). Soil organic matter chemistry in allophanic soils: a pyrolysis‐GC/MS study of a Costa Rican Andosol catena. *European Journal of Soil Science, 58*(6), 1330–1347.

Buurman, P., & Roscoe, R. (2011). Different chemical composition of free light, occluded light and extractable SOM fractions in soils of Cerrado and tilled and untilled fields, Minas Gerais, Brazil: a pyrolysis‐GC/MS study. *European Journal of Soil Science, 62*(2), 253–266.

Callahan, B. J., McMurdie, P. J., Rosen, M. J., Han, A. W., Johnson, A. J. A., & Holmes, S. P. (2016). DADA2: high-resolution sample inference from Illumina amplicon data. *Nature methods, 13*(7), 581–583.

Camenzind, T., Hättenschwiler, S., Treseder, K. K., Lehmann, A., & Rillig, M. C. (2018). Nutrient limitation of soil microbial processes in tropical forests. *Ecological Monographs, 88*(1), 4–21.

Carter, M. R. (2002). Soil quality for sustainable land management: organic matter and aggregation interactions that maintain soil functions. *Agronomy journal, 94*(1), 38–47.

Changes in fungal communities along a boreal forest soil fertility gradient. (2015). *New Phytologist, 207*(4), 1145–1158.

Chantigny, M. H. (2003). Dissolved and water-extractable organic matter in soils: a review on the influence of land use and management practices. *Geoderma, 113*(3–4), 357–380.

Chao, A. (1984). Nonparametric estimation of the number of classes in a population. *Scandinavian Journal of statistics*, 265–270.

Chen, Yongshan, Camps-Arbestain, Marta, Shen, Qinhua, . . . & Luz, M. (2018). The long-term role of organic amendments in building soil nutrient fertility: a meta-analysis and review. *Nutrient Cycling in Agroecosystems*.

Chen, C., Dynes, J. J., Wang, J., Karunakaran, C., & Sparks, D. L. (2014). Soft X-ray spectromicroscopy study of mineral-organic matter associations in pasture soil clay fractions. *Environmental Science & Technology, 48*(12), 6678–6686.

Chen, L., Liang, J., Qin, S., Liu, L., Fang, K., Xu, Y., . . . & Yang, Y. (2016). Determinants of carbon release from the active layer and permafrost deposits on the Tibetan Plateau. *Nature Communication, 7*, 13046.

Cho, H., Kim, M., Tripathi, B., & Adams, J. (2017). Changes in soil fungal community structure with increasing disturbance frequency. *Microbial Ecology, 74*(1), 62–77.

Cleveland, C. C., Townsend, A. R., & Schmidt, S. K. (2002). Phosphorus limitation of microbial processes in moist tropical forests: evidence from short-term laboratory incubations and field studies. *Ecosystems, 5*(7), 0680-0691.

Cline, L. C., & Zak, D. R. (2016). Soil microbial communities are shaped by plant‐driven changes in resource availability during secondary succession. *Ecology, 96*(12), 3374–3385.

Cotrufo, M. F., Soong, J. L., Horton, A. J., Campbell, E. E., Haddix, M. L., Wall, D. H., & Parton, W. J. (2015). Formation of soil organic matter via biochemical and physical pathways of litter mass loss. *Nature Geoscience, 8*(10), 776–779.

Curtin, D., Beare, M. H., Qiu, W., & Chantigny, M. H. (2015). Temperature dependence of organic matter solubility: Influence of biodegradation during soil-water extraction. *Soil Science Society of America Journal, 79*(3).

Curtin, D., Peterson, M. E., & Anderson, C. R. (2016). pH-dependence of organic matter solubility: base type effects on dissolved organic C, N, P, and S in soils with contrasting mineralogy. *Geoderma, 271*, 161–172.

Dahlgren, R., Saigusa, M., & Ugolini, F. (2004). The nature, properties and management of volcanic soils. *Advances in Agronomy, 82*(03), 113–182.

Dairy, N. (2012). New Zealand dairy statistics. *DairyNZ Ltd: Hamilton, New Zealand*.

Das, M. R., & Mahiuddin, S. (2007). The influence of functionality on the adsorption of p-hydroxy benzoate and phthalate at the hematite–electrolyte interface. *Journal of Colloid and Interface Science, 306*(2), 205–215.

Delgado-Baquerizo, M., Reich, P. B., Trivedi, C., Eldridge, D. J., Abades, S., Alfaro, F. D., . . . & Gallardo, A. (2020). Multiple elements of soil biodiversity drive ecosystem functions across biomes. *Nature ecology & evolution, 4*(2), 210–220.

Diagboya, P. N., Olu-Owolabi, B. I., & Adebowale, K. O. (2015). Effects of time, soil organic matter, and iron oxides on the relative retention and redistribution of lead, cadmium, and copper on soils. *Environmental Science and Pollution Research, 22*(13), 10331–10339.

Dixon, G. R., & Tilston, E. L. (2010). *Soil microbiology and sustainable crop production*: Springer Science & Business Media.

Duarte-Guardia, S., Peri, P., Amelung, W., Thomas, E., Borchard, N., Baldi, G., . . . & Ladd, B. (2020). Biophysical and socioeconomic factors influencing soil carbon stocks: a global assessment. *Mitigation and Adaptation Strategies for Global Change, 25*(6), 1129–1148.

Dumale Jr, W. A.; Tsuyoshi, M.; Kenta, H.; & Taku, N. (2011). SOC turnover and lime-CO_2 evolution during liming of an acid Andisol and Ultisol. *Open Journla of. Soil Science, 1*, 49−53

Dungait, J. A., Hopkins, D. W., Gregory, A. S., & Whitmore, A. P. (2012). Soil organic matter turnover is governed by accessibility not recalcitrance. *Global Change Biology, 18*(6), 1781–1796.

Eilers, K. G., Debenport, S., Anderson, S., & Fierer, N. (2012). Digging deeper to find unique microbial communities: the strong effect of depth on the structure of bacterial and archaeal communities in soil. *Soil Biology and Biochemistry, 50*, 58–65.

Eswaran, H., Van Den Berg, E., & Reich, P. (1993). Organic carbon in soils of the world. *Soil Science Society of America Journal, 57*(1), 192–194.

Eze, S., Palmer, S. M., & Chapman, P. J. (2018). Soil organic carbon stock in grasslands: Effects of inorganic fertilizers, liming and grazing in different climate settings. *Journal of environmental management, 223*, 74–84.

Fang, X.M., Zhang, X.L., Chen, F.S., Zong, Y.Y., Bu, W.S., Wan, S.Z., . . . & Wang, H. (2019). Phosphorus addition alters the response of soil organic carbon

decomposition to nitrogen deposition in a subtropical forest. *Soil Biology and Biochemistry, 133*, 119–128.

FAO, IFAD, UNICEF, WFP, WHO. FAO; Rome: 2020. The State of Food Security and Nutrition in the World 2018. Building Climate Resilience for Food Security and Nutrition.

Fierer, N., Bradford, M. A., & Jackson, R. B. (2007). Toward an ecological classification of soil bacteria. *Ecology, 88*(6), 1354–1364.

Fisk, M., Santangelo, S., & Minick, K. (2015). Carbon mineralization is promoted by phosphorus and reduced by nitrogen addition in the organic horizon of northern hardwood forests. *Soil Biology & Biochemistry*, *81*, 212–218.

Flato, G., Marotzke, J., Abiodun, B., Braconnot, P., Chou, S. C., Collins, W., . . . & Eyring, V. (2014). Evaluation of climate models. In *Climate change 2013: the physical science basis. Contribution of Working Group I to the Fifth Assessment Report of the Intergovernmental Panel on Climate Change* (pp. 741–866): Cambridge University Press.

Foley, J. A., Ramankutty, N., Brauman, K. A., Cassidy, E. S., Gerber, J. S., Johnston, M., . . . & Zaks, D. P. M. (2011). Solutions for a cultivated planet. *Nature, 478*(7369), 337–342.

Fornara, D. A., Steinbeiss, S., McNamara, N. P., Gleixner, G., Oakley, S., Poulton, P. R., . . . & Bardgett, R. D. (2011). Increases in soil organic carbon sequestration can reduce the global warming potential of long-term liming to permanent grassland. *Global Change Biology, 17*(5), 1925–1934.

Fuss, S., Lamb, W. F., Callaghan, M. W., Hilaire, J., Creutzig, F., Amann, T., . . . & Khanna, T. (2018). Negative emissions—Part 2: Costs, potentials and side effects. *Environmental Research Letters, 13*(6), 063002.

Ghaley, B. B., Wösten, H., Olesen, J. E., Schelde, K., Baby, S., Karki, Y. K., . . . & Ferrise, R. (2018). Simulation of soil organic carbon effects on long-term winter wheat (*Triticum aestivum*) production under varying fertilizer inputs. *Frontiers in plant science, 9*, 1158.

Godfray, H. C. J., Beddington, J. R., Crute, I. R., Haddad, L., Lawrence, D., Muir, J. F., . . . & Toulmin, C. (2010). Food security: the challenge of feeding 9 billion people. *science, 327*(5967), 812–818.

Gomes, L. C., Faria, R. M., de Souza, E., Veloso, G. V., Schaefer, C. E. G., & Fernandes Filho, E. I. (2019). Modelling and mapping soil organic carbon stocks in Brazil. *Geoderma, 340*, 337–350.

Gougoulias, C., Clark, J. M., & Shaw, L. J. (2014). The role of soil microbes in the global carbon cycle: tracking the below‐ground microbial processing of plant‐derived

carbon for manipulating carbon dynamics in agricultural systems. *Journal of the Science of Food and Agriculture, 94*(12), 2362–2371.

Greiner, E., Kumar, K., Sumit, M., Giuffre, A., Zhao, W., Pedersen, J., & Sahai, N. (2014). Adsorption of l-glutamic acid and l-aspartic acid to γ-Al2O3. *Geochimica et Cosmochimica Acta, 133*, 142–155.

Grządziel, J. (2017). Functional redundancy of soil microbiota–does more always mean better? *Polish Journal of Soil Science, 50*(1), 75.

Gu, B., Schmitt, J., Chen, Z., Liang, L., & McCarthy, J. F. (1994). Adsorption and desorption of natural organic matter on iron oxide: mechanisms and models. *Environmental science & technology, 28*(1), 38–46.

Guan, X. H., Chen, G. H., & Shang, C. (2006). Combining kinetic investigation with surface spectroscopic examination to study the role of aromatic carboxyl groups in NOM adsorption by aluminum hydroxide. *J Colloid Interface Sci, 301*(2), 419–427.

Guggenberger, G., & Zech, W. (1994). Composition and dynamics of dissolved carbohydrates and lignin-degradation products in two coniferous forests, NE Bavaria, Germany. *Soil Biology and Biochemistry, 26*(1), 19–27.

Hale, L., Feng, W., Yin, H., Guo, X., Zhou, X., Bracho, R., . . . & Zhou, J. (2019). Tundra microbial community taxa and traits predict decomposition parameters of stable, old soil organic carbon. *ISME J, 13*(12), 2901–2915.

Hall, S. J., Huang, W., & Hammel, K. E. (2017). An optical method for carbon dioxide isotopes and mole fractions in small gas samples: Tracing microbial respiration from soil, litter, and lignin. *Rapid Communications in Mass Spectrometry, 31*(22), 1938–1946.

Harsh, J., Chorover, J., & Nizeyimana, E. (2002). Allophane and imogolite. *Soil Mineralogy with Environmental Applications*, 7, 291–322.

Haynes, R. (1984). Lime and phosphate in the soil-plant system. In *Advances in Agronomy* (Vol. 37, pp. 249–315): Elsevier.

Haynes, R. J. (2005). Labile Organic Matter Fractions as Central Components of the Quality of Agricultural Soils: An Overview. *Advances in agronomy, 85*, 221–268.

Haynes, R. J., & Naidu, R. (1998). Influence of lime, fertilizer and manure applications on soil organic matter content and soil physical conditions: a review. *Nutrient Cycling in Agroecosystems, 51*(2), 123–137.

Hedley, M. J., & Bolan, N. S. (2003). Role of carbon, nitrogen, and sulfur cycles in soil acidification. In *Handbook of soil acidity* (pp. 43–70): CRC Press.

Hemingway, J. D., Rothman, D. H., Grant, K. E., Rosengard, S. Z., Eglinton, T. I., Derry, L. A., & Galy, V. V. (2019). Mineral protection regulates long-term global preservation of natural organic carbon. *Nature, 570*(7760), 228–231.

Herath, H., Camps-Arbestain, M., & Hedley, M. (2013). Effect of biochar on soil physical properties in two contrasting soils: an Alfisol and an Andisol. *Geoderma, 209*, 188–197.

Herath, H., Camps-Arbestain, M., Hedley, M. J., Kirschbaum, M. U. F., Wang, T., & van Hale, R. (2015). Experimental evidence for sequestering C with biochar by avoidance of CO_2 emissions from original feedstock and protection of native soil organic matter. *GCB Bioenergy, 7*(3), 512–526.

Hewitt, A. E., & Shepherd, T. G. (1997). Structural vulnerability of New Zealand soils. *Soil Research, 35*(3), 461–474.

Hiemstra, T., Antelo, J., Rahnemaie, R., & van Riemsdijk, W. H. (2010). Nanoparticles in natural systems I: the effective reactive surface area of the natural oxide fraction in field samples. *Geochimica et Cosmochimica Acta, 74*(1), 41–58.

Hiemstra, T., Mia, S., Duhaut, P. B., & Molleman, B. (2013). Natural and pyrogenic humic acids at goethite and natural oxide surfaces interacting with phosphate. *Environ Sci Technol, 47*(16), 9182–9189.

Hillel, D., & Rosenzweig, C. (2009). Carbon exchange in the terrestrial domain and the role of agriculture. *CSA News, 54*(6), 5–11.

Hönisch, B., Hemming, N. G., Archer, D., Siddall, M., & McManus, J. F. (2009). Atmospheric carbon dioxide concentration across the mid-Pleistocene transition. *Science, 324*(5934), 1551–1554.

Hou, D., O'Connor, D., Igalavithana, A. D., Alessi, D. S., Luo, J., Tsang, D. C., . . . & Ok, Y. S. (2020). Metal contamination and bioremediation of agricultural soils for food safety and sustainability. *Nature Reviews Earth & Environment, 1*(7), 366–381.

Hutchinson, J., Campbell, C., & Desjardins, R. (2007). Some perspectives on carbon sequestration in agriculture. *Agricultural and forest meteorology, 142*(2–4), 288–302.

Inagaki, T. M., Possinger, A. R., Grant, K. E., Schweizer, S. A., Mueller, C. W., Derry, L. A., . . . & Kögel-Knabner, I. (2020). Subsoil organo-mineral associations under contrasting climate conditions. *Geochimica et Cosmochimica Acta, 270*, 244–263.

Jansen, B., & Nierop, K. G. (2009). Methyl ketones in high altitude Ecuadorian Andosols confirm excellent conservation of plant-specific n-alkane patterns. *Organic Geochemistry, 40*(1), 61–69.

John, M. K. (1970). 2267141. Colorimetric determination of phosphorus in soil and plant materials with ascorbic acid. *Soil Science, 109*(4), 214–220.

Jones, D., & Willett, V. (2006). Experimental evaluation of methods to quantify dissolved organic nitrogen (DON) and dissolved organic carbon (DOC) in soil. *Soil Biology and Biochemistry, 38*(5), 991–999.

Kaiser, K., & Guggenberger, G. (2000). The role of DOM sorption to mineral surfaces in the preservation of organic matter in soils. *Organic Geochemistry, 31*(7–8), 711–725.

Kaiser, K., & Guggenberger, G. (2003). Mineral surfaces and soil organic matter. *European Journal of Soil Science, 54*(2), 219–236.

Kaiser, K., & Zech, W. (1997). Competitive sorption of dissolved organic matter fractions to soils and related mineral phases. *Soil Science Society of America Journal, 61*(1), 64–69.

Kamprath, E. J., & Adams, F. (2010). Soil acidity and liming. *Century of soil science. North Carolina*, 103–107.

Kang, S., Amarasiriwardena, D., & Xing, B. (2008). Effect of dehydration on dicarboxylic acid coordination at goethite/water interface. *Colloids and Surfaces A: Physicochemical and Engineering Aspects, 318*(1–3), 275–284.

Katoh, K., Misawa, K., Kuma, K. I., & Miyata, T. (2002). MAFFT: a novel method for rapid multiple sequence alignment based on fast Fourier transform. *Nucleic Acids Research*, 30(14), 3059–3066.

Keiluweit, M., Bougoure, J. J., Zeglin, L. H., Myrold, D. D., Weber, P. K., Pett-Ridge, J., . . . & Nico, P. S. (2012). Nano-scale investigation of the association of microbial nitrogen residues with iron (hydr)oxides in a forest soil O-horizon. *Geochimica et Cosmochimica Acta, 95*, 213–226.

Keiluweit, M., Wanzek, T., Kleber, M., Nico, P., & Fendorf, S. (2017). Anaerobic microsites have an unaccounted role in soil carbon stabilization. *Nature Communications, 8*(1), 1771.

Kemmitt, S., Lanyon, C., Waite, I., Wen, Q., Addiscott, T., Bird, N. R., . . . & Brookes, P. (2008). Mineralization of native soil organic matter is not regulated by the size, activity or composition of the soil microbial biomass—a new perspective. *Soil Biology and Biochemistry, 40*(1), 61–73.

Kleber, M. (2010). What is recalcitrant soil organic matter? *Environmental Chemistry, 7*(4), 320–332.

Kleber, M., Eusterhues, K., Keiluweit, M., Mikutta, C., Mikutta, R., & Nico, P. S. (2015). Chapter one-mineral–organic associations: formation, properties, and relevance in soil environments. *Advances in agronomy, 130*, 1–140.

Kleber, M., Sollins, P., & Sutton, R. (2007). A conceptual model of organo-mineral interactions in soils: self-assembly of organic molecular fragments into zonal structures on mineral surfaces. *Biogeochemistry, 85*(1), 9–24.

Kochian, L. V., Hoekenga, O. A., & Pineros, M. A. (2004). How do crop plants tolerate acid soils? Mechanisms of aluminum tolerance and phosphorous efficiency. *Annual Review of Plant Biology, 55,* 459-493.

Köchy, M., Hiederer, R., & Freibauer, A. (2015). Global distribution of soil organic carbon–Part 1: Masses and frequency distributions of SOC stocks for the tropics, permafrost regions, wetlands, and the world. *Soil, 1*(1), 351–365.

Kögel-Knabner, I., Guggenberger, G., Kleber, M., Kandeler, E., Kalbitz, K., Scheu, S., … & Leinweber, P. (2008). Organo-mineral associations in temperate soils: Integrating biology, mineralogy, and organic matter chemistry. *Journal of Plant Nutrition and Soil Science, 171*(1), 61–82.

Kögel-Knabner, I., & Amelung, W. (2021). Soil organic matter in major pedogenic soil groups. *Geoderma, 384*, 114785.

Kõljalg, U., Nilsson, R. H., Abarenkov, K., Tedersoo, L., Taylor, A. F., Bahram, M., ... & Larsson, K. H. (2013). Towards a unified paradigm for sequence-based identification of fungi. *Molecular Ecology, 22*(21), 5271–5277.

Kopittke, P. M., Dalal, R. C., Finn, D., & Menzies, N. W. (2017). Global changes in soil stocks of carbon, nitrogen, phosphorus, and sulphur as influenced by long-term agricultural production. *Global Change Biology, 23*(6), 2509–2519.

Kopittke, P. M., Dalal, R. C., Hoeschen, C., Li, C., Menzies, N. W., & Mueller, C. W. (2020). Soil organic matter is stabilized by organo-mineral associations through two key processes: The role of the carbon to nitrogen ratio. *Geoderma, 357*.

Kopittke, P. M., Hernandez‐Soriano, M. C., Dalal, R. C., Finn, D., Menzies, N. W., Hoeschen, C., & Mueller, C. W. (2018). Nitrogen‐rich microbial products provide new organo‐mineral associations for the stabilization of soil organic matter. *Global Change Biology, 24*(4), 1762–1770.

Kopittke, P. M., Menzies, N. W., Wang, P., McKenna, B. A., & Lombi, E. (2019). Soil and the intensification of agriculture for global food security. *Environment International, 132*, 105078.

Kov, R., Camps-Arbestain, M., Calvelo Pereira, R., Suárez-Abelenda, M., Shen, Q., Garbuz, S., & Macías Vázquez, F. (2018). A farm-scale investigation of the organic

matter composition and soil chemistry of Andisols as influenced by land use and management. *Biogeochemistry, 140*(1), 65–79.

Lal, R. (2004). Soil carbon sequestration impacts on global climate change and food security. *Science, 304*(5677), 1623–1627.

Lal, R. (2020). Soil organic matter content and crop yield. *Journal of Soil and Water Conservation, 75*(2), 27A–32A.

Lamichhane, S., Krishna, K. B., & Sarukkalige, R. (2016). Polycyclic aromatic hydrocarbons (PAHs) removal by sorption: a review. *Chemosphere, 148*, 336–353.

Lefevre, C., Rekik, F., Alcantara, V., & Wiese, L. (2017). *Soil organic carbon: the hidden potential*.

Lehmann, J., Hansel, C. M., Kaiser, C., Kleber, M., & Kgel-Knabner, I. (2020). Persistence of soil organic carbon caused by functional complexity. *Nature Geoence, 13*(8), 1–6.

Lehmann, J., & Joseph, S. (Eds.). (2015). *Biochar for environmental management: science, technology and implementation*. Routledge.

Lehmann, J., & Kleber, M. (2015). The contentious nature of soil organic matter. *Nature, 528*(7580), 60–68.

Lehmann, J., Solomon, D., Kinyangi, J., Dathe, L., Wirick, S., & Jacobsen, C. (2008). Spatial complexity of soil organic matter forms at nanometre scales. *Nature Geoscience, 1*(4), 238–242.

Lennon, J. T., Aanderud, Z. T., Lehmkuhl, B., & Schoolmaster Jr, D. R. (2012). Mapping the niche space of soil microorganisms using taxonomy and traits. *Ecology, 93*(8), 1867–1879.

Li, C., Yan, K., Tang, L., Jia, Z., & Li, Y. (2014). Change in deep soil microbial communities due to long-term fertilization. *Soil Biology and Biochemistry, 75*, 264–272.

Li, X. M., Sun, G. X., Chen, S. C., Fang, Z., Yuan, H. Y., Shi, Q., & Zhu, Y. G. (2018). Molecular chemodiversity of dissolved organic matter in paddy soils. *Environmental science & technology, 52*(3), 963–971.

Li, Y., Wang, T., Camps-Arbestain, M., Suárez-Abelenda, M., & Whitby, C. P. (2020). Lime and/or phosphate application affects the stability of soil organic carbon: Evidence from changes in quantity and chemistry of the soil water-extractable organic matter. *Environmental science & technology, 54*(21), 13908–13916.

Liang, C., Schimel, J. P., & Jastrow, J. D. (2017). The importance of anabolism in microbial control over soil carbon storage. *Nature microbiology, 2*(8), 1–6.

Lijklema, L. (1977). *Role of iron in the exchange of phosphate between water and sediments*. Paper presented at the Interactions Between Sediments and Fresh Water; Proceedings of an International Symposium.

Liu, C., Gong, X., Dang, K., Li, J., Yang, P., Gao, X., . . . & Feng, B. (2020). Linkages between nutrient ratio and the microbial community in rhizosphere soil following fertilizer management. *Environmental Research, 184*, 109261.

Loveday, J. (1974). Methods for analysis of irrigated soils. *Technical Communication, Commonwealth Bureau of Soils (UK)*.

Luo, R., Fan, J., Wang, W., Luo, J., Kuzyakov, Y., He, J.-S., . . . & Ding, W. (2019). Nitrogen and phosphorus enrichment accelerates soil organic carbon loss in alpine grassland on the Qinghai-Tibetan Plateau. *Science of The Total Environment, 650*, 303–312.

Lutzow, M. v., Kogel-Knabner, I., Ekschmitt, K., Matzner, E., Guggenberger, G., Marschner, B., & Flessa, H. (2006). Stabilization of organic matter in temperate soils: mechanisms and their relevance under different soil conditions - a review. *European Journal of Soil Science, 57*(4), 426–445.

Lützow, M. v., Kögel‐Knabner, I., Ekschmitt, K., Matzner, E., Guggenberger, G., Marschner, B., & Flessa, H. (2006). Stabilization of organic matter in temperate soils: mechanisms and their relevance under different soil conditions–a review. *European Journal of Soil Science, 57*(4), 426–445.

Ma, B., Lv, X., Cai, Y., Chang, S. X., & Dyck, M. F. (2018). Liming does not counteract the influence of long-term fertilization on soil bacterial community structure and its co-occurrence pattern. *Soil Biology & Biochemistry, 123*, 45–53.

Macíasa, F., & Camps-Arbestain, M. (2020). A biogeochemical view of the world reference base soil classification system. *Advances in Agronomy*, 295.

Malik, A. A., Martiny, J. B., Brodie, E. L., Martiny, A. C., Treseder, K. K., & Allison, S. D. (2020). Defining trait-based microbial strategies with consequences for soil carbon cycling under climate change. *The ISME journal, 14*(1), 1–9.

Marinho, M. A., Pereira, M. W., Vázquez, E. V., Lado, M., & González, A. P. (2017). Depth distribution of soil organic carbon in an Oxisol under different land uses: stratification indices and multifractal analysis. *Geoderma, 287*, 126–134.

Martin, M. (2011). Cutadapt removes adapter sequences from high-throughput sequencing reads. *EMBnet. journal, 17*(1), 10–12.

Mathew, I., Shimelis, H., Mutema, M., Minasny, B., & Chaplot, V. (2020). Crops for increasing soil organic carbon stocks – A global meta analysis. *Geoderma, 367*, 114230.

Matus, F., Rumpel, C., Neculman, R., Panichini, M., & Mora, M. (2014). Soil carbon storage and stabilisation in andic soils: a review. *Catena, 120*, 102–110.

McDaniel, P. A., Lowe, D. J., Arnalds, O., & Ping, C. L. (2012). Andisols.

McKenzie, H., & Wallace, H. S. (1954). The Kjeldahl determination of nitrogen: a critical study of digestion conditions-temperature, catalyst, and oxidizing agent. *Australian Journal of Chemistry, 7*(1), 55–70.

Metcalfe, D. B., Fisher, R. A., & Wardle, D. A. (2011). Plant communities as drivers of soil respiration: Pathways, mechanisms, and significance for global change. *Biogeosciences, 8*(8), 2047–2061.

Mikutta, R., & Kaiser, K. (2011). Organic matter bound to mineral surfaces: Resistance to chemical and biological oxidation. *Soil Biology and Biochemistry, 43*(8), 1738–1741.

Minasny, B., Malone, B. P., McBratney, A. B., Angers, D. A., Arrouays, D., Chambers, A., . . . & Das, B. S. (2017). Soil carbon 4 per mille. *Geoderma, 292*, 59–86.

Miyazawa, M., Takahashi, T., Sato, T., Kanno, H., & Nanzyo, M. (2013). Factors controlling accumulation and decomposition of organic carbon in humus horizons of Andosols. *Biology and Fertility of Soils, 49*(7), 929–938.

Mizota, C., & Van Reeuwijk, L. (1989). Clay mineralogy and chemistry of soils formed in volcanic material in diverse climatic regions. *Clay mineralogy and chemistry of soils formed in volcanic material in diverse climatic regions.*(2).

Mora, J. L., Guerra, J. A., Armas-Herrera, C. M., Arbelo, C. D., & Rodríguez-Rodríguez, A. (2014). Storage and depth distribution of organic carbon in volcanic soils as affected by environmental and pedological factors. *Catena, 123*, 163–175.

Murphy, J., & Riley, J. P. (1962). A modified single solution method for the determination of phosphate in natural waters. *Analytica chimica acta, 27*, 31–36.

Newcomb, C. J., Qafoku, N. P., Grate, J. W., Bailey, V. L., & De Yoreo, J. J. (2017). Developing a molecular picture of soil organic matter-mineral interactions by quantifying organo-mineral binding. *Nat Commun, 8*(1), 396.

Nierop, K. G., van Bergen, P. F., Buurman, P., & van Lagen, B. (2005). NaOH and $Na_4P_2O_7$ extractable organic matter in two allophanic volcanic ash soils of the Azores Islands—a pyrolysis GC/MS study. *Geoderma, 127*(1–2), 36–51.

Nunan, N., Schmidt, H., & Raynaud, X. (2020). The ecology of heterogeneity: soil bacterial communities and C dynamics. *Philos Trans R Soc Lond B Biol Sci, 375*(1798), 20190249.

Nuñez, J., Renslow, R., Cliff III, J. B., & Anderton, C. R. (2018). NanoSIMS for biological applications: current practices and analyses. *Biointerphases, 13*(3), 03B301.

Olsen, S. R., Cole, C. V., Watanable, F. S., & Dean, L. A. (1954). Estimation of available phosphorus in soils by extraction with sodium bicarbonate; Circular No. 939, United States Department of Agriculture: Washington, DC.

Pachauri, R. K., Allen, M. R., Barros, V. R., Broome, J., Cramer, W., Christ, R., . . . & Dasgupta, P. (2014). *Climate change 2014: synthesis report. Contribution of Working Groups I, II and III to the fifth assessment report of the Intergovernmental Panel on Climate Change*: IPCC.

Panichini, M., Neculman, R., Godoy, R., Arancibia-Miranda, N., & Matus, F. (2017). Understanding carbon storage in volcanic soils under selectively logged temperate rainforests. *Geoderma, 302*, 76–88.

Parfitt, R. L. (2009). Allophane and imogolite: role in soil biogeochemical processes. Clay minerals, 44(1), 135–155.

Paul, A., Balesdent, J., & Hatté, C. (2020). ^{13}C-^{14}C relations reveal that soil ^{13}C-depth gradient is linked to historical changes in vegetation ^{13}C. *Plant and Soil*, 447(1), 305–317.

Paustian, K., Lehmann, J., Ogle, S., Reay, D., Robertson, G. P., & Smith, P. (2016). Climate-smart soils. *Nature, 532*(7597), 49–57.

Pianka, E. R. (1970). On r-and K-selection. *The american naturalist, 104*(940), 592–597.

Plaza, C., Courtier-Murias, D., Fernández, J. M., Polo, A., & Simpson, A. J. (2013). Physical, chemical, and biochemical mechanisms of soil organic matter stabilization under conservation tillage systems: a central role for microbes and microbial by-products in C sequestration. *Soil Biology and Biochemistry, 57*, 124-134.

Possinger, A. R., Zachman, M. J., Enders, A., Levin, B. D., Muller, D. A., Kourkoutis, L. F., & Lehmann, J. (2020). Organo–organic and organo–mineral interfaces in soil at the nanometer scale. *Nature communications, 11*(1), 1–11.

Price, M. N., Dehal, P. S., & Arkin, A. P. (2010). FastTree 2–approximately maximum-likelihood trees for large alignments. *PloS one, 5*(3), e9490.

Pulleman, M., & Marinissen, J. (2004). Physical protection of mineralizable C in aggregates from long-term pasture and arable soil. *Geoderma, 120*(3), 273–282.

Qiu, Y., Lv, W., Wang, X., Xie, Z., & Wang, Y. (2020). Long-term effects of gravel mulching and straw mulching on soil physicochemical properties and bacterial and fungal community composition in the Loess Plateau of China. *European Journal of Soil Biology, 98*, 103188.

Rahnemaie, R., Hiemstra, T., & van Riemsdijk, W. H. (2007). Geometry, charge distribution, and surface speciation of phosphate on goethite. *Langmuir, 23*(7), 3680–3689.

Ramesh, T., Bolan, N. S., Kirkham, M. B., Wijesekara, H., Kanchikerimath, M., Rao, C. S., . . . & Choudhury, B. U. (2019). Soil organic carbon dynamics: Impact of land use changes and management practices: A review. *Adv. Agron*.

Ramírez, P. B., Fuentes-Alburquenque, S., Díez, B., Vargas, I., & Bonilla, C. A. (2020). Soil microbial community responses to labile organic carbon fractions in relation to soil type and land use along a climate gradient. *Soil Biology and Biochemistry, 141*, 107692.

Razanamalala, K., Razafimbelo, T., Maron, P.-A., Ranjard, L., Chemidlin, N., Lelièvre, M., . . . & Becquer, T. (2018). Soil microbial diversity drives the priming effect along climate gradients: a case study in Madagascar. *The ISME journal, 12*(2), 451–462.

Rousk, Johannes, Bååth, Erland, Brookes, Philip, C., . . . & Catherine. (2010). Soil bacterial and fungal communities across a pH gradient in an arable soil. *Isme Journal Multidisciplinary Journal of Microbial Ecology*.

Rumpel, C., Amiraslani, F., Koutika, L.-S., Smith, P., Whitehead, D., & Wollenberg, E. (2018). Put more carbon in soils to meet Paris climate pledges. In: Nature Publishing Group.

Rumpel, C., Baumann, K., Remusat, L., Dignac, M.-F., Barré, P., Deldicque, D., . . . & Chabbi, A. (2015). Nanoscale evidence of contrasted processes for root-derived organic matter stabilization by mineral interactions depending on soil depth. *Soil Biology and Biochemistry, 85*, 82–88.

Rumpel, C., & Kögel-Knabner, I. (2010). Deep soil organic matter—a key but poorly understood component of terrestrial C cycle. *Plant and Soil, 338*(1–2), 143–158.

Sáiz-Jiménez, C., & De Leeuw, J. (1986). Chemical characterization of soil organic matter fractions by analytical pyrolysis-gas chromatography-mass spectrometry. *Journal of Analytical and Applied Pyrolysis, 9*(2), 99–119.

Schimel, J., Balser, T. C., & Wallenstein, M. (2007). Microbial stress‐response physiology and its implications for ecosystem function. *Ecology, 88*(6), 1386–1394.

Schindelin, J., Arganda-Carreras, I., Frise, E., Kaynig, V., Longair, M., Pietzsch, T., . . . & Schmid, B. (2012). Fiji: an open-source platform for biological-image analysis. *Nature methods, 9*(7), 676–682.

Schipper, L., Parfitt, R., Fraser, S., Littler, R., Baisden, W., & Ross, C. (2014). Soil order and grazing management effects on changes in soil C and N in New Zealand pastures. *Agriculture, Ecosystems & Environment, 184*, 67–75.

Schipper, L. A., Baisden, W. T., Parfitt, R. L., Ross, C., Claydon, J. J., & Arnold, G. (2007). Large losses of soil C and N from soil profiles under pasture in New Zealand during the past 20 years. *Global Change Biology, 13*(6), 1138–1144.

Schmidt, M. W., Torn, M. S., Abiven, S., Dittmar, T., Guggenberger, G., Janssens, I. A., . . . & Trumbore, S. E. (2011). Persistence of soil organic matter as an ecosystem property. *Nature, 478*(7367), 49–56.

Schneider, M. P. W., Scheel, T., Mikutta, R., Hees, P. V., & Kalbitz, K. (2010). Sorptive stabilization of organic matter by amorphous Al hydroxide. *Geochimica et Cosmochimica Acta, 74*(5), 1606–1619.

Schweizer, S. A., Hoeschen, C., Schluter, S., Kogel-Knabner, I., & Mueller, C. W. (2018). Rapid soil formation after glacial retreat shaped by spatial patterns of organic matter accrual in microaggregates. *Glob Chang Biol, 24*(4), 1637–1650.

Scott, E. E., & Rothstein, D. E. (2014). The dynamic exchange of dissolved organic matter percolating through six diverse soils. *Soil Biology and Biochemistry, 69*, 83–92.

Seifert, A.-G., Roth, V.-N., Dittmar, T., Gleixner, G., Breuer, L., Houska, T., & Marxsen, J. (2016). Comparing molecular composition of dissolved organic matter in soil and stream water: Influence of land use and chemical characteristics. *Science of the Total Environment, 571*, 142–152.

Shahbaz, M., Kuzyakov, Y., Sanaullah, M., Heitkamp, F., Zelenev, V., Kumar, A., & Blagodatskaya, E. (2017). Microbial decomposition of soil organic matter is mediated by quality and quantity of crop residues: mechanisms and thresholds. *Biology and Fertility of Soils, 53*(3), 287–301.

Shannon, C. E. (1948). A mathematical theory of communication. *The Bell system technical journal, 27*(3), 379–423.

Shannon, P., Markiel, A., Ozier, O., Baliga, N. S., Wang, J. T., Ramage, D., ... & Ideker, T. (2003). Cytoscape: a software environment for integrated models of biomolecular interaction networks. *Genome Research*, 13(11), 2498–2504.

Shen, Q., Suarez-Abelenda, M., Camps-Arbestain, M., Pereira, R. C., McNally, S. R., & Kelliher, F. M. (2018). An investigation of organic matter quality and quantity in acid soils as influenced by soil type and land use. *Geoderma, 328*, 44–55.

Shukla, P., Skea, J., Calvo Buendia, E., Masson-Delmotte, V., Pörtner, H., Roberts, D., . . . & Van Diemen, R. (2019). IPCC, 2019: Climate Change and Land: an IPCC special report on climate change, desertification, land degradation, sustainable land management, food security, and greenhouse gas fluxes in terrestrial ecosystems.

Silva-Sánchez, A., Soares, M., & Rousk, J. (2019). Testing the dependence of microbial growth and carbon use efficiency on nitrogen availability, pH, and organic matter quality. *Soil Biology and Biochemistry, 134*, 25–35.

Smith, P., House, J. I., Bustamante, M., Sobocka, J., Harper, R., Pan, G., . . . & Pugh, T. A. (2016). Global change pressures on soils from land use and management. *Glob Chang Biol, 22*(3), 1008–1028.

Šnajdr, J., Valášková, V., Merhautová, V. r., Herinková, J., Cajthaml, T., & Baldrian, P. (2008). Spatial variability of enzyme activities and microbial biomass in the upper layers of Quercus petraea forest soil. *Soil Biology and Biochemistry, 40*(9), 2068–2075.

Solaw, F. (2011). The state of the world's land and water resources for food and agriculture. *Rome, Italy*.

Sollins, P., Homann, P., & Caldwell, B. A. (1996). Stabilization and destabilization of soil organic matter: mechanisms and controls. *Geoderma, 74*(1–2), 65–105.

Spielvogel, S., Prietzel, J., & Kgel-Knabner, I. (2008). Soil organic matter stabilization in acidic forest soils is preferential and soil type-specific. *European Journal of Soil Science, 59*(4), 674–692.

Spohn, M., & Schleuss, P.-M. (2019). Addition of inorganic phosphorus to soil leads to desorption of organic compounds and thus to increased soil respiration. *Soil Biology and Biochemistry, 130*, 220–226.

Stockmann, U., Adams, M. A., Crawford, J. W., Field, D. J., Henakaarchchi, N., Jenkins, M., . . . & Zimmermann, M. (2013). The knowns, known unknowns and unknowns of sequestration of soil organic carbon. *Agriculture, Ecosystems & Environment, 164*, 80–99.

Su, Y., He, Z., Yang, Y., Jia, S., Yu, M., Chen, X., & Shen, A. (2020). Linking soil microbial community dynamics to straw-carbon distribution in soil organic carbon. *Scientific reports, 10*(1), 1–12.

Suárez-Abelenda, M., Kaal, J., Camps-Arbestain, M., Knicker, H., & Macías, F. (2014). Molecular characteristics of permanganate-and dichromate-oxidation-resistant soil organic matter from a black-C-rich colluvial soil. *Soil research, 52*(2), 164–179.

Takahashi, T., & Dahlgren, R. A. (2016). Nature, properties and function of aluminum–humus complexes in volcanic soils. *Geoderma, 263*, 110–121.

Tan, X., Nie, Y., Ma, X., Guo, Z., Liu, Y., Tian, H., . . . & He, W. (2021). Soil chemical properties rather than the abundance of active and potentially active microorganisms control soil enzyme kinetics. *Science of the Total Environment, 770*, 144500.

Tarnocai, C., Canadell, J., Schuur, E. A., Kuhry, P., Mazhitova, G., & Zimov, S. (2009). Soil organic carbon pools in the northern circumpolar permafrost region. *Global biogeochemical cycles, 23*(2).

Tegelaar, E., De Leeuw, J., Derenne, S., & Largeau, C. (1989). A reappraisal of kerogen formation. *Geochimica et Cosmochimica Acta, 53*(11), 3103–3106.

Tiessen, H., Cuevas, E., & Chacon, P. (1994). The role of soil organic matter in sustaining soil fertility. *Nature, 371*(6500), 783–785.

Tilman, D., Balzer, C., Hill, J., & Befort, B. L. (2011). Global food demand and the sustainable intensification of agriculture. *Proceedings of the national academy of sciences, 108*(50), 20260-20264.

Trumbore, S. (2009). Radiocarbon and soil carbon dynamics. *Annual Review of Earth and Planetary Sciences, 37*, 47–66.

Undurraga P.; Zagal E.; Sepúlveda G.; & Valderrama N. (2009). Dissolved organic carbon and nitrogen in Andisol for six crop rotations with different soil management intensity. *Chilean Journal of Agricultural Research, 69*(3), 445−54.

Upton, R. N., Checinska Sielaff, A., Hofmockel, K. S., Xu, X., Polley, H. W., & Wilsey, B. J. (2020). Soil depth and grassland origin cooperatively shape microbial community co‐occurrence and function. *Ecosphere, 11*(1), e02973.

Verde, J. R., Arbestain, M. C., & Macías, F. (2010). Influence of agricultural practices on the stability of organo-Al complexes in an alu-andic Andosol: a laboratory study. *Soil science, 175*(8), 390–397.

Vogel, C., Mueller, C. W., Hoschen, C., Buegger, F., Heister, K., Schulz, S., . . . & Kogel-Knabner, I. (2014). Submicron structures provide preferential spots for carbon and nitrogen sequestration in soils. *Nature Communications, 5*, 2947.

Von Lützow, M., Kögel-Knabner, I., Ludwig, B., Matzner, E., Flessa, H., Ekschmitt, K., . . . & Kalbitz, K. (2008). Stabilization mechanisms of organic matter in four temperate soils: Development and application of a conceptual model. *Journal of Plant Nutrition and Soil Science, 171*(1), 111–124.

Wagai, R., Kajiura, M., Asano, M., & Hiradate, S. (2015). Nature of soil organo-mineral assemblage examined by sequential density fractionation with and without sonication: Is allophanic soil different? *Geoderma, 241–242*, 295–305.

Wagai, R., Kajiura, M., Uchida, M., & Asano, M. (2018). Distinctive roles of two aggregate binding agents in allophanic Andisols: Young carbon and poorly-crystalline metal phases with old carbon. *Soil Systems, 2*(2), 29.

Wang, C., Qu, L., Yang, L., Liu, D., Morrissey, E., Miao, R., . . . & Bai, E. (2021). Large‐scale importance of microbial carbon use efficiency and necromass to soil organic carbon. *Global Change Biology*.

Wang, H., Xu, W., Hu, G., Dai, W., Jiang, P., & Bai, E. (2015). The priming effect of soluble carbon inputs in organic and mineral soils from a temperate forest. *Oecologia, 178*(4), 1239–1250.

Wang, T., Camps-Arbestain, M., Hedley, M., Singh, B. P., Calvelo-Pereira, R., & Wang, C. (2014). Determination of carbonate-C in biochars. *Soil Research, 52*(5).

Wei, X., Zhu, Z., Liu, Y., Luo, Y., Deng, Y., Xu, X., . . . & Ge, T. (2020). C:N:P stoichiometry regulates soil organic carbon mineralization and concomitant shifts in microbial community composition in paddy soil. *Biology and Fertility of Soils, 56*(8), 1093–1107.

Weishaar, J. L., Aiken, G. R., Bergamaschi, B. A., Fram, M. S., Fujii, R., & Mopper, K. (2003). Evaluation of specific ultraviolet absorbance as an indicator of the chemical composition and reactivity of dissolved organic carbon. *Environmental science & technology, 37*(20), 4702–4708.

Weissert, L., Salmond, J., & Schwendenmann, L. (2016). Variability of soil organic carbon stocks and soil CO2 efflux across urban land use and soil cover types. *Geoderma, 271*, 80–90.

Weng, L., Vega, F. A., & Van Riemsdijk, W. H. (2011). Competitive and synergistic effects in pH dependent phosphate adsorption in soils: LCD modeling. *Environ Sci Technol, 45*(19), 8420–8428.

Weng, L. P., Koopal, L. K., Hiemstra, T., Meeussen, J. C., & Van Riemsdijk, W. H. (2005). Interactions of calcium and fulvic acid at the goethite-water interface. *Geochimica et Cosmochimica Acta, 69*(2), 325–339.

Whitman, T., Pepe-Ranney, C., Enders, A., Koechli, C., Campbell, A., Buckley, D. H., & Lehmann, J. (2016). Dynamics of microbial community composition and soil organic carbon mineralization in soil following addition of pyrogenic and fresh organic matter. *The ISME journal, 10*(12), 2918–2930.

Whitman, T., Zhu, Z., & Lehmann, J. (2014). Carbon mineralizability determines interactive effects on mineralization of pyrogenic organic matter and soil organic carbon. *Environmental Science & Technology, 48*(23), 13727–13734.

Wiesmeier, M., Urbanski, L., Hobley, E., Lang, B., von Lützow, M., Marin-Spiotta, E., . . . & Kögel-Knabner, I. (2019). Soil organic carbon storage as a key function of soils - A review of drivers and indicators at various scales. *Geoderma, 333*, 149–162.

WRB, I. W. G. (2015). World reference base for soil resources 2014, update 2015: International soil classification system for naming soils and creating legends for soil maps. In (pp. 192): Fao Rome.

Xu, G., Chen, J., Berninger, F., Pumpanen, J., Bai, J., Yu, L., & Duan, B. (2015). Labile, recalcitrant, microbial carbon and nitrogen and the microbial community

composition at two Abies faxoniana forest elevations under elevated temperatures. *Soil Biology & Biochemistry*.

Xu, P., Liu, Y., Zhu, J., Shi, L., Fu, Q., Chen, J., . . . & Huang, Q. (2020). Influence mechanisms of long-term fertilizations on the mineralization of organic matter in Ultisol. *Soil and Tillage Research, 201*.

Yang, C., Liu, N., & Zhang, Y. (2019). Soil aggregates regulate the impact of soil bacterial and fungal communities on soil respiration. *Geoderma, 337*, 444–452.

Yang, W., Zhang, D., Cai, X., Xia, L., Luo, Y., Cheng, X., & An, S. (2019). Significant alterations in soil fungal communities along a chronosequence of Spartina alterniflora invasion in a Chinese Yellow Sea coastal wetland. *Science of The Total Environment, 693*, 133548.

Ye, G., Lin, Y., Luo, J., Di, H. J., Lindsey, S., Liu, D., . . . & Ding, W. (2020). Responses of soil fungal diversity and community composition to long-term fertilization: Field experiment in an acidic Ultisol and literature synthesis. *Applied Soil Ecology, 145*, 103305.

Zhao, F. J., Ma, Y., Zhu, Y. G., Tang, Z., & McGrath, S. P. (2015). Soil contamination in China: Current status and mitigation strategies. *Environmental science & technology, 49*(2), 750–759.

Zheng, M. H., Huang, C., & Wang, J. M. (2015). Responses of soil acid phosphatase and beta-glucosidase to nitrogen and phosphorus addition in two subtropical forests in southern China. *European Journal of Soil Biology, 2015,68*(-), 77–84.

Zheng, Q., Hu, Y., Zhang, S., Noll, L., & Wanek, W. (2019). Soil multifunctionality is affected by the soil environment and by microbial community composition and diversity. *Soil Biology and Biochemistry, 136*, 107521.

Zhonga, Y., Yanb, W., Wanga, R., Wanga, W., & Shangguanb, Z. (2018). Decreased occurrence of carbon cycle functions in microbial communities along with long-term secondary succession. *Soil Biology and Biochemistry, 123*, 207–217.

Zieger, A., Kaiser, K., Ríos Guayasamín, P., & Kaupenjohann, M. (2017). Massive carbon addition to an organic-rich Andosol did not increase the topsoil but the subsoil carbon stock. *Biogeosciences Discussions, 2017*(November), 1–30.

Zimmerman, A. R., Gao, B., & Ahn, M. Y. (2011). Positive and negative carbon mineralization priming effects among a variety of biochar-amended soils. *Soil Biology and Biochemistry, 43*(6), 1169–1179.

Appendix IV. Statement of contribution doctorate with publications/manuscripts

MASSEY UNIVERSITY
TE KUNENGA KI PŪREHUROA
UNIVERSITY OF NEW ZEALAND

GRADUATE RESEARCH SCHOOL

STATEMENT OF CONTRIBUTION
DOCTORATE WITH PUBLICATIONS/MANUSCRIPTS

We, the candidate and the candidate's Primary Supervisor, certify that all co-authors have consented to their work being included in the thesis and they have accepted the candidate's contribution as indicated below in the *Statement of Originality*.

Name of candidate:	Yang Li
Name/title of Primary Supervisor:	Marta Camps-Arbestain/Prof. Dr
In which chapter is the manuscript /published work:	Chapter 3

Please select one of the following three options:

(●) The manuscript/published work is published or in press

- Please provide the full reference of the Research Output:

Li, Y., Wang, T., Camps-Arbestain, M., Suárez-Abelenda, M., & Whitby, C. P. (2020). Lime and/or Phosphate Application Affects the Stability of Soil Organic Carbon: Evidence from Changes in Quantity and Chemistry of the Soil Water-Extractable Organic Matter. Environmental science & technology, 54(21), 13908–13916.

( ) The manuscript is currently under review for publication – please indicate:

- The name of the journal:

- The percentage of the manuscript/published work that was contributed by the candidate:

- Describe the contribution that the candidate has made to the manuscript/published work:

( ) It is intended that the manuscript will be published, but it has not yet been submitted to a journal

Candidate's Signature:	Yang Li Digitally signed by Yang Li Date: 2021.11.02 14:29:53 +08'00'
Date:	02-Nov-2021
Primary Supervisor's Signature:	
Date:	2-Nov-2021

This form should appear at the end of each thesis chapter/section/appendix submitted as a manuscript/ publication or collected as an appendix at the end of the thesis.

MASSEY UNIVERSITY
TE KUNENGA KI PŪREHUROA
UNIVERSITY OF NEW ZEALAND

GRADUATE RESEARCH SCHOOL

STATEMENT OF CONTRIBUTION
DOCTORATE WITH PUBLICATIONS/MANUSCRIPTS

We, the candidate and the candidate's Primary Supervisor, certify that all co-authors have consented to their work being included in the thesis and they have accepted the candidate's contribution as indicated below in the *Statement of Originality*.

Name of candidate:	Yang Li
Name/title of Primary Supervisor:	Marta Camps-Arbestain/Prof. Dr
In which chapter is the manuscript /published work:	Chapter 4

Please select one of the following three options:

(●) The manuscript/published work is published or in press

- Please provide the full reference of the Research Output:

Li, Y., Camps-Arbestain, M., Whitby, C. P., Wang, T., Mueller, C. W., Hoeschene, C., Beare, M. H. (2021). Functional complexity explains the depth-dependent response of organic matter to liming at the nanometer scale. Geoderma (accepted)

( ) The manuscript is currently under review for publication – please indicate:

- The name of the journal:

- The percentage of the manuscript/published work that was contributed by the candidate:

- Describe the contribution that the candidate has made to the manuscript/published work:

( ) It is intended that the manuscript will be published, but it has not yet been submitted to a journal

Candidate's Signature:	Yang Li Digitally signed by Yang Li Date: 2021.11.02 14:34:04 +08'00'
Date:	02-Nov-2021
Primary Supervisor's Signature:	Marta Camps
Date:	2-Nov-2021

This form should appear at the end of each thesis chapter/section/appendix submitted as a manuscript/ publication or collected as an appendix at the end of the thesis.

MASSEY UNIVERSITY
TE KUNENGA KI PŪREHUROA
UNIVERSITY OF NEW ZEALAND

GRADUATE RESEARCH SCHOOL

STATEMENT OF CONTRIBUTION
DOCTORATE WITH PUBLICATIONS/MANUSCRIPTS

We, the candidate and the candidate's Primary Supervisor, certify that all co-authors have consented to their work being included in the thesis and they have accepted the candidate's contribution as indicated below in the *Statement of Originality*.

Name of candidate:	Yang Li
Name/title of Primary Supervisor:	Marta Camps-Arbestain/Prof. Dr
In which chapter is the manuscript /published work:	Chapter 5

Please select one of the following three options:

○ The manuscript/published work is published or in press

- Please provide the full reference of the Research Output:

◉ The manuscript is currently under review for publication – please indicate:

- The name of the journal:

Science of the Total Environment

- The percentage of the manuscript/published work that was contributed by the candidate: 70.00

- Describe the contribution that the candidate has made to the manuscript/published work:

The candidate and chief supervisor designed the experiment. The candidate conducted the experiment, and data analyses with assistance of Dr. Tao Wang. The data interpretation and manuscript writing were carried out with assistance of all supervisors.

○ It is intended that the manuscript will be published, but it has not yet been submitted to a journal

Candidate's Signature:	Yang Li Digitally signed by Yang Li Date: 2021.11.02 14:47:34 +08'00'
Date:	02-Nov-2021
Primary Supervisor's Signature:	Marta Camps
Date:	2-Nov-2021

This form should appear at the end of each thesis chapter/section/appendix submitted as a manuscript/ publication or collected as an appendix at the end of the thesis.